# ASTROPHYSICAL PHENOMENA REVEALED BY SPACE VLBI

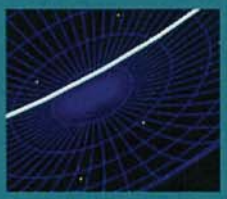

Proceedings of the VSOP Symposium,
January 2000

Edited by

H. Hirabayashi, P.G. Edwards and D.W. Murphy

# Astrophysical Phenomena Revealed by Space VLBI

**Proceedings of the VSOP Symposium**
**held at**
**the Institute of Space and Astronautical Science**
**19–21 January 2000**

Edited by
H. Hirabayashi, P.G. Edwards and D.W. Murphy

Published by the Institute of Space and Astronautical Science
Yoshinodai 3–1–1, Sagamihara, Kanagawa 229-8510, Japan

Printed by Work-1 Co. Ltd
Sagamihara, Japan



Astrophysical Phenomena Revealed by Space VLBI
Proceedings of the VSOP Symposium
held at the Institute of Space and Astronautical Science
on 19–21 January 2000
edited by H. Hirabayashi, P.G. Edwards and D.W. Murphy
ISBN 4-9980848-0-1 C3444

*Astrophysical Phenomena Revealed by Space VLBI*
*H. Hirabayashi, P.G. Edwards and D.W. Murphy (eds.)*

# Contents

*Astrophysical Phenomena Revealed by Space VLBI*
*H. Hirabayashi, P.G. Edwards and D.W. Murphy (eds.)*

# Preface

This volume contains the proceedings of the VLBI Space Observatory Programme (VSOP) symposium held at the Institute of Space and Astronautical Science from Wednesday 19 January to Friday 21 January, 2000. The symposium marked both the tenth anniversary of the first VSOP symposium held in December 1989 and the third anniversary of HALCA's launch. The 1989 symposium, the proceedings of which were published in *Frontiers of VLBI* (Universal Academy Press), attracted 50 participants from abroad, and a similar number travelled to Japan for the 2000 symposium. *Frontiers of VLBI* captures a time when, buoyed by the success of the TDRSS experiments, the future for space VLBI was full of promise.

This promise was realized with the launch of the MUSES-B satellite on 12 February 1997 and the subsequent deployment of its mesh antenna – capping many years of planning and effort. These proceedings reflect the wide range of science being conducted with VSOP observations: from studies of pulsars and the interstellar medium, to galactic masers, to high-redshift quasars. Highlights of the conference included the growing interplay between observations of jets and the increasingly sophisticated magneto-hydrodynamic simulations, and the complementary nature of multi-wavelength observations, and these are showcased in the color figures on the following pages.

VSOP observations offer a gain in linear resolution of $\sim$3, and often an even greater improvement in the area of the synthesized beam, and the contributions to this volume reflect the greatly enhanced science these gains allow. Aside from resolution, perhaps the main difference with ground VLBI is the fact that the precession of HALCA's elliptical orbit results in the beam (or optical transfer function) changing with time, which results in observations for survey-type program having to be spread over the $\sim$1.5 year nodal precession timescale.

The high noise temperature of HALCA's 22 GHz receiver has been the major disappointment of the mission, however the successful detection of 22 GHz fringes to HALCA during the outburst of the Orian-KL water vapor maser demonstrates that the rest of the VSOP system performed admirably at this frequency, lending confidence to efforts to push to even higher frequencies in the next generation missions described in these proceedings.

We wish to thank all those who helped in the organization and running of the symposium, including the members of the Science Organizing Committee (H. Hirabayashi, D. Jauncey, R. Preston, L. Gurvits and P. Edwards) and the many members of the Local Organizing Committee, especially S. Kameno, K. Fujisawa, T. Bushimata, I. Avruch and Y. Asaki and his band of helpers during the meeting. The efforts of post-symposium tour leaders J. Lovell and D. Murphy are also appreciated. Special thanks are given to Y. Miyaji, T. Nagano and M. Tanaka for all their work at the registration desk and behind the scenes. Funding from the Ministry of Education, Science, Sports and Culture for the symposium is also gratefully acknowledged.

Finally, our thanks to all symposium participants, and especially to the authors for preparing their manuscripts within four weeks, allowing the proceedings to be printed and distributed in less than three months from the symposium.

H. HIRABAYASHI
P.G. EDWARDS
D.W. MURPHY

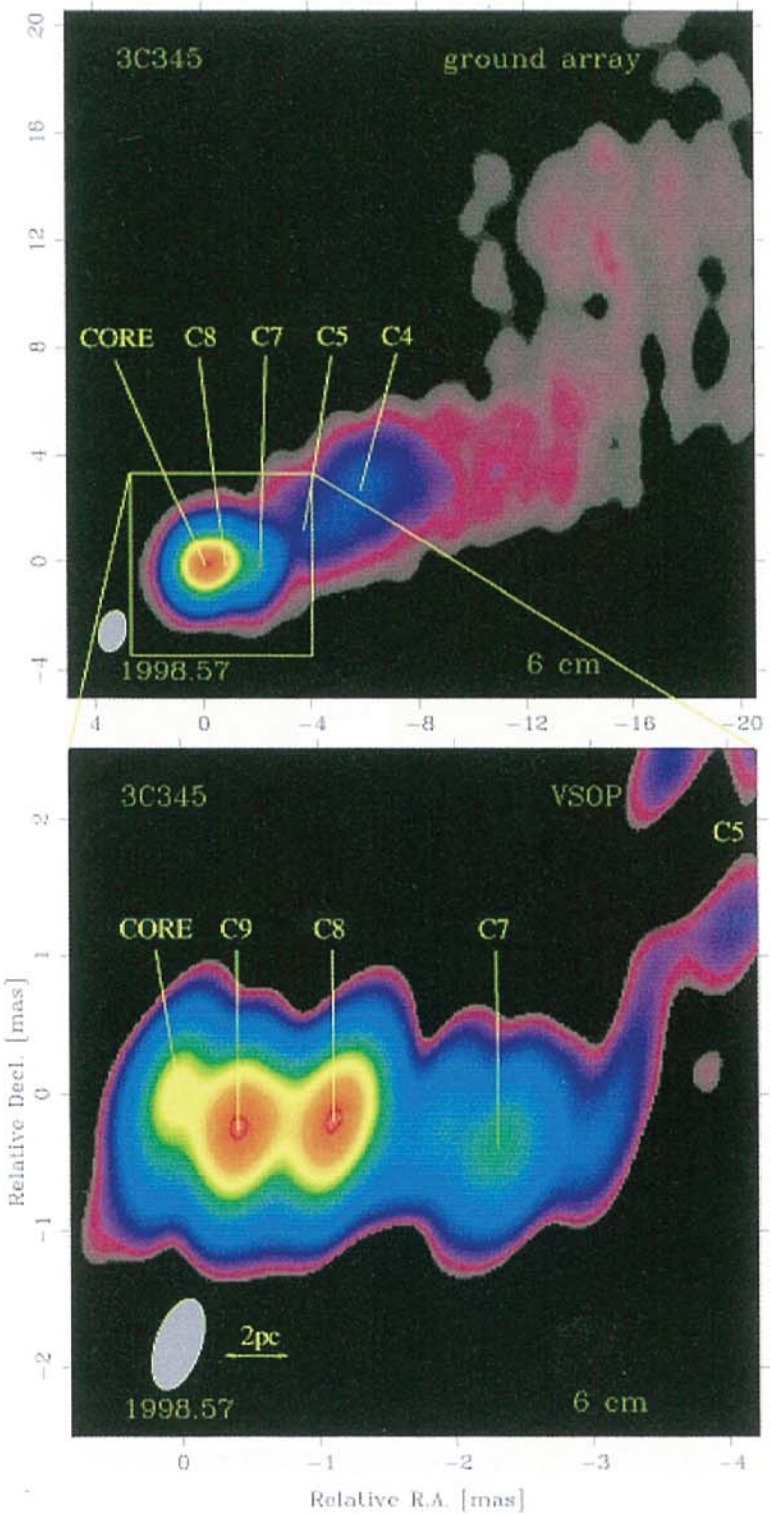


Color Figure 1: Ground-only (top) and VSOP (bottom) images at 5 GHz of the quasar 3C345. The resolution gained by the addition of data from HALCA allows the inner jet components to be much more clearly discerned (Klare et al., page 21).

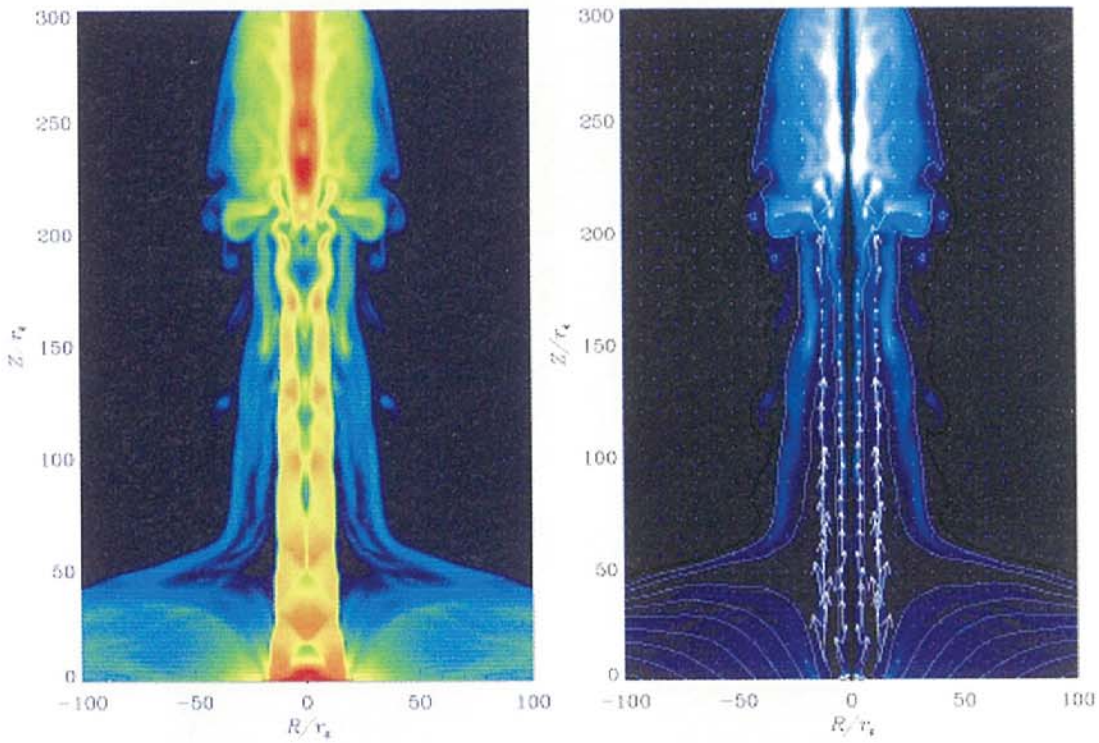


Color Figure 2a: (left) Magnetic pressure intensity plot for a simulated fast jet produced by a Keplerian accretion disk around a black hole (at [0,0]), with red indicating the highest magnetic pressure (Meier and Koide, page 31). Such a plot is similar to the appearance of a total intensity radio image (if the field/particle ratio is uniform). The knot-like intensity enhancements along the jet are caused by X-shocks occurring where the flow compresses. These knots move at pattern speeds considerably less than the flow speed of the jet. Distances are in gravitational units ($r_g = GM/c^2$).

Color Figure 2b: (right) Plot of magnetic field components and poloidal ($V_R$, $V_Z$) jet velocity vectors for the simulation at left. The contours show the poloidal magnetic field lines while the intensity image shows the azimuthal field strength ($B_\phi$). Polarization images of jets with strong poloidal field will have magnetic vectors along the contours (generally parallel to the body of the jet here), whereas regions with strong azimuthal field will have magnetic vectors perpendicular to the jet. The magnetic structure of this simulated jet is rather similar to some of the jets observed by Moellenbrock et al. (these proceedings).

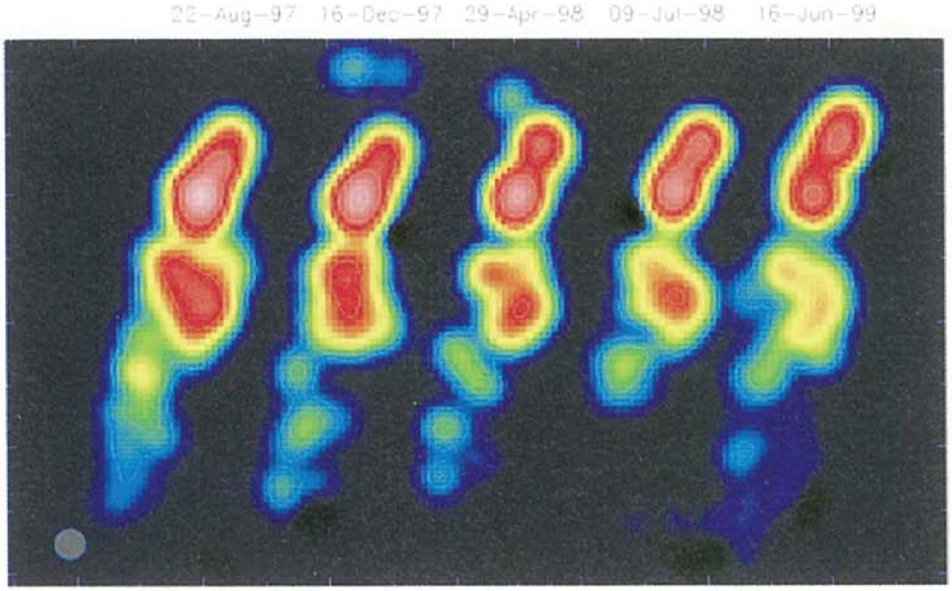


COLOR FIGURE 3: Five epoch VSOP 5 GHz images of 1928+734 (Murphy et al., page 47). All images have been convolved with the same circular 0.5 milli-arcsecond beam (shown at bottom left). Evolution of the core and jet components can clearly be seen.

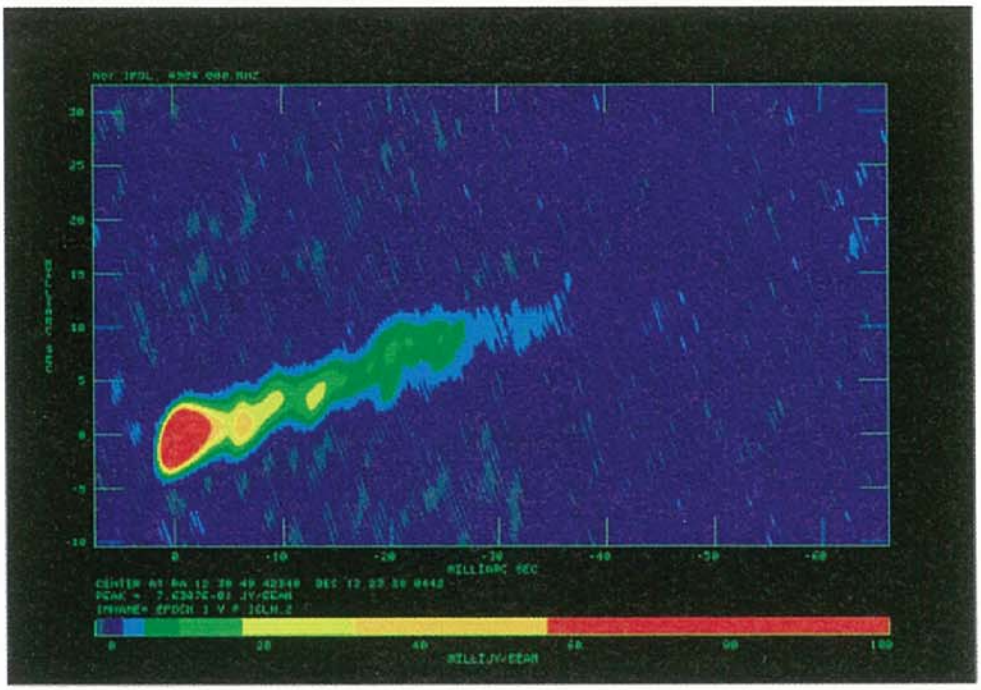

COLOR FIGURE 4: First epoch (1997 December 20) VSOP image of the Vir A jet at 5 GHz (Junor et al., page 13). Although Hubble Space Telescope observations have indicated superluminal motion of jet components on the arc-second scale, VSOP monitoring shows no evidence for such motions on the milli-arcsecond scale.

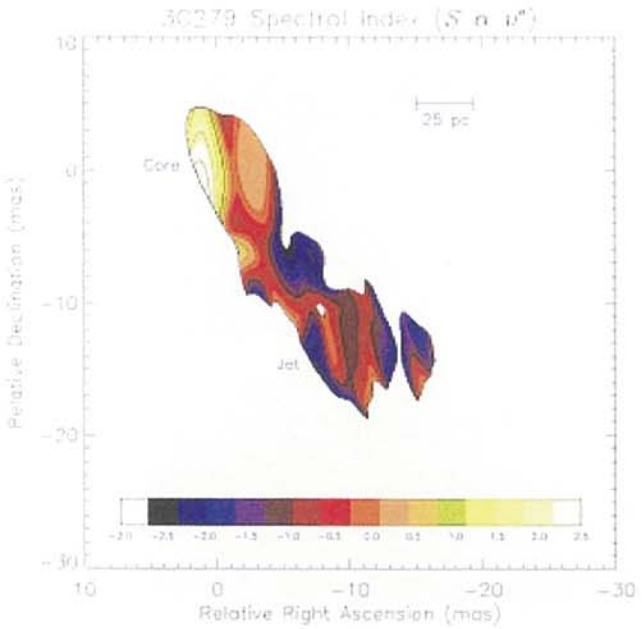


Color Figure 5: The spectral index map of 3C 279 produced from a 1.6 GHz VSOP image and the ground-only 5.0 GHz image made on consecutive days in January 1998 (Hirabayashi et al., page 25). The quasar core at left shows a highly inverted core (i.e. positive spectral index) indicating strong synchrotron self-absorption.

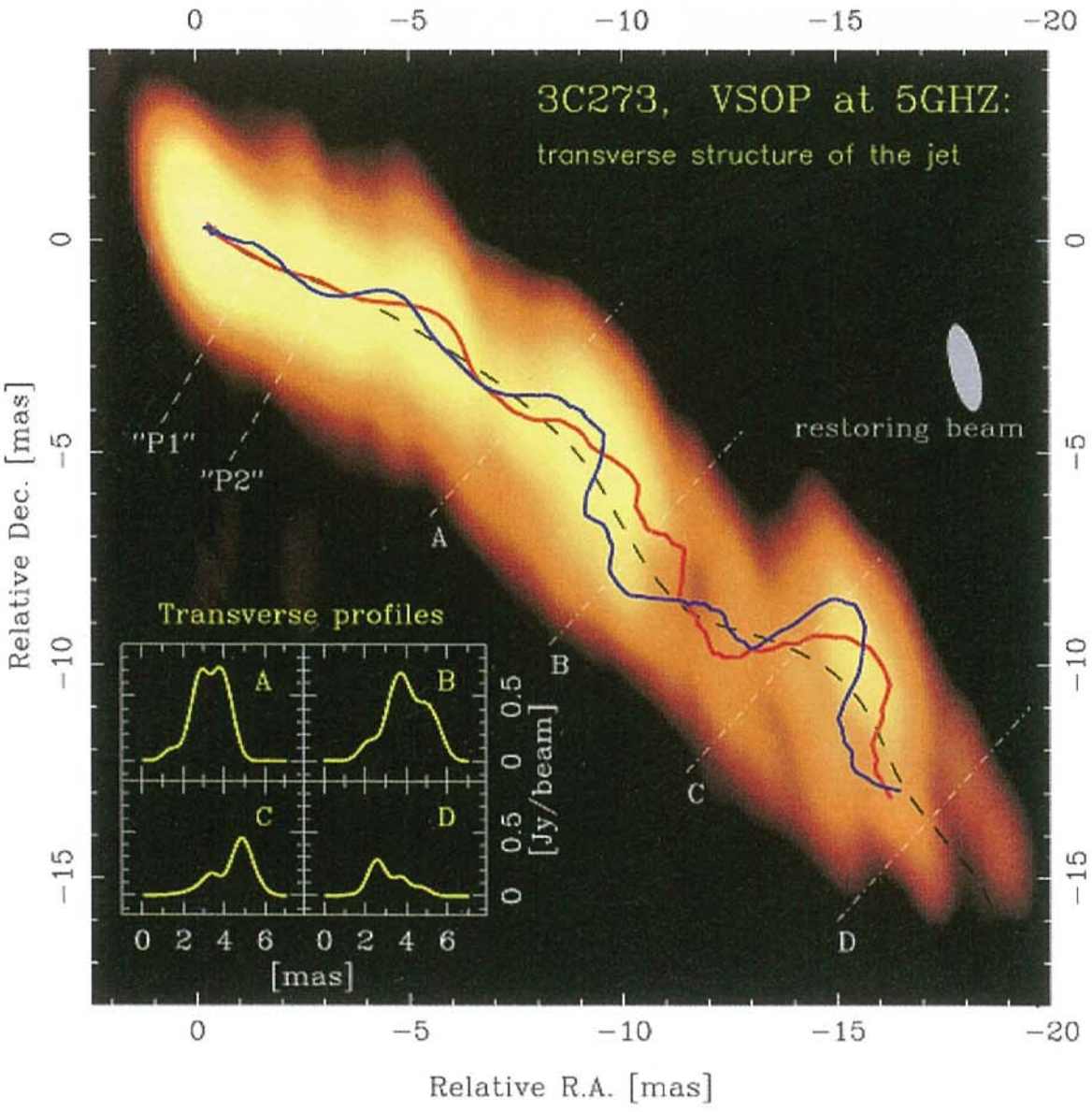

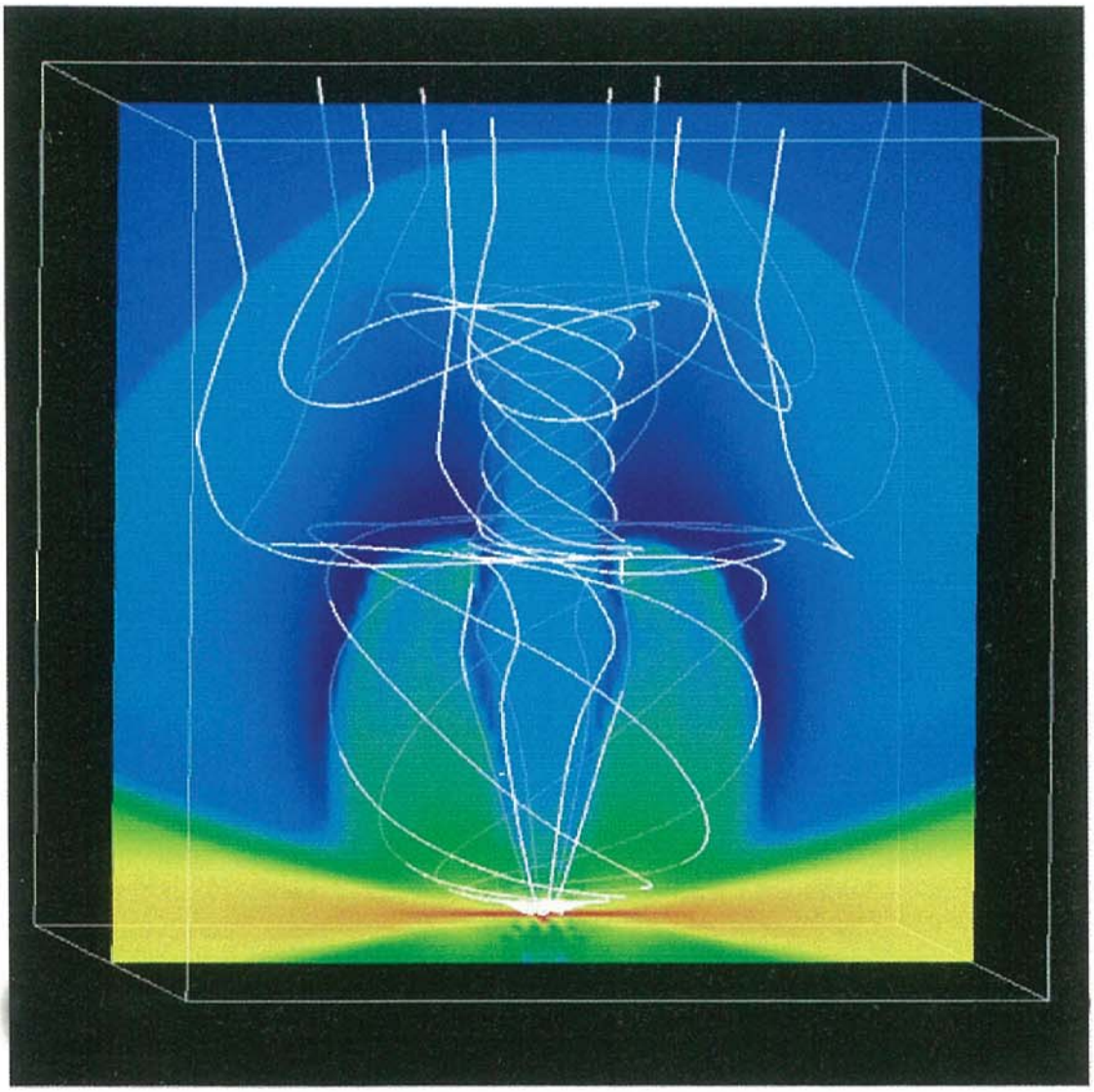

COLOR FIGURE 7: Simulation by T. Kudoh and K. Shibata showing a typical example of a magnetically driven jet ejected from accretion disk. The white lines show the magnetic field lines, and the colors represent particle density. Note that a beautiful bow shock is created ahead of a jet, with magnetic field lines strongly twisted below, but not at, the bow shock (Shibata, page 29).

---

← COLOR FIGURE 6: A 5 GHz VSOP image of the parsec-scale radio jet of 3C273 (Lobanov et al. page 239). The dot-dashed white lines denote the locations of the 4 flux density profiles shown in the inset. Two emitting features, denoted P1 and P2, can be identified in the jet, the locations of which are shown on the image by the red and blue lines.

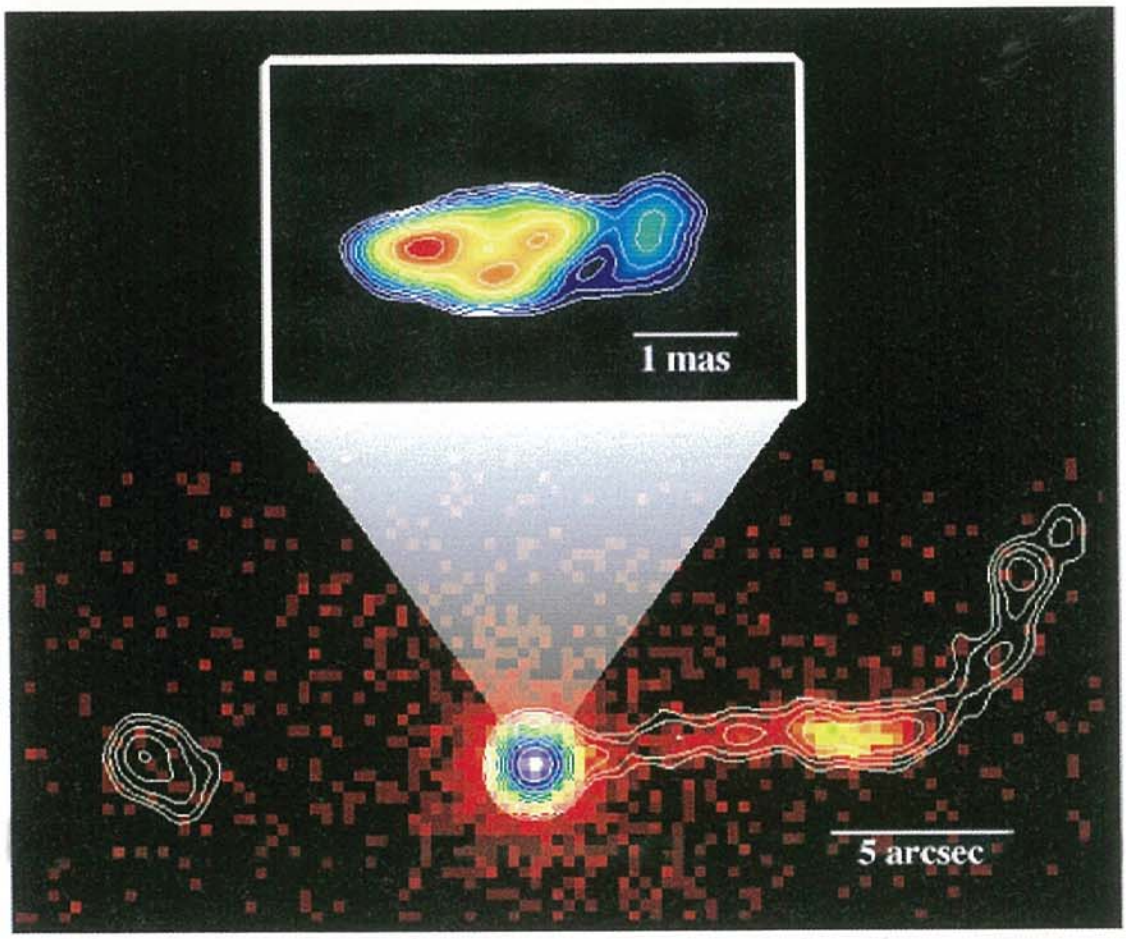


Color Figure 8: A 5 GHz VSOP image of PKS 0637−752 (top) and an overlay of the Australia Telescope Compact Array 8.6 GHz (contours) and Chandra X-ray (colours) images (bottom). The ATCA image has been restored with a circular beam with FWHM of 0.84 arcsec, which is the half-power point of the Chandra PSF. With the unexpected discovery of the X-ray jet in this quasar, the relationship between the parsec-scale and kilo-parsec scale jets in core-dominated quasars has attracted renewed attention (Lovell et al., page 215).

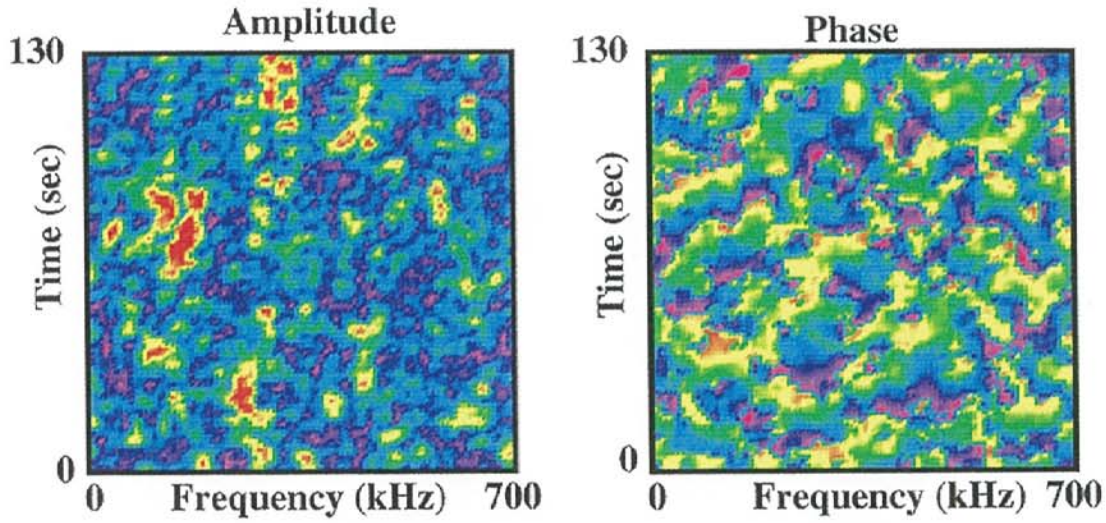


COLOR FIGURE 9: Speckle pattern of the Vela pulsar, observed on the HALCA-Tidbinbilla baseline at 1.6 GHz (Gwinn et al., page 117).

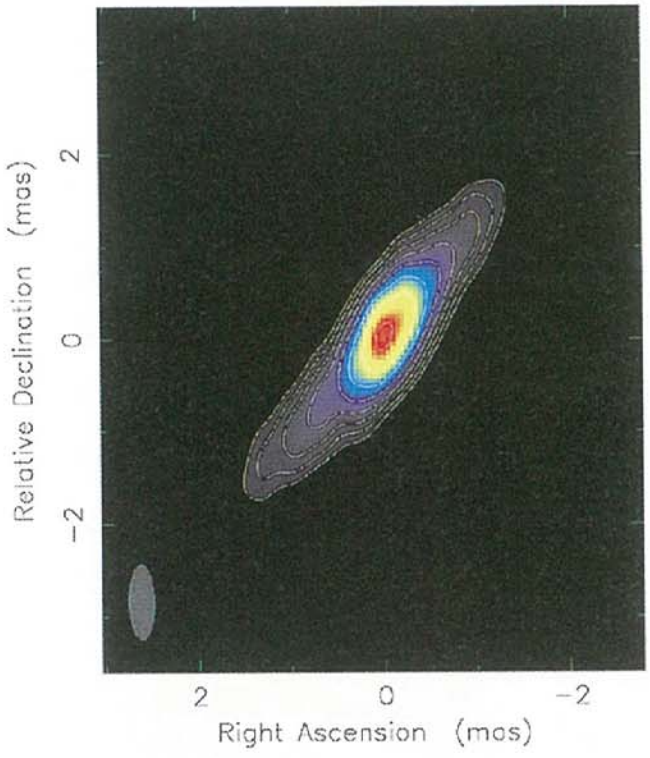


COLOR FIGURE 10: The 22 GHz VSOP image from March 1998 of the Orion-KL water vapour maser spot that underwent an outburst in 1997–1998. The map peak is $1.3\times10^5$ Jy/beam and beam size is 0.80 milli-arcseconds × 0.27 milli-arcseconds. Details of the outburst and evolution of the elongated shape evident in the image are described by Kobayashi et al. (page 109).

*Astrophysical Phenomena Revealed by Space VLBI*
*H. Hirabayashi, P.G. Edwards and D.W. Murphy (eds.)*

# Welcoming Remarks

Haruto Hirosawa

*ISAS, Yoshinodai 3-1-1, Sagamihara, Kanagawa 229-8510, Japan*

In December 1989, we had an international symposium on the VLBI Space Observatory Programme (VSOP) here at ISAS, Sagamihara, where we welcomed fifty participants from outside Japan. Now we have the second international symposium on VSOP also here at Sagamihara, where we are welcoming again more than fifty participants from abroad. I would like to ask our international colleagues here who also attended the first symposium: "Did you really expect at the time of the first symposium that we could reach the success, the level of success that we presently have?" I suppose a majority of answers might be "no".

The HALCA project (the name of the satellite was MUSES-B until launch) formally started in April 1989. Around December 1989, the development of the ISAS's new satellite launcher, named M-V, was not yet formally started, though the MUSES-B spacecraft was assumed to be carried into orbit by the first launch of the M-V rocket. At the initial phase of the spacecraft development, the large deployable antenna based on an idea of the tension-wired-truss, which formed the main dish from complicated wire networks and meshes, still required a large number of studies and experiments. The international cooperation for conducting space VLBI observations after the spacecraft was launched seemed to be very extensive and to require broad aspects of preparations.

We can say now that we have arrived at a great success. On February 12, 1997, the satellite HALCA was successfully launched by the M-V rocket and was injected into the planned orbit. About two weeks after the launch, the HALCA's eight-meter-diameter antenna was successfully deployed. On March 24, 1997, the HALCA antenna was first directed towards a celestial radio source and signals detected. In the middle of May 1997, fringes were first detected on a baseline formed by HALCA and a ground radio telescope. In the middle of June, 1997, the first space-VLBI images were generated from cooperative observations between HALCA and ground radio telescopes. After this sequence of events, the VSOP project gradually moved into a science observations phase, and as all you recognize, a large number of scientific results have been generated by VSOP. I am convinced that this second VSOP sym-

posium itself is clear evidence of the success of HALCA and the VSOP project.

The success of the VSOP is not only achieved by the success of the HALCA spacecraft, but also by both the international collaborations among space organizations, radio astronomy observatories and other institutions, and the cooperation among a large number of scientists from all over the world. The international cooperation realized for VSOP is on an unprecedented scale, which has never existed before in the field of space science. Representing my Japanese VSOP colleagues, I would like to express our sincere thanks to the international partner organizations and observatories, the international colleagues of the VSOP team, and radio astronomers from abroad, all who have deeply contributed to the success of HALCA and the VSOP mission.

Thank you very much.

*Astrophysical Phenomena Revealed by Space VLBI*
*H. Hirabayashi, P.G. Edwards and D.W. Murphy (eds.)*

# VSOP Current Status

H. Hirabayashi

*ISAS, Yoshinodai 3-1-1, Sagamihara, Kanagawa 229-8510, Japan*

**Abstract**

HALCA was launched on 12 February 1997. The current status of the VLBI Space Observatory Programme (VSOP) mission is described.

## 1 Introduction

The Institute of Space and Astronautical Science (ISAS) launched the first space VLBI (Very Long Baseline Interferometry) satellite, HALCA, on 1997 February 12. After completing a series of engineering experiments to verify space VLBI observations, the first VLBI fringes and images were obtained in May and June 1997, respectively. HALCA is being operated for science observations at 1.6 and 5 GHz for the VSOP (VLBI Space Observatory Programme) project in cooperation with many organizations and radio telescopes around the world. HALCA's status earlier in the mission has been reviewed by Hirabayashi (1998), Hirabayashi et al. (1998), Lovell et al. (1999) and Hirabayashi and Hirosawa (2000): in this paper more recent science activities of the mission are described.

## 2 The HALCA Satellite

HALCA's orbit has an apogee height of 21,400 km, perigee height of 560 km, inclination angle of 31°, and orbital period of 6.3 hours. The 8 m main reflector and the sub-reflector supporting structure were deployed in orbit. The satellite as it appears after full deployment in orbit is shown in Figure 1.

The on-board radio astronomy subsystem is composed of low-noise amplifiers for three frequency bands, 1.60–1.73 GHz, 4.7–5.0 GHz and 22.0–22.3 GHz, down-converters, two video converters, two high speed samplers, a formatter, two frequency-synthesizers, and a calibration signal generator (Hirosawa and Hirabayashi 1997, Hirabayashi et al. 2000).

The HALCA radio-telescope has typical system temperatures of 75 K at 1.6 GHz and 95 K at 5 GHz, with an antenna aperture efficiency

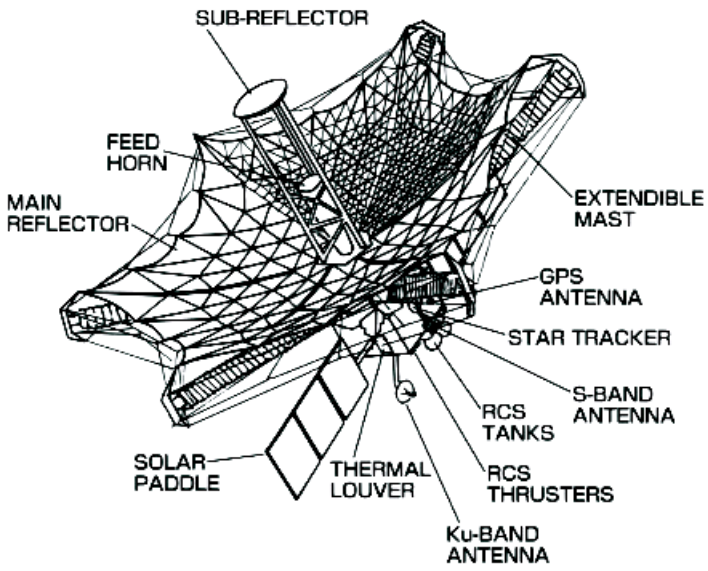


Figure 1: The fully deployed HALCA satellite.

of about 30% at 1.6 GHz. The 22 GHz system temperature is unexpectedly high, and it is believed that the 22 GHz waveguide connecting the feed horn and the front-end was possibly impaired due to heavy vibrations during launch.

## 3 In-Orbit Checkout

After a series of experiments as an engineering satellite — deployment of the 8 meter antenna, precise attitude control of spacecraft with a large antenna, transfer of phase reference signal, high data rate telemetry, etc. — the Usuda 64 m antenna and HALCA, via Usuda 10m tracking antenna, observed the quasar PKS 1519−273 at 1.6 GHz on 1997 May 7. The tapes were processed with the VSOP correlator at the National Astronomical Observatory (NAO), Mitaka, and the first HALCA-ground fringes were found on May 13. Subsequent three station interferometry with HALCA, the Usuda 64 m antenna and the Kashima 34 m showed stable closure phases confirming the success of the observations and paving the way for the imaging experiments.

In June 1997, the Canadian correlator at the Dominion Radio As-

trophysical Observatory (DRAO), Penticton, and the VLBA (Very Long Baseline Array) correlator of the National Radio Astronomy Observatory (NRAO), Socorro, detected fringes at 1.6 GHz. In July 1997, fringes at 5 GHz were first detected at Socorro, then at Penticton and at Mitaka. In mid-June 1997, the first 1.6 GHz images were generated and in July the first 5 GHz images were produced and an angular resolution of $\sim$0.3 mas achieved.

In April 1998, 22 GHz fringes to HALCA were first detected at Socorro for the bursting water maser in Orion-KL (Kobayashi et al., these proceedings). Imaging at 22 GHz has only been possible for this source because of the sensitivity problems, with little HALCA contribution because of the extended maser size.

HALCA has had some operational problems resulting in a observing being stopped because of telemetry signal loss, attitude control loss, etc. However, as far as electric power is concerned, it seems HALCA will be able to operated for at least five years from launch (Murata, these proceedings).

## 4 VSOP International Operation

HALCA is commanded from the Sagamihara Operations Center at ISAS six times a week by 2.1 GHz telemetry through the Kagoshima Space Center. For VLBI observations real-time two-way telemetry support is required with uplink at 15.3 GHz and data downlinked at 14.2 GHz at 128 mega-bits per second. Five 15 GHz-band tracking stations are employed: at Usuda (Japan), operated by ISAS; Green Bank (USA), operated by NRAO; and Goldstone (USA), Madrid (Spain), and Tidbinbilla (Australia) operated by NASA/JPL. Range-rate data from this ground telemetry network is also used for ISAS and JPL orbit determination.

A number of ground radio telescopes have committed time for simultaneous observations with VSOP. Commitments of ground radio telescope time for the mission have been negotiated through the Global VLBI Working Group (GVWG), formed under URSI Commission J. Participating telescopes include those of the Very Long Baseline Array (VLBA), the European VLBI Network (EVN), the Asia-Pacific Telescope (APT), and individual telescopes.

The recording format of the VLBI data is dependent upon the ground facilities involved. Three different tape formats are used: S2, VSOPT and VLBA/MkIV. Depending on the participating ground tele-

scopes, VSOP observations are correlated at the 10-station VSOP correlator in Mitaka, the 20-station VLBA correlator in Socorro, the 6-station S2 correlator in Penticton. Experiments involving two or more formats require conversion of some tapes at Mitaka, which has two S2/VSOPT and two VLBA/VSOPT bi-directional copiers.

## 5 Science Activities of VSOP

Scientific observations are classified into two categories; the peer reviewed General Observing Time Program and the mission-led Survey Program. The first Announcement of Opportunity covered observations for the 17 month period to the end of 1998, and the second Announcement of Opportunity solicited proposals for the calendar year 1999. The VSOP World Wide Web site (http://www.vsop.isas.ac.jp/) contains additional information and pictures of mission activities.

Observations of 4–7 hours are used for Survey Program observations. The Survey Program deals with a statistical sample of nearly 300 sources to be observed at 5 GHz with typically 3–4 ground telescopes, and is described in more detail in the papers in these proceedings by Fomalont et al., Moellenbrock et al, and Lovell et al.

Table 1: Summary of VSOP Observations to January 2000

| Year | GOT observations | Survey observations | Test observations | Total |
|---|---|---|---|---|
| 1997 | 49 | 20 | 25 | 94 |
| 1998 | 109 | 65 | 9 | 183 |
| 1999 | 183 | 45 | 9 | 237 |
| Total | 341 | 130 | 43 | 514 |

Scientific observations are being routinely undertaken at 1.6 and 5 GHz. A summary of VSOP observing to date is given in Tables 1 and 2. About fifty Survey Program observations have been extracted from GOT observations, and so the grand total of observed Survey sources is now 180 sources (Fomalont et al. these proceedings). Of the GOT observations, 131.5 were made at 1.6 GHz and and 209.5 at 5 GHz (with one observation conducted simultaneously at 1.6 and 5 GHz – see Murphy et

Table 2: Summary of observations by correlator

| Correlator | GOT observations | Survey observations |
|---|---|---|
| Socorro | 229 | – |
| Penticton | 88 | 105 |
| Mitaka | 24 | 25 |

al., these proceedings). Approximately 200 AO1 observations and 140 A02 observation have been made, with some ambiguity in these numbers due to shares, mergers and continuing programs.

## 6 VSOP Historical Notes

The year of HALCA's launch was half a century after the first detection by the so-called cliff-top interferometer in Sydney (Bolton and Stanley 1948). The first successful VLBI experiments in Canada and soon after in the USA were done in 1967, thirty years before HALCA's launch. The first space VLBI experiment with TDRSS was successful in 1986 (Levy et al. 1986), paving the way for dedicated imaging space VLBI to come 10 years later. The idea of space VLBI had been talked about, and concepts developed, by many people related to various missions like QUASAT, RadioAstron, and IVS before HALCA was finally launched.

In the year VSOP was budgeted, we had a space VLBI symposium here at ISAS, and this was 10 years and 2 months before this symposium. To make the VSOP mission successful, we had worked together with international colleagues with lots of efforts. We shared the ten years and we are now ten years older!

HALCA is now 3 years old. She had observed so many varieties of AGN features. But as Shakespeare stated as for the beauty of Cleopatra in *Antonio and Cleopatra*, "AGE (AGN?) cannot wither her, nor custom stale Her infinite variety."

**Acknowledgements.** The VSOP Project is led by the Japanese Institute of Space and Astronautical Science, with significant contributions from National Astronomical Observatory of Japan, the Jet Propulsion Laboratory, the U.S. National Radio Astronomy Observatory, the Canadian Dominion Radio Astrophysical Observatory, the Australia Tele-

scope National Facility, the European VLBI Network, the Joint Institute for VLBI in Europe, and the directors and staff of many of the world's radio observatories. The author would like to express his sincere thanks to a large number of international members of the VSOP team for the collaborations on the VSOP for long years. Philip Edwards is thanked for his help in the preparation of this paper.

## References

Bolton, J.G. & Stanley, G.J. 1948, *Nature*, **161**, 312

Hirabayashi, H. 1998, in *ASP Conf. Ser.* **144***: IAU Coll. 164: Radio Emission from Galactic and Extragalactic Compact Sources*, eds. J.A. Zensus, G.B. Taylor & J.M. Wrobel (San Francisco: Astron. Soc. Pac.), 11

Hirabayashi, H., Hirosawa, H., Kobayashi, H. et al. 1998, *Science*, **281**, 1825 and erratum **282**, 1995

Hirabayashi, H. & Hirosawa, H. 2000, *Adv. Sp. Res.*, **26** 589

Hirabayashi, H. et al. 2000, to be submitted to *PASJ*

Hirosawa, H., & Hirabayashi, H. 1997 *Advances in the Astronautical Sciences*, **96**, 229

Levy, G.S., Linfield, R.P., Ulvestad, J.S. et al. 1986, *Science*, **234**, 187

Lovell, J.E.J., Hirabayashi, H., Kobayashi, H. et al. 1999 *NewAR*, **43**, 515

*Astrophysical Phenomena Revealed by Space VLBI*
*H. Hirabayashi, P.G. Edwards and D.W. Murphy (eds.)*

# HALCA's Operating Efficiency & Lifetime

Y. Murata[1] & the HALCA operation group[1,2]

[1] *ISAS, Yoshinodai 3-1-1, Sagamihara, Kanagawa 229-8510, Japan*
[2] *NAO, Ohsawa 2-21-1, Mitaka, Tokyo 181-8588, Japan*

**Abstract**

We describe the current status of HALCA and the future prospects of the mission. HALCA must be operated in a three-reaction wheel mode from the middle of October 1999, affecting the operating efficiency of HALCA. The mission lifetime may exceed 5 years, if there are no unexpected problems.

## 1 HALCA History and Status

We have operated HALCA (Hirabayashi et al. 1998) for about 3 years, undertaking General Observing Time (GOT) observations from 13 July 1997. About 510 observations have been made, of which roughly 340 are GOT observations, 130 are Survey Program observations, and 40 are test observations.

On several occasions HALCA has stopped observing for an extended period, sometimes due to trouble with the on-board system. One such problem is the hanging-up of the on-board telemetry. We experienced this problem for the first time on 31 August 1998. It took about 2 months to recover, which was required for understanding the problem and establishing the recovery plan. We had the same trouble on 16 November 1998, 22 February 1999, and 16 November 1999. Each time we succeeded in recovering with a shorter down-time than previously. Another problem is that one of the four reaction wheels was broken on 7 October 1999, resulting in the loss of the attitude control for about 2 weeks. We could not move to the safe-hold mode due to the lack of the thruster fuel required for safe-hold maneuvers. After recovering from this accident, observing re-started in December 1999, however HALCA lost attitude control again toward the end of December, and was in free-spin mode at a time of the symposium.

## 2 Recovery Plan/Operation

We had to wait for a number of conditions to be met for recovery: the thermal condition of the reaction wheels and the batteries and also the

angular momentum of the satellite. The angular momentum has to be compensated by the three reaction wheels. Finally we also needed to care about the satellite's sun angle after recovery, with a sun angle of 180° (the sun is located toward the $-z$ direction, or bottom of the satellite) desired. Recovery efforts started in the week following the symposium because we found the HALCA conditions were good. We successfully regained attitude control on 5 February 2000. We started Ku tracking from February 15, and are, at the time of writing, preparing to start the observation starting from the beginning of March. We have the apogee eclipse "season", during which eclipses last about 90 minutes, from April 12 to May 9, after which HALCA enters a "no eclipse" season again. The decision on when to change the attitude of HALCA, e.g. from sun angles near $\sim 180°$ to those near 90°, will be made at this time.

## 3 Operation Efficiency with Three Reaction Wheels

We need at least three reaction wheels to have 3-axis control of the satellite's attitude. However, the four reaction wheels of HALCA were symmetrically located, and were designed so that the total angular momentum of the satellite was zero. Thus there was no need to worry about the intrinsic angular momentum of HALCA when we had four reaction wheels for attitude control. However, it is impossible to have zero-momentum attitude control with three reaction wheels, and we must switch to biased-momentum control. This means the rotation speed of each reaction wheel after the maneuver is different from that before the maneuver. Large maneuvers may make the rotation speeds of the wheels exceed their limits. Allowed maneuvers are now typically 10°–30°, depending on the exact conditions of the maneuver.

During the perigee passage after a maneuver the accumulated angular momentum is dumped by the magnetic torquer, restoring the reaction wheel rotation speeds to their nominal values. It would be possible therefore to make a maneuver every orbit, if the magnetic torquer worked perfectly. However, we need to study how the reaction wheel rotation speeds changed in real operations. It seems that one maneuver per two orbits is the optimistic view, and that having to check the rotation speeds before every maneuver during a Kagoshima commanding pass is the pessimistic view.

The total capacity for momentum accumulation from external perturbations has become smaller in three reaction wheel mode. The main

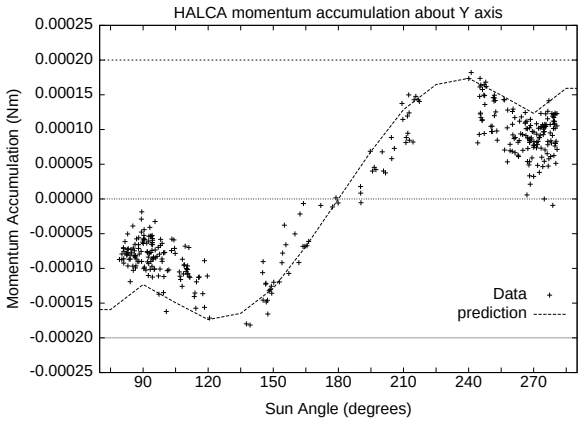


Figure 1: The torque around the $y$ axis of HALCA versus the sun angle measured from HALCA's $+z$ axis. The "+" signs are the measured data, and dashed lines show the expectation from a simple model.

external force is solar ram pressure. Figure 1 shows the torque due to solar ram pressure versus sun angle (measured from the HALCA $+z$ axis). It is difficult to maintain HALCA's attitude when perturbations exceed the momentum accumulation of about 0.0001 Nm per orbit, which comes from the capacity of the reaction wheels. So only the solution is attitudes with sun angles of 165°–195°. But this situation reduces the science which can be done, because we can only observe sources in the anti-sun direction, and there is a large area of sky which cannot be observed with this attitude. So we are now studying the possibility that HALCA observes in the sun angle range 260°–280°, which has a larger sky coverage than that of 165°–195°. We can offset the range of the momentum accumulation from ±0.0001 Nm to 0.0–0.0002 Nm, for example, by changing the parameters of the momentum dumping with the magnetic torquer. It seems that the sun angles of 80°–100° is another solution, but we have more experience in the 260°–280° range than at 80°–100°. We need to get more data and study it carefully.

Because of the maneuver limitations, it is difficult to make a large attitude change in one day. We must pick sources close to the previous source. If we must monitor the rotation speed of the reaction wheels, it will take 2–3 days to maneuver to the next source, and so the efficiency of maneuvering is reduced. Multi-frequency observations of the same source, e.g. 1.6 GHz on one day and 5.0 GHz the next, increase the observing efficiency.

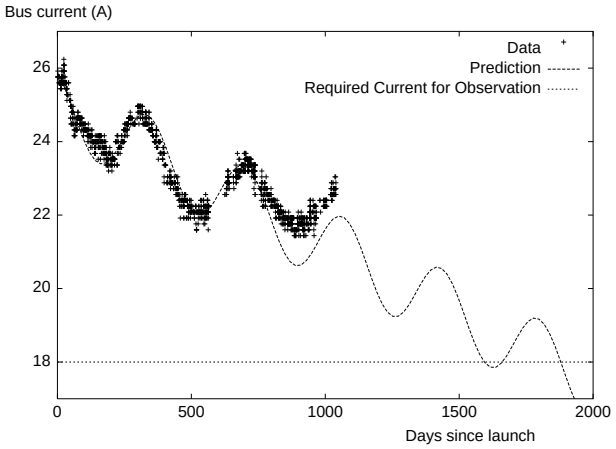


Figure 2: The time from launch in days and the output from the solar battery measured as the bus current. The required current for observing is more than 18 A. The plotted curve assumes the degradation is linear.

## 4 What Will Decide HALCA's Life-Time?

It was originally thought that the solar panel degradation would limit the HALCA's life-time to 3–5 years. However, current data for the degradation indicates that we can observe for more than 5 years (Figure 2). We now think the solar panels might not decide the life time of HALCA. The thruster fuel is nearly finished and so we will not use the thrusters in normal operations. The thrusters were not used in the last two recovery operations, and so this also might not limit HALCA's life-time, however the lack of thrusters does make recovery operations riskier, and so may have an effect on HALCA's life-time. Perhaps the most likely problem is the failure of on-board instrumentation. We have already experienced problems with the reaction wheels and the data handling unit. Most of the components were designed assuming a 3–5 year life-time, however HALCA's repeated system shutdowns and re-starts have probably stressed some components, reducing their life-time.

**Acknowledgements.** We gratefully acknowledge the participants of the symposium. The good results of the VSOP observations encourage us very much.

## References

Hirabayashi, H., Hirosawa, H., Kobayashi, H. et al. 1998, *Science*, **281**, 1825 and erratum **282**, 1995

*Astrophysical Phenomena Revealed by Space VLBI*
*H. Hirabayashi, P.G. Edwards and D.W. Murphy (eds.)*

# Multi-Epoch Global+VSOP/HALCA Observations of Virgo A at $\lambda 6\,\mathrm{cm}$

W. Junor [1], J.A. Biretta [2], F.N. Owen [3] & M.C. Begelman [4]

[1] *UNM, 800 Yale Blvd., N.E., Albuquerque, NM 87131, USA*
[2] *STScI, 3700 San Martin Drive, Baltimore, MD 21218, USA*
[3] *NRAO, P.O. Box 0, Socorro, NM 87801, USA*
[4] *JILA/University of Colorado, Box 440, Boulder, CO 80309, USA*

**Abstract**

Images from 4 epochs of VSOP+Global observations at $\lambda 6\,\mathrm{cm}$ of the nearby active galaxy, Vir A, are presented. No proper motions are detected in 1.5 years to a limit of $\approx 10^{-2}\,c$. Sequential brightening of two components on either side of the jet's axis is seen, however.

## 1 Introduction

The nearby ($D = 14.7\,\mathrm{Mpc}$) E0p galaxy M87 in the Virgo Cluster is the host for the bright radio source Virgo A (3C274, J1230+1223). This active galaxy contains the prototype extragalactic jet (Curtis 1918). The jet is roughly $25''$-long and has been studied extensively across the electromagnetic spectrum. Jets are conduits for the transport of material and energy from the center of an active galactic nucleus (AGN) to the outer regions of the galaxy. The central "engine" in an AGN is believed to be a super-massive black hole with an orbiting accretion disk fed by material raining in from the host galaxy. In M87, there is distinct evidence for a central mass of $\approx 3 \times 10^9\,M_\odot$ (Harms et al., 1994; Macchetto et al., 1997). The mechanism by which jets are formed and collimated is uncertain though magneto-hydrodynamic (MHD) models are currently favored. In these models, MHD "fluid" from the accretion disk is accelerated along poloidal magnetic field lines threading the disk to Alfvénic speeds which are much greater than the local sound speed. These models have the advantage of removing angular momentum from the accretion disk. (See Livio 1999 for a review.) Collimation of the MHD wind is achieved through "hoop stresses" where the field becomes predominantly toroidal. Since the field lines are anchored in the accretion disk, a toroidal field will be generated naturally by the rotation

of the disk. Recent work by Junor et al. (1999) indicates that collimation of the Vir A jet begins within a projected distance of a few tens of Schwarzchild radii ($r_S$) of the core and is not complete until several $\times 10^3\, r_S$ from the central engine.

## 2 Global + VSOP/HALCA Images of Vir A Jet

The VLBI core of Vir A was observed with VSOP/HALCA and global arrays on four occasions at $\lambda 6$ cm. Vir A is one of the sources in VSOP's *Key Sources* program. Table 1 summarizes the details of these observations. The quoted beam is for the best 'V'-weighted image *i.e.* using the fourth root of the visibility weights to emphasize the contribution of the highest spatial frequencies to the image. The data were analyzed within NRAO's AIPS package. The images are shown in Figure 1 and Color Figure 4.

Table 1: Observing summary for Vir A at $\lambda 6$ cm

| Epoch | Antennas | Beam (mas×mas, °) | Figure |
|---|---|---|---|
| 1997.97 | VLBA, EB, RZ, Y, NZ | 2.03, 0.38, +17.1 | 1 |
| 1999.27 | VLBA, GZ, Y, TZ | 2.83, 0.40, −12.3 | |
| 1999.32 | VLBA, EB, GZ, HH, Y, TZ | 2.33, 0.51, −2.1 | 2 |
| 1999.49 | VLBA, EB, GZ, TZ | 2.28, 0.93, +6.4 | |

## 3 Discussion

Although superluminal motion has been seen reliably on VLA and HST scales (Biretta et al. 1995; Biretta et al. 1999), observed proper motions on VLBI scales seem to be moderately sub-luminal at best (Reid et al. 1989; Junor & Biretta, 1995; Biretta & Junor, 1995). A similar result is seen with these VSOP images; proper motions are $\leq 10^{-2}\, c$ although there is some evidence for brightening and dimming of static features. The rapid sampling of the 4 epochs goes some way to overcoming reservations about the results derived from earlier VLBI with limited temporal sampling. The bright component at $\approx 8$ mas from the

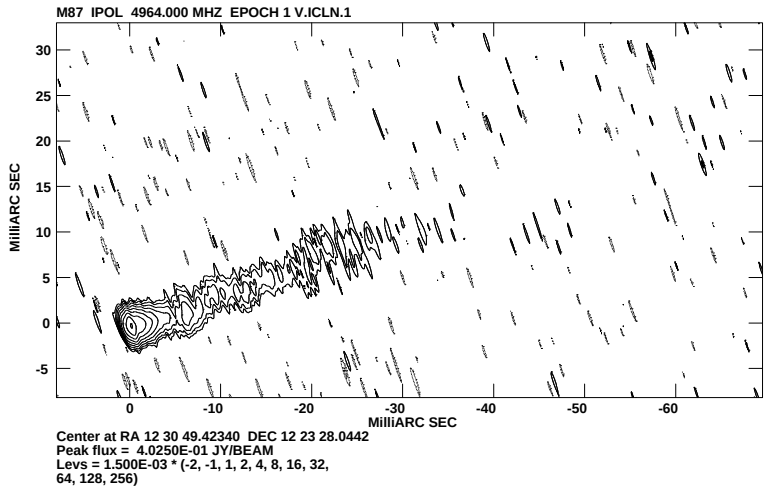


Figure 1: Epoch 1997.97 image of Vir A VLBI core at $\lambda 6$ cm. Noise floor is 0.52 mJy beam$^{-1}$. Beam is 2.03 mas$\times$0.38 mas in PA=+17.1°.

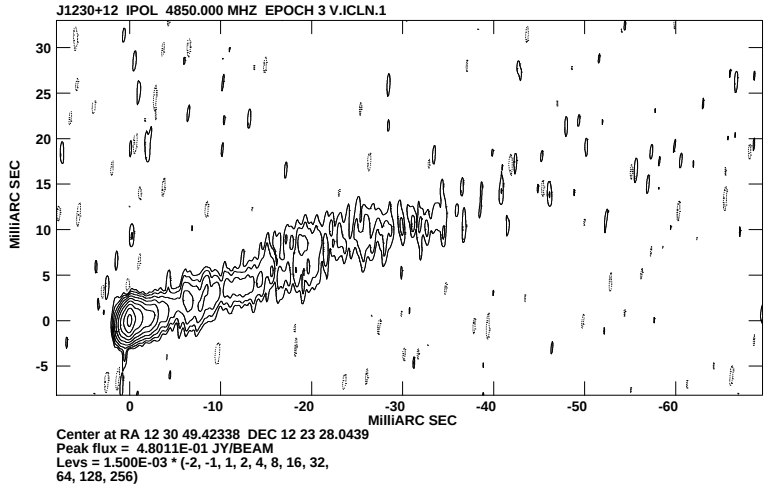


Figure 2: Epoch 1999.32 image of Vir A VLBI core at $\lambda 6$ cm. Noise floor is 0.56 mJy beam$^{-1}$. Beam is 2.33 mas$\times$0.51 mas in PA=−2.1°.

core appears to move laterally, but other observations with higher transverse resolution reveal this to be a blending of two bright components on either side of the jet's axis. These components have flared sequentially in brightness thus giving rise to an apparent motion of $\approx 0.24\,c$. Uniformly- and naturally-tapered images made from these data show that the jet is clearly limb-brightened on scales larger than $\approx 20$ mas. Other VLBI images at a variety of resolutions (Junor, Biretta & Livio, 1999; Junor & Biretta, 1995; Biretta & Junor, 1995; Junor et al. $\lambda 4$ cm images, in preparation) also show limb-brightened structures. This suggests that the emission from the jet is related to slowly-moving surface phenomena though this is hard to reconcile with the need for relativistic speeds for the jet and counter-jet (Sparks et al. 1992). Further support for larger synchrotron emissivity from the surface of the jet rather than from throughout the jet comes from recent VLBA polarimetry results (Junor, Biretta & Wardle, in preparation) which show that the **B** field lies along the jet edges and that the field is smaller on the jet's axis.

**Acknowledgements.** We gratefully acknowledge the VSOP Project, which is led by the Japanese Institute of Space and Astronautical Science in cooperation with many organizations and radio telescopes around the world. WJ thanks the National Science Foundation and JPL for support.

## References

Biretta, J.A. and Junor, W. 1995, *Proc.Nat.Acad.Sci. USA*, **92**, 11364

Biretta, J.A., Zhou, F. & Owen, F.N. 1995, *ApJ*, **447**, 582

Biretta, J.A., Sparks, W.B. & Macchetto, F. 1999, *ApJ*, **520**, 621

Curtis, H.D. 1918, *Publ. Lick Obs.*, **13**, 55

Harms, R.J., Ford, H.C., Tsvetanov, Z.I., *et al.* 1994, *ApJ*, **435**, 35

Junor, W. and Biretta, J.A. 1995, *AJ*, **109**, 500

Junor, W., Biretta, J.A, & Livio, M. 1999, *Nature*, **401**, 891

Livio, M. 1999, *Physics Reports*, **311**, 225

Macchetto, F.D., Marconi, A., Axon, D.J., *et al.* 1997, *ApJ*, **489**, 579

Reid, M.J., Biretta, J.A., Junor, W., *et al.* 1989, *ApJ*, **336**, 112

Sparks, W.B., Fraix-Burnet, D., Macchetto, F. *et al.* 1992, *Nature*, **355**, 804

*Astrophysical Phenomena Revealed by Space VLBI*
*H. Hirabayashi, P.G. Edwards and D.W. Murphy (eds.)*

# Space-VLBI Observations of the Core-Jet in the Nearby Spiral Galaxy M81

Norbert Bartel & Michael F. Bietenholz

*York University, Toronto M3J 1P3, Canada*

**Abstract**

M81 hosts the closest active galactic nucleus that can be imaged with VSOP. With a linear resolution of about 2,000 AU at 5 GHz the image shows the highest detail of any map of the core-jet yet. The jet can be traced over 3.5 mas or 12,000 AU and appears wavy with its orientation changing between about 60° and 70° reminiscent of a helical structure. On average the core-jet points towards the relatively weak lobe-like structure seen on kiloparsec scales and is approximately oriented along the rotation axis of the galaxy. The core-jet has structural similarities to the powerful AGN of radio galaxies and quasars and physical similarities to Sgr A*, and may therefore shed light on the structure and nature of the central source of our own Galaxy.

The nearby galaxy M81 is a grand-design spiral that resembles our own Galaxy in type, size, and mass (Figure 1). Like our Galaxy, it contains a nuclear radio source (see Kellermann et al. 1976 for first detection) that is most likely associated with a supermassive black hole in the gravitational center of the galaxy. But while the nucleus of our Galaxy, Sgr A*, is largely hidden behind scattering clouds of gas, M81's nucleus is virtually unaffected by scatter broadening at most radio frequencies. M81 is also, at a distance of 3.65 Mpc (Freedman et al. 1994) the nearest spiral galaxy with an active galactic nucleus (AGN) and, with the radio galaxy Cen A, the nearest galaxy with an AGN altogether. Its center consists of a stationary core with a short, one-sided, jittery jet (Bietenholz et al. 2000) towards the north-east.

The VSOP observations were made with a ground array of 12 telescopes at 5 GHz on 1 May 1999. Left circular. pol. (IEEE convention) was recorded with a bit rate of 128 Mb/s. The total flux density of the central source in M81 (M81*) was $158 \pm 8$ mJy. About 40% of all scans on baselines between HALCA and any of the ground array telescopes resulted in detections. The $(u, v)$ coverage for the data with detections of M81* is given in Figure 2 (left part). The data were correlated with the processor in Socorro, NM, U.S.A. and further reduced with AIPS.

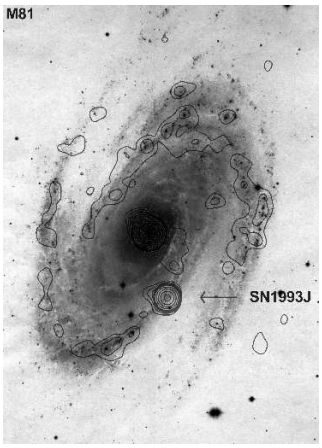


Figure 1: The galaxy M81 at 5.0 GHz observed with the VLA in the D array at 1997.87 superimposed on an optical image (Sandage, The Hubble Atlas of Galaxies, 1961). The radio contour levels are at 0.14, 0.3, 0.5, 0.7, 1, 2, 4, 8, 15, 20, 40, and 80 mJy/beam. The nucleus is the brightest source in M81 at 120 mJy/beam. The second brightest source is supernova 1993J. The width of the image is 13 arcmin on the sky. North is up and east to the left.

The following figures show three images of M81*, made with data from three different array configurations. In Figure 2 (right part) we show the image made with ground array data only. In Figure 3 we show images made with data from HALCA baselines only (left) and with the complete, VSOP, data set (right). The first image shows a rather compact source, elongated along the north-west south-east axis. Details become visible in the next two images obtained with HALCA. The image with data from HALCA baselines only shows that the source is more complex. Full details become apparent in the last image, from all the data. It appears now that the structure is wavy, changing its orientation over 3.5 mas from about 70° for the dominant component to about 60° and back to 70° for the structure further to the north-west.

The wavy structure in the image is a new feature never before seen in M81*. It is further supported if one considers ground array VLBI observations of the source at 8.4 GHz. From previous M81* work (Ebbers et al. 1998) we know that the higher frequency emission emanates predominantly at locations a bit south-west of the peak emission at 5 GHz. From astrometric work by Bietenholz et al. (2000) it follows then that

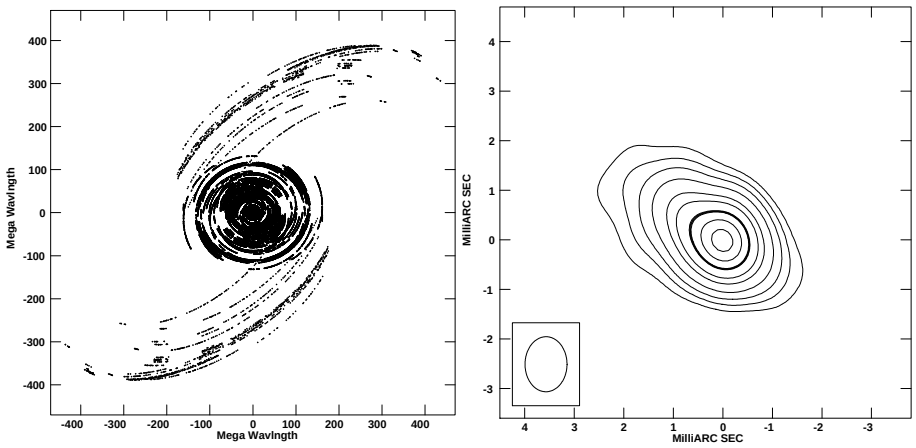


Figure 2: Left part: the $(u, v)$ coverage for the VSOP observations for scans with detections only. The "wings" refer to baselines with HALCA. The ground array telescopes were the Effelsberg 100 m, Germany, the 130m (equivalent) phased VLA, near Socorro, NM, the Green Bank 43 m, WV, and nine 25 m VLBA antennas, all NRAO, U.S.A. Right part: image from ground array data only. The convolving beam here and hereafter is plotted in the lower left corner. The contours are at $-1$, 1, 2.5, 5, 10, 20, 30, **50**, 70, 90% of the peak brightness of 75 mJy/beam.

the stationary core is approximately located at the lower south-west contours. The dominant component at 8.4 GHz is expected to have a p.a. of 55–60°, in contrast to the 70° p.a. of the dominant component at 5 GHz. It is therefore conceivable that the wavy structure starts close to the stationary core with a p.a. of about 55–60° and oscillates in its orientation along the jet with a period of about 2 mas or 7,000 AU. A wavy structure may indeed be expected for a jet emanating from the vicinity of an accretion disk and a black hole. The magnetic field lines are expected to be warped due to the rotation of the central system, and charged particles travelling along the helical lines may give rise to radio structure that appears wavy in projection.

In terms of the length of the jet and its luminosity, M81* appears to be a scaled-down version of the core of radio galaxies and quasars — but probably a scaled-up version of the nucleus of our own Galaxy, Sgr A*. M81*'s radio spectrum is strikingly similar to that of Sgr A*, save for the higher turn-over frequency of the latter indicating that Sgr A* is a more compact source (Reuter & Lesch 1996). However M81*'s

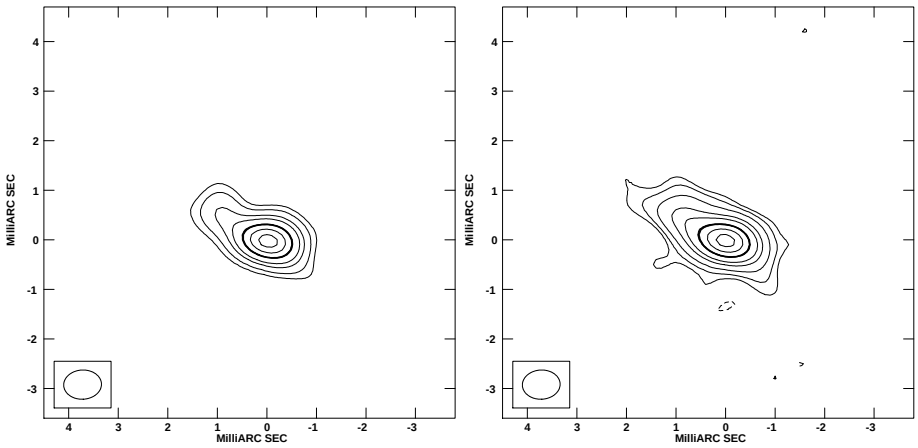


Figure 3: Left: image from data from baselines with HALCA only. Right: image from the full VSOP data set. The same beam was used for better comparison. The contours are at $-5$, 5, 10, 20, 30, **50**, 70, 90% of the peak brightness of 75 mJy/beam and at $-2.5$, 2.5, 5, ... % of the peak brightness of 70 mJy/beam for the two maps, respectively.

luminosity is four orders of magnitude higher than that of Sgr A*, and the jet is at least two orders of magnitude longer than any that may exist in Sgr A* (Lo et al. 1998; Krichbaum et al. 1998).

We gratefully acknowledge support provided through the VSOP Project.

## References

Bietenholz, M.F., Bartel, N. & Rupen, M.P. 2000, *ApJ*, in press

Ebbers, A., Bartel, N., Bietenholz, M.F., Rupen, M.P. & Beasley, A.J. 1998 in *ASP Conf. Ser.* **144***: IAU Coll. 164* , eds. J.A. Zensus, G.B. Taylor & J.M. Wrobel (San Francisco: A. S. P.), 203

Freedman, W.L. et al. 1994 *ApJ*, **427**, 628

Kellermann, K.I., Shaffer, D.B., Pauliny-Toth, I.I.K., Preuss, E. & Witzel, A. 1976 *ApJ*, **210**, L121

Krichbaum, T.P. et al. 1998, *A&A*, **335**, L106

Lo, K.Y., Shen, Z.-Q., Zhao, J.-H. & Ho, P.T.P. 1998, *ApJ*, **508**, L61

Reuter, H.-P. & Lesch, H. 1996, *A&A*, **310**, L5

*Astrophysical Phenomena Revealed by Space VLBI*
*H. Hirabayashi, P.G. Edwards and D.W. Murphy (eds.)*

# A Sharper View into the Parsec-Scale Jet of 3C 345

J. Klare, J.A. Zensus, E. Ros & A.P. Lobanov

*Max-Planck-Institut für Radioastronomie, Bonn, Germany*

**Abstract**

We present images from VSOP observations of 3C 345 at 6 cm, for two epochs separated by 1 year. In the VSOP images, the inner jet of 3C 345 is resolved into several components, which cannot be disentangled from each other in the ground VLBI images. The components show superluminal motions, with different trajectories and large variations in the flux densities. These observations help us to obtain better constrains for the models of 3C 345.

## 1 Introduction

The quasar 3C 345 ($16^{\rm m}$, z=0.595) is an archetypical source for studies at superluminal motions. Several partially resolved enhanced emission regions (components) are observed in the jet, after being ejected from the core at apparent speeds of $2c$–$20c$ along strongly bent trajectories (e.g. Zensus et al. 1995). This may be caused by a periodic process driven by Kelvin-Helmholtz instabilities (Hardee, 1987, Steffen et al., 1995, Qian et al., 1996) or a binary black hole system (Lobanov 1996). The ejection angles of the components vary, and the component trajectories differ significantly. The curvature of the component trajectories increases near the core, while the trajectories appear to straighten farther away from the core. This makes the innermost region a better indicator of the jet kinematics. It is therefore important to investigate the behaviour of the jet components at a very early stage of their evolution in order to constrain the kinematics of the jet components. This makes 3C 345 a prime candidate for high-resolution imaging with VSOP.

## 2 Observations and Imaging

We present here images from two out of 8 observations made for our VSOP monitoring program of 3C 345 (see Table 1). The observations presented here were made at 6 cm in 1998.57 and 1999.50. 3C 345 was

observed for 14 h and 10 h, respectively. The data were processed at the NRAO[1] VLBA correlator in Socorro, New Mexico, USA. Calibration and fringe-fitting were done in AIPS, and imaging was performed using Difmap. Model fitting by elliptical Gaussian components was applied to quantify the flux densities and positions of the jet components.

Table 1: VSOP monitoring program of 3C 345

| Epoch | $\lambda$ (cm) | Pol. | Array |
|---|---|---|---|
| 1998.22 | 6 | No | HALCA, VLBA, EB, Y |
| 1998.22 | 18 | No | HALCA, VLBA, GO, Y |
| **1998.57** | **6** | **No** | **HALCA, VLBA, EB, Y** |
| 1998.66 | 18 | Yes | HALCA, VLBA, EB, Y |
| **1999.50** | **6** | **Yes** | **HALCA, VLBA, EB** |
| 1999.50 | 18 | Yes | HALCA, VLBA, EB, GO, RO |
| 1999.69 | 6 | Yes | HALCA, VLBA, Y |
| 1999.69 | 18 | Yes | HALCA, VLBA, GO |

EB: Effelsberg, Y: phased VLA, GO: Goldstone, RO: Robledo

## 3 Evolution of the Jet Components

The baselines to HALCA are about 3 times larger than the longest ground baselines, leading to a likewise improvement in image resolution. At $\lambda = 6$ cm, the interferometric beam including the space baselines in east-west direction is $\sim 0.34$ mas (1st epoch) and $\sim 0.37$ mas (2nd epoch) while the ground array yields only $\sim 1$ mas resolution. With this improved image resolution, we are able to identify the synchrotron self-absorbed core and three inner jet components (C9, C8 and C7) to the west (Figure 1, left). In the ground-array image the core and these components appear blended into a single one.

To compare both epochs, we have restored both images with a circular beam of 0.4 mas, and we have also modelled the visibilities with Gaussian components. The big change of the inner few parsecs within one year is evident (Figure 1, right). The flux of the core has more than doubled (from 0.8 Jy to 1.8 Jy), while its shape became slightly elongated in east-west direction in 1999.50. At this epoch, the single-dish flux density at 6 cm has also increased (UMRAO) which, according to the

[1]The National Radio Astronomy Observatory (NRAO) is operated by Associated Universities, Inc., under cooperative agreement with the National Science Foundation.

flare model of Lobanov & Zensus (1999), is a reliable hint that a new jet feature (C10) has been recently emitted from the central region. Our later VSOP observations should help to identify the expected new jet feature.

The components C9 and C8 appear almost merged into one single component. However, a detailed analysis shows that the distance between C9 and C8 became smaller — only about 0.11 mas. The bigger effect is the change of the flux density. The flux of C9 increased from 2.6 Jy to 3.0 Jy, while the flux of C8 dropped from 2.4 Jy to only 1.3 Jy. With a component distance of 0.55 mas and a beam size of 0.37 mas, the big flux difference between C9 and C8 causes the apparent dominance of the brighter feature over the fainter. C8 has an angular speed of only 0.18 mas/yr, which corresponds to an apparent speed of $3.6\,h^{-1}c$ (for a flat universe cosmology, with $H_0 = 100h\,\mathrm{km\,s^{-1}Mpc^{-1}}$). The trajectories of C9 and C7 show faster proper motions, of 0.3 mas/yr ($5.8\,h^{-1}c$) and 0.28 mas/yr ($5.5\,h^{-1}c$). Also, the proper motion of C7 along 1996 was 0.35 mas/yr $\widehat{=}$ $6.8\,h^{-1}c$ (Ros et al. 2000), at the same core distances as C8. The observed relative weakness of C8 may arise from its lower observed speed. A detailed analysis of the kinematics and the component evolution will be presented in Klare et al. (in preparation).

## 4 Conclusions and Future Work

The VSOP observations provide a good opportunity for high resolution imaging and allow us to trace the components in the vicinity of radio source cores better than ground VLBI. We have successfully imaged 3C 345 at 6 cm with the VSOP. The observations presented here, combined with the other epochs (Table 1, data reduction in progress) and also at the other wavelength (18 cm), and adding polarimetric imaging should help us to constrain the models of 3C 345.

**Acknowledgements.** We gratefully acknowledge the VSOP Project, which is led by the Japanese Institute of Space and Astronautical Science in cooperation with many organizations and radio telescopes around the world. This research has made use of data of the Michigan Radio Astronomy Observatory which is supported by the National Science Foundation and by funds from the University of Michigan.

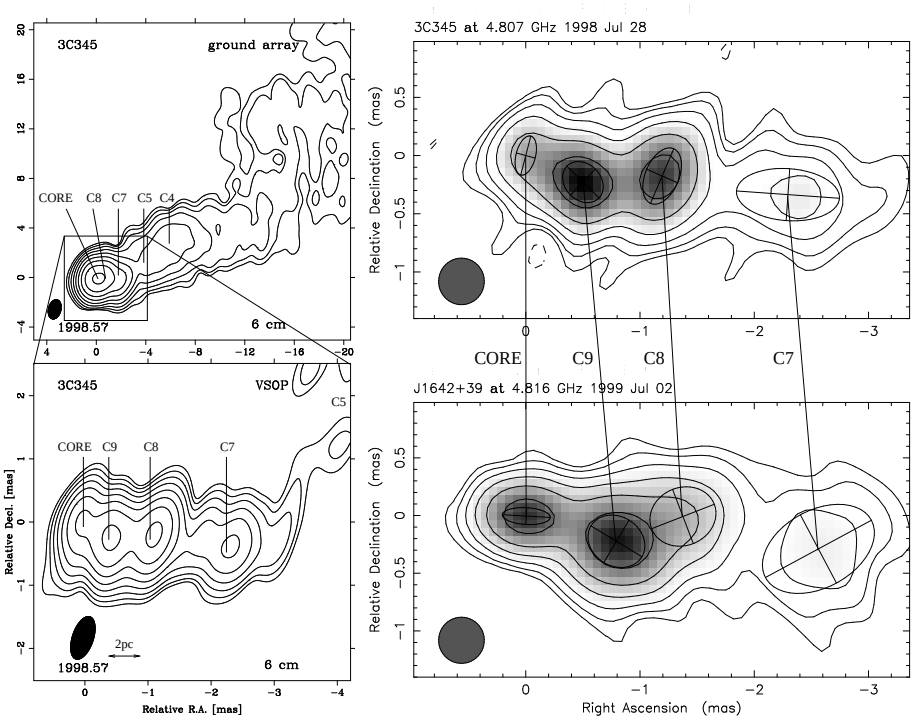


Figure 1: Total intensity flux images of 3C 345 - Left: VSOP resolves the core into several components (see also Colour Figure 1). Right: Evolution of the inner jet components, epochs 1998.57 and 1999.50

## References

Hardee P.E., 1987, *ApJ*, **318**, 78

Klare J., Zensus J.A., Ros E. et al., *A&A*, in preparation

Lobanov A.P., 1996, in *Physics of the Parsec-Scale Structure in the Quasar 3C 345*, (NMIMT, Socorro, USA: Ph.D. thesis)

Lobanov A.P. & Zensus A.P., 1999, *ApJ*, **521**, 509

Qian S.J., Krichbaum T.P., Zensus J.A. et al., 1996, *A&A*, **308**, 395

Ros E., Zensus J.A., Lobanov A.P., 2000, *A&A*, **354**, 55

Steffen W., Zensus J.A., Krichbaum T.P. et al., 1995, *A&A*, **302**, 335

Zensus, J.A., Cohen M.H., Unwin S.C., 1995, *ApJ*, **35**, 433

*Astrophysical Phenomena Revealed by Space VLBI*
*H. Hirabayashi, P.G. Edwards and D.W. Murphy (eds.)*

# 3C279 Results Derived from Two-Frequency VSOP Observations

H. Hirabayashi[1], P.G. Edwards[1], B.G. Piner[2], A.E. Wehrle[2], S.C. Unwin[2], J.E.J. Lovell[3], R. Okayasu[1], T. Kii[1] and F. Makino[4]

[1] *ISAS, Yoshinodai 3-1-1, Sagamihara, Kanagawa 229-8510, Japan*
[2] *JPL/Caltech, 4800 Oak Grove Rd, Pasadena, CA 91109, USA*
[3] *ATNF, PO Box 76, Epping, NSW 1710, Australia*
[4] *NASDA, Sengen 2-1-1, Tsukuba, Ibaraki, Japan*

**Abstract**

A series of VSOP observations of 3C 279 have been made at 1.6 and 5 GHz during the AO1 and AO2 periods. The milli-arcsecond scale structure of 3C 279 is dominated by the core and the jet component C4. The spectral index map obtained from the 1.6 GHz VSOP and 5 GHz ground-only maps shows an inverted spectrum at the core indicating synchrotron self-absorption. Due to the evolution of the VSOP beam, AO2 images show much finer details of parsec-scale components.

## 1 Introduction

The blazar 3C 279 ($z$=0.536) is a prominent EGRET gamma-ray source, displaying significant long-term variability and an episode of short-term flaring (Wehrle et al. 1998). 3C 279 was selected as a VLBI Space Observatory Programme (VSOP) Key Science Project source, and a series of VSOP observations have been made of 3C 279 to study the parsec-scale structure and its evolution, and to search to connections between the gamma-ray activity and the milli-arcsecond scale structure, such as the emergence of new jet components. This paper reviews the AO1 observations and presents first results from AO2 observations.

## 2 AO1 Observations

3C 279 was observed during the AO1 phase of the mission on 1998 January 9 at 1.6 GHz and 1998 January 10 at 5 GHz. The ground telescope arrays were made up of nine elements of the Very Long Baseline Array (VLBA) with the addition of the 70 m telescopes at Goldstone and Tidbinbilla at 1.6 GHz, and the Usuda 64 m at 5 GHz.

### 2.1 Jet Motions and Brightness Temperature

Preliminary images from these datasets are presented in Edwards et al. (1999) and Hirabayashi et al. (2000), with more detailed analysis given in Piner et al. (2000). The 5 GHz VSOP image shows that the parsec-scale radio emission is dominated by a double structure consisting of the compact core and the bright jet component 'C4' located 3 mas from the core at a position angle of $-115°$. In the 1.6 GHz image C4 is brighter than the core indicating synchrotron self-absorption in the core.

A total of six elliptical Gaussian components are required to fit the 5 GHz VSOP data (Piner et al. 2000). The first three of these components are interior to 1 mas, and represent the core and two components of the inner jet. The region interior to 1 mas is a complex region with multiple components and a stationary feature at $\sim$1 mas (Piner et al. these proceedings; Wehrle et al. 2000).

The component C4 has been moving along a position angle of $-115°$ for over 10 years (e.g. Unwin et al. 1989; Lister et al. 1998; Wardle et al. 1998) This position angle differs significantly from that of the kpc-scale emission and previous parsec-scale jet components, which had position angles of approximately $-140°$. The brightness distribution of C4 is asymmetric, with the leading edge being sharper than the trailing material, and the trailing material being located at position angles between $-115°$ and $-140°$ (Piner et al. 2000). The sharp leading edge of C4 is suggestive of a shock front, which is confirmed by polarization observations that show the leading edge of C4 has a magnetic field transverse to the jet (Lister et al. 1998; Wardle et al. 1998).

Our highest brightness temperature lower limit of $\sim 5 \times 10^{12}$ K for component C4 at 1.6 GHz (see Piner et al. 2000) implies a Doppler factor lower limit of 5 for the inverse Compton brightness temperature limit (Kellermann and Pauliny-Toth 1969). This Doppler factor is similar to that inferred from gamma-ray observations (Wehrle et al. 1998).

### 2.2 Spectral Index Map

The spectral index map made by comparing the matched resolution 1.6 GHz VSOP image and 5 GHz VLBA image (Piner et al. 2000) is shown in Color Figure 5 on page xvi of these proceedings. The color bar at the bottom of the image indicates the value of the spectral index ($S \propto \nu^{\alpha}$). Spectral index contours are also plotted at intervals of 0.5, from $-2.5$ to 2.5. The beam is the average of the 1.6 GHz VSOP beam and the 5 GHz VLBA beam: $3.1 \times 1.1$ mas at a position angle of 16°.

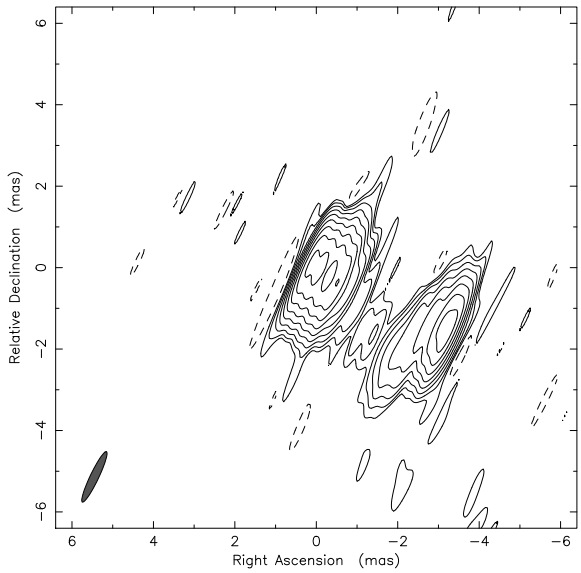


Figure 1: Preliminary image of the first 5 GHz AO2 observation on 15 March 1999. The map peak is 2.6 Jy, with contours of $-1$, 1, 2, 4 ... 256 $\times$ 7.6 mJy/beam. The beam FWHM is 1.4$\times$0.2 mas at a PA of $-26°$.

The core of 3C 279 has an inverted spectrum with steep spectral index gradients. The spectral index in the core region ranges from $\sim 1.0$ at the western edge to the theoretical limiting value for synchrotron self-absorption of 2.5 (assuming a constant magnetic field) over a small region at the eastern edge. The highly inverted spectrum at the eastern edge may imply the detection of a homogeneous compact component in this region, although a varying magnetic field in this region would complicate this interpretation.

The jet component C4 has a flat spectrum with $\alpha$ approximately 0.25. This is unusual, as jet components usually have steeper spectra ($\alpha < 0$), and may be indicative of a stronger shock, which in turn may explain why C4 has remained prominent for longer than previous jet components. The spectral index appears to vary smoothly between the front and trailing portions of C4, which suggests the trailing material may be physically associated with the leading edge and not an apparent connection due to our line of sight. Beyond C4 the spectral index steepens, a sign of a general tendency of energy loss of the emitting particles along the jet.

## 3 AO2 Observations

Due to the precession of HALCA's orbit, the first half of 1999 allowed VSOP observation to be made with a $(u, v)$-coverage offering maximum resolution along the jet. A preliminary image of the first AO2 epoch in March 1999 is shown in Figure 1. The jet components within 1 mas of the core, revealed by model-fitting in the AO1 data, are clearly seen in the AO2 image. Several more 5 GHz observations and another 1.6 GHz observation were made between March and July 1999, which will enable us to study the evolution of 3C 279 from AO1 to AO2 and shorter time-scale variations within AO2. Studying the evolution and motions of new components, changes in the brightness temperature of components and in the shocked edge of C4 are the main aims of these monitoring observations.

**Acknowledgements.** We gratefully acknowledge the VSOP Project, which is led by ISAS in cooperation with many organizations and radio telescopes around the world. The VLBA is operated by the National Radio Astronomy Observatory, a facility of the NSF operated under cooperative agreement by Associated Universities, Inc.

## References

Edwards, P.G., Hirabayashi, H., Lovell, J.E.J. et al. 1999, *Astron. Nachr.*, **320**, 230

Kellermann, K.I. & Pauliny-Toth, I.I.K. 1969, *ApJ*, **155**, L71

Hirabayashi, H., Edwards, P.G., Wehrle, A.E. et al. 2000, *Adv. Sp. Res.*, **26**, 689

Lister, M.L., Marscher, A.P., & Gear, W.K. 1998, *ApJ*, **504**, 702

Piner, B.G., Edwards, P.G., Wehrle, A.E. et al. 2000, *ApJ*, in press

Unwin, S.C., Cohen, M.H., Biretta, J.A., Hodges, M.W., & Zensus, J.A. 1989, *ApJ*, **340**, 117

Wardle, J.F.C., Homan, D.C., Ojha, R. & Roberts, D.H. 1998, *Nature*, **395**, 457

Wehrle, A.E., Pian, E., Urry, C.M. et al. 1998, *ApJ*, **497**, 178

Wehrle, A.E., et al. 2000, in preparation

*Astrophysical Phenomena Revealed by Space VLBI*
*H. Hirabayashi, P.G. Edwards and D.W. Murphy (eds.)*

# MHD Simulations of Jets from Magnetized Accretion Disk

Kazunari Shibata

*Kwasan Observatory, Kyoto University, Yamashina, Kyoto 607-8471, Japan*

In the last 10 years, magnetohydrodynamic (MHD) simulations of jets ejected from magnetized accretion disks, such as that shown in Color Figure 7, have developed significantly through the rapid development of supercomputers:

1. It has been found that the terminal velocity and mass flux of jets in nonsteady MHD models show basically the same scaling laws as those found for steady MHD models (Kudoh and Shibata 1995, 1997; Kudoh et al. 1998).

2. Nevertheless, magnetized accretion disks and jets never reach steady state because of magneto-rotational instability occurring in magnetized accretion disks (Kudoh et al. 1998). Disks are full of flares and bursts, and very energetic jets are intermittently produced in association with them (Hayashi et al. 1996; Kuwabara et al. 2000).

3. 3D simulations of MHD jets from accretion disks have started to be performed, which show that the MHD jet is dynamically stable for the kink instability at least for several Keplerian orbits even if the magnetic field in the jet is highly twisted (Matsumoto and Shibata 1997).

4. Self-consistent general relativistic MHD simulations have been performed for the first time on jets from disks around a black hole, which revealed the formation of shock waves and ejection of jets from near to the hole inside $3r_s$, where $r_s$ is the Schwarzchild radius. At present, the maximum Lorentz factor of jets found in these nonsteady simulations is about 2, though this limit is basically due to difficulty of simulations of high Lorentz factor MHD plasmas (Koide et al. 1998, 1999, 2000).

Although these are remarkable achievements, it is still difficult to construct self-consistent time-dependent MHD models of jets from near to the black hole to the scale of VSOP jets. The reader is referred to Shibata and Kudoh (1999) for a review of recent studies on time-dependent MHD simulations of jets from accretion disks.

## References

Hayashi, M.R., Shibata, K. & Matsumoto, R. 1996, *ApJ*, **468**, L37

Koide, S., Shibata, K. & Kudoh, T. 1998, *ApJ*, **495**, L63

Koide, S., Shibata, K. & Kudoh, T. 1999, *ApJ*, **522**, 727

Koide, S., Meier, D., Kudoh, T. & Shibata, K., 2000, *ApJ*, in press

Kudoh, T. & Shibata, K. 1995, *ApJ*, **452**, L41

Kudoh, T. & Shibata, K. 1997, *ApJ*, **474**, 362

Kudoh, T., Matsumoto, R. & Shibata, K. 1998, *ApJ*, **508**, 186

Kuwabara, T., Shibata, K., Kudoh, T. & Matsumoto, R. 2000, *PASJ*, submitted

Matsumoto, R. & Shibata, K. 1997, in *Proc. Accretion Phenomena and Related Outflows, (IAU Colloq. 163)*, eds. D.T. Wickramasinghe, G.V. Bicknell & L. Ferrario, 443

Shibata, K. & Kudoh, T. 1999, in *Proc. Star Formation 1999*, ed. T. Nakamoto, (Nobeyama Radio Observatory), 263

*Astrophysical Phenomena Revealed by Space VLBI*
*H. Hirabayashi, P.G. Edwards and D.W. Murphy (eds.)*

# Magnetohydrodynamic Production Of Highly Relativistic Jets

D.L. Meier [1] and S. Koide [2]

[1] *Jet Propulsion Laboratory, Pasadena, California, USA*
[2] *Toyama University, Toyama, Japan*

**Abstract**

Recently, several groups around the world have begun to test theories of jet formation using magnetohydrodynamic (MHD) simulations (computer simulations of magnetized gas flow around black holes). While it is now generally accepted that jets, including relativistic ones, are accelerated and collimated by magnetized accretion disks, the Lorentz factors that have been achieved in these simulations still do not approach those suggested by Space VLBI observations. In this paper we discuss some of our recent simulations of MHD jet formation that indicate how highly relativistic outflows might be produced.

## 1 Introduction

Space VLBI studies of individual compact extragalactic radio sources indicate co-moving brightness temperatures of $3 - 5 \times 10^{12} K$ (Shen et al. 2000; Preston et al. 2000) and lower limits on some sources in the VSOP survey up to $10^{13} K$ or higher (Lovell et al. 2000). Assuming $\sim 10^{11} K$ for an intrinsic synchrotron source at rest, these results imply lower limits on the jet Lorentz factor of $8-12$ and 50, respectively, where $\Gamma_{min} \equiv (1 - V_{min}^2/c^2)^{-1/2} = 0.5\, T_{B,co-moving}/T_{B,intrinsic}$.

The leading model for producing and collimating relativistic jets is the magnetohydrodynamic (MHD) acceleration model, (e.g., Shibata 2000). While able to account for jet collimation, relativistic velocity, and magnetic fields, as well as fit in well with the black hole accretion model for active galactic nuclei (AGN), the MHD model has one potential problem. The terminal jet speeds obtained in numerical simulations are only of order the escape velocity at the foot point of the jet. This means that, even when the black hole is spinning rapidly, and the accretion disk inner edge reaches almost to the horizon, it is still very difficult to achieve jet Lorentz factors much above 3 — considerably slower than the speeds indicated by the observations.

In this paper we review some of the relevant properties of numerical simulations of MHD jet acceleration and discuss a physical process called the *magnetic switch* (Meier et al. 1997) which may aid in producing high Lorentz factor flow. That is, if the magnetic field anchored in a rotating Keplerian accretion disk threads a tenuous corona above the disk, then magnetic forces in that corona can significantly exceed gravitational forces, leading to very rapid acceleration and terminal jet speeds that depend on the properties of the rotating field and accelerated plasma, rather than the properties of the gravitational field. High Lorentz factors are potentially achievable in this case.

## 2 Review of Numerical Simulations of Jet Production by Magnetized Accretion Disks

Simulations of jet production by magnetized accretion disks falls into two general categories: a) steady-state and b) time-dependent. While the goal of all MHD acceleration studies is to understand the origin of jets, the immediate purpose of the steady-state simulations is to reproduce the results of the analytic and semi-analytic work — particularly those of Blandford & Payne (1982) — but without the restrictive assumption of self-similarity. The purpose of time-dependent simulations, on the other hand, is to study the initial transient effects associated with jet acceleration. As accretion and jet production are expected to be rather unsteady processes, such simulations provide some additional realism over the steady-state models.

### 2.1 Steady-State Simulations

We will use the results of Krasnopolsky et al. (1999) as an example, but there have been many other papers on the subject recently (e.g., Ustyugova et al. 1995; Ouyed et al. 1997). The cylindrically-symmetric computational region is a rectangular area, bounded on the left by the rotation axis, at the bottom by an accretion disk boundary condition, and at the top and right by "outflow" boundaries (see Figure 1). A poloidal $(R, Z)$ magnetic field is anchored in the differentially-rotating disk and matter is injected from the lower boundary along the field lines at a speed slower than the escape speed. It is important to note that, while the axial field and velocity ($B_Z$ and $V_Z$) and azimuthal velocity ($V_\phi$) are fixed on the lower boundary, the radial components ($B_R$ and $V_R$) and azimuthal field ($B_\phi$) are allowed to change as the solution is

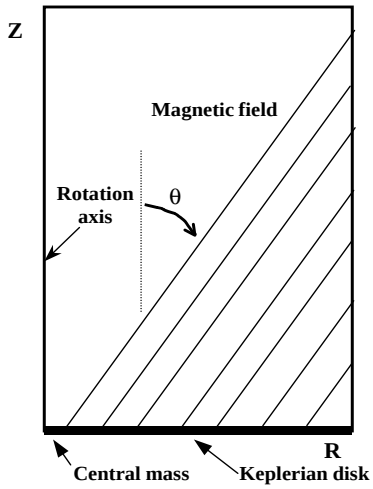


Figure 1: Initial conditions for steady-state simulations. Pseudo-relativistic simulations are similar, but have a hole in the disk center at $R = 6GM/c^2$.

obtained. The curvature and twist of the field lines is determined by the solution, and their slope and azimuthal pitch at the lower disk boundary are adjusted to be consistent with that solution. Note that the disk extends inward *all the way to the rotation axis*, requiring the gravitational potential of the central object to be smoothed at small radii to avoid a singularity. Typical results are shown in Figure 1 of Krasnopolsky et al. (1999), and they are indeed very similar to Blandford & Payne's (1982) semi-analytic results. The field lines must have a polar angle of $\theta > 30^\circ$ in order for magnetically-driven outflow to commence. However, well above the disk the field lines bend toward the axis, resulting in a magnetically-collimated wind or jet. The accelerating flow passes through a series of critical points, eventually reaching a terminal velocity of order the escape speed at the foot of the jet.

## 2.2 Time-Dependent Simulations

### 2.2.1 Fully General Relativistic Jet Production Near Rotating Black Holes

As the central engine is believed to be a rotating black hole, the full jet acceleration problem will involve MHD processes in curved spacetime near the horizon. Koide et al. (1999) have shown that, once a special

relativistic MHD code has been developed, it is fairly straightforward to add the stationary Kerr geometry, allowing such processes to be studied.

Our fully relativistic simulations begin with a rather thick accretion disk, with inner edge at $R = 6\,GM/c^2 \equiv 6\,r_g$, threaded by a weak axial magnetic field (internal Alfven velocity of $V_A = 0.01c$). In addition to the disk, a freely-falling halo fills the remainder of the computational grid, which extends from $2.2\,r_g$ to $40\,r_g$ in spherical radius and from 0 to $\pi/2$ in polar angle. Five different scenarios were simulated in a series of papers: 1) non-rotating Schwarzschild black hole with a non-rotating (ADAF-like) disk; 2) non-rotating black hole with a rotating Keplerian disk; 3) rotating Kerr black hole with angular momentum parameter $j \equiv J/(GM^2/c) = 0.95$ and non-rotating disk; 4) rotating black hole with two kinds of Keplerian disk: co-rotating with the black hole and counter-rotating against the black hole's rotation. The simulations are followed for a fairly short period of time — on the order of $\sim 100\tau_g \equiv 100\,GM/c^3$.

In all cases except the co-rotating, Keplerian/Kerr case, the simulation reached the point when a significant portion of the disk had accreted into the hole, allowing the rotation of the disk or geometry and MHD processes to run their course. In the latter case, because co-rotating orbits at $6r_g$ are stable, and the field weak, the simulation evolved on a secular time scale and could not be run to completion because of cost and numerical problems. Work on this case is continuing.

As expected, in the Schwarzschild cases no significant MHD-driven outflow develops unless the disk is rotating; and the outflow velocity is of order the escape velocity from the last stable orbit of $6r_g$ ($0.4c$).

In the Kerr cases, however, a powerful jet results *even when the disk is not rotating*. The main driver is the rotating geometry itself, rather than the rotation of the accretion disk. The disk falls rapidly into the ergospheric region ($R < 2r_g$), where the accreting matter must rotate with the black hole geometry. This rotation drives an MHD jet in a manner similar to the non-relativistic rotating disk simulations (see Shibata 2000). This process is closely-related to those discussed by Blandford & Znajek (1977), Punsly & Coroniti (1990), and Meier (1999). Our analysis shows that angular momentum, but not energy, is extracted from the hole. That is, while jet acceleration spins down the hole, more mass is gained by accretion itself than is expelled in jet energy. The highest jet speeds achieved so far in these simulations are of order the escape velocity from deep within the ergosphere ($\Gamma < 3$).

The counter-rotating disk case (Koide et al. 2000) behaves in a similar manner, since retrograde orbits are *unstable* at $R = 6r_g$. As the disk plunges rapidly into the ergosphere, the frame dragging actually reverses its spin, and a black-hole-rotation-driven MHD jet again ensues.

### 2.2.2 Pseudo-Relativistic Simulations of Black Hole Accretion Systems

While understanding the fully relativistic problem is the goal, the simulations described in the previous subsection have a few numerical drawbacks. Because the disk has a finite thickness, and because the simulations can handle only a modest density contrast across the grid, it is not possible to study the behavior of very tenuous coronae. Furthermore, because fully relativistic simulations must solve a nonlinear algebraic equation for the Lorentz factor in each cell at each time step, there is a possibility that one of these millions of solutions will diverge, bringing the entire simulation to a halt. This is a significant problem as the magnetic field becomes more dominant and the Lorentz factor higher.

To study the strong field situation in very tenuous coronae, and to follow the evolution to many thousands of $\tau_g$, we have employed the simpler non-relativistic simulations — with an infinitely thin disk boundary condition — and interpreted them in a relativistic manner (Lind et al. 1994; Meier et al. 1997; Meier et al. 2000). That is, as long as the inertia of the magnetic field and internal energy are small ($c_{sound} < c$; $V_A < c$), the non-relativistic MHD equations have the same form as the relativistic ones if the velocity $V$ is replaced with the proper velocity $U \equiv \Gamma V$. When $U$ exceeds $c$ (unity here), it can be identified with the Lorentz factor $\Gamma$. Thus, these pseudo-relativistic simulations account for the inertia of the kinetic energy, which will be important even for a cold gas.

The initial conditions for these simulations are very similar to those of the steady state ones in Figure 1, except that the disk is truncated interior to the last stable orbit, and $B_R$, $V_R$, and $B_\phi$ are all *fixed* on the lower boundary, as would be the case in an actual accretion disk. These conditions result in a new magnetic field structure during the simulation (Figure 2). The anchored field lines at the inner edge of the disk are bent inward, creating a substantial $B_R$ in the corona, which is then wound up by the differential rotation into $B_\phi$, expelling plasma upward and pinching it into a collimated jet. One such simulation is shown at late times (a time in gravitational units, $\tau_g = GM/c^3$, of 700)

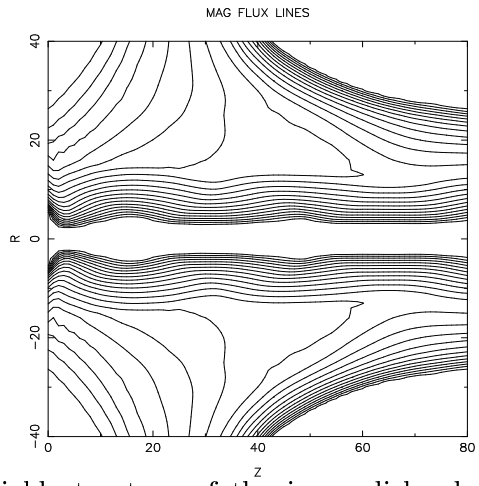


Figure 2: Field structure of the inner disk edge. Image is rotated 90°clockwise from Figure 1 and includes both negative and positive $R$ regions. The black hole is at the origin and length units are in $r_g$.

in Color Figure 2. It bears a striking resemblance, in both morphology and magnetic field structure, to the observations of Moellenbrock et al. (2000). This highly-collimated inner jet appears to compete with the outer, loosely-collimated wind found in the steady state simulations: in the $\sim 80$ simulations we have run, we see either the inner jet or wind, but rarely both at the same time.

### 2.2.3 The Magnetic Switch

Because the field is anchored on the boundary, and because we have control over the density of the injected material, the pseudo-relativistic simulations can study the case where the field dominates the dynamics in a very tenuous corona. We have found that an important transition in the character of the outflow occurs when the MHD power input $L_{MHD} \equiv B^2_{corona} R^4_{corona} \Omega^2/4c$ (where $R_{corona}$ is the size of the coronal region ejecting the jet and $\Omega$ its angular velocity) exceeds a critical value $L_{crit} \equiv E_{escape}/\tau_{free-fall} = 4\pi\rho_{corona} R^2_{corona} (GM/R_{corona})^{3/2}$ (Meier et al. 1997; Meier 1999). $L_{crit}$ can be considered to be the MHD equivalent of the Eddington limit: for $L_{MHD} < L_{crit}$, gravity dominates, whereas magnetic forces dominate above the critical value. For $L_{MHD} > L_{crit}$, the jet is initially unbound an accelerates rapidly to a terminal velocity that depends only on the properties of the injected matter and rotating

magnetic field ($\Gamma_{jet} = L_{MHD}/\dot{M}c^2$), not on the escape velocity from the black hole region. As a result, high Lorentz factors are possible when the mass loss rate $\dot{M}$ is low and the MHD power high. This appears to occur both in the case of the inner jet and the outer MHD wind. So far, our simulations have achieved Lorentz factors of $\Gamma_{jet} = 10 - 20$ and could potentially go much higher when we begin to take the magnetic inertia into account and explore the very large field regime.

To summarize, we find that the fastest and most powerful jets are produced when the central black hole rotates rapidly, the accreting material falls rapidly into the ergosphere, and the material accelerated in the jet is of very low density.

## 3 Discussion

These results suggest two possible scenarios for MHD production of highly relativistic jets in AGN. Both involve low density, advection-dominated flows (ADAFs). In the first case the entire disk is an ADAF, rapidly plunging into the ergosphere, and the jet is produced very near the black hole. Most of the outflow is at the escape velocity ($\Gamma < 3$), but high Lorentz factors can be achieved in very low density, magnetically-dominated "coronal holes". In the second scenario, the magnetic field is anchored in a thin, dense Keplerian disk, and only the corona is advection-dominated. Either an inner jet or outer wind is possible in this case. Again much of the outflow is at the local escape velocity, but high Lorentz factor flow can occur in very low density coronal holes.

The outer relativistic wind is a tempting model for M87, because the observations indicate a large opening angle in the jet collimation region (see Junor et al. 2000). However, such a structure also can be obtained, even in the inner jet case, if that jet is accelerated from a satellite black hole orbiting around the large $3 \times 10^9 M_\odot$ hole rather than from a large accretion disk around the central hole. As the period of such an orbiting satellite is $\sim 10$ years, if this model is viable, we should see variations in the 43 GHz structure of the M87 core over the next few years.

## 4 Conclusions

Magnetically-driven outflow from accretion disks around black holes appears to have two main components: a slowly-collimating wind from the disk surface and a highly-collimated jet from the disk inner edge.

Both types of outflow are subject to magnetic switching, with a critical MHD power analogous to the Eddington limit for radiative acceleration. When $L_{MHD} < L_{crit}$, gravity is important and $V_{jet} \sim V_{escape}$ ($\Gamma < 3$). When $L_{MHD} > L_{crit}$, gravity is unimportant and $\Gamma_{jet} \sim L_{MHD}/\dot{M}c^2$, allowing high Lorentz factors if the MHD power is high and mass loss is low. When the black hole rotates, the jet is accelerated from the frame-dragged matter inside the ergosphere. The strongest and fastest jets occur when the material plunges rapidly into the ergosphere, as in the case of an ADAF or when the disk counter-rotates with respect to the hole's rotation.

**Acknowledgements.** We gratefully acknowledge the VSOP Project, which is led by the Japanese Institute of Space and Astronautical Science in cooperation with many organizations and radio telescopes around the world. Part of this research was carried out at the Jet Propulsion Laboratory, California Institute of Technology, under contract to the National Aeronautics and Space Administration.

## References

Blandford, R. & Payne, D. 1982, *MNRAS*, **199**, 883

Blandford, R. & Znajek, R. 1977, *MNRAS*, **179**, 433

Junor, W. et al. 2000, *these Proceedings*

Koide, S., Shibata, K., & Kudoh, T. 1999, *ApJ*, **522**, 727

Koide, S., Meier, D., Shibata, K., & Kudoh, T. 2000, *ApJ*, in press

Krasnopolsky, et al. 1999, *ApJ*, **526**, 631

Lind, K., Meier, D., & Payne, D. 1994, *B.A.A.S.*, **184**

Lovell, J. et al. 2000, *these Proceedings*

Meier, D. et al. 1997, *Nature*, **388**, 350

Meier, D. 1999, *ApJ*, **482**, 753

Meier, D. et al. 2000, in preparation

Moellenbrock, G. et al. 2000, *these Proceedings*

Ouyed, R. & Pudritz, R. 1997, *ApJ*, **482**, 712

Preston, R.A. et al. 2000, *these Proceedings*

Punsly, B. & Coroniti, F. 1990, *ApJ*, **354**, 583

Shen, Z.-Q. et al. 2000, *these Proceedings*

Shibata, K. 2000, *these Proceedings*

Ustyugova, G. et al. 1995, *ApJ*, **439**, L39

*Astrophysical Phenomena Revealed by Space VLBI*
*H. Hirabayashi, P.G. Edwards and D.W. Murphy (eds.)*

# High-Frequency Observations of Blazars

A.P. Marscher[1], S.G. Marchenko-Jorstad[1,2], J.R. Mattox[1], A.E. Wehrle[3] & M.F. Aller[4]

[1] *Institute for Astrophysical Research, Boston University, 725 Commonwealth Ave., Boston, MA 02215, USA*
[2] *Astronomical Institute, St. Petersburg State University, Bibliotechnaya Pl. 2, Petrodvorets, St. Petersburg 198904, Russia*
[3] *Jet Propulsion Laboratory, 4800 Oak Grove Dr., Pasadena, CA 91109, USA*
[4] *Astronomy Department, 817 Dennison Bldg., University of Michigan, Ann Arbor, MI 48109-1090, USA*

**Abstract**

We report on the results of high-frequency VLBA observations of 42 $\gamma$-ray bright blazars monitored at 22 and 43 GHz between 1993.9 and 1997.6. In 1997 the observations included polarization-sensitive imaging. The cores of $\gamma$-ray blazars are only weakly polarized, with EVPAs (electric-vector position angles) usually within 40° of the local direction of the jet. The EVPAs of the jet components are usually within 20° of the local jet direction. The apparent speeds of the $\gamma$-ray bright blazars are considerably faster than in the general population of bright compact radio sources. Two X-ray flares (observed with RXTE) of the quasar PKS 1510−089 appear to be related to radio flares, but with the radio leading the X-ray variations by about 2 weeks. This can be explained either by synchrotron self-Compton emission in a component whose variations are limited by light travel time or by the Mirror Compton model.

## 1 Introduction

The operation of the VLBA has enabled us to make high dynamic-range, fine-resolution images of strong compact radio sources at frequencies of 22 and 43 GHz. This allows significant advancements in our exploration of the regions in the jets of blazars closer to the central engine than has heretofore been possible.

In order to explore the properties of the jets of $\gamma$-ray bright blazars at the highest possible resolution, the first four authors monitored 42 EGRET-detected blazars with the VLBA, mostly at 22 and 43 GHz.

Starting in 1997, near the end of the project, observations were carried out in dual-polarization mode so that polarized intensity images could be made. Here we describe the salient results obtained thus far from this study.

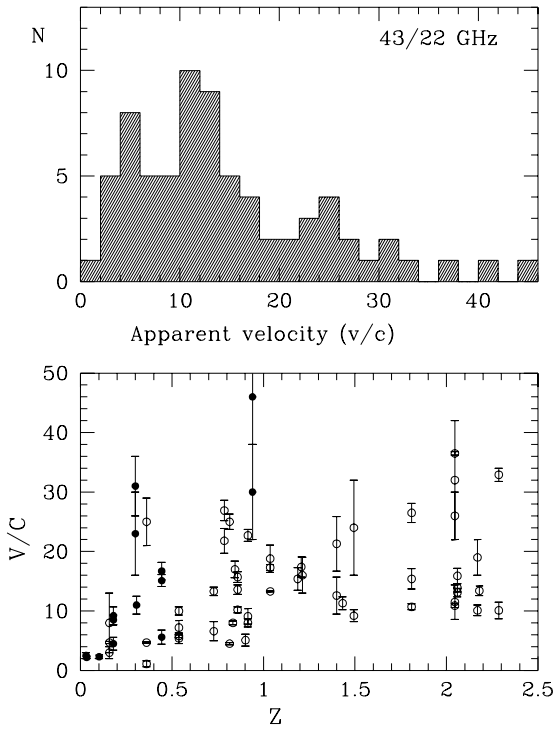


Figure 1: *Top panel:* Histogram of apparent velocities of jet components with proper motions detected (72 components in 33 sources). *Bottom panel:* Correlation plot of apparent velocities vs. redshift. BL Lac objects are denoted by filled circles, quasars by open circles.

In addition, starting in December 1996, three of us (APM, SGM-J, and MFA) began a campaign of weekly X-ray monitoring of the rapidly variable quasar PKS 1510−089 with the *Rossi* X-ray Timing Explorer (*RXTE*) to accompany the regular monitoring of the radio emission at 14.5, 8.0, and 4.8 GHz at the University of Michigan Radio Astronomy Observatory (UMRAO). The purpose is to determine whether the X-ray and radio variations are related in this object, which in the past has shown no significant time lags across radio frequencies (Tornikoski et al. 1994). We discuss preliminary results from this ongoing project below.

## 2 Results of the $\gamma$-Ray Blazar Monitoring Program

In the jets of the $\gamma$-ray blazar sample, we have found 26 stationary components in 20 sources and 72 moving components in 33 sources. Standing features are therefore quite common close to the core. The apparent velocity distribution of the moving components is given in Figure 1. The apparent speeds range from sub-$c$ (Mkn 421) to $> 40c$ (0235+164) for $H_0 = 65\,\mathrm{km\,s^{-1}\,Mpc^{-1}}$, $q_0 = 0.1$. The peak of the apparent velocity distribution is at $11c$, but there is a long high-velocity tail to the distribution: 13 of the sources (18 components) show motions at speeds exceeding $20c$. The distribution of apparent velocities of the general population of bright, flat-spectrum radio sources is quite different (Pearson et al. 1998), heavily weighted toward low speeds.

In general, for blazars in which more than one superluminal component is detected, the apparent velocities are not the same. For example, in PKS 0528+134 the speeds range from 4 to $13c$. If the separation from the core is deprojected in a crude fashion (e.g., by assuming that the fastest component is moving at the optimal angle for superluminal motion — the result does not depend strongly on the details of the deprojection scheme), there is a positive correlation of apparent speed with linear distance from the core for the sample.

Many of the jets of the $\gamma$-ray blazars are strongly bent. Examples are shown in Figure 2. Furthermore, a number of the jets of $\gamma$-ray blazars are quite broad within a few mas of the core, which suggests that they are being viewed nearly end-on.

The high apparent velocities, correlation of apparent velocity with distance from the core, strong apparent bending, and broad features in the jet, are all expected for a sample that is biased toward objects with relativistic jets that lie very close to the line of sight near the core. In such cases, the Doppler boosting of the high-energy emission will be maximal and the projection effects will be amplified compared with jets that, for example, lie at angles that maximize the proper motions. Seen in projection, jets pointing nearly at us appear broader and more strongly bent than do jets that lie at larger angles to the line of sight. Furthermore, the proper motion is less than its maximum value for such jets. If the jet bends, it will almost always bend away from the line of sight, since there is a very limited range in direction in which it could be to point even closer to the line of sight. Components farther down the jet will then have higher proper motions.

The polarized intensity images shown in Figure 2 are representative

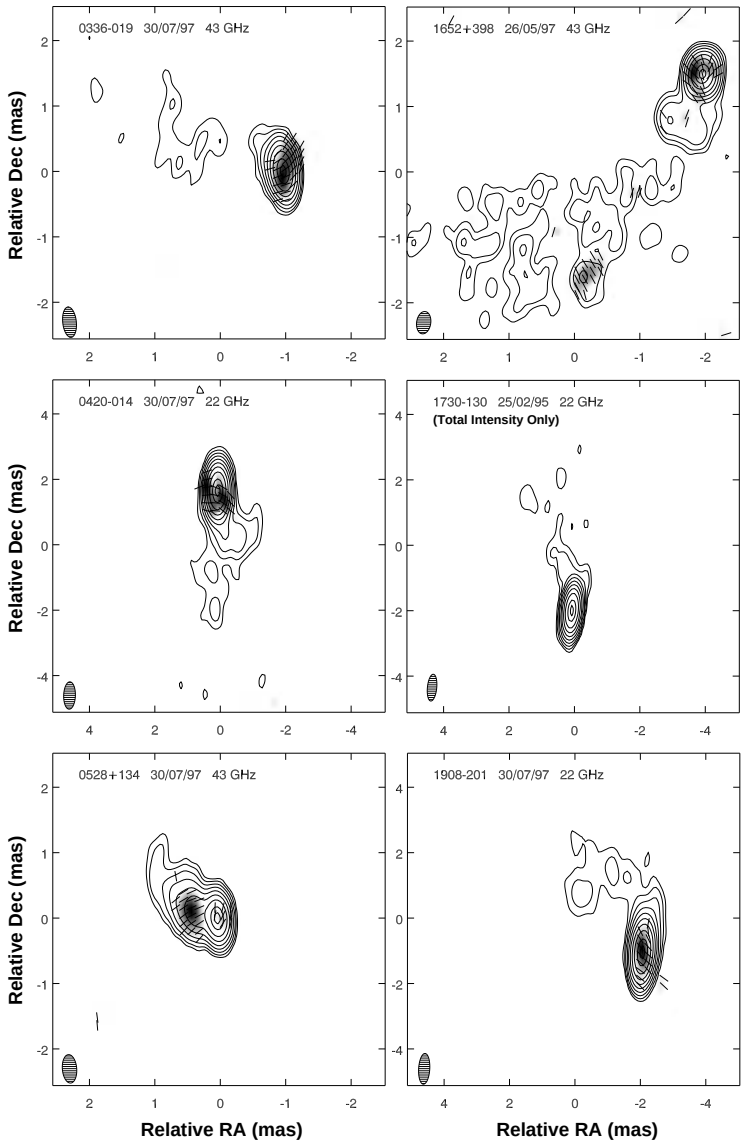


Figure 2: VLBA images of 6 blazars with strongly bent jets. The contours correspond to factors of 2 in total intensity, with the highest at 64%. The gray-scale shows polarized intensity, while the lines indicate the direction of the electric vectors. The maximum total intensities in Jy beam$^{-1}$ (fractional polarizations of the cores) are: 0336−019: 1.73 (1.9%); 0420−014: 3.00 (0.5%); 0528+134: 1.74 (0.7%); 1652+398 (Mkn 501): 0.23 (1.2%); 1730−130: 7.81 (no polarized intensity image); 1908−201: 2.41 (1.4%).

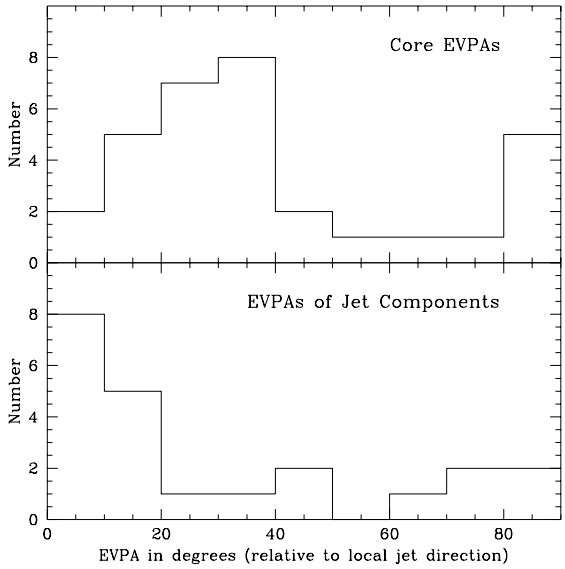


Figure 3: *Top panel:* Histogram of polarization electric-vector position angles (EVPAs), minus the local direction of the jet axis, of the cores of 32 of the blazars in the sample (4 other sources had core polarizations below the detection threshold). *Bottom panel:* The same for 22 jet components with significant polarization detected.

of the entire sample. The core polarizations are very low — all less than 6% and most less than 3%, with 25% (9 blazars) less than 1%. The electric-vector position angles (EVPAs) have a rather broad distribution relative to the local jet direction (see Figure 3, top panel), although there is a deficit of EVPAs between 40° and 80°. The EVPAs of the cores therefore tend to favor orientations somewhat parallel to the jets, but still at oblique angles, although 16% have EVPAs transverse to the jet. The substantial number of oblique EVPAs might suggest further bending closer to the central engine (so that the fields would be transverse to the inner jet direction), which can be tested with higher frequency or space-VLBI observations at 22 or 43 GHz. The distribution of the EVPAs of the jet components (see Fig. 3, bottom panel) is even more uneven, favoring magnetic fields that are either parallel or transverse to the jets. There is essentially no difference between the polarization properties of BL Lac objects and quasars, unlike what is found at 5 GHz (Cawthorne et al. 1993).

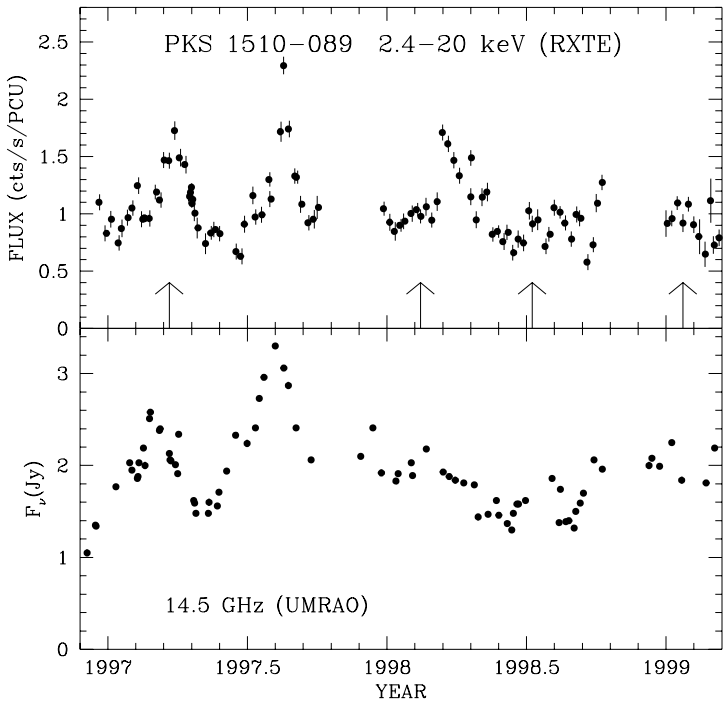


Figure 4: *Top panel:* X-ray light curve (flux is in photon counts per second per detector) of PKS 1510−089. *Bottom panel:* Radio light curve at 14.5 GHz. In the two major flares in 1997, the radio variations led the X-ray by about 2 weeks. The arrows indicate epochs of extrapolated zero separation between superluminally moving knots and the core.

## 3 Nearly Simultaneous X-Ray and Radio Flares in PKS 1510−089

Figure 4 shows the 2.4–20 keV X-ray and 14.5 GHz radio light curves of the quasar PKS 1510−089. In 1997 there were two strong flares at each waveband. It is noteworthy that the timescale of the flares was many weeks, which allowed good time sampling despite the fact that observations occurred only weekly. The second flare has a very similar profile at both wavebands. It is apparent from Fig. 4 that the radio variations *led* the X-ray by about two weeks. Of course, this needs to be confirmed with further observations, especially in light of the early-1998 X-ray flare that had no strong radio counterpart; we are continuing to monitor the source through early October 2000.

How can the radio lead the X-ray flare? There are two possibilities.

One is the "Mirror Compton" model of Ghisellini & Madau (1996), in which the synchrotron flare first scatters off one or more clouds near the jet so that the relativistic electrons in the jet see the flare blue-shifted and time-delayed and scatter these photons to X-ray and $\gamma$-ray energies. This predicts that longer time delays should correspond to weaker X-ray flares. The other possibility is that the X-rays are synchrotron self-Compton (SSC) emission from the jet. If the variations are limited by light-travel effects, then the electrons receive most of the synchrotron photons (which they will subsequently scatter to high energies) time-delayed. In this case the X-ray peak cannot occur any later than when the synchrotron flare has decayed to about 60% of its peak value (Sokolov & Marscher 2000), a condition that is satisfied by the two flares in PKS 1510−089 in 1997.

## 4 Conclusions

The association of high-energy emission with the relativistic jets in blazars is demonstrated by the coincidence of $\gamma$-ray (Marchenko-Jorstad et al., these proceedings) and X-ray flares with radio flares and/or superluminal ejections. The properties of the $\gamma$-ray blazars are consistent with a population that is more strongly beamed than the general population of strong, compact radio sources (Lister & Marscher 1999). The stronger beaming of the $\gamma$-rays occurs in the case of Compton scattering of photons from outside the jet because of the blue-shifting of these seed photons in the jet frame. In the SSC case, the extra beaming comes from the K-correction owing to the steeper spectral index (typically $\sim -1$) of the $\gamma$-ray emission relative to the radio emission ($\sim 0$).

The polarization of the cores and jets of both quasars and BL Lac objects favors magnetic fields that lie transverse to the jet direction, although there are many sources in which the core polarizations are oblique by 20–40°. There is no significant difference between the polarization properties of BL Lac objects and quasars at 22 or 43 GHz.

The images shown here reveal cores that are still nearly unresolved. In order to explore the nature of the cores of blazar jets and to understand the production of energy and acceleration of relativistic electrons in the jets, we need the angular resolution provided by VLBI with antennas in space, as well as multiwavelength monitoring missions and campaigns. In addition, continued theoretical effort, especially 3D relativistic MHD simulations, is needed to interpret the results.

**Acknowledgements.** This work was supported in part by NASA through CGRO Guest Investigator grants NAG5-7323 and NAG5-2508, and by U.S. National Science Foundation grant AST-9802941. The University of Michigan Radio Astronomy Observatory is funded in part by a grant from the U.S. National Science Foundation.

## References

Cawthorne, T.V., Wardle, J.F.C., Roberts, D.H. & Gabuzda, D.C. 1993, *ApJ*, **416**, 519

Ghisellini, G. & Madau, P. 1996, *MNRAS*, **280**, 67

Lister, M.L. & Marscher, A.P. 1999, *Astroparticle Phys.*, **11**, 65

Pearson, T.J., Browne, I.A.W., Henstock, D.R. et al. 1998, in *ASP Conf. Ser.* **144***: IAU Coll. 164: Radio Emission from Galactic and Extragalactic Compact Sources*, eds. J.A. Zensus, G.B. Taylor & J.M. Wrobel (San Francisco: Astron. Soc. Pac.), 17

Sokolov, A.S. & Marscher, A.P. 2000, in preparation

Tornikoski, M., Valtaoja, E., Teräsranta, H., et al. 1994, *A&A*, **289**, 673

*Astrophysical Phenomena Revealed by Space VLBI*
*H. Hirabayashi, P.G. Edwards and D.W. Murphy (eds.)*

# VSOP Monitoring of 1928+738

D.W. Murphy [1], R.A. Preston [1], A. Polatidis [2], J.E. Conway [2],
H. Hirabayashi [3], Y. Murata [3], H. Kobayashi [4]

[1] *JPL, MS238-332, 4800 Oak Grove Drive, Pasadena CA 91109, USA*
[2] *Onsala Space Observatory,S-439 92 Onsala, Sweden*
[3] *ISAS, Yoshinodai 3-1-1, Sagamihara, Kanagawa 229-8510, Japan*
[4] *NAO, Ohsawa 2-21-1, Mitaka, Tokyo 181-8588, Japan*

**Abstract**

In the paper we present the results from a VSOP monitoring campaign on the low redshift ($z$=0.3) circumpolar superluminal quasar 1928+738. Our five epochs of data show that there have been substantial structural changes in this source near the core on the time-scale of a few months.

## 1 Introduction

1928+738 is in the S5 polar cap sample and has been well studied on both the arcsecond-scale and mas-scale. Proper motions have been detected in several distinct jet components with values that lie in the range 0.27–0.36 mas yr$^{-1}$ (Hummel et al. 1992; Ros et al. 1999) which leads to apparent speeds in the range 4.8–6.5 $c$ for $H_0 = 65\,\mathrm{km\,s^{-1}\,Mpc^{-1}}$. The 22 GHz work of Hummel et al.(1992) showed that the motion of the VLBI components in 1928+738 was not consistent with simple linear expansion along a fixed position angle (PA) for all components. Indeed, 1928+738 was one of the first sources for which helical jet motion was proposed. Expanding upon this work, Roos et al. (1993) proposed that a massive binary black hole (MBBH) system is responsible for the sinusoidal jet ridge line observed at 22 GHz over a 5 year period. The phase of this sinusoid, in the plane of the sky, varies by $\approx 0.28$ mas yr$^{-1}$, which implies a period in the rest frame of the quasar of 2.9 years within the framework of a ballistic relativistic jet model. A period this short is unlikely to be caused by geodetic precession of the primary black hole as the implied gravitational lifetime is then extremely short (~10 years!). A more realistic scenario is to assume that the observed period is associated with the binary orbital period. An alternative to the ballistic relativistic jet model is to assume that the observed wiggles in the jet are caused by Kelvin-Helmholtz (KH) instabilities also driven by the orbital motion of the MBBH system.

## 2 1928+738 VSOP Images

Figure 1, and Color Figure 3, show 5 GHz images of the core and inner jet region of 1928+738 from our five epochs of data. These epochs are 1997 August 22, 1997 December 16, 1998 April 29, 1998 July 9 and 1999 June 16. Each image has a size of 6 mas by 6 mas and our typical observation included the use of HALCA, the VLBA, Effelsberg and a second European antenna.

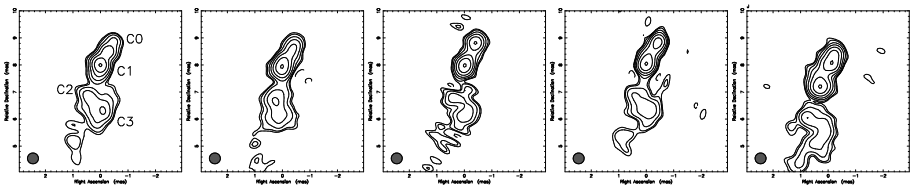


Figure 1: 5 GHz images from the 5 epochs of 1928+738 monitoring.

As can be seen, there are very distinct structural changes in this region during the period of our monitoring observations. The core is located in the northern most part of the image and is not a bright feature on the early images. In the later 3 epochs the core can be seen to be flaring and in the last epoch there is evidence of the ejection of a new component. However, at a distance of roughly 2.3 mas from the core the jet goes through a large apparent bend followed by another large bend after which the jet has roughly the same position angle as the initial jet direction.

## 3 Component Properties

We have model-fitted the core region of 1928+738 using 4 components which we call C0, C1, C2, and C3. The location of these components are shown in the first image in Figure 1. C0 is the core while C1, C2, C3 are jet components located progressively further down the jet from the core. Figure 2 shows the proper motion of these components with respect to the core. Least squares fitting gives proper motion of the components C1, C2, and C3 to be 0.34 $\pm$ 0.07, 0.09 $\pm$ 0.08, and 018 $\pm$ 0.07 mas $^{-1}$ respectively. For $H_0 = 65$ km s$^{-1}$ Mpc$^{-1}$, this corresponds to apparent speeds (in units of $c$) to be 6.1$\pm$1.3, 1.6$\pm$1.4, and 3.2$\pm$1.3 for components C1, C2, and C3 respectively. These speeds are similar to

what has been derived in previous studies of this source (Hummel et al. 1992 and Ros et al. 1999). The behavior exhibits several features which are now seen in increasing numbers of VLBI sources. Namely, we have both stationary (C2) and moving components (C1, C3). Furthermore there is evidence that the apparent speed increases as we go away from the core since the speed of C3 is higher than that of C1. This may be explained as either real acceleration of the jet or by simple projection effects namely that the jet is curving slightly away from our line of sight as the it leaves the core. An examination of the position angle (PA) variations of the components, as displayed in Figure 3, shows that C1 and C3 are moving away from the core at different PAs. There is some evidence for the PA of each component to be changing with time and for there to be oscillations about this linear PA evolution. Such PA changes seem to rule out simple ballistic motion for the components and oscillations in a helical jet seems an attractive explanation worth pursuing further.

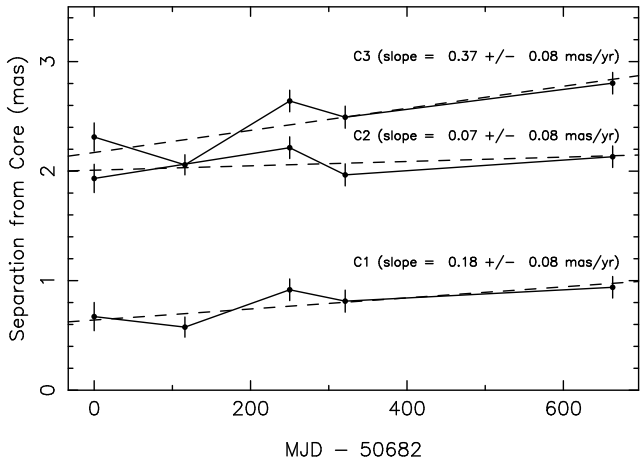


Figure 2: Separation of components from the core (C0).

## 4 Summary

We have imaged 1938+378 at 5 epochs that span a time range of almost 2 years. In that time, we have observed a variety of structural changes in the inner jet region near the region. As is the case for an increasing number of sources real jet motions can be very different from the simple

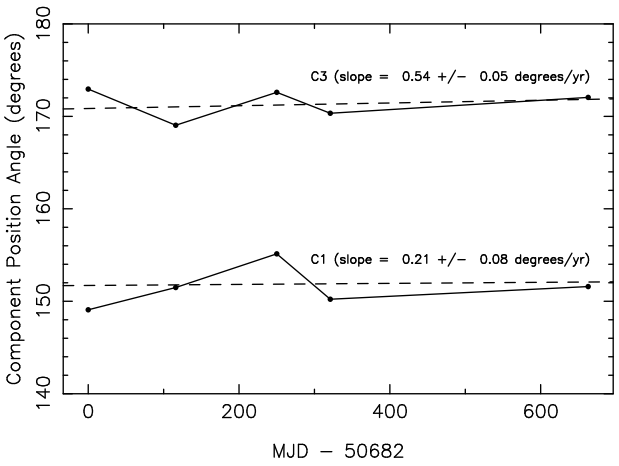


Figure 3: Position angle evolution for C1 and C3.

model of a straight jet with components moving at constant apparent speed. In 1928+738, we have examples of a variety of different phenomena: stationary components, components moving with different speeds along different position angles which themselves are changing with time. More work is needed to clarify under what new framework the diverse motions exhibited by the inner jet components of this source can now be explained.

**Acknowledgements.** We gratefully acknowledge the VSOP Project, which is led by the Japanese Institute of Space and Astronautical Science in cooperation with many organizations and radio telescopes around the world.

## References

Hummel, C.A., Schalinski, C.J., Krichbaum, et al. 1992, *A&A*, **257**, 489

Roos, N., Kaastra, J.S., & Hummel, C A. 1993, *AJ*, **409**, 130

Ros, E., Marcaide, J. M., Guirado, J. C., et al. 1999, *A&A*, **348**, 381

*Astrophysical Phenomena Revealed by Space VLBI*
*H. Hirabayashi, P.G. Edwards and D.W. Murphy (eds.)*

# A VSOP Observation of 3C 84

K. Asada[1], S. Kameno[2], M. Inoue[2], Z.-Q. Shen[2],
S. Horiuchi[2] & D.C. Gabuzda[3]

[1] *Department of Physics, Science University of Tokyo, Shinjuku-ku, Tokyo 162-8601, Japan*
[2] *NAO, Ohsawa 2-21-1, Mitaka, Tokyo 181-8588, Japan*
[3] *JIVE, Postbus 2, 7990 AA, Dwingeloo, The Netherlands*

**Abstract**

We present 5 GHz VSOP and 15 GHz global VLBI images of 3C 84. Our VSOP observation reveals a double-ridgeline structure in the southern component for the first time at this low frequency. We conclude that a jet and its back flow form this double-ridgeline structure. An inverted spectrum in the northern component indicates free-free absorption. This result is consistent with previous observations.

## 1 Introduction

The compact radio source 3C 84 in the Seyfert galaxy NGC 1275 is one of the strongest radio sources and a near-by (z=0.018) active galactic nucleus (AGN). It has been a prime target of Very Long Baseline Interferometry (VLBI) observations. Previous VLBI observations revealed a very complicated structure of 3C 84. It has a jet to the south and counter-jet to the north and a bright, flat-spectrum core. The counterjet shows a strong low-frequency cut off, while the main jet shows no low-frequency cut off. The asymmetric distribution of this cut off seems to be due to free-free absorption in a volume that surrounds the core and lies in front of the counterjet but is behind the main jet (Vermeulen and Readhead 1994; Romney et al. 1995). From previous VLBA observations at 15 GHz, it has been reported that the southern jet has a double-ridgeline structure in the east-west direction (Venturi et al. 1993).

## 2 Observations and Data Reduction

On 1996 November 21, we observed this source for 10 hrs with a global VLBI network at 15 GHz. We used the VLBA, the phased-VLA, and

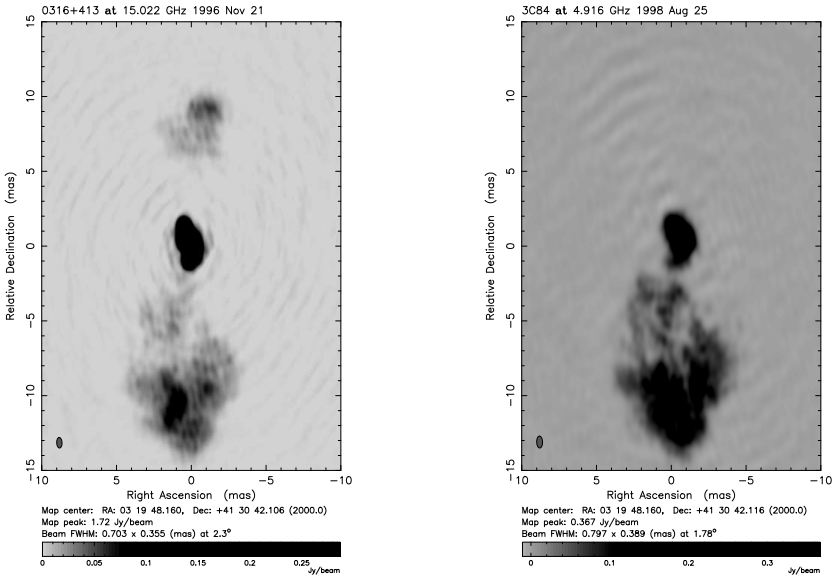


Figure 1: Clean images of 3C 84 at observing epochs 1996.89 with global VLBI at 15 GHz (left) and 1998.65 with VSOP at 5 GHz (right)

Effelsberg 100-m antenna. On 1998 August 25, we observed again for 14 hrs with the VLBI Space Observatory Programme (VSOP) at 5 GHz. At this time we used the VLBA, the phased-VLA, and the Space VLBI satellite HALCA. Amplitude calibration for each antenna and fringe fitting were performed with AIPS. Imaging, deconvolution, and self-calibration were performed using Difmap.

## 3 Results and Discussion

### 3.1 The Southern Jet

Images of both of our global VLBI and VSOP observations are shown in Fig. 1. Our VSOP observation at 5 GHz reveals a transversal structure of the southern jet in the east-west direction (see Fig 1). A double-ridgeline structure is shown clearly which has been already observed at a higher frequency. A spectral index distribution which is obtained by a comparison between 15 and 5 GHz is shown in Fig 2. The spectral index along the central ridgeline decreases from the north to the south,

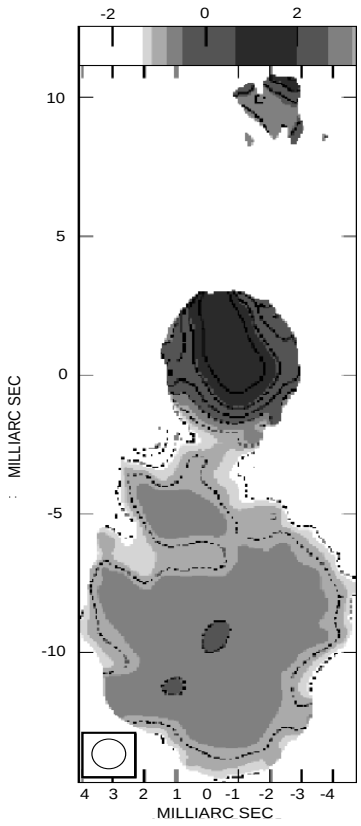


Figure 2: Spectral index distribution which is obtained by comparison between the 15 GHz global VLBI image and the 5 GHz VSOP image.

while that along the eastern ridgeline decreases from the south to the north. It is widely accepted that decay of spectral indices is caused by a energy loss in relativistic plasma. Hence the decay can be an indicator of a plasma age. A jetstream to the south forms the central ridgeline, while a back flow froms the southern hot spot form the eastern ridgeline. In the image taken by the VSOP at 5 GHz, there is another ridgeline parallel to the central and the eastern ridgeline in the southern jet. This western ridgeline can be a part of back flow, too.

The southern jet has a wiggled structure in the image taken by VSOP at 5 GHz (see Fig 1). Generally, there are many possibilities which is cause of the apparent wiggled jet structure such as the Kelvin-Helmholtz instability, or so on. Our spectral index map suggests that

the central ridgeline is the jet, while the eastern and western ridgeline is the back flow. Therefore, the wiggled structure in the main jet might be due to the Kelvin-Helmholtz instability between the jet and the back flow.

### 3.2 The Northern Jet

In the northern counterjet, there is a component which shows a spectral index $\alpha > 2.5$. It indicates that free-free absorption (FFA) is preferred as a reason of the low-frequency cutoff rather than synchrotron self-absorption (SSA). Furthermore, the spectral index increases from the counterjet to the core. This spectral index gradient is explained by a torus-like FFA absorber surrounding the core and lying in front of the counterjet but is behind the main jet. This idea is consistent with results of the previous observations.

## 4 Summary

We present the results of VSOP and global VLBI observations of 3C 84. From these observations, we produced a spectral index map to discuss the plasma age, and the absorption feature. A double-ridgeline structure is found in the southern jet in the image of the 5 GHz VSOP observation. Our spectral index map suggests a jet forms the central ridgeline, a back flow forms the eastern and western ridgelines, and the wiggled structure might be caused by Kelvin-Helmholtz instability between the jet and the back flow. Our spectral index map shows an inverted spectrum with its spectral index $\alpha > 2.5$ in the counterjet. This result is consistent with the previous idea which the core is surrounded by a torus like FFA absorber.

## References

Romney, J.D., Benson J.M., Dhawan V. et al. 1995, Proc. Natl. Acad. Sci. USA **92**, 11360

Venturi T., Readhead A. C. S., Marr J. M. & Backer D. C. 1993, *ApJ*, **411**, 522

Vermeulen R. C. & Readhead A. C. S. 1994, *ApJ*, **430**, L41

*Astrophysical Phenomena Revealed by Space VLBI*
*H. Hirabayashi, P.G. Edwards and D.W. Murphy (eds.)*

# VLBI Monitoring of 3C 279 at 22 and 43 GHz: 1991-1997

B.G. Piner[1], A.E. Wehrle[1], S.C. Unwin[1], A.C. Zook[2],
W. Xu[3] & A.P. Marscher[4]

[1] *Jet Propulsion Laboratory, California Institute of Technology, USA*
[2] *Department of Physics and Astronomy, Pomona College, USA*
[3] *IPAC, California Institute of Technology, USA*
[4] *Department of Astronomy, Boston University, USA*

**Abstract**

We present results obtained from VLBI monitoring of the relativistic jet in 3C 279 at 22 GHz from 1991 to 1997 (18 epochs), and at 43 GHz from 1995 to 1997 (10 epochs). Measured speeds for all detected components are presented. Component C4 has followed a nonlinear path out from the core, and the motion of this component is discussed in detail.

## 1 Introduction and Observations

The blazar 3C 279 is one of the most famous and well-studied quasars. We have been studying this source intensively with VLBI, using both ground and space-based VLBI observations. Results from our collaborative VLBI Space Observatory Programme (VSOP) monitoring observations are presented by Hirabayashi et al. in these proceedings. This paper presents results from high-frequency 22 and 43 GHz ground-based VLBI observations conducted between 1991 and 1997. The earlier observations (1991–1994) were conducted with the global VLBI network and partial Very Long Baseline Array (VLBA); later observations (1994–1997) were conducted with the full VLBA. Observations at 43 GHz did not begin until 1995. We have recorded a total of 18 epochs of observation at 22 GHz between 1991 and 1997, and 10 epochs at 43 GHz between 1995 and 1997. Sample images of 3C 279 at 22 and 43 GHz are shown in Figure 1.

## 2 Components and Speeds

A total of eight components (named C4, C5, C5a, C6, C7, C7a, C8, and C9) have been identified and tracked by model fitting. These component

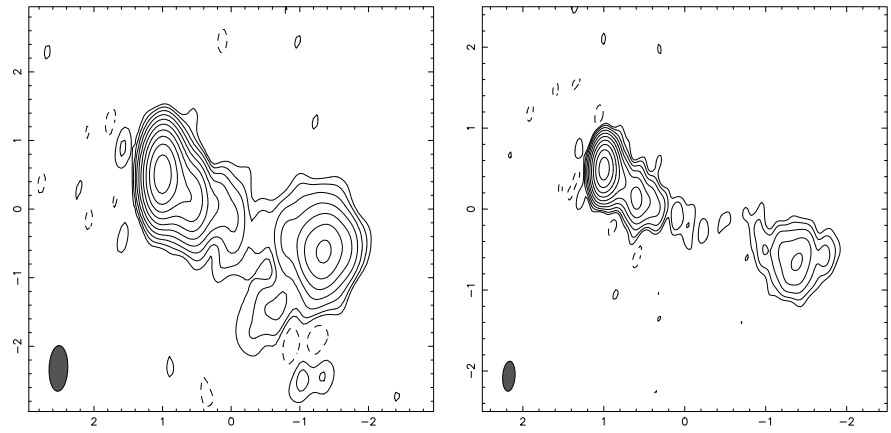

Figure 1: 22 GHz (left) and 43 GHz (right) images of 3C 279 from 1995 Mar 19. The peak flux densities are 12.3 and 13.6 Jy beam$^{-1}$, the contour levels are 15 and 18 mJy beam$^{-1}$ × -1,1,2,4,...512, and the beam sizes are 0.67 × 0.27 mas at -2° and 0.37 × 0.15 mas at -4° for the 22 and 43 GHz images respectively.

names have been chosen to maintain consistency with the C5, C6, and C7 of Leppänen et al. (1995) and the C8 of Lister et al. (1998). The outward motion of these components is shown in Figure 2. The bright component C4 currently at ∼3 mas has been extremely long lived, with an ejection time in the mid 1980s. The component C5 at ∼1 mas is stationary, and other superluminal components interior to C5 fade and disappear as they approach C5. The bright component C8 (which was as bright as 9 Jy) was ejected near the time of the EGRET flare in early 1996, although the formal ejection time is several sigma before the flare. Component speeds measured by fitting to component separations vs. time are ($H_0$=70 km s$^{-1}$ Mpc$^{-1}$ and $q_0$=0.1): 7.5 ± 0.2 $c$ for C4, −0.6 ± 0.5 $c$ for C5, 6.8 ± 1.0 $c$ for C5a, 5.8 ± 0.4 $c$ for C6, 5.0 ± 0.4 $c$ for C7, 4.8 ± 0.2 $c$ for C7a, and 5.4 ± 0.2 $c$ for C8.

## 3 3-Dimensional Motion of C4

Component C4 has followed a nonlinear path out from the core, and we use this path and the apparent speed of C4 to model the 3-dimensional trajectory of this component, using the method described by Zensus et al. (1995) for 3C345. Polynomials were fit to $x(t)$ and $y(t)$ (Figure 3$a$).

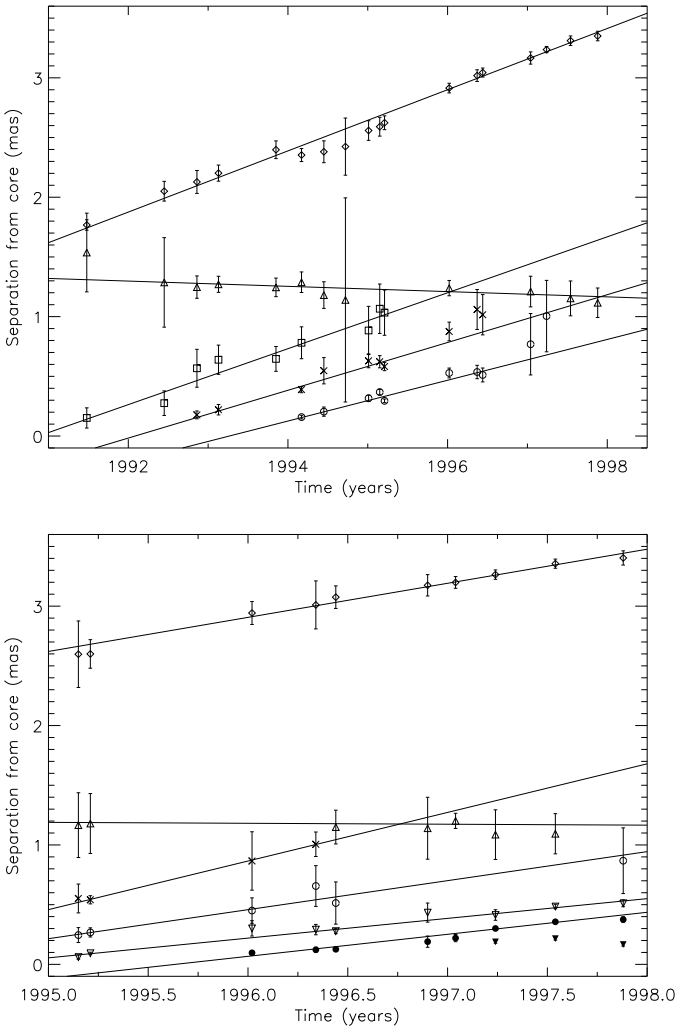


Figure 2: Distances from the core of model components as a function of time at 22 GHz (top) and 43 GHz (bottom). Diamonds represent C4, triangles C5, squares C5a, crosses C6, circles C7, inverted triangles C7a, filled circles C8, and filled inverted triangles C9. Error bars have been set to be proportional to the beam size and inversely proportional to the square root of the component SNR (component surface brightness/ rms surface brightness). The lines shown are the best fits to motion with constant speed.

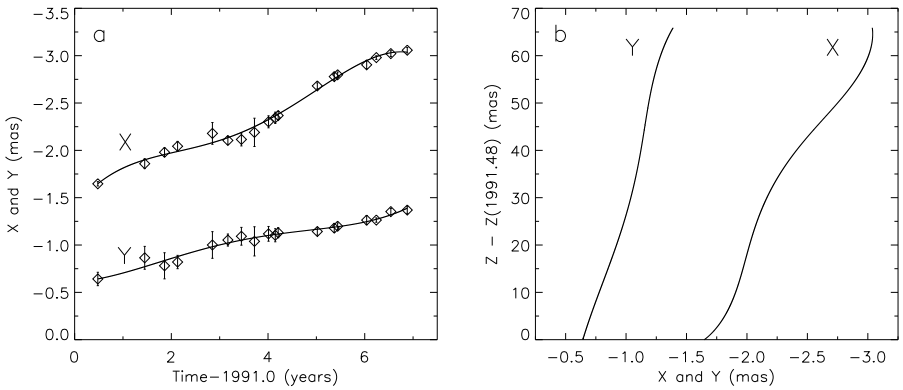


Figure 3: ($a$): $x$ and $y$ position of C4 vs. time. The lines show polynomial fits to the motion. ($b$): Derived motion of C4 in the $(x, z)$ and $(y, z)$ planes.

Fourth order polynomials were required for adequate fits. The apparent speed was found from $\beta_{app}(t) = (\dot{x}(t)^2 + \dot{y}(t)^2)^{1/2}$, and a constant $\Gamma$ slightly larger than the minimum $\Gamma$ required for the maximum $\beta_{app}(t)$ was assumed ($\Gamma = 13$). The viewing angle was then solved for, taking the small angle solution because the large angle solution gives large changes in Doppler factor that would be seen as large changes in flux. From the viewing angle, $z(t)$ can be calculated and the complete 3D trajectory determined. The motion in the $(x, z)$ and $(y, z)$ planes is shown in Figure 3$b$. C4 appears to follow a low pitch angle helical path in the $(x, z)$ plane.

**Acknowledgements.** Part of the work described in this paper has been carried out at the Jet Propulsion Laboratory, California Institute of Technology, under contract with the National Aeronautics and Space Administration. A.E.W. acknowledges support from the NASA Long Term Space Astrophysics Program. The National Radio Astronomy Observatory is a facility of the National Science Foundation operated under cooperative agreement by Associated Universities, Inc.

## References

Leppänen, K.J., Zensus, J.A., & Diamond, P.J. 1995, *AJ*, **110**, 2479

Lister, M.L., Marscher, A.P., & Gear, W.K. 1998, *ApJ*, **504**, 702

Zensus, J.A., Cohen, M.H., & Unwin, S.C. 1995, *ApJ*, **443**, 35

*Astrophysical Phenomena Revealed by Space VLBI*
*H. Hirabayashi, P.G. Edwards and D.W. Murphy (eds.)*

# VSOP Observations of 3C 216

Z. Paragi[1], S. Frey[1], I. Fejes[1], R.W. Porcas[2],
R.T. Schilizzi[3,4] & T. Venturi[5]

[1] *FÖMI Satellite Geodetic Observatory, Penc, Hungary*
[2] *Max-Planck-Institut für Radioastronomie, Bonn, Germany*
[3] *Joint Institute for VLBI in Europe, Dwingeloo, The Netherlands*
[4] *Leiden Observatory, Leiden, The Netherlands*
[5] *Istituto di Radioastronomia, Bologna, Italy*

**Abstract**

We present VLBI Space Observatory Programme (VSOP) observations of the extremely misaligned quasar 3C 216. The observed brightness temperature of the radio core is comparable to the inverse Compton limit, and the source emission is probably relativistically boosted towards us.

## 1 Introduction

We carried out VSOP observations of 3C 216 ($z = 0.67$), a peculiar compact steep spectrum (CSS) quasar. The source is remarkable for its jet extending from the core to 140 mas, oriented almost perpendicularly to the arcsecond scale structure (Fejes et al. 1992). The jet follows a gently curved path, with underlying wiggles, and ends in a sharp bend (Akujor et al. 1996). These earlier observations could be interpreted with a precessing jet scenario; however, the very high rotation measure observed in the bend (Venturi & Taylor 1999) and the recently detected HI absorption in the source (Pihlström et al. 1999) indicate that the jet is probably deflected by an interstellar cloud in the host galaxy.

In the innermost part of the source, components emerge at superluminal speeds (Barthel et al. 1988). Venturi et al. (1993) showed that deceleration takes place in the inner few mas (10–20 parsecs). There is also a quasi-stationary component at $\sim 1.5$ mas from the radio core at 5 GHz. Our main goal was to investigate this region in more detail.

## 2 Observations, Data Reduction and Imaging

The observations took place on 14/15 February 1999 using HALCA, the 43m Green Bank telescope and the western part of the European VLBI

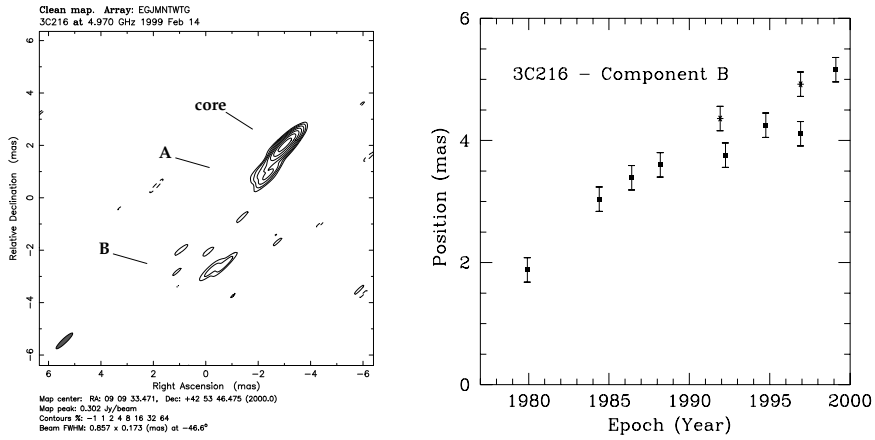


Figure 1: **a** Full resolution space VLBI image. Contour levels are $-1$, 1, 2, 4, 8, 16, 32, 64% of the peak brightness of 302 mJy/beam, the size of the restoring beam is $0.86 \times 0.17$ mas at $PA = -47°$. **b** Motion of the superluminal component B from the earliest VLBI observations. The 1979–89 data are taken from Barthel et al. (1988) and Venturi et al. (1993), the 1991–98 data are taken from Venturi et al. (in prep.). Asterisks indicate observations at 8.4 GHz

Network (EVN) at 5 GHz. There were three tracking passes during the 8.5 hour experiment using the Green Bank, Tidbinbilla and Goldstone tracking stations. The data were correlated at the NRAO-VLBA correlator. We experimented with a variety of cellsizes and data weighting in imaging, in order to reconstruct the source structure on different spatial scales.

## 3 Results

The space VLBI image is shown in Fig. 1a. Components are labelled in the same way as in Venturi et al. (1993). The results of model fitting of the self-calibrated data are listed in Table 1. The core region is resolved; however, the clean beam is highly elongated roughly along the jet direction. Using a 0.5 mas circular restoring beam, Component A is apparently well separated from the core (image not shown). The separation is estimated as $1.25 \pm 0.05$ mas. This is not in agreement with

the results of model fitting; an elongated component closer to the core (0.87 mas) gives the best fit to the data (see Table 1.). Component B is clearly resolved, and seems to be edge brightened on the western side. It is difficult to estimate the positional uncertainty of component B; we will use 0.2 mas in further analysis (as well as for other epochs). The position angle of the inner jet components ($PA = 152°$) is slightly misaligned with respect to the 100 mas scale jet ($PA = 146 - 149°$).

In order to scale angular sizes to projected linear sizes, we used $H_0 = 100\,h\,\mathrm{km\,s^{-1}\,Mpc^{-1}}$ and $q_0 = 0.5$; 1 mas corresponds to $3.9\,h^{-1}$pc at the distance of 3C 216. The observed brightness temperatures of the source components are listed in Table 1. For the radio core, $T_\mathrm{b} = 7.85 \times 10^{11}$ K, which is comparable to the inverse Compton limit.

## 4 Discussion

The position of component B from earlier VLBI measurements is shown in Fig. 1b. These data are consistent with a constant proper motion of $0.14 \pm 0.01$ mas/yr between 1979 and 1999. This corresponds to $\beta_\mathrm{app} = (3.0 \pm 0.2)\,h^{-1}$ apparent transverse velocity.

The nature of component A is rather unclear. Its separation from the core is 1.25 mas (in the super-resolved image), compared to the earlier reported quasi-stationary position of 1.4–1.6 mas (Venturi et al. 1993). The beam orientation is not suitable to decide whether this feature is a separate component, or just an extension to the core emission. As we could not model the source structure with a stable component at a distance of 1.25 mas in the model-fitting process, the latter seems more favorable. It is very probable that the "core" and "component A" together form the so-called ultracompact jet region of 3C 216 (see Lobanov 1998). In this case we can apply the equipartition jet model of Blandford and Königl (1979) in which the limiting brightness temperature is about $3 \times 10^{11}\,\delta^{5/6}$ K. A comparison with the observed value results in a lower limit to the Doppler factor: $\delta \gtrsim 3.17$.

A lower limit to the Lorentz factor of the jet ($\gamma$) and an upper limit to the viewing angle to the line of sight ($\theta$) can be calculated using $\beta_\mathrm{app}$ and $\delta$ determined above. Our results are $\gamma \gtrsim 3.16$ and $\theta \lesssim 18.4°$ (assuming $h = 0.7$). Much higher Doppler factors for 3C 216 have been determined by other methods ($\delta = 33$ in Ghisellini et al. 1992 and $\delta = 65$ in Güijosa & Daly 1996). These Doppler factors would result in very large Lorentz factors of $\gamma \gtrsim 16$ and much smaller angles to the line

Table 1: Fitted elliptical Gaussian model parameters of the source

| Component | $S$ (mJy) | $r$ (mas) | $\Theta$ (°) | $a$ (mas) | $b/a$ | $\Phi$ (°) | $T_{\rm b}$ ($10^{12}$ K) |
|---|---|---|---|---|---|---|---|
| Core | 381.6 | 0.00 | – | 0.36 | 0.31 | −32 | 0.785 |
| A | 122.8 | 0.87 | 151.5 | 1.37 | 0.21 | −62 | 0.025 |
| B | 45.1 | 5.16 | 152.3 | 1.93 | 0.14 | −31 | 0.007 |

of sight, but are not in contradiction with our lower and upper limits determined from $\delta \gtrsim 3.17$.

**Acknowledgements.** We gratefully acknowledge the VSOP Project, which is led by the Japanese Institute of Space and Astronautical Science in cooperation with many organizations and radio telescopes around the world. This research has been partially supported by the Hungarian Space Office.

## References

Akujor, C.E., Porcas, R.W. & Fejes, I. 1996, in *Extragalactic Radio Sources* eds. R. Ekers, C. Fanti & L. Padrielli (Dordrecht: Kluwer), 83

Blandford, R.D. & Königl, A. 1979, *ApJ*, **232**, 34

Barthel, P.D., Pearson, T.J. & Readhead, A.C.S. 1988, *ApJ*, **329**, L51

Fejes, I., Porcas, R.W. & Akujor C.E. 1992, *A&A*, **257**, 459

Ghisellini, G., Celotti, A., George, I.M. & Fabian A.C. 1992, *MNRAS*, **258**, 776

Güijosa, A. & Daly, R.A. 1996, *ApJ*, **461**, 600

Lobanov, A.P. 1998, *A&A*, **330**, 79

Pihlström, Y.M., Vermeulen, R.C., Taylor, G.B. & Conway, J.E. 1999, *ApJ*, **525**, L13

Venturi, T., Pearson, T.J., Barthel, P.D. & Herbig, T. 1993, *A&A*, **271**, 65

Venturi, T. & Taylor, G.B. 1999, *AJ*, **118**, 1931

*Astrophysical Phenomena Revealed by Space VLBI*
*H. Hirabayashi, P.G. Edwards and D.W. Murphy (eds.)*

# Multi-Frequency VSOP Observations of 3C 380

S. Kameno[1], Z.-Q. Shen[1], M. Inoue[1], K. Fujisawa[1] & K. Wajima[2]

[1] *NAO, Osawa 2-21-1, Mitaka, Tokyo 181-8588, Japan*
[2] *ISAS, Yoshinodai 3-1-1, Sagamihara, Kanagawa 229-8510, Japan*

**Abstract**

We report the first-epoch VSOP observations of the superluminal quasar 3C 380 at L- and C-band. A straight motion with a constant apparent speed of the component A is preferred, suggesting ballistic ejection from the core. The opening angle of the jet is $\sim 20°$ at both the pc- and kpc-scale. The distribution of spectral indices along the jet reveals shell-like spectral enhancements at the knots, possibly indicating an adiabatic expansion of the plasma blobs.

## 1 Introduction

The quasar 3C 380 is one of the most powerful radio sources at a redshift $z = 0.692$. This object is classified as a compact steep-spectrum (CSS) source, with an overall size of 10 kpc and a steep spectrum $\alpha = \frac{d \log S_\nu}{d \log \nu} = -0.7$ (Fanti et al. 1990). If we assume a Hubble constant of $H_0 = 75$ km s$^{-1}$ Mpc$^{-1}$, 1 mas corresponds to 6 pc. VLA observations revealed

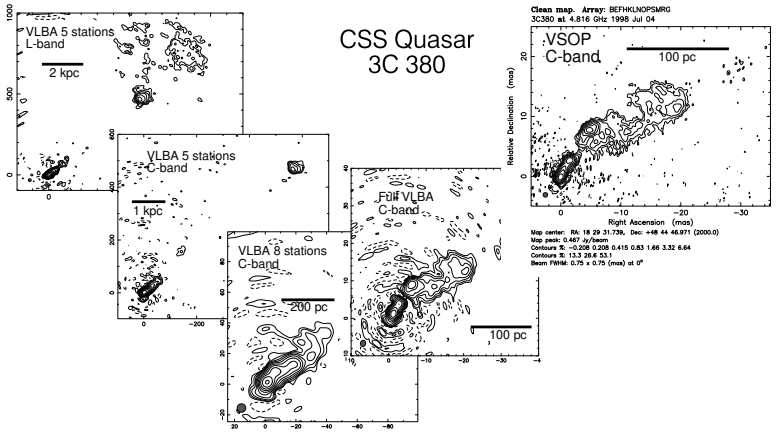


Figure 1: Images of 3C 380 in various scales with different arrays.

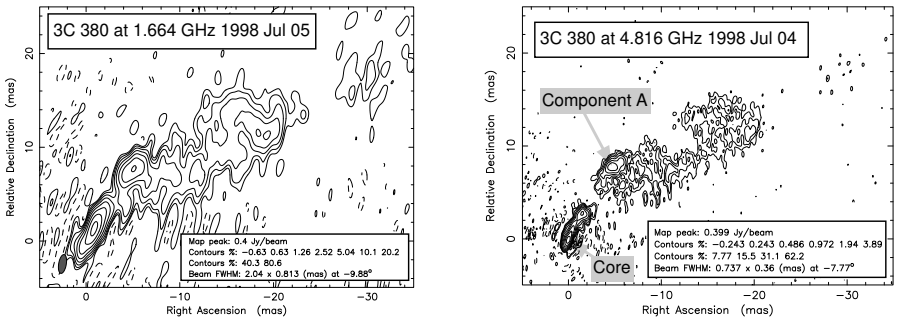


Figure 2: Full-resolution images of 3C 380 at 1.7 (*left*) and 5 GHz (*right*).

a one-sided jet emanating from the core to the north-west, a hot spot at 6 kpc from the core, and a cocoon-like radio lobe with a radius of $\sim 10$ kpc (O'Dea et al. 1999). The jet shows a kinked structure on the 100-pc scale (Polatidis & Wilkinson 1998, hereafter PW98). Several knots are identified along the jet. PW98 have monitored the motion of knot A, which is located $\sim 50$ pc from the core, revealing an apparent superluminal motion $\beta_{\rm app} = 5.9 \pm 0.7$. They found that this component curved along the bending jet and that its apparent speed changed from $\beta_{\rm app} = 2$ to 10, leading them to consider the intersection of oblique shocks. This idea suggests an astrophysical interest; 3C 380 can be a good probe to investigate the interaction between a relativistic jet and the ambient gas. Simultaneous VSOP observations at 1.7 and 5 GHz will provide a distribution of spectral indices along the jet, and enable us to verify the interaction.

## 2 VSOP Observations and Results

Our VSOP observations at 1672 MHz (L-band) and 4824 MHz (C-band) were carried out for 12 hours on July 5 and 4, 1998, respectively. Figure 1 shows the images at various scales and resolutions by different arrays. With the most compact array, which consists of PT, LA, FD, OV, and KP, we detect the hot spot 6 kpc from the core at a position angle (PA) of $-50°$. Full-resolution VSOP images are shown in Figure 2. We obtain resolutions of $2.0 \times 0.8$ mas at PA $-9.°9$ and $0.74 \times 0.36$ mas at PA $-7.°8$ at L- and C-band, respectively, with uniform weighting. Component A is clearly identified at both frequencies.

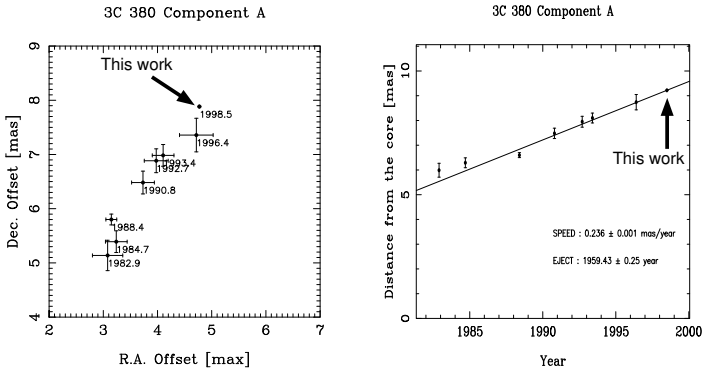


Figure 3: (*left*): Relative position of the component A from the core. Data points before 1996.4 are citations from PW98. (*right*): Angular distance of the component A from the core. The solid line indicates the best-fit linear motion.

## 3 Discussion

### 3.1 Jet Motion

The distance of the component A from the core is $9.22 \pm 0.01$ mas at a PA of $323.^{\circ}8$. It is plotted in Figure 3 together with previous measurements by PW98. Although PW98 mentioned that the component A changed its direction and speed in 1988.4, our result indicates a straight motion with a constant apparent speed. The average proper motion of $\mu = 0.236 \pm 0.001$ mas yr$^{-1}$ corresponds to $\beta_{\rm app} = 6.33 \pm 0.03$. The PA of $329^{\circ}.3$ is almost the same as that of the location of the component A. It may indicate a ballistic motion of the component A from the core.

### 3.2 Parsec- and Kiloparsec-Scale Jets

The jet has a straight extension from the core to the component A at $\sim$50 pc at a PA of $\sim 330^{\circ}$. In the low-resolution L-band image (see Figure 1), an extended diffuse emission at $\sim 6$ kpc can be seen at PA $\sim 330^{\circ}$. We also see another straight ridge at PA $\sim 310^{\circ}$ from the 60 pc to 6 kpc scale. Considering the ballistic motion of the component A, the opening angle of $\sim 20^{\circ}$ is due to changes of the direction of the jet ejection.

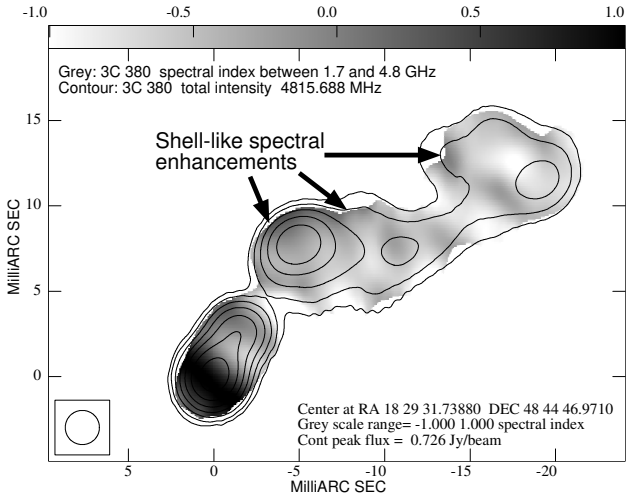


Figure 4: Spectral indices between L- and C-band (*grey scale*), overlaid on the total intensity image at C-band (*contour*). Both are restored with a 2 mas circular Gaussian beam.

### 3.3 Distribution of Spectral Index

The distribution of the spectral indices between L- and C-band is shown in Figure 4. While the inner 10 pc from the core is optically thick, downstream from component A shows an optically-thin feature with a negative spectral index. We found shell-like spectral enhancements along the jet, as shown in Figure 4. They are associated with the knots, and the radius of the shell is larger further downstream. We consider that these features indicate adiabatic expansion of plasma blobs.

**Acknowledgements.** We gratefully acknowledge the VSOP Project, which is led by the Japanese Institute of Space and Astronautical Science in cooperation with many organizations and radio telescopes around the world.

### References

Fanti, R., Fanti, C. Schilizzi, R. et al. 1990, *A&A*, **231**, 333

O'Dea, C., de Vries, W. Biretta, J. et al. 1999, *AJ*, **117**, 1143

Polatidis, A. & Wilkinson, P. 1998, *MNRAS*, **294**, 327 (PW98)

*Astrophysical Phenomena Revealed by Space VLBI*
*H. Hirabayashi, P.G. Edwards and D.W. Murphy (eds.)*

# VSOP Observations of Cen A

Kenta Fujisawa

*NAO, Ohsawa 2-21-1, Mitaka, Tokyo 181-8588, Japan*

**Abstract**

We have observed and imaged Centaurus A at light-month scale. The jet near the core bends by 60 degrees at 2 light-month from the core. Because of the large viewing angle of Cen A, this bending is not apparent but a true one. Discussions about physical mechanisms of bending jet are presented.

## 1 Introduction

We have observed Centaurus A (Cen A, NGC 5128) at unprecedented high resolution. The processes by which the jets of Active Galactic Nuclei (AGN) are formed and collimated have been investigated. Cen A is a unique object which lets us study the physical processes of the radio jet of AGN because of its proximity of only 3.5 Mpc from our Galaxy. One milli-arc-second (mas) is 24 light-days at this distance, and one can image the structure of light-month scale by VLBI. Structures in such small-scale near the central region reflect the process of jet formation. The angle between our line of sight and the jet is large, 50–80° (Tingay et al. 1998), while typical AGN jets are seen end-on. This side-on jet is a good opportunity for investigating the jet structure with less ambiguity.

## 2 Observation

Observations of Cen A were carried out in 1999 January. Although these observations were in the course of VLBI Space Observatory Programme (VSOP, Hirabayashi et al. 1998), no fringe was found at upper limit of 0.1 Jy for space baselines at all epochs. The observation was made at 5 GHz, standard VSOP mode. The participanting telescopes are phased 6 telescopes of Australian Telescope compact array (ATCA), Mopra, and three VLBA (MK, FD, OV) telescopes. Left circular polarization data were recorded on S2 terminals at Australian sites (ATCA and Mopra), and VLBA terminal at VLBA sites. Those tapes of two different types were copied to VSOP tape at the Mitaka correlation center of National Astronomical Observatory in Japan, and correlated.

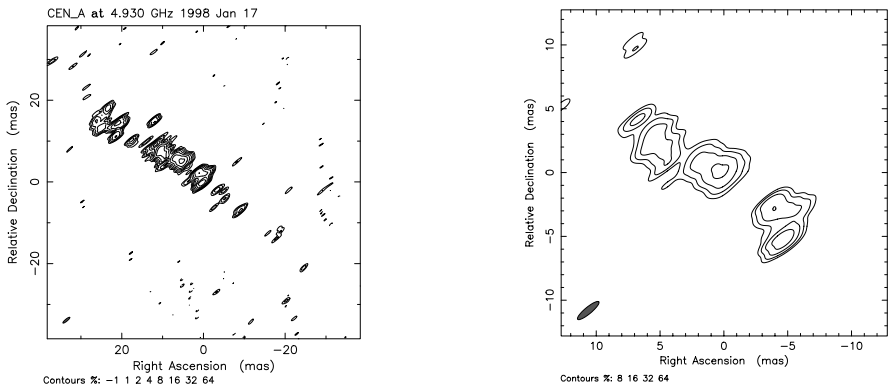


Figure 1: (left) Image of Cen A. (right) A close-up region of core.

Fringes with enough Signal-to-Noise ratios were found at all ground-ground baselines. The data including space baselines were rejected for the reductions later. The data were processed using AIPS in the normal procedure. The image was made with mapping software Difmap. The uniform weighting was applied for high-resolution imaging, and the final beamsize of $2.15\times0.52$ mas with position angle of $-50.4$ degree from north was achieved. The obtained image is shown in Figure 1.

## 3 Result and Discussion

There is no dominant component in the image of Cen A. A large, complex structure elongates from southwest to northeast at 30 mas range at PA$=60^\circ$ with a compact peak near the edge of southwest. Also three complex components are seen at 7 mas, 10 mas, and 23 mas from the peak, respectively. This 30 mas scale structure well coincides with the previous 5 GHz image by Tingay et al. (1998). They identified the core as the most southwest component, which is coincide with the peak in our image. Although further considerations would be required, we identify the peak as the core. Figure 1 (right) shows a close-up of the region of core component. It is clear that the jet is not straight. The jet starts from the core toward about north (PA$=0^\circ$) until 3 mas, then bends to PA$=60^\circ$. No brightness enhancement is seen at the locus of bending.

### 3.1 Bending Jet

It is known that jets of AGN often exhibit strong bends on the pc scale. Such bends, however, are believed to be apparent. The bending angles in such jets are intrinsically small, but amplified by their small viewing angle (e.g. Conway and Murphy 1995).

The viewing angle of Cen A is large, 50–80° (Tingay et al. 1998), and the observed large bending at light-month scale jet is not an apparent one. The apparent angle of bending of the innermost jet of Cen A is 60° at 2 mas from the core. The true angle of bending $\Phi$ is expressed as follows: $\cos\Phi \leq \sqrt{\cos^2\phi + \cos^2\theta \sin^2\phi}$, where $\phi$ is apparent angle of bending, and $\theta$ is angle between the large-scale jet and the line of sight. To determine the geometry of the bending jet, one more parameter $p$, the position angle of the small-scale jet around the large-scale jet, is required. Setting $\phi$=60° and $\theta$=65° (the median of 50° and 80°), we have $\Phi$ >30°. The extreme case, $\Phi$=30°, is a conservative estimation and probably $\Phi$ >45°.

The observed structure around the core might be different from the true one due to the strong absorption. The absorption is significant below 8 GHz, but negligible at higher frequencies. The bending structure is slightly seen at 22 GHz image (Tingay, private communication). Therefore, it is supposed that the bending structure observed at 5 GHz is real, not an absorption effect. Hence we conclude that the jet of Cen A bends with angle of at least 30°, probably >45°, at 2 light-month scale.

### 3.2 Formation of Bending Jet

A simple model for the bending jet is squeezing with unseen matter, like a large molecular cloud. The jet collides with the matter and then changes its direction, as observed in some Compact-Steep Spectrum sources (CSSs) or Giga-Hertz Peaked Spectrum sources (GPSs) . However, this is not likely to be the case for Cen A. No brightness enhancement is observed at the locus of bending, while such a jet colliding with ambient matter should cause a shock and a brightness enhancement. A large fraction of kinetic energy would be released as observed in CSS/GPS sources.

Another model of jet bending is the change of jet ejection angle. The large-scale jet knots could be ejected when the jet ejection angle was toward the PA= 60°, and the innermost knots could be ejected toward north. This model is also not to be likely the case. The jet in

Cen A is straight at scales from sub-pc to kpc, at a PA of 60°. If this changing angle of ejection model would be true, the ejection angle had been fixed for at least $10^3$ year, and recently changed suddenly. This model would be tested with monitoring of the innermost component.

It is a widely accepted idea that the magnetic field plays a significant role for jet creation. A collimating structure is reported for M87 (Vir A, Junor et al. 1999). They found a jet with opening angle of 60° under 0.1 pc scale. The wide-opened jet is collimated into a limb-brightened narrower jet continuing up to 1 kpc. Junor et al. (1999) noted that magneto-hydrodynamic (MHD) models involving accretion disks are favored for the acceleration and collimation of jets based on the collimating structure found in M87 (Shibata and Uchida, 1985; Ouyed and Pudritz 1997). The structure of bending jet in Cen A is quite similar to one side of two ridges of collimating jet of M87. Moreover, the spatial scale of bending is roughly the same (a few light-months). Thus the jet in Cen A could be bent due to the same origin with that of M87, although it is not certain why only one side of ridges is seen in Cen A.

Tingay et al. (1998) suggested that there is a high-speed, unseen jet, based on the internal structure change of knots. They discussed that the observed knots are slow-moving patterns of the flow. The bending jet could be a filament structure enclosing the high-speed jet along with their interpretation.

These possible interpretations of the bending jet would be tested by future monitoring the changing of the structure.

**Acknowledgements.** The author gratefully acknowledges the VSOP Project, which is led by the Japanese Institute of Space and Astronautical Science in cooperation with many organizations and radio telescopes around the world.

## References

Tingay, S.J. et al. 1998, *AJ*, **115**, 960

Hirabayashi, H. et al. 1998, *Science*, **281**, 1825

Conway, J.E. & Murphy, D.W. 1993, *ApJ*, **411**, 89

Junor, W., Biretta, J.A. & Livio, M. 1999, *Nature*, **401**, 891

Shibata, K. & Uchida, Y. 1985, *PASJ*, **37**, 31

Ouyed, R. & Pudritz, R.E. 1997, *ApJ*, **482**, 712

*Astrophysical Phenomena Revealed by Space VLBI*
*H. Hirabayashi, P.G. Edwards and D.W. Murphy (eds.)*

# VSOP Observations of a Sub-Parsec Accretion Disk

D.L. Jones, A.E. Wehrle, B.G. Piner & D.L. Meier

*Jet Propulsion Laboratory, California Institute of Technology, USA*

**Abstract**

The physical conditions in the inner parsec of accretion disks believed to orbit the central black holes in active galactic nuclei can be probed by imaging the absorption of background radio emission by ionized gas in the disk. We report high angular resolution observations of the nearby galaxy NGC 4261 which show evidence for free-free absorption by a thin, nearly edge-on disk at several frequencies. The angular width, and probably the depth, of the absorption appears to increase with decreasing frequency, as expected. Because free-free absorption is much larger at lower frequencies, the longest possible baselines are needed to provide adequate angular resolution; observing at higher frequencies to improve resolution will not help.

## 1 Introduction

The nearby FR-I radio galaxy NGC 4261 (3C270) is a good candidate for the detection of free-free absorption by ionized gas in an inner accretion disk. The galaxy is known to contain a central black hole with a mass of $5 \times 10^8$ $M_\odot$, a nearly edge-on nuclear disk of gas and dust with a diameter of $\approx 100$ pc, and a large-scale symmetric radio structure which implies that the radio axis is close to the plane of the sky. At an assumed distance of 40 Mpc, 1 milliarcsecond (mas) corresponds to 0.2 pc. Previous VLBA observations of this galaxy revealed a parsec-scale radio jet and counterjet aligned with the kpc-scale jet (see Figure 1). The opening angle of the jets is less than $20^\circ$ during the first 0.2 pc and $< 5^\circ$ during the first 0.8 pc. At 8.4 GHz we found evidence for a narrow gap in radio brightness at the base of the parsec-scale counterjet, just east (left) of the brightest peak which we identified as the core based on its inverted spectrum between 1.6 and 8.4 GHz (see the left part of Figure 2, from Jones and Wehrle 1997). We tentatively identified this gap as the signature of free-free absorption by a nearly-edge on inner disk with a width $<<$ 0.1 pc and an average electron density of $10^3 - 10^8$ cm$^{-3}$ over the inner 0.1 pc.

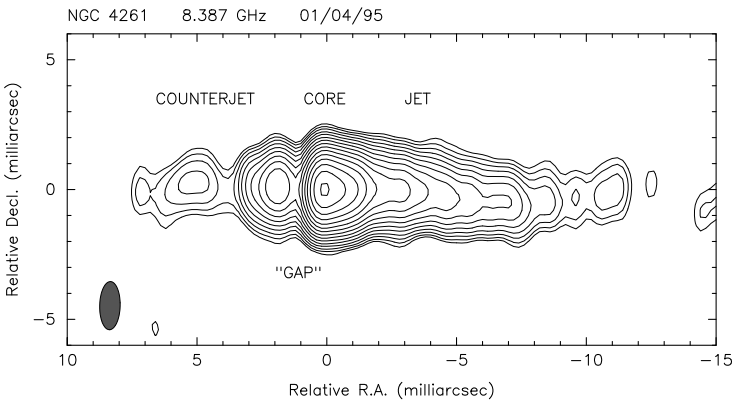


Figure 1: VLBA image of NGC 4261 at 8.4 GHz. The contours increase in steps of $\sqrt{2}$ starting at $\pm 0.75\%$ of the peak, which is 99 mJy/beam. The restoring beam is $1.86 \times 0.79$ mas with major axis PA $= -1.3°$.

## 2 Observations

We observed NGC 4261 at 1.6 and 4.9 GHz with HALCA and a ground array composed of 7 VLBA antennas plus Shanghai, Kashima, and the DSN 70-m Tidbinbilla antennas at 1.6 GHz (22 June 1999) and 8 VLBA antennas plus the phased VLA at 4.9 GHz (27 June 1999). During both epochs the VLBA antennas at St. Croix and Hancock were unavailable, as was the North Liberty antenna at 1.6 GHz. Data were recorded as two 16-MHz bandwidth channels with 2-bit sampling by the Mark-III/VLBA systems and correlated at the VLBA processor in Socorro. Both channels were sensitive to left circular polarization.

Fringe-fitting was carried out in AIPS after applying *a priori* amplitude calibration. For VLBA antennas we used continuously measured system temperatures, for the VLA we used measured $T_A/T_{SYS}$ values with an assumed source flux density of 5 Jy, and for the remaining antennas we used typical gain and system temperature values obtained from the VSOP web site. Fringes were found to all antennas at 1.6 GHz except HALCA, but the signal/noise ratio to Shanghai and Kashima was very low and these data were not used. The *a priori* amplitude calibration for Tidbinbilla was dramatically incorrect for unknown reasons. We calibrated Tidbinbilla by imaging the compact structure of the source using VLBA data, then holding the VLBA antenna gains fixed and allowing the Tidbinbilla gain to vary. This produced a good match

in correlated flux density where the projected VLBA and Tidbinbilla baselines overlap. At 4.9 GHz fringes were found to all antennas, including HALCA. A similar correction to the *a priori* amplitude calibration for HALCA and the phased VLA was applied.

In both observations we found that averaging in frequency over both 16-MHz channels in AIPS produced large, baseline-dependent amplitude reductions even though the post-fringe-fit visibility phases were flat and continuous between channels. Averaging over frequency within each 16-MHz band separately fixed this problem. Difmap was used for detailed data editing, self-calibration, and image deconvolution. Both 16-MHz bands were combined during imaging.

Imaging within Difmap used uniform weighting with the weight of HALCA data increased by a factor of 500. Several iterations of phase-only self calibration, followed by amplitude self calibration iterations with decreasing time scales, resulted in good fits ($\chi^2 \approx 1$) between the source model and the data.

## 3 Results

### 3.1 1.6 GHz

Although our image at 1.6 GHz does not include data from HALCA, it does have more than twice the angular resolution of our previous 1.6 GHz image (Jones and Wehrle 1997) due to the addition of Tidbinbilla. The previous image showed a symmetric structure, with the jet and counter-jet extending west and east from the core. No evidence for absorption is seen in this image. However, with higher resolution we do detect a narrow gap in emission just east of the core, at the base of the counterjet. The width of the gap is less than 2 mas.

### 3.2 4.9 GHz

We detected fringes to HALCA at 4.9 GHz when the projected Earth-space baselines were less than one Earth diameter. The HALCA data fills in the $(u, v)$ coverage hole between continental VLBA baselines and those to Mauna Kea, and also increases the north-south resolution by a factor of two. Our 4.9 GHz image is shown in Figure 2. Note that the gap in emission is again seen just east of the peak. A careful comparison of brightness along the radio axis at 4.9 and 8.4 GHz shows that the gap is both deeper and wider at 4.9 GHz, as expected from free-free absorption. The region of the gap has a very inverted spectrum, the brightest peak

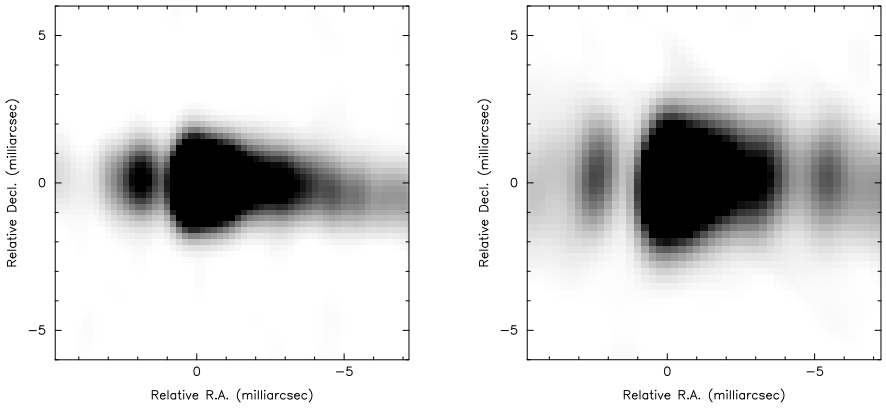


Figure 2: Grey-scale images of the nucleus of NGC 4261 at 8.4 GHz (left) and 4.9 GHz (right), with identical fields of view.

(core) has a slightly less inverted spectrum, and the distant parts of both the jet and counterjet have steep spectra.

## 4 Summary

Our observations at 1.6 and 4.9 GHz appear to confirm the free-free absorption explanation for the sub-parsec radio morphology in NGC 4261. Measurements of the optical depth in the absorbed region and the distance between the absorption and the core as a function of frequency will allow the radial distribution of electron density in the inner parsec of the disk to be determined.

**Acknowledgements.** We gratefully acknowledge the VSOP Project, which is led by the Japanese Institute of Space and Astronautical Science in cooperation with many organizations and radio telescopes around the world. This research was carried out at the Jet Propulsion Laboratory, California Institute of Technology, under contract with the U.S. National Aeronautics and Space Administration.

## References

Jones, D.L. & Wehrle, A.E. 1997, *ApJ*, **484**, 186

*Astrophysical Phenomena Revealed by Space VLBI*
*H. Hirabayashi, P.G. Edwards and D.W. Murphy (eds.)*

# Detection of the VLBI-Scale Counter Jet in NGC 6251

H. Sudou[1], Y. Taniguchi[1], Y. Ohyama[2], S. Kameno[2],
S. Sawada-Satoh[2], M. Inoue[2], O. Kaburaki[1], & T. Sasao[2],

[1] *Astronomical Institute, Tohoku Univ., Aoba, Sendai 980-8578, Japan*
[2] *NAO, Osawa 2-21-1, Mitaka, Tokyo 181-8588, Japan*

**Abstract**

Mapping the central 5 pc region of the nearby radio galaxy NGC 6251 with a 0.2 pc resolution using VLBI at two radio frequencies, 5 GHz and 15 GHz, we have found the sub-pc-scale counter jet for the first time in this radio galaxy. This discovery allows us to investigate the jet acceleration based on the relativistic beaming model (Ghisellini et al. 1993).

## 1 Introduction

The genesis of powerful radio jets from active galactic nuclei is one of the long standing problems in astrophysics (Bridle & Perley 1984). Although global morphological properties give us very important information, the very inner regions in the radio jets also provide hints to understanding the genesis of radio jets. In order to investigate radio galaxies at sub–milli-arcsecond angular resolution, we have performed new high-resolution VLBI observations of NGC 6251 using HALCA (Hirabayashi et al. 1998). We use a distance to NGC 6251 of 94.4 Mpc (for a Hubble constant $H_0 = 75$ km s$^{-1}$ Mpc$^{-1}$). Note that 1 mas (milli-arcsecond) corresponds to 0.48 pc at this distance.

## 2 Observations

NGC 6251 was observed at 5 GHz using VSOP on 30 April 1998 and at 15 GHz using VLBA on 2 June 1998. Details of the observations are summarized in Table 1. In order to perform beam-size-matched comparison between 5 GHz and 15 GHz, we restored the two images with a same spatial resolution of $0.50 \times 0.50$ mas.

Table 1: Observations.

| Epoch | $\nu$ (GHz) | Stations | Peak Int. (Jy/beam) | RMS noise (mJy/beam) | DR[1] |
|---|---|---|---|---|---|
| 1998.33 | 5 | VLBA, HALCA, EB[2] | 0.13 | 0.50 | 260 |
| 1998.42 | 15 | VLBA | 0.34 | 0.25 | 1400 |

[1]DR : Dynamic range; [2]EB : Effelsberg 100-m telescope

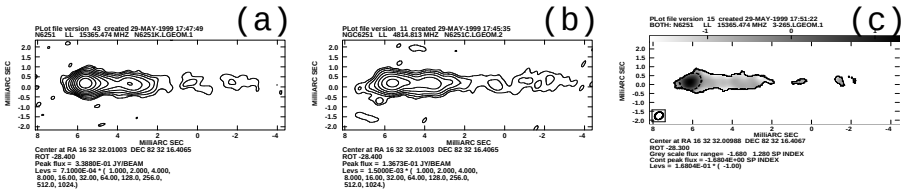


Figure 1: The images of NGC 6251 at 15 GHz (a) and at 5 GHz (b). The images are rotated clockwise on the sky by 28°. The spectral index map is shown in (c). Here the spectral index $\alpha$ is defined as $S_\nu \propto \nu^\alpha$.

## 3 Results

Our final maps at 15 GHz and 5 GHz are shown in Figure 1a and 1b, respectively. Although the secondary peak is seen at both frequencies, its angular distance from the 15 GHz brightest peak is larger by 0.3 mas (0.14 pc) than that at 5 GHz. This difference may be attributed to the different opacity toward the central engine at 5 GHz and 15 GHz.

Here we apply two new methods for the registration using correlation functions between intensity profiles and between wiggling patterns of the radio jet at the two frequencies. The correlation function of intensity profiles exhibits the maximum correlation coefficient $\simeq 0.98$ at an offset of $0.30 \pm 0.11$ mas, indicating that the peak at 5 GHz is shifted to the jet direction from that at 15 GHz. Analysis of wiggling patterns gives an offset of $0.60 \pm 0.36$ mas with a correlation coefficient of $\simeq$0.66. Since these two offsets were obtained using two independent methods, we adopt a weighted average of the two offsets. Thus the best offset of $0.42 \pm 0.14$ mas is obtained. Using this offset, we register the two images and obtain a spectral index image of the radio jet as shown in Figure 1c. An optically thin component on the opposite side of the jet can be seen. We conclude that this is the real counter jet.

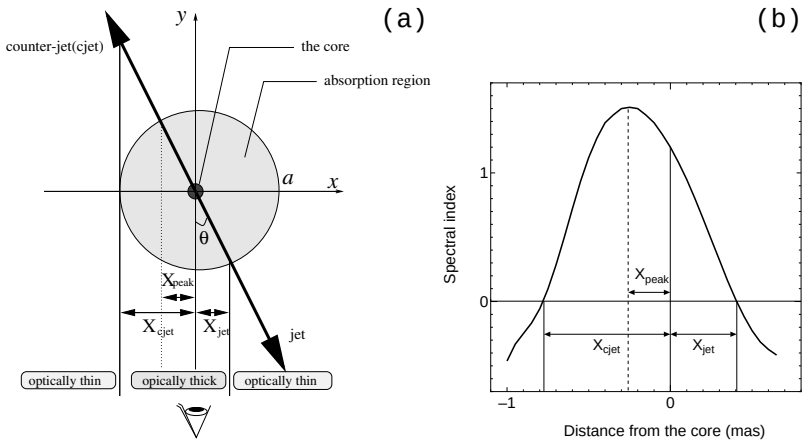


Figure 2: A schematic illustration of the spherical-absorption model (a), and spectral index variation along the radio jet of NGC 6251 (b).

## 4 Discussions

We assume for simplicity that the core is surrounded by a plasma sphere with a radius of $a$ and the radio emission from the inner part of the jets (i.e., both the jet and the counter jet) suffer from free-free absorption. The approaching jet escapes from the plasma sphere at a projected distance of $x = a \times \sin\theta_{\rm jet}$ and thus the spectral index is its intrinsic value here. The counter jet suffers the effect of free-free absorption until $x = -a$. It is also noted that the path length is longest at $x = -a \times \sin\theta_{\rm jet}$. As shown in Figure 2a, we define the following projected distances; $X_{\rm jet} = X_{\rm peak} = a \times \sin\theta_{\rm jet}$ and $X_{\rm cjet} = a$. Then we are able to estimate $\theta_{\rm jet} = \sin^{-1}\left(\frac{X_{\rm jet}}{X_{\rm cjet}}\right)$. We adopt the 15 GHz brightest peak as the core, because the optical depth at 15 GHz is sufficiently small in the case of free-free absorption. In Figure 2b, we show the observed spectral index variation along the radio jet. We estimate $X_{\rm peak} \approx 0.24$ mas, $X_{\rm jet} \approx 0.41$ mas, and $X_{\rm cjet} \approx 0.80$ mas. Then we obtain $\theta_{\rm jet} \simeq 31°$.

Adopting the so-called Doppler beaming model, the jet–to–counter-jet intensity ratio $R$ can be written as a function of projected distance $x$, $R(x) = \left[\frac{1+\beta_{\rm jet}(x)\cos\theta_{\rm jet}(x)}{1-\beta_{\rm jet}(x)\cos\theta_{\rm jet}(x)}\right]^{2-\alpha(x)}$, where $\beta_{\rm jet}(x) = v_{\rm jet}(x)/c$. In Figure 3a, we measured $R$ as a function of $x$. It is shown that $R$ is estimated to be systematically larger at 5 GHz than those at 15 GHz. This is probably due to stronger absorption at 5 GHz than at 15 GHz. It is shown that

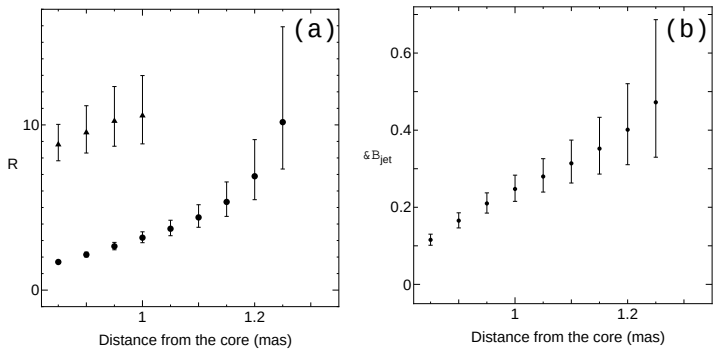


Figure 3: The jet/counter jet flux density ratio $R$ as a function of the projected distance from the brightest peak at 15 GHz for the 5GHz data (filled triangles) and for the 15 GHz data (filled circles) (a), and jet velocity $\beta_{\rm jet}$ as a function of projected distance from the brightest peak at 15 GHz (b).

$R$ at 15 GHz increases from 1.7 at 0.85 mas (0.4 pc) to 10 at 1.25 mas (0.6 pc) with projected distance from the core. If this increase is just caused by the Doppler beaming, it is suggested that $\beta_{\rm jet}$ increases with distance, because $\theta_{\rm jet}$ does not appear to vary significantly. Figure 3b shows that the jet is accelerated from $\beta_{\rm jet} \approx 0.1$ at 0.4 pc to $\beta_{\rm jet} \approx 0.5$ at 0.6 pc. This provides the first direct evidence for the acceleration in the sub-pc-scale radio jet.

**Acknowledgements.** We gratefully acknowledge many staff members of VLBA and VSOP who operated observations without whom this study would not have been possible.

## References

Bridle, A.H. & Perley, R.A. 1984, *ARA&A*, **22**, 319,

Ghisellini, G., Padovani, P., Celotti, A. & Maraschi, L. 1993, *ApJ*, **407**, 65

Hirabayashi, H., Hirosawa, H., Kobayashi, H. *et al.* 1998, *Science*, **281**, 1825 and erratum **282**, 1995

*Astrophysical Phenomena Revealed by Space VLBI*
*H. Hirabayashi, P.G. Edwards and D.W. Murphy (eds.)*

# A Study of Young Radio-Loud AGN Using Space-VLBI

Ignas Snellen[1] *, Wolfgang Tschager[2], Richard Schilizzi[3,2]
Huub Röttgering[2] & George Miley[2]

[1] *Institute of Astronomy, Madingley Road, Cambridge CB3 0HA, UK*
[2] *Sterrewacht Leiden, Postbus 9513, 2300 RA Leiden, The Netherlands*
[3] *Joint Institute for VLBI in Europe, Postbus 2, 7990 AA, Dwingeloo, The Netherlands*

**Abstract**

Gigahertz Peaked Spectrum (GPS) sources form a key element in the study of the onset and evolution of radio-loud AGN, since they are most likely the young counterparts of extended radio sources. Here we discuss space-VLBI observations of GPS sources, which enable us to obtain unprecedented angular resolution at frequencies near their spectral turnovers. Observed peak brightness temperatures of $10^{10.5-11}$ Kelvin indicate that synchrotron self absorption is responsible for their spectral turnovers. This is in close agreement with previous size – spectral turnover statistics for GPS sources. The combination of these new space-VLBI observations with ground-based VLBI observations taken at an earlier epoch, confirm the young ages for the most compact GPS galaxies of several hundred years.

## 1 Young Radio-Loud AGN

Although radio-loud Active Galactic Nuclei (AGN) have been studied for several decades, still not much is known about their birth and subsequent evolution. The recent identification of a class of very young radio sources can be considered as a major breakthrough in this respect, since it has opened many unique opportunities for radio source evolution studies.

Unfortunately, the nomenclature and use of acronyms in this field of research is rather confusing. This is mainly caused by the different ways in which young radio sources are selected. Selection of young sources is made in two ways, the first based on their broadband radio spectra,

*This research was supported by the European Commission, TMR Programme, Research Network Contract ERBFMRXCT96-0034 "CERES", and the TMR Access to Large-scale Facilities programme under contract No. ERBFMGECT950012

and the second based on their compact morphology. A convex shaped spectrum, peaking at about 1 GHz distinguishes young radio sources from other classes of compact radio sources. In this case they are called Gigahertz Peaked Spectrum (**GPS**) radio sources (e.g., O'Dea et al. 1991; O'Dea 1998). Similar objects, which are typically an order of magnitude larger in size, have their spectral turnovers shifted to the 10−100 MHz regime, causing them to be dominated at cm wavelengths by the optically thin parts of their spectra. These are called Compact Steep Spectrum (**CSS**) radio sources to distinguish them from the general population of extended steep spectrum sources (e.g., Fanti et al. 1990).

On the other hand, young radio sources are found in multi-frequency VLBI surveys, in which they can be recognised by compact jet/lobe-like structures on both sides of their central core. They are called Compact Symmetric Objects (**CSO**, Wilkinson et al. 1994). Their double sided structures clearly distinguish them from the large majority of compact sources showing one-sided core-jet morphologies. This implies that the luminosities of CSO are unlikely to be substantially enhanced by Doppler boosting. Larger versions of CSOs are subsequently called Medium Symmetric Objects (**MSO**) and Large Symmetric Objects (**LSO**).

The overlap between the classes of CSO and GPS galaxies is large and we believe that they can be considered to be identical objects. However, note that a substantial fraction of GPS sources are optically identified with high redshift quasars, which in general show core-jet structures (Stanghellini et al. 1997). The relationship between GPS quasars and GPS galaxies/CSO is not clear and under debate (Snellen et al. 1999). We therefore believe it is wise to restrict evolution studies to GPS galaxies and CSOs.

### Evidence for Youth

Although it was always speculated that GPS sources were young objects, only recently has strong evidence been found to support this hypothesis. Monitoring several GPS sources over a decade or more using VLBI, allowed Owsianik & Conway (1998) and Owsianik, Conway & Polatidis (1998) to measure the hotspot advance speeds of several prototype GPS sources to be $\sim 0.1h^{-1}c$. These imply dynamical ages of typically $10^{2-3}$ years.

Additional proof for youth comes from analysis of the overall radio spectra of the somewhat larger CSS sources. Murgia et al. (1999) show that their spectra can be fitted with synchrotron aging models, implying

ages of typically $10^{3-5}$ years.

The work of these authors shows that GPS/CSO sources are very young and most likely the progenitors of large, extended radio sources. This makes them key objects for radio source evolution studies.

### Tools for Radio Source Evolution Studies

Several authors have used number count statistics and linear size distributions to constrain the luminosity evolution of radio sources (Fanti et al. 1995; Readhead et al. 1996; O'Dea & Baum 1997). All these studies find an excess of young objects in relation to the number of old, extended radio sources. This over-abundance of GPS and CSS sources has generally been explained by assuming that a radio source significantly decreases in luminosity over its lifetime. In this way, sources are more likely to contribute to flux density limited samples at young than at old age, causing the apparent excess.

However, in addition to their over-abundance, GPS galaxies are found to be significantly more biased towards high redshift than large extended radio galaxies (Snellen & Schilizzi 2000). This is puzzling since classes of sources representing similar objects at different stages of their evolution are expected to have similar birth functions and redshift distributions. Furthermore, it suggests that the interpretation of their number count statistics, which are averaged over a large redshift range, is not so straightforward. We have postulated a simple evolution scenario which can resolve these puzzles. We argue that the luminosity evolution of a radio-loud AGN during its first $10^5$ years is qualitatively very different from that during the rest of its lifetime. This may be caused by a turnover in the density profile of the interstellar/intergalactic medium at the core-radius of the host galaxy, resulting in an increase in luminosity for young, and a decrease in luminosity for old radio-loud AGN with time. Such a luminosity evolution results in a flatter collective luminosity function for the young objects, causing their bias towards higher redshifts, and their over-abundance at bright flux density levels (Snellen et al. 2000).

An alternative explanation is that GPS sources are indeed young AGN, but mainly short-lived objects, which will never evolve into extended radio sources (Readhead et al. 1994). In that case, the two populations are not directly connected, and no similar cosmological evolution or redshift distribution is necessary.

Table 1: Status of VSOP observations.

| Name | id | $z$ | Date of Obs 5 GHz | Date of Obs 1.6 GHz |
|---|---|---|---|---|
| 0108+388 | Gal | 0.669 | 1999.08.06 | 1999.08.05 |
| 0248+430 | QSO | 1.316 | 1999.02.15 | 1999.08.18 |
| 0552+398 | QSO | 2.370 | 1999.03.23 | 1999.01.15 |
| 0615+820 | QSO | 0.710 | 1999.09.18 | tbd |
| 0646+600 | QSO | 0.460 | 1999.09.20 | 1999.09.27 |
| 1333+459 | QSO | 2.450 | 1998.06.22 | 1999.05.28 |
| 1404+286 | Gal | 0.077 | 1998.06.30 | tbd |
| 2021+614 | Gal | 0.227 | 1997.11.16 | 1999.09.28 |
| 1550+582 | QSO | 1.324 | 1998.07.02 | – |
| 1622+665 | Gal | 0.201 | 1998.05.24 | – |
| 0636+680 | QSO | 3.180 | 1999.09.19 | – |

## 2 Space-VLBI Observations of GPS Sources

In general, the angular resolution of VLBI observations at a certain observing frequency is limited by the size of the earth. The combination of ground VLBI stations with the Japanese satellite HALCA (part of the VLBI Space Observatory Programme VSOP), achieves a resolution typically 3 times higher than this ($\sim 1.5$ mas and $\sim 0.5$ mas at 1.6 and 5 GHz respectively). In particular, the study of GPS sources benefits from VSOP, since observing at a higher frequency to achieve a similar resolution is often not an option, because of their steep fall-off in flux density towards high frequency. Furthermore, their physical properties are most interesting around their spectral turnover, where differences in spectral indices within the source are more prominent than at high frequency.

We have been awarded VSOP observing time for 11 and 8 of the brightest and most compact GPS sources at 5.0 and 1.6 GHz respectively. Details and status of the observations are listed in Table 1. At the time of writing, all targets at 5 GHz, and 6 of the 8 sources at 1.6 GHz have been observed.

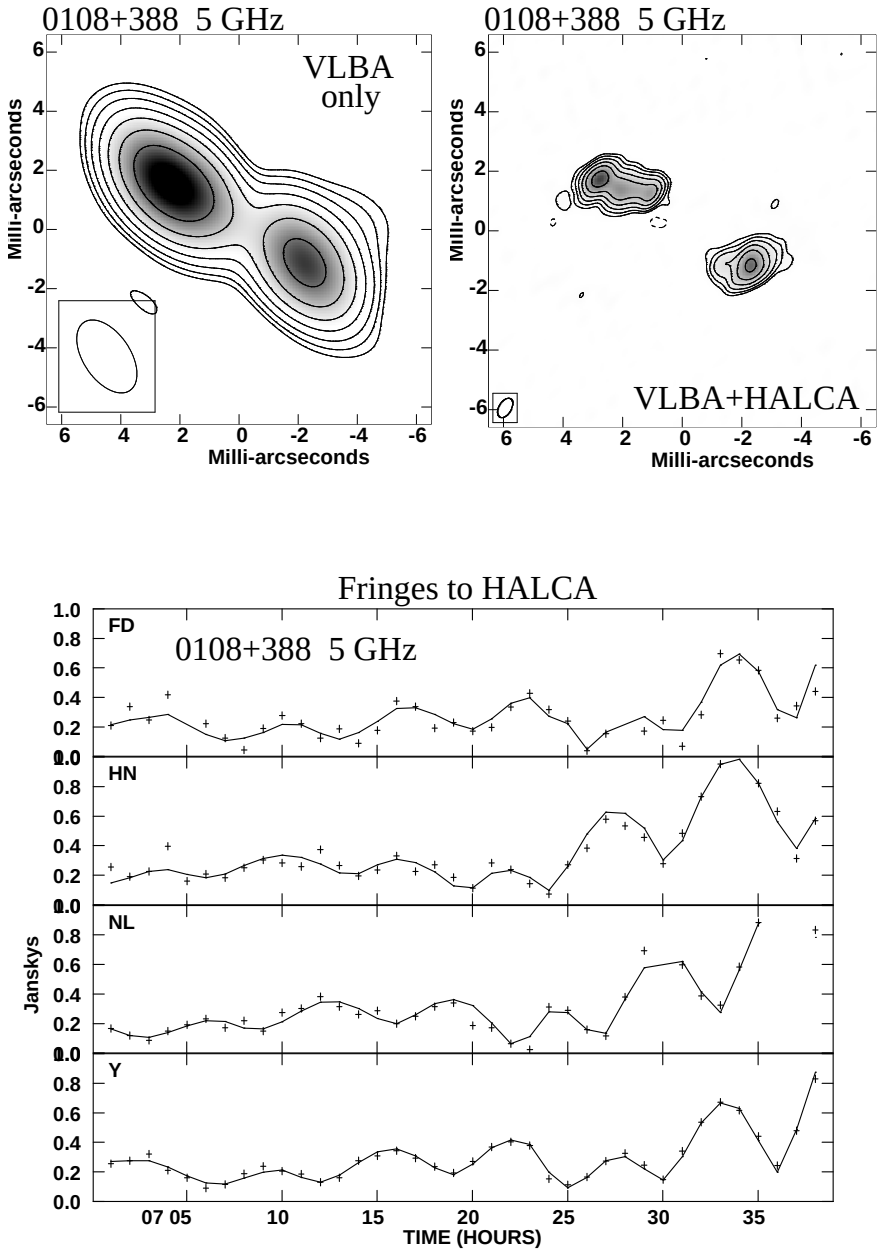


Figure 1: VSOP observations of 0108+388 at 5 GHz. The upper left panel shows the VLBA only image, the upper right panel shows the VLBA+HALCA image, and the lower panel shows some of the fringes of the VLBA antennas and the VLA to HALCA.

### First Results and Discussion

A large fraction of the sources have now been imaged. Some examples are shown in Figures 1 and 2. Additional observations have been taken at 15 GHz with the VLBA to match the 5 GHz VSOP data in resolution, which will allow detailed spectral decompositions of the objects. In particular, this may sched new light on the nature of the GPS quasars and the role of Doppler boosting in these sources.

One of the first results of these observations are the high brightness temperatures observed of typically $10^{10.5-11}$ Kelvin. This indicates that these objects must be near their synchrotron self absorption (SSA) turnover at the observed frequency, making it very likely that indeed SSA is the cause of their spectral peaks. This is in agreement with the statistical arguments of Snellen et al. (2000), who found that among samples of GPS and CSS sources, the ratio of component size, as derived from the spectral peak assuming SSA, and overall angular size, are constant and very similar to those found for large extended radio sources. This not only implies self-similar evolution, but also provides strong evidence for SSA. Note however, that several authors argue that free-free absorption can not be ruled out for the smallest GPS galaxies (Kameno et al., these proceedings; Marr et al., these proceedings)

A valuable spin-off from these high angular resolution VSOP observations come from their comparison with ground-based VLBI images taken at an earlier epoch. Following the method of Owsianik & Conway (1998), we use these to derive dynamical ages for GPS sources. In this way, we find that the two dominant components at 5 GHz of 2021+614 (Fig. 2), have a larger separation at the epoch of the VSOP observations, compared to data from Conway et al. (1994) taken in 1982 and 1987. The increase in separation indicates a hotspot advance speed of $\sim 0.1$c, which implies an age of $\sim 400$ years for these components (Tschager et al. 2000). Preliminary analysis of 0108+388 (fig 1) shows an advance speed of 15 $\mu$as/yr, consistent with what is found by Owsianik, Conway & Polatidis (1998; 9 $\mu$as/yr). These observations confirm the young ages of a few hundred years for the most compact GPS galaxies.

## 3 Summary

GPS galaxies and CSO are now identified as classes of young radio sources. They form a key element in the investigation of the evolution of radio-loud AGN. We report on VSOP observations of 11 and

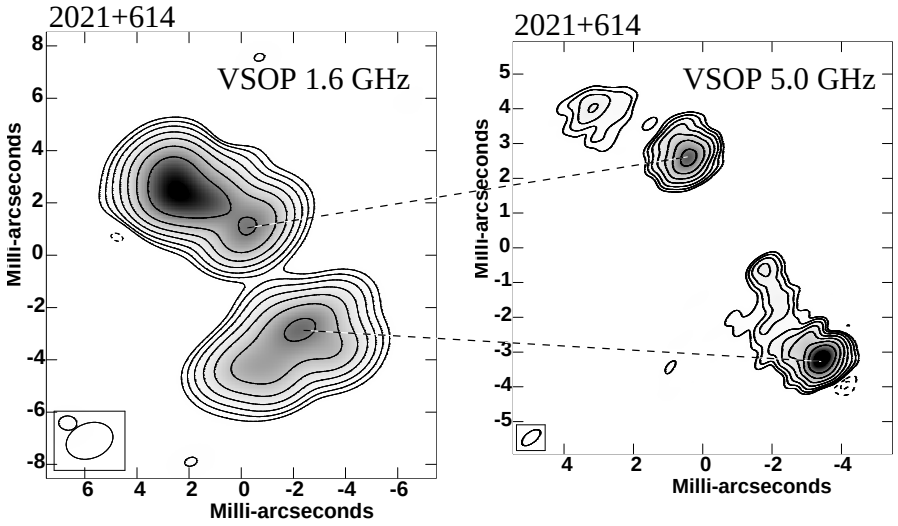


Figure 2: VSOP observations of 2021+614 at 1.6 and 5 GHz. The dotted lines connect the two dominant features at 5 GHz with their position at 1.6 GHz. Note the importance of sufficient resolution near the spectral turnover frequency, where the differences in spectral index between the components are most prominent.

8 bright GPS sources at 5.0 and 1.6 GHz frequency respectively. First analysis indicates high brightness temperatures consistent with synchrotron self absorption as the cause of their spectral turnover. Comparison with ground-based VLBI datasets taken at earlier epochs confirm the very young ages for the most compact GPS galaxies of a few hundred years.

**Acknowledgements.** We gratefully acknowledge the VSOP Project, which is led by the Japanese Institute of Space and Astronautical Science in cooperation with many organizations and radio telescopes around the world.

## References

Conway, J.E., Myers, S.T., Pearson, T.J. et al. 1994, *ApJ*, **425**, 568

Fanti, R., Fanti, C., Schilizzi, R.T. et al. 1990, *A&A*, **231**, 333

Fanti, C., Fanti, R., Dallacasa, D. et al. 1995, *A&A*, **302**, 317

Kameno, S. et al., *these Proceedings*

Marr, J. et al., *these Proceedings*

Murgia, M., Fanti, C., Fanti, R., Gregorini, L., Klein, U., Mack, K-H., Vigotti, M., 1999, *A&A*, **345**, 769

O'Dea, C.P., Baum, S.A., Stanghellini, C., 1991, *ApJ*, **380**, 66

O'Dea, C.P., Baum, S.A., 1997, *AJ*, **113**, 148

O'Dea, C.P., 1998, *PASP*, **110**, 493

Owsianik, I. & Conway, J.E., 1998, *A&A*, **337**, 69

Owsianik, I., Conway, J.E., Polatidis, A.G., 1998, *A&A*, **336**, L37

Readhead, A.C.S, Xu, W., Pearson, T.J., 1994, in *Compact Extragalactic Radio Sources*, eds J.A. Zensus & K.I. Kellermann, 19

Readhead, A.C.S., Taylor, G.B., Xu, W., Pearson, T.J., Wilkinson, P.N., 1996, *ApJ*, **460**, 634

Snellen, I.A.G., Schilizzi, R.T., Bremer, M.N et al. 1999, *MNRAS*, **307**, 149

Snellen, I.A.G., & Schilizzi, R.T., 2000 Proc. 'Lifecycles of Radio Galaxies' workshop, ed. J. Biretta et al., to appear in *New Astronomy Reviews*

Snellen, I.A.G., Schilizzi, R.T., Miley, G.K. et al. 2000, *MNRAS*, submitted

Stanghellini, C., O'Dea, C.P., Baum, S.A., Dallacasa, D., Fanti, R., Fanti, C., 1997, *A&A*, **325**, 943

Tschager, W., Schilizzi, R.T., Röttgering,, H.J.A., Snellen, I.A.G., Miley, G.K., 2000, submitted to *A&A*

Wilkinson, P.N., Polatidis, A.G., Readhead, A.C.S., Xu, W. and Pearson, T.J., 1994, *ApJ*, **432**, L87

*Astrophysical Phenomena Revealed by Space VLBI*
*H. Hirabayashi, P.G. Edwards and D.W. Murphy (eds.)*

# Pentachromatic VSOP and VLBA Survey of GPS Sources

S. Kameno[1], S. Sawada-Satoh[1], K. M. Shibata[1], M. Inoue[1] & K. Wajima[2]

[1] *NAO, Osawa 2-21-1, Mitaka, Tokyo 181-8588, Japan*
[2] *ISAS, Yoshinodai 3-1-1, Sagamihara, Kanagawa 229-8610, Japan*

**Abstract**

We report an early results of the GPS survey project using the VSOP and the VLBA at 5 frequencies. All 9 objects observed with the VLBA at 3 frequencies show a convex spectrum, which can be fit by the free-free absorption model. We find a significant difference in the FFA opacities between QSO- and RG-type samples. This result is consistent with Barthel's unified scheme between quasars and radio galaxies.

## 1 Introduction

GHz-Peaked Spectrum (GPS) sources are powerful radio sources, which have a compact overall size ($<$ 1 kpc) and a convex radio spectrum peaked at a GHz frequency (O'Dea et al. 1991). Their morphology and steep spectrum above the peak indicate that most of radio emission comes from double lobes. Since their lobes are extremely small, they are considered to be at a young stage ($10^3 - 10^5$ yrs) of the evolution (O'Dea 1998). There are two explanations for the spectral cut-off at low frequencies; synchrotron self-absorption (SSA) (Snellen 1997) and free-free absorption (FFA) (Bicknell et al. 1997). Our VSOP observation (Kameno et al. 2000) showed that FFA is preferable rather than SSA for the GPS source OQ 208. To confirm how common is FFA in GPS sources, we are conducting a pentachromatic (1.6, 2.3, 4.8, 8.4, and 15.4 GHz) GPS survey for 18 objects using the VSOP and the VLBA. Here we report early results for 9 sources at 3 frequencies with the VLBA.

## 2 The Sample, Observations, and Data Analysis

We selected 18 sample objects, based on the GPS catalog by de Vries et al. (1997), under the criteria: (1) the peak frequency $\nu_{\rm max}$ stands within our observing range, i.e., 1.6 GHz $< \nu_{\rm max} <$ 15 GHz, (2) since all sources

must be bright enough to be detected with the VSOP and the VLBA, we put the criteria $S_{1.6\mathrm{GHz}} > 0.1\,\mathrm{Jy}$, $S_{5\mathrm{GHz}} > 0.5\,\mathrm{Jy}$, and $S_{15\mathrm{GHz}} > 0.2\,\mathrm{Jy}$. We observed 9 of 18 objects with the VLBA in 24 hours on 1998 December 15. Every object was observed at 3 frequencies with 2–6 scans. After the correlation process with the NRAO VLBA correlator, we took fringe fitting with AIPS and imaging with Difmap.

Table 1: Flux densities and FFA parameters of each component

| Object & Optical ID | Component | Flux density 2.3 GHz (mJy) | 8.4 GHz (mJy) | 15.4 GHz (mJy) | $S_0$ (Jy) | $\tau_0$ |
|---|---|---|---|---|---|---|
| 0108+388 (Sy2) | A | 591± 3 | 574± 3 | 262± 2 | 16.1±1.5 | 11.6±0.75 |
| | B | 429± 3 | 286± 4 | 152± 2 | 8.2±1.5 | 9.7±1.25 |
| NGC1052 (Sy2) | A | 969± 6 | 1796± 6 | 1311± 2 | 70.0±1.9 | 17.4±0.47 |
| | B | <5.6 | 77± 1 | 489± 1 | | |
| | C | 13± 2 | 247± 2 | 189± 2 | 12.6±2.6 | 57.9±18.3 |
| 0248+430 (QSO) | A | 173± 2 | 92± 2 | 65± 1 | 3.0±1.2 | 9.2±2.82 |
| | B | 5± 1 | 8± 2 | 7± 1 | 0.3±1.4 | 16.5±50.1 |
| | C | 63± 2 | 549± 3 | 354± 1 | 21.0±1.6 | 28.0±4.20 |
| 0646+600 (QSO) | A | 360± 1 | 882± 2 | 866± 2 | 37.3±1.4 | 19.4±0.51 |
| | B | 402± 1 | 280± 1 | 120± 1 | 7.6±1.0 | 9.6±0.82 |
| 0738+313 (QSO) | A | 2635±15 | 2627± 4 | 2156± 5 | 88.8±1.8 | 13.0±0.30 |
| | B | 187±16 | 981± 4 | 912± 5 | 43.4±2.6 | 36.2±3.77 |
| 1333+459 (QSO) | A | 168± 6 | 319± 1 | 252± 1 | 10.9±0.8 | 17.8±2.76 |
| | B | 372± 9 | 204± 1 | 91± 1 | 5.5±0.7 | 8.2±1.66 |
| 1843+356 (QSO) | A | 828± 2 | 225± 1 | 98± 2 | 5.8±0.9 | 4.0±0.94 |
| | B | 143± 2 | 221± 1 | 119± 2 | 6.6±1.1 | 14.6±1.96 |
| 2050+364 (RG) | A | 1892±10 | 876± 3 | 247± 2 | 22.1±1.4 | 6.9±0.47 |
| | B | 553± 9 | 136±13 | 65± 2 | 3.8±2.1 | 3.9±3.31 |
| | C | 800±11 | 229±23 | 77± 3 | 5.2±2.5 | 3.6±2.82 |
| | D | 752± 4 | 250± 8 | 48± 3 | 5.8±2.1 | 4.5±2.08 |
| 2149+056 (RG) | A | 771±20 | 572± 8 | 393± 6 | 18.8±0.8 | 12.5±0.49 |
| | B | 111± 4 | 47± 1 | 28± 1 | 1.3±0.9 | 1.9±4.01 |

## 3 Results and Discussion

We show all images by uniform weighting in Figure 1. Based on the images, we estimated a flux density of each lobe component using IMFIT in AIPS. We try model fitting based on the model: an optically thin synchrotron emission from the lobe is absorbed by external FFA plasma, $S_\nu = S_0 \nu^\alpha \exp(-\tau_0 \nu^{-2.1})$. Here, $S_\nu$ is the observed flux density, $S_0$ is the intrinsic flux density at 1 GHz, $\nu$ is the frequency, $\alpha$ is the intrinsic spectral index of the synchrotron emission, and $\tau_0$ is the FFA coefficient. The flux densities and fitting results are shown in Table 1 and Figure 2.

From the FFA fit, we find a significant difference between QSO-type and RG- or Sy2-type GPS samples. QSO-type sources show asymmetric

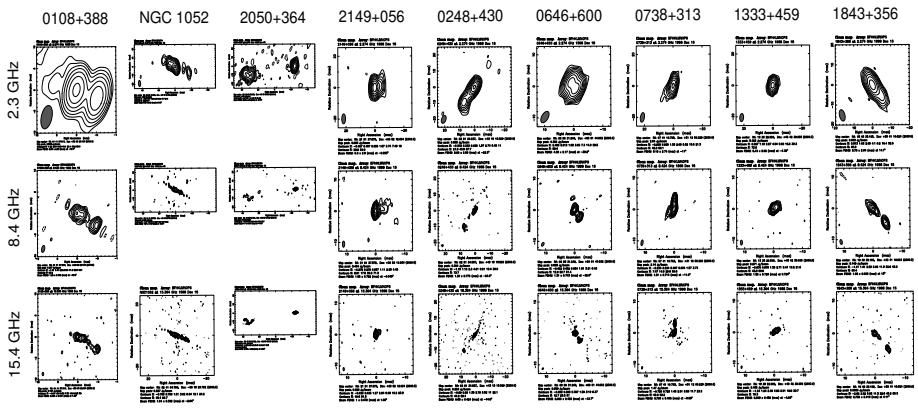


Figure 1: Trichromatic images of the GPS sources at 2.3, 8.4, and 15.4 GHz. Contours start at $\pm 3\sigma$ level, increasing by factors of 2.

FFA opacities towards double lobe, while RG- or Sy2-type sources have symmetric opacities. The histogram of the FFA opacity ratio $R$, defined as $R = \tau_{0\mathrm{A}}/\tau_{0\mathrm{B}}$ ($\tau_{0\mathrm{A}} > \tau_{0\mathrm{B}}$), clearly exhibits the difference (see Figure 3). We think that this result is related with Barthel's unified scheme between RGs and QSOs (Barthel 1989). If the line of sight is close to the jet axis, as thought to be QSO-type, a large difference of the path length in external plasma towards lobes causes an asymmetric FFA. In case of RG- or Sy2-type sample, the line of sight is nearly perpendicular to the jet axis, so that small difference in the path length results in a relatively symmetric FFA (see Figure 4).

## References

Barthel, P. 1989, *ApJ*, **336**, 606

Bicknell, G., Dopita, M. & O'Dea, C. 1997, *ApJ*, **485**, 112

de Vries, W., Barthel, P. & O'Dea, C. 1997, *A&A*, **321**, 105

Kameno, S., Horiuchi, S., Shen, Z.-Q. et al. 2000, *PASJ*, **56**, 1

O'Dea, C. 1998, *PASP*, **110**, 493

O'Dea, C., Baum, S. & Stanghellini, C. 1991, *ApJ*, **380**, 66

Snellen, I. 1997, *A Population Study of Faint Gigahertz Peaked Spectrum Sources*, PhD Thesis, Leiden Observatory.

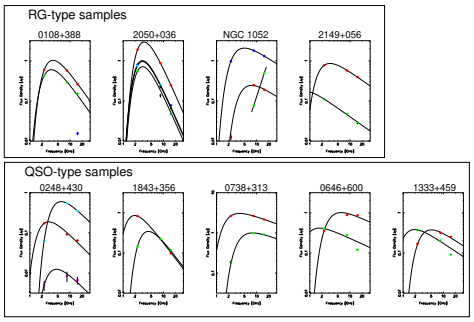


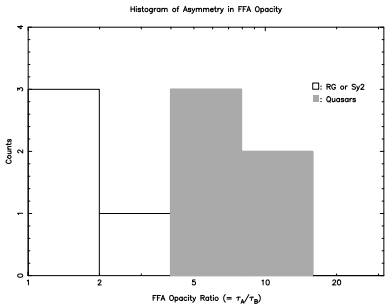


Figure 2: (left) Flux densities of each component at three frequencies (dots with an error bar) and the best-fit FFA model (solid lines).

Figure 3: (right) A histogram of the FFA asymmetry $R = \tau_{0\mathrm{A}}/\tau_{0\mathrm{B}}$. Open and filled areas indicate RG- and QSO-type sources, respectively.

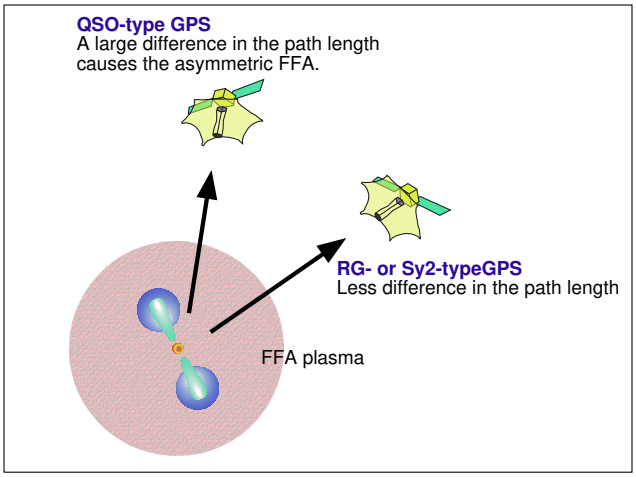


Figure 4: A schematic diagram of a GPS source. If the line of sight is close to the jet axis (QSO-type), a large difference in the path length causes asymmetric FFA. An RG-type source, on the contrary, has small difference in the path length, since the line of sight is nearly perpendicular to the jet axis.

*Astrophysical Phenomena Revealed by Space VLBI*
*H. Hirabayashi, P.G. Edwards and D.W. Murphy (eds.)*

# Free-Free Absorption by a Gas Disk in the GPS Radio Galaxy 0108+388

J.M. Marr[1], G.B. Taylor[2] & F. Crawford III[3]

[1] *Union College, Schenectady, NY, USA*
[2] *NRAO, Socorro, NM, USA*
[3] *MIT, Cambridge, MA, USA*

**Abstract**

We have observed the gigahertz-peaked spectrum source 0108+388 with the VLBA at a range of frequencies above and below the spectral peak. The activity that dominates the radio emission from 0108+388, which is also classified as a Compact Symmetric Object, is thought to be less than 1000 years old. Here we present evidence for a disk of gas in the central tens of parsecs that causes free-free absorption at low frequencies and may have triggered the recent onset of radio frequency activity. The spectral index maps obtained from our observations reveal that the radio spectra of a large area of the map turn over at about the same frequency, indicating that the turnover is due to foreground free-free absorption, rather than synchrotron self-absorption. The morphologies of the spectral index maps further show that the absorbing material is non-uniform and is suggestive of an edge-on disk centered on the core of the active galaxy. A rough model of free-free absorption by a disk of gas that fits the observed opacity maps is obtained.

We have observed the Gigahertz-Peaked Spectrum ("GPS") radio galaxy 0108+388 with the VLBA[1] at two frequencies above the spectral turnover, at the turnover frequency, and at two frequencies below the turnover. The sequence of maps reveal the point-by-point spectra of the radio emission and the morphology of the absorption. If the turnover is due to free-free ("f-f") absorption, one expects the whole source, or large parts of it, to get fainter with decreasing frequencies as the optical depth of the foreground screen increases. If the turnover is due to synchrotron self-absorption (or "SSA"), on the other hand, then small pieces of the source, where the magnetic field and electron density are greatest, will be opaque at higher frequencies and will decrease in intensity with decreasing frequency, while the more diffuse and lower magnetic field parts continue to increase in intensity.

[1]The VLBA is operated by the National Radio Astronomy Observatory, which is a facility of the National Science Foundation operated under cooperative agreement by Associated Universities, Inc.

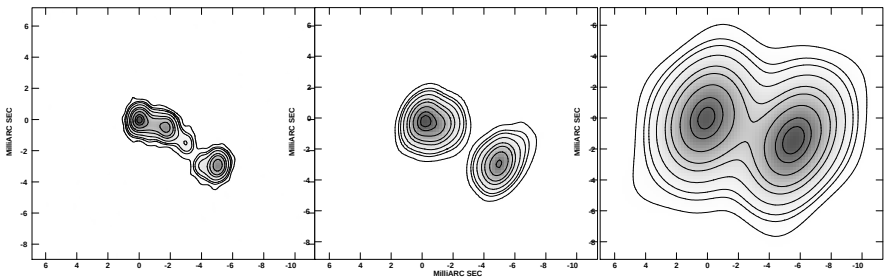


Figure 1: Clean maps at 15.3, 5.0, and 1.7 GHz. The displayed contours correspond to 1, 3, 5, 10, 20, 30, 50, 75, and 90% of the peak flux densities, which are 0.130, 0.396, and 0.221 Jy/beam, respectively.

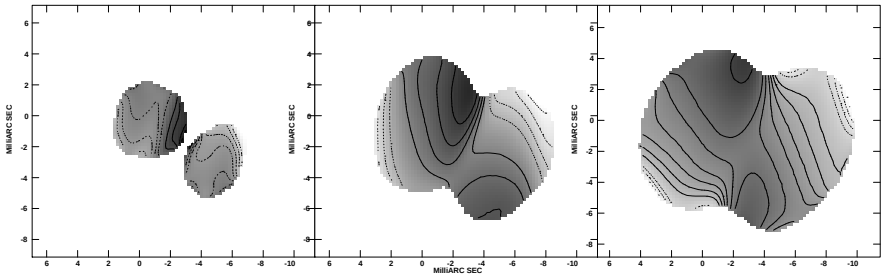


Figure 2: Spectral Index Maps between: 15.3 and 8.4 GHz, 8.4 and 5.0 GHz, 5.0 and 2.7 GHz, and 2.7 and 1.3 GHz. The contours represent spectral index values of $-3$, $-2$, $-1.6$, $-1.2$, $-0.9$, $-0.6$, $-0.3$, $+0.3$, 0.6, 0.9, 1.2, 1.6, 2.0, and 3.0, where $F_\nu \propto \nu^\alpha$.

Observations were made at 8.415, 4.983, 2.267, and 1.663 GHz on 24 June 1996 and at 15.349 and 8.415 GHz on 3 February 1997. The CLEAN maps at 15.3, 8.4, and 1.7 GHz are displayed in Fig. 1.

Spectral index maps between neighboring frequency bands were made from data sets that were edited to yield identical resolutions. The three lower frequency spectral index maps are shown in Fig. 2. The spectral index map between the two highest frequencies, not shown, is consistent with that found by Taylor et al. (1996); the two major components have steeply declining spectra and a small component in the middle, inferred to be the core, has an inverted spectrum. In the spectral-index map between 8.4 and 5.0 GHz, the spectra of the inner regions of the two major components are flatter, but the outer regions are still steeply inverted. Between 5.0 and 2.3 GHz, the spectra of all but the easternmost and westernmost edges are inverted. Between 2.3 and 1.7 GHz, the spectral index map looks similar to that between 2.3 and 5.0 GHz, except that the spectral indices are larger and the region

of inverted spectra encompasses almost the whole source. In both of the two lower frequency spectral index maps the region with inverted spectra appears to run across the map in the north-south direction. The most steeply inverted spectra are located in two areas north and south of the core at the edge of the mapped region.

The turnover of the composite spectrum at 5.0 GHz clearly results from the majority of the source turning over at this frequency. This is in conflict with the expectations for SSA but is consistent with f-f absorption by foreground gas. Additionally, the peak spectral index is 3.2, which is sufficiently greater than the maximum allowable spectral index with SSA. The general character of the spectral index distributions is also suggestive of an edge-on disk centered on the core.

To directly map the absorbing gas we made opacity maps. The creation of the opacity maps involves comparison of maps at all the observed frequencies (as described below), so we edited all data sets to have the same $(u,v)$ range. These truncated data sets had aspect ratios of only 9.0 but the resulting maps still had good fidelity; the final maps look very much like the 2.3 and 1.7 GHz clean maps made with the full data sets and the signal to noise ratios are higher. The fidelity of these maps result because the structure of this source is quite simple.

At each point in the map, we use the spectral index between 15.3 and 8.4 GHz to extrapolate the flux densities at 8.4 GHz to the lower frequencies. This produces reasonable estimates of the flux densities at 2.3 and 1.7 GHz in the absence of the absorbing medium. The optical depths at each point in the map at 2.3 and 1.7 GHz are then inferred by comparing the observed flux-densities with the extrapolated flux-densities. However, since the optical depths at 8.4 GHz are not really zero, the extrapolation of the spectrum produces a small error. We improve the inferred optical depths by iterating the procedure. The inferred optical depths at 2.3 and 1.7 GHz are used to infer the optical depths at 8.4 and 15.3 GHz (assuming f-f absorption), which are then used to correct the 8.4 and 15.3 GHz maps to produce maps of the unabsorbed flux-densities. These modified maps are then used to recreate the 1.7 and 2.3 GHz maps of the unabsorbed flux-densities, which are used, in turn, in the creation of improved opacity maps.

The resultant opacity maps at 2.3 and 1.7 GHz are shown in Fig. 3. These maps show that the maximum absorption occurs at two points north and south of the center and that the absorbing medium is extended in the north-south direction, roughly perpendicular to the jet axis.

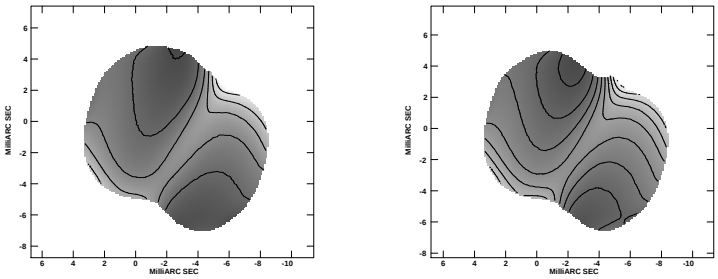


Figure 3: Opacity maps at 2.7 GHz and 1.3 GHz. The contours represent optical depths of 0.4, 0.8, 1.2, 1.6, 2.0, 2.4, 2.8, 3.2 and 3.6.

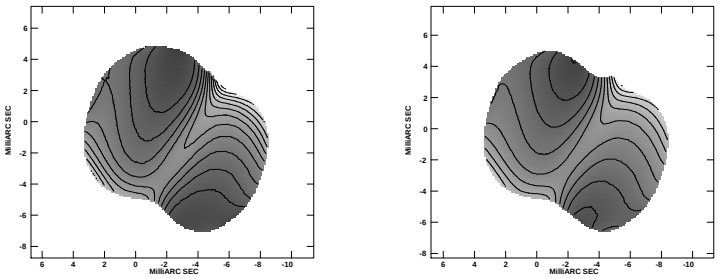


Figure 4: Maps of $\tau_\nu \times \nu^{2.1}$ at 2.7 and 1.3 GHz. The displayed contours represent values of 1, 2, 3, 4, 5, 6, 7, 8, 9, 10, 11, and 12.

To check for consistency in the f-f model we remove the frequency dependence in our two opacity maps (by multiplying by $\nu^{2.1}$). These maps, shown in Fig. 4, are essentially identical, indicating that f-f absorption fits the spectrum at each point in the map.

Using the maps in Fig. 4 we roughly model the size and conditions of the absorbing medium. We find the maps fit a disk of gas with radius $\approx 180$ pc, $\langle N_e \rangle \approx 600\,\mathrm{cm}^{-3}$, and $\langle T_e \rangle \approx 10^4$K. Comparing to the HI absorption results of Carilli et al. (1998) we estimate a ratio of the column depths of $\langle N_e \rangle$ to $N_{HI}$ of $\frac{3500}{T_S}$, where $T_S$ is the spin temperature of the HI atoms.

**Acknowledgements.** This research was aided, in part, by funding from the Dudley Observatory. We are also grateful for the friendly assistance of Vivek Dhawan and the staff at the National Radio Astronomy Observatory.

## References

Carilli, C.L., Menten, K.M., Reid, M.J. et al. 1998, *ApJ*, **494**, 175

Taylor, G.B., Readhead, A.C.S., & Pearson, T.J. 1996, *ApJ*, **463**, 95

*Astrophysical Phenomena Revealed by Space VLBI*
*H. Hirabayashi, P.G. Edwards and D.W. Murphy (eds.)*

# Masers from Space: A Review and a Preview of Space VLBI Maser Observations

P.J. Diamond

*MERLIN/VLBI National Facility, Jodrell Bank Observatory*
*Macclesfield, SK11 9DL, England*

**Abstract**

A review is presented of the current state of spectral line observations performed with VSOP. The historical context is discussed and the limitations due to sensitivity, intrinsic size and the effects of interstellar scattering are described. A preview of what might be possible with proposed future space VLBI missions, VSOP-2 and ARISE, is also presented. The principal conclusions are that SiO masers are probably not a viable target due to their intrinsic sizes but that $H_2O$ megamasers and $H_2O$ masers in regions of star formation will be a prime target for the future.

## 1 Introduction

Prior to the launch of HALCA, there was much excitement at the prospect of space VLBI observations of maser sources. Unlike continuum interferometry, the fixed observing frequency of a line limits the resolution possible with ground-based VLBI. The only way to increase the spatial resolution is to fly a radio telescope. HALCA is equipped with three receivers; it is useful to examine what molecular masers or absorption lines might have been detected with those systems.

HALCA's L-band receiver can observe between 1.60 and 1.73 GHz, this means that all four ground-state transitions of OH can be observed. Such masers are to be found in regions of star formation (SFR), circumstellar envelopes (CSE), in the shock-excited regions around supernova remnants (SNR), in the thin atmospheres of comets and as megamasers in the inner regions of other galaxies. OH is also seen in absorption towards the nuclei of active galactic nuclei.

The C-band system covers the frequency range 4.7 to 5.0 GHz. Maser emission also exists in this band; Jy-level excited-state OH masers and $H_2CO$ are observed in SFR, both molecules are also observed in

absorption against the continuum emission of some galaxies. Potentially, the K-band system at 22 GHz had the greatest prospects of yielding new and exciting results since strong, compact masers are known to exist in SFR, CSE and the nuclei of galaxies. Unfortunately, as we are all aware, the K-band system was damaged, possibly through vibration during the launch and was rendered almost inoperable.

Although there are many possible types of maser accessible to HALCA, observations of the sometimes weak emission are not possible due to the severe sensitivity limitations imposed by the constraints of the spacecraft. Table 1 lists the pre-launch estimates of the $7\sigma$ noise in a 1 minute integration for each observing band on a HALCA-VLBA baseline, apart from the degradation of the K-band system these estimates were remarkably accurate.

Table 1: Pre-launch estimates of $7\sigma$ noise in 1 minute integration on HALCA-VLBA 25m baseline.

| Observing band | 16 MHz (mJy) | 15kHz (mJy) | Comment |
|---|---|---|---|
| L | 131 | 4200 | |
| C | 147 | 4700 | No C-band masers detectable |
| K | 400 | 12000 | K-band sensitivity degraded |

The limitations apparent in Table 1 meant that, on sensitivity grounds alone, only OH masers in SFR, CSEs and SNR and the various types of $H_2O$ maser would be accessible to HALCA.

However, there are other limitations. Masers resident in different types of object appear to have a wide variety of intrinsic sizes. OH masers in the envelopes of evolved stars appear, in general, to have sizes $>$ 20 milliarcsec (Bowers et al. 1980) and would not therefore be detectable on space-ground baselines. There are some exceptions to this, Norris et al. (1984) showed that the most-blue shifted peak of the 1612 MHz OH maser emission towards the OH/IR star OH127.8-0.0 was compact on trans-Atlantic baselines. This phenomenon has since been observed in several other stars (Sivagnanam et al. 1988; van Langevelde et al. 2000) and is attributed to the special location of the blue-shifted masers, they appear to lie directly along the line-of-sight to the star and probably amplify the compact thermal emission originating in the stellar photosphere (see Figure 1).

In the complex gaseous structures surrounding SNR shock-excited 1720 MHz OH masers are known to be reasonably common. However, recent MERLIN and VLBA results by Claussen et al. (1999) show that they have large intrinsic sizes ranging from 50 $\longrightarrow$ 180 milliarcsec.

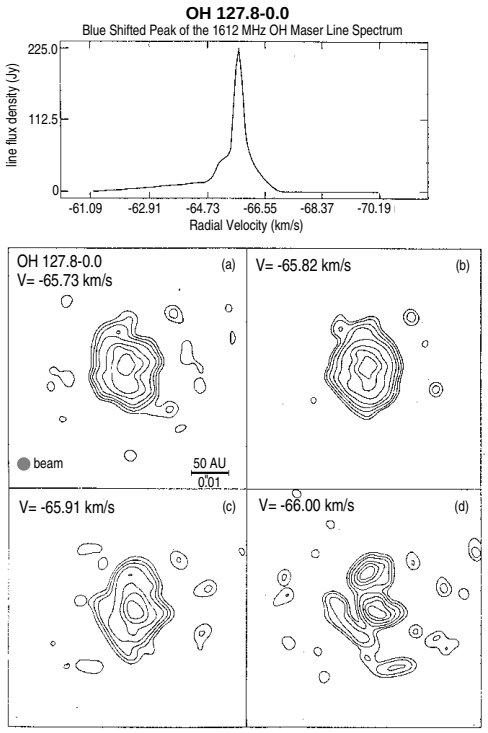


Figure 1: Single-dish spectrum and global VLBI images of OH 1612 MHz maser emission in four velocity channels around the blue-shifted peak of OH127.8-0.0 (Diamond et al., in preparation).

All four transitions of the ground-state of OH are to be found towards SFR, however, the intrinsic sizes of such masers are difficult to determine. Some appear to be dominated by scattering (see below), while maser physics also appears to play a role. For example, Reid et al. (1980) have shown the 1665 MHz OH masers in W3(OH) to be $\sim 5$ milliarcsec in size, while Masheder et al. (1994) determined the sizes of the 1720 MHz masers in the same source to be $< 1.2$ milliarcsec. This latter

measurement implies that, for W3(OH) at least, the measured size of the 1665 MHz masers must be intrinsic.

Most $H_2O$ maser sources have compact emission detectable on the long ground-space baselines except for those in CSEs. Several groups have shown that such masers have sizes ranging from $0.2 \longrightarrow 1.2$ milliarcsec (Spencer et al. 1979; Diamond et al. 1987).

## 2 The Bane of Spectral Line VLBI: Scattering

Radio waves from distant sources propagate through the interstellar medium (ISM) and are affected by their passage. Free electrons in the ISM have a number density $\delta n_e$ that varies over scales from 100km to 1 kpc. This results in variations in the refractive index of the medium ($\delta n_r \sim (-r_e \lambda^2 / 2\pi)\delta n_e$) which in turn result in a phase perturbation that manifests itself in a variety of observable phenomena; namely: angular broadening, angular wander, pulsar pulse broadening, pulse time fluctuations and intensity scintillations. For the study of masers with long-baseline interferometers the principal problem is the angular broadening of the maser spots.

The angular diameter resulting from scattering is related to the scattering measure:

$$SM = \int_0^D C_N^2 \, ds \tag{1}$$

where $C_N^2$ denotes the power in the fluctuation spectrum along the line of sight. Taylor and Cordes (1993) provide a relationship between the scattered angular diameter and the scattering measure valid for galactic sources:

$$SM = (\frac{\Theta}{71mas})^{5/3} \nu_{GHz}^{11/3} \tag{2}$$

Numerous studies of pulsars, masers and extragalactic sources have demonstrated the reality of the scattering process. In some cases the scattering can be extreme, Frail et al. (1994) showed that the angular diameter of some OH masers in OH/IR stars close to the Galactic Centre exceeded 1000 milliarcsec. Diamond et al. (1988) showed, from a global VLBI survey of some 60 OH sources, that there was a tendency for angular sizes of masers to increase with distance implying that, in general, interstellar scattering determines the angular size and therefore the brightness temperatures.

However, once again there are exceptions. Kemball et al. (1988) performed a single-baseline VLBI survey with Medicina and Hartebeesthoek of 16 strong 1665 MHz OH masers in SFR. Surprisingly, they detected three sources, all with sizes $\sim 1$ milliarcsec; the size predicted by our understanding of scattering was 20 milliarcsec. This result implied that there may be holes in the scattering screen.

## 3 HALCA and OH Masers

As the above discussion makes clear the potential spectral line targets available to HALCA are somewhat limited. However, successful observations of OH masers in SFR OH34.26+0.15, one of the sources detected by Kemball et al. (1988), have recently been reported by Slysh et al. (2000). Using a ground array of ATNF, Mopra, Tidbinbilla, Usuda, Shanghai and Bear Lakes co-observing with HALCA they successfully detected fringes to the spacecraft. The maser spots were only partially resolved with the major and minor axes of the strongest peak estimated at $2.6 \pm 0.5$ and $0.3 \pm 0.3$ milliarcsec respectively. It is possible that the masers spots are composed of still smaller, unresolved features. A lower limit to the brightness temperature of $6 \times 10^{12}$K results from these measurements. Such a value exceeds the maximum values of $T_B$ predicted by some maser models by an order of magnitude. In order to accommodate such high values it is probable that the maser emission is not isotropic but is highly beamed.

Slysh et al. point out that a distant pulsar (14.5 kpc) and an extragalactic source which lie within $10'$ and 0.76 degrees of OH34.26+0.15 respectively are both very heavily scattered, having angular sizes $> 200$ milliarcsec when scaled to 1665 MHz. OH34.26+0.15 lies at a distance of 3.8 kpc and so the obvious conclusion is that the source of the heavy scattering lies beyond the maser source. Slysh et al. therefore suggest that their space VLBI results suggest a large scale deviation in the distribution of the scattering material in the Galaxy.

## 4 HALCA and $H_2O$ Masers

Due to the degradation of the K-band system it was not expected that any celestial source could be observed by HALCA, however, nature provided a surprise in the form of a massive outburst of an $H_2O$ maser in Orion-KL. Such outbursts have been observed before. Between 1979

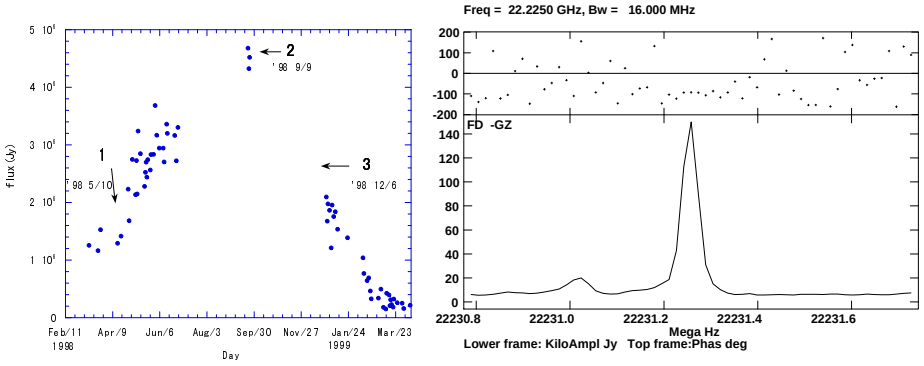


Figure 2: a) Time evolution of the peak flux density of the 8 km/s feature in Orion-KL, data taken with the Kagoshima 6-m telescope; b) Scalar averaged spectrum of the $H_2O$ maser emission in Orion-KL on the baseline FD–HALCA.

and 1988 a maser at a velocity of 8 km/s flared to a flux density of 7 MJy. During that time a global VLBI observation by Matveyenko et al. (1988) revealed the burst region to have a linear structure with a clear velocity gradient along it indicative of rotation. Matveyenko et al. (1988) proposed a model in which the individual masers denoted long coherent paths in a structure similar to the rings around Saturn.

In the early Spring of 1998 the same region flared again, eventually reaching a flux density of $\sim 5$ MJy. Fig 2a shows the time evolution of the burst as seen from the 6-m radio telescope in Kagoshima. On March 3, 1998 an observation was performed using the VLBA and HALCA, fringes were found at the VLBA correlator on April 9, 1998. Fig 2b shows the scalar-averaged amplitude and phase spectrum for a minute interval on the baseline Fort Davis–HALCA. Kobayashi et al. (these proceedings) discuss the nature of the peculiar linear structure of the maser region as determined from VLBA monitoring.

## 5 The Future

There are two proposed space missions of interest to spectral line observers: VSOP-2 and ARISE. Currently, it is planned to equip VSOP-2 at 5 (or 8) GHz, 22 GHz and 43 GHz; ARISE would be similarly equipped but with an additional receiver at 86 GHz. The sensitivities are such that both antennas would be able to detect hundreds if not thousands of $H_2O$ and SiO masers if compact structure is present. The apogee for each spacecraft is planned to be $\sim 40,000$ km, the resultant resolution at 22, 43 and 86 GHz will be 60, 30 and 15 $\mu$arcsec respectively. Such a high apogee will, in all likelihood, preclude observations of SiO masers. Numerous VLBA observations of v=1, J=1-0 SiO masers at 43 GHz have demonstrated that fringes are rarely detected on the long 8000 km baselines of the array, implying that the intrinsic sizes of such masers is $> 200\mu$arcsec. Despite several attempts, no transatlantic fringes towards 43 GHz SiO maser sources have yet been detected. 86 GHz observations of the v=1, J=2-1 transition appear to generate the same result. Although such observations are still in their infancy, CMVA observations of several sources have not detected compact emission on intra-USA baselines.

The principal target of future space VLBI missions will be $H_2O$ masers, in particular megamasers in the nuclei of other galaxies and masers in SFR. Since the discovery of the Keplerian rotating disc of gas traced by $H_2O$ maser emission by Miyoshi et al. (1995) a cottage industry has developed attempting to determine the detailed structures of the known megamaser sources and also to detect new sources.

There appear to be two types of megamaser source; the first is of the class exemplified by NGC4258 (Miyoshi et al. 1995) which contains a sub-parsec scale disc of gas in Keplerian rotation about a $39 \times 10^6 M_\odot$ black-hole. A continuum jet is known to be emerging along the rotation axis of the system (Herrnstein et al. 1997). Other similar sources are NGC1068, NGC4945, Circinus, NGC3079 and IC2560. A second type of galaxy (e.g. NGC1052: Claussen et al. 1998) exhibits maser emission that appears to lie along the continuum jets. The detailed study of these objects at the high resolution available to space-VLBI will enable astronomers to measure the masses of the supermassive black holes that lurk in the centre of these galaxies, to probe the accretion disc structure, to measure the distances using proper motion studies (e.g. Herrnstein et al. 1999) and to study the jet physics.

Another prime target will be the study and monitoring of the $H_2O$

masers in regions of star formation. Gwinn (1994) and others have demonstrated that scattering in the ISM affects $H_2O$ masers as well as OH, though to a lesser extent since the angular broadening varies approximately as $\lambda^2$. So, some masers will be resolved on the longest space VLBI baselines. However, Migenes et al. (1999) in a pre-VSOP survey have observed several 10s of sources with compact structures on long ground baselines suggesting that there will be many accessible targets.

Astronomers will be able to study the detailed structure of the maser regions, the small-scale structure and shapes of the masers themselves but above all they will be able to perform frequent monitoring of the changing structures in such objects. Long-term proper motion studies have revealed the distances and overall dynamics of some masers; for example Gwinn et al. (1992) have determined the distance to the $H_2O$ maser in W49(N) to be $11.4 \pm 1.2$ kpc and have shown that the masers are expanding in a bipolar manner from a common point presumed to be a newly born star.

However, space VLBI observations could perform such measurements much more quickly, more accurately and enable studies of the complex motions that probably exist in such regions. Observations with VSOP-2 or ARISE would be able to watch a typical $H_2O$ maser in W49N move its own diameter in 3-4 weeks. One can imagine that 'movies' analogous to the SiO movie of TX Cam (Diamond & Kemball, in preparation) could be produced in this manner.

**Acknowledgements.** Ian Avruch is thanked for his help in preparing Figure 1 for publication.

## References

Bowers, P.F., Reid M.J., Johnston, K.J. et al. 1980, *ApJ*, **242**, 1088

Claussen, M.J., Diamond, P.J., Braatz, J.A. et al. 1998, *ApJ*, **500**, L129

Claussen, M.J., Goss. W.M., Frail, D.A., et al. 1999, *ApJ*, **522**, 349

Diamond, P.J., Johnston, K.J., Chapman, J.M. et al. 1987, *A&A*, **174**, 95

Diamond, P.J., Martinson, A., Dennison, B et al. 1988 in *Radio Wave Scattering in the Interstellar Medium* (New York: American Institute of Physics), 195

Frail, D.A., Diamond, P.J., Cordes, J.M. et al. 1994, *ApJ*, **427**, L43

Gwinn, C.R., Moran J.M. & Reid, M.J. 1992, *ApJ*, **393**, 149

Gwinn, C.R. 1994, *ApJ*, **429**, 253

Herrnstein, J.R., Moran, J.M., Greenhill, L.J. et al. 1997, *ApJ*, **475**, L17

Herrnstein, J.R., Moran, J.M., Greenhill, L.J. et al. 1999, *Nature*, **400**, 539

Kemball, A.J., Diamond, P.J. & Mantovani, F., 1988, *MNRAS*, **234**, 713

Masheder, M.R.W., Field, D., Gray, M.D. et al. 1994, *A&A*, **281**, 871

Matveyenko, L.L., Graham, D.A. & Diamond, P.J. 1988, *Soviet Astron. Letters*, **14**, 468

Migenes, V., Horiuchi, S., Slysh, V.I. et al. 1999, *ApJS*, **123**, 487

Miyoshi, M., Moran, J.M., Herrnstein, J.M. et al. 1995, *Nature*, **373**, 127

Norris, R.P., Booth, R.S., Diamond, P.J. et al. 1984, *MNRAS*, **208**, 435

Reid, M.J., Haschick, A.D., Burke, B.F. et al. 1980, *ApJ*, **239**, 89

Sivagnanam, P., Diamond P.J., Le Squeren, A.M. et al. 1988, *A&A*, **194**, 157

Slysh, V.I. et al. 2000, *MNRAS*, in press

Spencer, J.H., Johnston, K.J., Moran, J.M. et al. 1979, *ApJ*, **230**, 449

Taylor, J.H. & Cordes, J.M., 1993, *ApJ*, **411**, 674

van Langevelde, H.J. et al. 2000, *A&A*, in press

*Astrophysical Phenomena Revealed by Space VLBI*
*H. Hirabayashi, P.G. Edwards and D.W. Murphy (eds.)*

# Polarization Structure of the Orion-KL Water Masers

Shinji Horiuchi [1], V. Migenes [2] & S. Deguchi [3]

[1] *NAO, Ohsawa 2-21-1, Mitaka, Tokyo 181-8588, Japan*
[2] *University of Guanajuato, Guanajuato, Mexico*
[3] *Nobeyama Radio Observatory, Minamisaku, Nagano 384-1305, Japan*

**Abstract**

Water masers in the star forming region Orion-KL started an outburst in 1997. Our VLBA polarimetry observations reveal that the future bursting maser spot exhibited ∼70% fractional linear polarization with a modest total total flux density of ∼ 30 Jy during the early stage of the burst. These results suggest that this latest bursting phenomenon has an origin similar to the super maser event of 1979.

## 1 Introduction

The observations of maser polarization provide information on the magnetic field direction in dense protostellar gas, which may be crucial to understanding the process of star-formation and confinement in mass outflows from protostars, but which is difficult to obtain by other means. In this paper we report our results from VLBA (Very Long Baseline Array) polarization imaging of the high-mass star-forming region Orion-KL. Information on the field structure on the scale of $10^{12}$-$10^{15}$ cm enables us to compare directly various theories of protostar formation.

## 2 Polarization Mapping with VLBA

The observation was made on 1 February 1997 for 8 hours with the full VLBA array. Among the spots we have identified in the velocity range $-40\,\mathrm{km\,s^{-1}}$ to $50\,\mathrm{km^{-1}}$, about half show a strong degree of linear polarization of $20 \sim 50\%$, with a few exceptional spots yielding linear polarizations of about 70%.

## 3 Super Masers and Polarization

The Orion-KL water masers are special due to their extremely strong emission. A super burst event of the masers was firstly discovered in 1979

and lasted a few years (e.g. Garay et al. 1989). The second burst event was discovered in December 1997 and reached a peak flux of $3.5\times10^6$ Jy in September 1998 (Omodaka et al. 1999). Our VLBA observation was carried out about ten months before this latest burst. Space VLBI observations at the burst epoch were carried out by VSOP (Kobayashi et al. 2000) and the Japanese VLBI network (Omodaka et al. 1999). A VLBA image of this region in 1995 appears in Matveyenko et al. (1998).

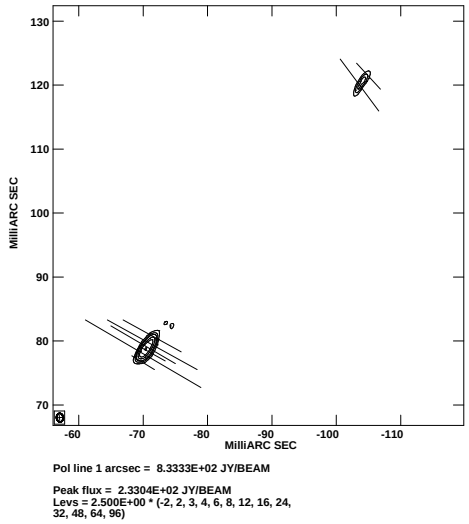


Figure 1: Linear polarization map of pre-burst spot (lower) in Orion-KL. The lines indicate the fractional polarization at this epoch (1997.09).

The highest flux peak in our map coincides with the burst spot position in the 1980's and 1990's within the accuracy of the absolute position of the VLBA of about 0.1 arcsecond. However there are several features in this region within a 100 milli-arcsecond radius. From comparison of the relative positions of several features among these maps, we found that the bursting spot is imaged in our February 1997 data and yields a 30 Jy flux and 70% fractional polarization. This flux density is consistent with the light curve of the burst event (Omodaka et al. 1999) assuming an exponential dependence in the flux density increase. The spot is not present in the 1995 map of Matveyenko et al. (1998).

## 4 Discussion

Using the Mizusawa radio telescope Horiuchi and Kameya (2000) started a monitoring program of the linear polarization of the maser in December 1998, during a phase of rapid flux density decrease after the burst (Figure 2). They found that the total flux density of $2.4\times10^6$ Jy (December 1998) exhibited about 46% linear polarization. Over the next six months they found that the total intensity decreased by about two orders of magnitude while the fractional linear polarization gradually fell to 30%. There is also systematic variation in the polarization angle. It was 25° on 1998 December 21 and shifted almost uniformly to 40° in two months, though varied less rapidly since. These bursts with high fractional linear polarization are clearly unique events that require their own explanation, different from that of other water maser features.

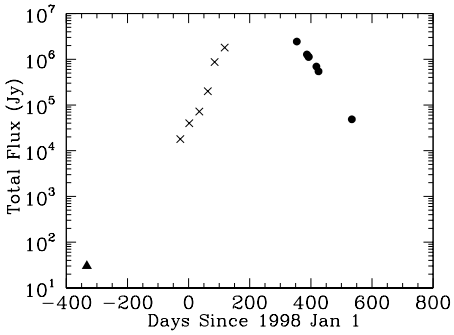


Figure 2: Total flux variation of the present burst: triangles, this work; crosses, Omodaka et al. (1998); circles, Horiuchi and Kameya (2000).

The monitoring observations of the super burst event in 1980's indicated that the time scale of such an event is ∼10 years (Garay et al. 1989), while the present burst lasted only ∼3 years. This suggests no periodicity in the water maser burst events of this region, although we must continue to monitor in the coming several years to confirm this. The polarization characteristics plotted as a function of total intensity are common for the two events, although the time scales of the flux variations differ. When the maser was strong (i.e., greater than $5\times10^5$ Jy), the degree of polarization decreased with flux density. Our results of 40% polarization at several million Jy agree well with the range measured by Garay et al. (1989). Our results for the present burst demonstrate similar variations in polarization degree and the position angle, though with

differences in absolute position angle and time scale. The difference in the polarization angle may be accounted for by the position-angle difference of the maser elongation of the bursting spots. The present bursting maser spot has an elongated structure with aspect ratio of about 10 and position angle of $-40°$, as observed by VSOP in March 1998 (Kobayashi et al. 2000). Assuming that the burst spot has not changed its structure significantly, we find that the (E-vector) polarization angle is nearly perpendicular to the elongation of the bursting spots, similar to the superburst in the 1980's (Matveenko et al. 1988).

The mechanism by which we observe such extremely high brightness masers may be related to the several interacting masers located along the line of sight (Deguchi & Watson 1989). Boboltz et al. (1998) have suggested that the symmetric intensity variation of a water maser flare in W49 can be explained with two interacting maser clouds model; a system with a maser passing across the line of sight toward another background maser. From monitoring observations at Kagoshima (Omodaka et al. 1998) and from this work, we have found a symmetric variation of the total flux before and after the burst peak, which suggests that the interacting masers model is applicable (Figure 2). On the other hand, the polarization characteristics seem not to vary symmetrically in time around the peak of total intensity. Our result shows that the polarization degree decreased monotonically during the decay phase.

## References

Boboltz, D.A., Simoneti, J.H. & Dennison, P.J. et al. 1998, *ApJ*, **509**, 256

Deguchi, S. & Watson W.D. 1989, *ApJ*, **340**, L17

Garay, G., Moran, J.M. & Haschick, A.D. et al. 1989, *ApJ*, **338**, 244

Horiuchi, S. & Kameya O. 2000, *PASJ*, in press

Kobayashi, H. 2000, *these Proceedings*

Matveenko, L.I., Graham, D.A.& Diamond, P.J. 1988, *Sov. Ast. Lett.*, **14**, 468

Matveyenko, L.I., Diamond, P.J & Graham, D.A. 1998, *Ast. Lett.*, **24**, 623

Omodaka, T., Maeda, T. & Mochiduki, N. 1998, IAUC, 6893

Omodaka, T., Maeda, T., Miyoshi, M. et al. 1999, *PASJ*, **51** 333

*Astrophysical Phenomena Revealed by Space VLBI*
*H. Hirabayashi, P.G. Edwards and D.W. Murphy (eds.)*

# Monitoring of the Orion-KL Water Maser Outburst

H. Kobayashi [1], T. Shimoikura [2], T. Omodaka [2]
& P.J. Diamond [3]

[1] *NAO, Ohsawa 2-21-1, Mitaka, Tokyo 181-8588, Japan*
[2] *University of Kagoshima, Kohrimoto 1-21-35, Kagoshima 890-0065, Japan*
[3] *MERLIN, University of Manchester, Jodrell Bank Observatory, Macclesfield Cheshire SK11 9DL, United Kingdom*

**Abstract**

In December 1997 the Orion-KL water maser source was discovered to be undergoing an outburst and, in February 1998, a VSOP observation successfully yielded fringes on the source from HALCA to several VLBA antennas (see Color Figure 10). This confirmed the capabilities of the 22 GHz VSOP observing system elements, i.e. phase transfer, onboard frequency stability, and orbit determination accuracy. Following the VSOP observation, we monitored the Orion burst maser with VLBA-only observations at 2 week intervals. The outburst peaked at $5\times10^6$ Jy in September 1998, and then declined to a few times $10^5$ Jy, which is its normal intensity. By tracing the structure and velocity changes of the maser spots from the outburst phase to the declining phase, we find there are two velocity components at the region of the flaring water maser with a 0.2 km/s velocity difference. The separation of two components is observed to decrease as the maser intensity increases and, at the time of the outburst peak, the position of two maser components coincide. This strongly suggests that the overlapping of the two masers causes the luminous outburst.

## 1 Introduction

An ultra-luminous outburst of an Orion-KL water maser was first observed from 1983 to 1984 (Matveyenko et al. 1988, Garay et al. 1989). At that time, the total flux density reached values as large as $\sim6.7\times10^6$ Jy — around 200 times stronger than usual. In December 1997 another outburst of the Orion-KL water masers was discovered using the 6 m telescope of the University of Kagoshima (Omodaka et al. 1999). Two theoretical models have been proposed for such outbursts. One is a

coplanar model, in which a thin plane passes through the line of sight and the optical depth of the maser emission becomes larger (Elitzur et al. 1992). The other is an overlapping maser spot model, in which two maser spots lie along the same line of sight, with the background maser emission being amplified by the foreground maser. For this model, the two maser spots must coincide not only in position but also velocity (Boboltz et al. 1998). There has not been observational clear evidence to support either model, mostly because there were no VLBI monitoring observations during the last burst!

After the previous outburst, a VLBI image was obtained (Matveenko et al. 1998). For the investigation of the maser burst mechanism, it is very important to obtain frequent VLBI observations with high spatial-resolution during the outburst.

## 2 Observations

Monitoring observations were performed with the VLBA. Observations were carried out from 1998 May 10 to 1999 February 10 at two week intervals. In total, 16 days were used with a 3 hour observation each day. The typical synthesized beam size is $0.3\,\mathrm{mas} \times 0.7\,\mathrm{mas}$ with a position angle of around $0^\circ$. The velocity resolution was $0.05\,\mathrm{km/s}$. Fringes were detected on all VLBA baselines, confirming that the maser spots are compact.

## 3 Results

In Figure 1, the intensity profile of the water maser outburst is shown. It increased from December 1997 to September 1998, reaching a peak of $4.8 \times 10^6$ Jy, a little less than the previous outburst. In the previous burst, the maser intensity oscillated during the increasing phase, however this time the intensity changed more smoothly. This suggests the latest burst was simpler than the previous one.

Figure 2 shows three maps of the maser region at the velocity of peak intensity from the epochs 1, 2, and 3 indicated on Figure 1. They show that there are two components at the position of the maser burst, with the weaker component apparently passing through the stronger component. As the absolute position is uncertain, it is impossible to know which is stationary. When the two components coincided, the intensity of the burst maser was at its peak.

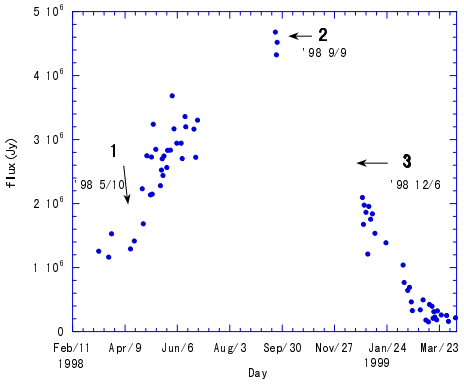


Figure 1: Time profile of peak flux of the bursting 7.6 km/s maser component.

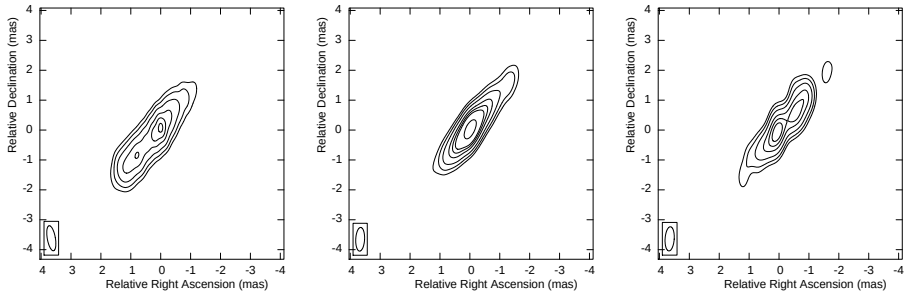


Figure 2: Three epoch maps of the bursting 7.6 km/s maser components. The dates are indicated on Figure 1. The maps shows the apparent passage of the weaker component across the stronger component. Contour levels are 2, 4, 8, 16, 24, 32, 64 and 128 by $10^4$ Jy/beam. The peak fluxes are $3.5\times10^5$, $9.2\times10^5$ and $4.7\times10^5$ Jy/beam, respectively.

## 4 Discussions

The maps of the Orion-KL maser burst show two components interacting with each other. This result therefore seems to support models in which overlapping masers produce strong bursts. The position of the current maser burst is the same as that of the previous burst. The apparent transverse velocity of one maser with respect to the other is 7.4 km/s. If the two maser components constitute a binary system, the total mass is around 0.1 $M_\odot$ and the separation length is around 3 AU. Such values are typical for the usual parameters of water maser spots.

**Acknowledgements.** We gratefully acknowledge the VSOP Project, which is led by ISAS in cooperation with many organizations and radio telescopes around the world. The National Radio Astronomy Observatory is a facility of the National Science Foundation operated under cooperative agreement by Associated Universities, Inc.

## References

Boboltz, D.A., Simoneti, J.H. & Dennison, P.J. et al. 1998, *ApJ*, **509**, 256

Elitzur, M., Hollenbach, C.J. & McKee, C.F 1992, *ApJ*, **394**, 221

Garay, G., Moran, J.M. & Haschick, A.D. et al. 1989, *ApJ*, **338**, 244

Matveyenko, L.I., Graham, D.A.& Diamond, P.J. 1988, *SvAL*, **14**, 468

Matveyenko, L.I., Diamond, P.J & Graham, D.A. 1998, *SvAL*, **24**, 623

Omodaka, T., Maeda, T., Miyoshi, M. et al. 1999, *PASJ*, **51**, 333

*Astrophysical Phenomena Revealed by Space VLBI*
*H. Hirabayashi, P.G. Edwards and D.W. Murphy (eds.)*

# VSOP Observations of PSR B0329+54

Anthony Minter

*NRAO, P.O. Box 2, Green Bank, West Virginia, U.S.A.*

## 1 Introduction

The pulsar B0329+54 was observed on 22 August 1998 using the HALCA satellite, the VLBA, the 140 foot telescope in Green Bank and the DSN's 70 meter telescopes in Goldstone and Madrid. The observations where at 1634 to 1666 MHz with 64 channels in two IFs resulting in a spectral resolution of 0.5 MHz. The VSOP observations were performed from 06:00 to 18:00 UT on August 22, 1998. These observations used the Green Bank, Goldstone, Madrid and Usuda tracking stations and the NRAO's VLBA correlator.

The IF at the 140 foot telescope was split with one output going to the VLBA recorder and with the other going to the spectrum analyzer. The spectrum analyzer was used to produce a dynamic spectrum of the pulsar in the frequency range 1600 to 1670 MHz. The data were integrated for 90 seconds with a frequency resolution of 0.078125 MHz and 128 phase bins across the full pulsar cycle.

## 2 Correlation

The data were correlated using the VLBA correlator. Two passes of the data were made. The first pass correlated the data in the standard fashion while the second made use of pulsar gating. The gate was centered on the main pulse of 0329+54 and had a total passband of 15% of the pulse cycle. The timing information obtained from the 140 foot telescope spectrum analyzer observations during the VSOP observations of 0329+54 was used to determine the exact time that the pulsar gate was turned on and off.

Fringes for 0329+54 were found at all times on ground to space baselines for both the standard correlation and the gated correlations. Only the gated data will be discussed here. Figure 1 shows the $(u, v)$ coverage obtained for this observation.

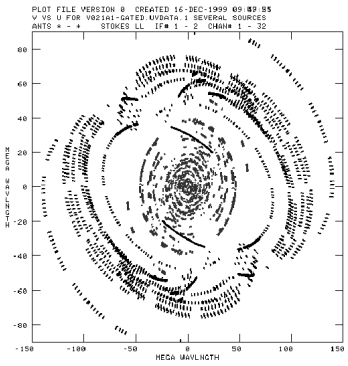


Figure 1: $(u, v)$ plot of valid data from VSOP observations of PSR B0329+54 (V021a1). The black (outer) points indicate space-ground baselines and the grey (inner) points indicate ground-ground baselines. The $u$ axis range is $\pm 150$ M$\lambda$ and the $v$ axis range is $\pm 90$ M$\lambda$.

## 3 Dynamic Spectra

The dynamic spectrum of 0329+54 from the 140 foot data is shown in Figure 2. The dynamic spectrum plots the flux versus time and frequency. This conveniently displays the "twinkling" of the pulsars signal due to the turbulent plasma located between the pulsar and the observer. The data shown in Figure 2 represent a preliminary calibration of the data and the uncalibrated bandpass edges of the 4 IFs can easily be seen. The data were integrated over the entire pulse to produce the dynamic spectra shown in Figure 2.

In the dynamic spectrum shown in Figure 2 there are several interesting features that should be noted. The first is that the flux rises by about a factor of ten at certain frequencies and times. Secondly, the flux brightenings are periodic both in frequency and in time, with the lower frequencies leading the higher frequencies. This is indicative of the turbulent plasma creating two (or more) dominate paths over which the pulsar emission can reach the Earth. The light along these multiple paths produce interference fringes at the Earth resulting in the features seen in Figure 2. This will be referred to as a multiple imaging event for the remainder of the paper.

In Figure 2 we also show a dynamic spectrum produced using the correlated flux from the HALCA to 140 foot telescope baseline data.

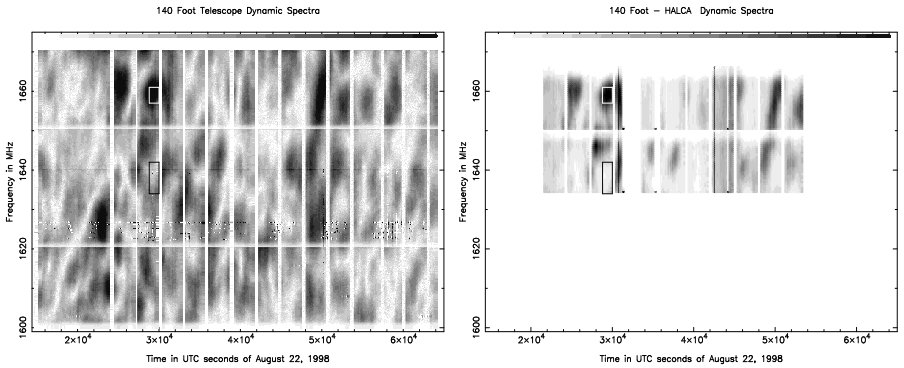


Figure 2: Dynamic spectrum of PSR B0329+54 using the 140 foot telescope on August 22, 1998 (left) and using the correlated flux on the HALCA to 140 foot baseline (right). The "bar" at the top of the images indicates the flux level with white being the lowest flux and black being the largest. Interference from the Iridium satellites can be seen from 1620 to 1627 MHz. The two boxes in each dynamic spectra indicate the data used for producing the images in Figure 3.

Roughly the same features are seen in this dynamic spectrum and in the one produced using only the 140 foot telescope data. The subtle differences can provide information on the size scale, distance or velocity of the turbulent plasma creating the multiple imaging events.

### 3.1 Multiple Imaging Event

In Figure 2 two boxes are shown for each dynamic spectra. The data within these boxes were used to produce the images shown in Figure 3. One data set was chosen such that it was during a multiple imaging event and could display multiple images of the pulsar and possibly image wander. The other data set was chosen at a time where multiple images would not be expected.

In Figure 3 the grey scale represents the multiple image data set (upper box in Figure 2) and the contours represent the single image data set (lower box in Figure 2). The total flux in the multiple imaging event is approximately 290 mJy while it is approximately 30 mJy in the "normal" image. These fluxes are the average pulsar flux integrated over the full pulse cycle. The total flux of the brightest component during the multiple imaging event is approximately 250 mJy while the secondary

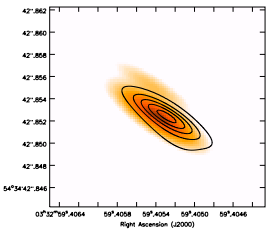


Figure 3: The contours show an image of 0329+54 produced during a period of low flux. The contours are derived from the data shown in the lower box in Figure 2. The grey scale image shows another image of 0329+54 derived from a period of high flux. This image is derived from the data in the upper box in Figure 2.

image is approximately 40 mJy. The two images of the pulsar during the multiple imaging event are separated by about 2.9 mas ($\sim$ 3.5 A.U. at 1 kpc). Also it can be seen that the images have been shifted by about 1.5 mas as would be expected from this type of phenomena (Gupta, Rickett and Lyne 1988). However, this data is not phase referenced. It is fortunate that these observations involved HALCA since the multiple images would not have been resolved from ground only VLBI experiments.

**Acknowledgements.** I gratefully acknowledge the VSOP Project, which is led by the Japanese Institute of Space and Astronautical Science in cooperation with many organizations and radio telescopes around the world. I would also like to thank the schedulers and fate, whose combined forces fortuitously allowed these observations to occur during an interstellar fringing event.

## References

Gupta, Y., Rickett, B., Lyne, A. 1988, in AIP Conf. Proc. 174, Radio Wave Scattering In The Interstellar Medium, ed. J.M. Cordes, B.J. Rickett and D.C. Backer (New York: AIP), 140.

*Astrophysical Phenomena Revealed by Space VLBI*
*H. Hirabayashi, P.G. Edwards and D.W. Murphy (eds.)*

# Observations of the Vela Pulsar Using VSOP

C.R. Gwinn[1], J.E. Reynolds[2], D.L. Jauncey[2], A.K. Tzioumis[2], B. Carlson[3], S. Dougherty[3], D. Del Rizzo[3], H. Hirabayashi[4], H. Kobayashi[4], Y. Murata[4], P.G. Edwards[4], J.F.H. Quick[5], C.S. Flanagan[5] & P.M. McCulloch[6]

[1] *UCSB, Santa Barbara, California 93106, USA*
[2] *ATNF, Epping, New South Wales, 2121, Australia*
[3] *DRAO, Penticton, British Columbia, V2A 6K3, Canada*
[4] *ISAS, Yoshinodai 3-1-1, Sagamihara, Kanagawa 229-8510, Japan*
[5] *HRAO, Krugersdorp, Transvaal, South Africa*
[6] *University of Tasmania, Hobart, 7001, Tasmania, Australia*

**Abstract**

Scattering in the interstellar plasma acts as an AU-scale lens to resolve the emission region of the Vela pulsar. In the observer plane, scattering produces a speckle pattern. Observations of this pattern on short baselines provide a measure of the size of the source. Observations on long baselines provide information about the spatial structure of the pulsar's emission region. Observations of this pattern for the Vela pulsar are in good agreement with theory, and should provide a picture of the Vela pulsar as a function of pulse phase.

## 1 Introduction

Pulsars exhibit rapid rotation and extremely strong gravitational and magnetic fields. This combination drives a strong electron-positron wind from near the surface of the star to beyond the light cylinder, where corotating material travels at lightspeed (Goldreich and Julian 1969). This wind may form the beam of radio waves that sweeps across the observer each rotation period, creating the observed pulses. Although this picture of pulsar magnetospheres is widely accepted, the physical mechanism, and even the location, of radio-wave generation remain unknown (Lyne and Graham-Smith 1998).

To improve understanding of pulsar emission mechanisms, we seek to resolve and image the pulsar's emission region. Scattering by plasma fluctuations in the interstellar plasma deflects radio waves, acting as

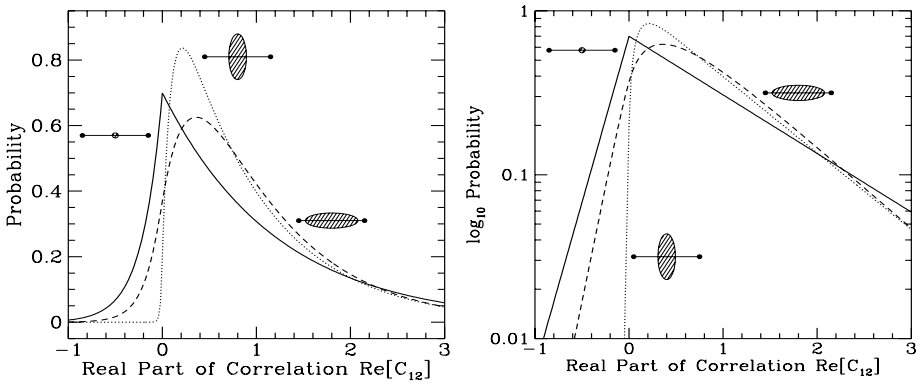


Figure 1: Expected distribution of the real part of the visibility, on a long baseline. Sold line: point source. Dotted line: source elongated perpendicular to baseline. Dashed line: elongated along baseline. Left panel: Linear scale. Right panel: Semilog scale.

an enormous, highly corrupt lens in interstellar space. In the plane of the observer, this lens produces a speckle pattern. Color Figure 9 shows an example of the speckle pattern for the Vela pulsar, observed on the HALCA-Tidbinbilla baseline. This pattern is the convolution of the point-source response with a diffraction-limited image of the source. The diffraction limit is set by the aperture of the scattering disk, the region in interstellar space from which the observer receives radiation (Gwinn et al. 1998). Because the angular size $\theta$ of the scattering disk increases with wavelength $\lambda$ as $\theta \propto \lambda^2$, the linear resolution afforded by this technique actually increases with wavelength.

The Vela pulsar is an excellent candidate for speckle studies of pulsar structure, because it is strong, heavily scattered, and is an archetypical member of the class of young pulsars. It lies at a distance of about 500 pc. From ground-based observations, we have inferred a size for the pulsar of about 500 km (Gwinn et al. 1997, 2000). At 18 cm observing wavelength, the scattering disk has a diameter of about 3 AU (full width at half maximum of major axis). At the pulsar, the linear resolution of this "lens" is about 1000 km.

## 2 Statistics of the Speckle Pattern

In strong scattering, the observer receives radiation from a variety of paths, with relative phases differing by many turns. Consequently, the

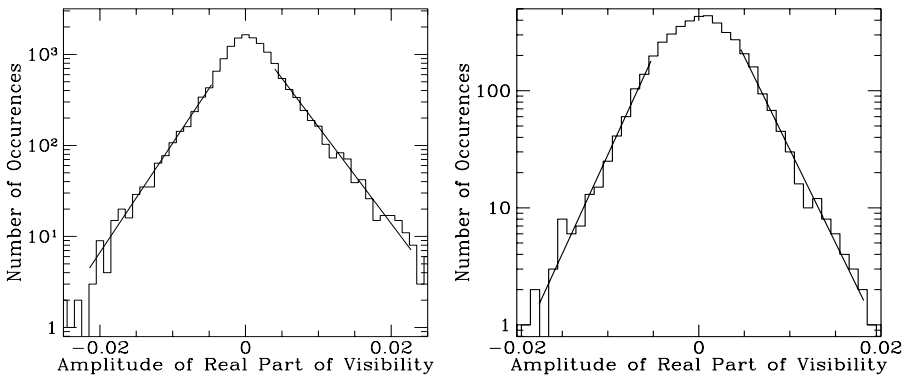


Figure 2: Distributions of amplitude of correlated flux density on a long baseline. Left: Hartebeesthoek-Tidbinbilla baseline. Right: HALCA-Tidbinbilla baseline. Each plot shows one fringe area, 4 MHz×30 sec for left plot and 4 MHz×10 sec for right.

electric field in the plane of the observer has statistics of a random walk. For a point source, the electric field is consequently drawn from a Gaussian distribution, and its square modulus, the intensity, is drawn from an exponential distribution (Goodman 1985). For a small but extended source, the distribution is a weighted sum of 3 exponentials; it resembles an exponential distribution with the small intensities missing (Gwinn et al. 1998).

On long baselines, correlated flux density of the source is the product of the electric fields at the 2 antennas. It is thus the product of factors drawn from 2 correlated Gaussian distributions. The distribution of the real part of the flux density can be shown to be a superposition of positive-going and a negative-going exponentials, along positive and negative directions. Figure 1 shows an example. If the source is resolved, the distribution becomes rounded near 0, and the scales of the exponentials change. The form of this change depends on the size of the source, the length of the baseline, and the orientation of the source relative to the baseline, if it is elongated.

## 3 Observations and Comparison with Theory

On 10 Dec 1997, we observed the Vela pulsar using HALCA and ground radio telescopes at Tidbinbilla (64-m diameter), Mopra (22-m), and Hartebeesthoek (26-m). We recorded data with the S2 recording sys-

tem. Tapes were analyzed at the LBA correlator in Australia to obtain a pulse ephemeris, and then correlated at the Canadian S2 correlator in Penticton. This analysis made heavy use of the capabilities of the Penticton correlator for high spectral resolution, rapid time sampling, pulsar gating, and extraordinarily careful treatment of statistics of input signals. The data were exported to UC Santa Barbara, where they were edited and fringed.

Figure 2 shows sample data for short time intervals, of one fringe area in each case. Because the scale is semilogarithmic, we expect the distributions to asymptotically approach straight lines, at amplitudes far from zero. As the figure shows, this is the case. Note also that the scales of the positive- and negative-going exponentials are different for the Hartebeesthoek-Tidbinbilla baseline, and are nearly the same for the longer HALCA-Tidbinbilla baseline. This is also in accord with predictions of the theory.

A solution for the structure of the pulsar will require fits to the distributions shown in Figure 2 including effects of noise and of averaging in frequency and time (Gwinn et al. 2000). This inversion will also benefit from measurements with the baseline at different position angles and with different lengths. The HALCA-Tidbinbilla baselines afford many such measurements, closely spaced in time, so that they are well suited to such an inversion. Efforts to image the pulsar using VSOP data, with resolution of hundreds of km, are underway.

**Acknowledgements.** We gratefully acknowledge the VSOP Project, which is led by the Japanese Institute of Space and Astronautical Science in cooperation with many organizations and radio telescopes around the world. We thank the US National Science Foundation for financial support.

## References

Goldreich, P., & Julian, W. H. 1969, *ApJ*, **157**, 869

Goodman, J.W. 1985, *Statistical Optics*, (New York: Wiley)

Gwinn, C.R., , Britton, M.C., Reynolds, J.E. et al. 1998, *ApJ*, **505**, 928

Gwinn, C.R., Ojeda, M.J., Britton, M.C. et al. 1997, *ApJ*, **483**, L53

Gwinn, C.R., Britton, M.C., Reynolds, J.E. et al. 2000, *ApJ*, in press

Lyne, A.G., & Graham-Smith, F. 1998, *Pulsar astronomy*, 2nd ed. (Cambridge: Cambridge University Press)

*Astrophysical Phenomena Revealed by Space VLBI*
*H. Hirabayashi, P.G. Edwards and D.W. Murphy (eds.)*

# Multi-Frequency VSOP Polarization Observations of the BL Lacertae Object 1803+784

D.C. Gabuzda

*JIVE, Postbus 2, 7990 AA Dwingeloo, The Netherlands, and Astro Space Center, Lebedev Physical Institute, 53 Leninsky pr., Moscow, 117924 Russia*

**Abstract**

Very Long Baseline Interferometry (VLBI) polarization observations provide information about the magnetic-field structures of the parsec-scale jets in active galactic nuclei. Comparison of polarization observations obtained nearly simultaneously at different frequencies can reveal the presence of Faraday rotation due to thermal plasma along the line of sight from the source to the observer or mixed in with the non-thermal emitting plasma. VLBI polarization observations at 5 and 1.6 GHz were obtained of the compact BL Lacertae object 1803+784 on successive days in July 1998 with global ground arrays plus the orbiting HALCA antenna. The 5 GHz image revealed a smoothly bent jet structure, with the magnetic field transverse all along the jet. This may indicate the presence of a series of relativistic shocks, but more likely reflects the toroidal component of a helical magnetic field associated with the VLBI jet. Comparison of the 1.6 GHz VSOP image and 5 GHz ground-only image suggests that the rotation-measure distribution of 1803+784 is non-uniform on milliarcsecond scales.

## 1 Introduction

BL Lacertae objects are active galactic nuclei with weak, sometimes undetectable, optical line emission and strong variability in total intensity and linear polarization over a broad range of wavelengths from ultraviolet to radio. Their arcsecond-scale radio structures are compact, and their integrated radio spectra are flat or inverted. It is believed that synchrotron radiation is the dominant emission mechanism virtually throughout the spectrum. The origin of the relative low luminosity of their optical line emission is not clear.

VLBI polarization observations of a complete sample of 1 Jy radio-selected BL Lacertae objects have shown a tendency for the dominant magnetic fields in the parsec-scale jets of these sources to be transverse to the local jet direction (Gabuzda, Pushkarev, & Cawthorne 1999, 2000). This has usually been interpreted as evidence for the presence of relativistic shocks that compress an initially tangled **B** field so that the dominant field lies in the plane of compression, perpendicular to the direction of propagation of the shock (Laing 1980; Hughes, Aller, & Aller 1989). It has seemed natural to associate transverse **B** fields in the jets of AGN with shocks, since these jets are obviously very energetic, and the components in which these transverse fields are detected are usually compact.

The BL Lacertae object 1803+784 has a redshift $z = 0.68$ (Witzel et al. 1988). The VLBI jet extends nearly directly west (Witzel et al. 1988; Gabuzda et al. 1992), though 5 GHz and 8.4 GHz VLBI polarization images suggested motion near the core in position angle about $-60°$ (Gabuzda et al. 1994; Gabuzda & Cawthorne 1996). The total intensity structure shows a remarkably persistent stationary feature roughly 1.2 mas west of the core, which has been detectable in VLBI images at centimeter wavelengths for more than a decade. Based on analyses of centimeter-wavelength $P$ images, it was proposed that this feature was associated with a transverse shock.

## 2 Results at 5 GHz – Evidence for Toroidal Fields

The ground array for the 5 GHz VSOP observations of 1803+784 on July 21, 1998 included nine VLBA antennas (all but Brewster) plus the 100-m Effelsberg dish. Figure 1 shows the resulting $(u, v)$ coverage; the HALCA baselines provided about a factor of three increase in resolution East–West and a factor of 1.5 North–South. The 5 GHz data reduction and results are described by Gabuzda (1999). We summarize these results below.

Figure 2 shows the 5 GHz VSOP total intensity ($I$) image with polarization vectors $\chi$ superimposed. We can see that, unlike previous centimeter-wavelength ground-based VLBI images, the brightest feature is not at the easternmost edge of the source emission: there is a weaker feature to the east of the brightest component, which is at the phase center. This suggests that the brightest feature is actually a knot in the innermost VLBI jet, rather than the core. Without spectral in-

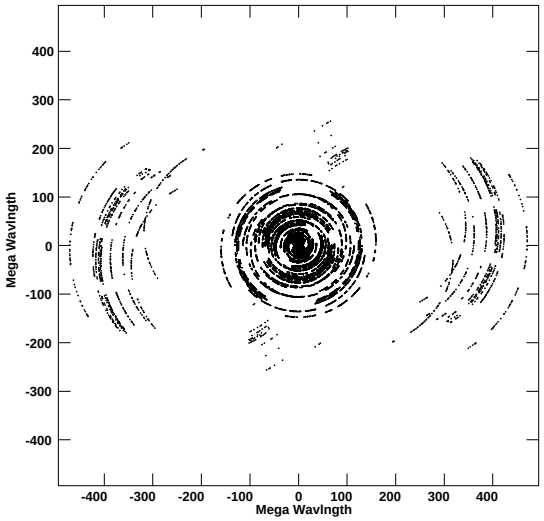


Figure 1: $(u, v)$ coverage obtained for the 5 GHz VSOP observations of 1803+784 on July 21, 1998. The coverage for the 1.6 GHz observations one day earlier is very similar.

dex information, it is impossible to conclusively determine whether the easternmost feature is the 5 GHz core (optically thick) or a counterjet (optically thin). However, the fact that this feature is only modestly polarized, $\sim 3\%$, suggests that it is probably the core.

The well-known stationary jet feature is clearly visible to the west at a distance of $\sim 1.3$ mas from the phase center. The extra resolution provided by the HALCA baselines shows that the jet curves northward and then southward between the easternmost feature (which we take to be the core) and the bright feature at the western end of the jet. The $\chi$ vectors clearly follow this bending of the jet, remaining aligned with the local jet direction as the jet curves. The degree of polarization in the jet ranges from 5% to nearly 20%, indicating that the associated emission is optically thin. Thus, the $\chi$ distribution implies that there is a transverse **B** field all along the observed VLBI jet.

This type of magnetic-field structure could, in principle, be due to a series of shocks propagating along the VLBI jet, with each shock compressing the local **B** field so that it is transverse to the local flow direction. However, this explanation seems somewhat contrived. In addition, the polarized emission is relatively smooth, and is not concentrated only in the brightest and most compact features. This suggests that another

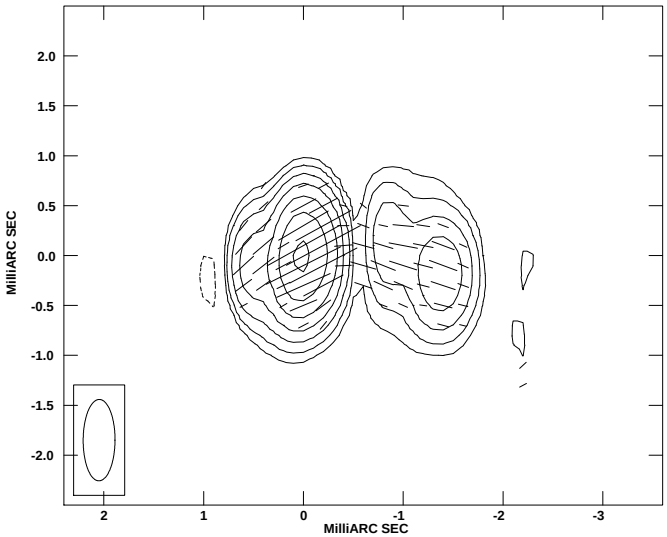


Figure 2: 5 GHz total intensity image for 1803+784 on July 21, 1998. The bottom contour is ±1.4% of the peak flux density of 1.07 mJy/beam, and the contours increase in multiples of 2. The sticks show superposed $\chi$ vectors for the linear polarization distribution.

interpretation is more likely: we are seeing the dominant toroidal component of a helical **B** field associated with the VLBI jet. This does not preclude the possibility that some of the knots of jet emission are associated with shocks; but it does provide a natural explanation for the fact that the observed jet **B** field remains transverse even as the jet bends fairly severely. The images presented here provide the first clear and direct evidence for the presence of toroidal magnetic fields on parsec scales.

## 3 Results at 1.6 GHz – Evidence for Non-Uniform Faraday Rotation

The ground array for the 1.6 GHz VSOP observations of 1803+784 on July 20, 1998 included the ten VLBA antennas, the phased VLA, and the 70-m Goldstone dish. The $(u, v)$ coverage is similar to that in Figure 1.

The resolutions of the VSOP 1.6 GHz images and the ground-only 5 GHz images from the following day are very nearly the same. Figure 3 shows the two sets of $I$ and $P$ images of the inner-jet region; the 1.6 GHz structure actually extends much further from the core, and will

be considered in more detail in a separate paper. At both frequencies, the structure observed in this region is very simple, and is dominated by a double roughly corresponding to the core and the nearly stationary feature to the west. This enables a relatively straightforward comparison of the images at the two frequencies.

Most surprising is the different behavior shown by the polarization position angles for the two features. In the simplest case in which the polarization of each of the components is subject to the same amount of Galactic (foreground) Faraday rotation, and this is the only Faraday rotation present, we would expect to observe the same rotation in $\chi$ between 1.6 and 5 GHz for both of the components. Even a cursory inspection of the images in Figure 3 shows that this is not the case.

This indicates a more complicated frequency dependence for the $\chi$ angles than is expected for a uniform foreground Faraday screen. Unfortunately, we cannot test for the $\lambda^2$ dependence expected for Faraday rotation, since we have data at only two frequencies. However, one obvious possibility is that there is Faraday rotation *local* to 1803+784, which is different for the two features.

We would like to derive reliable estimates for the separate rotation measures for the two components in the 1.6 GHz VSOP and 5 GHz ground images, in order to remove their effect from the higher resolution 5 GHz VSOP image. However, this is not so straightforward: rotation measure estimates are subject to $n\pi$ ambiguities, which can only be removed reliably when data are available at three or (preferably) more frequencies. In the case of our two-frequency 1803+784 data, even if we limit our consideration to $\chi$ ambiguities of $\pm 180^\circ$, there are two possible differences in the 1.6 GHz and 5 GHz polarization angles for each component, which cannot be distinguished based on the available data. These imply two possible rotation measures for each component, of comparable magnitude but opposite sign: roughly +25 or –85 rad/m$^2$ for the core region and –50 or +60 rad/m$^2$ for the western component.

The corresponding rotations at 5 GHz are $+5^\circ$ or $-17^\circ$ for the core region and $+10^\circ$ or $-12^\circ$ for the western component. The two possible rotation measures for the core region imply the same general $\chi$ behavior: either way, $\chi$ remains aligned with the direction of the inner VLBI jet. The choice of rotation measure for the western component could affect our interpretation: if the rotation measure is close to +60 rad/m$^2$, the derotated $\chi$ vectors will align even better with the local direction of the downward curving jet; if the rotation measure is close to –50 rad/m$^2$,

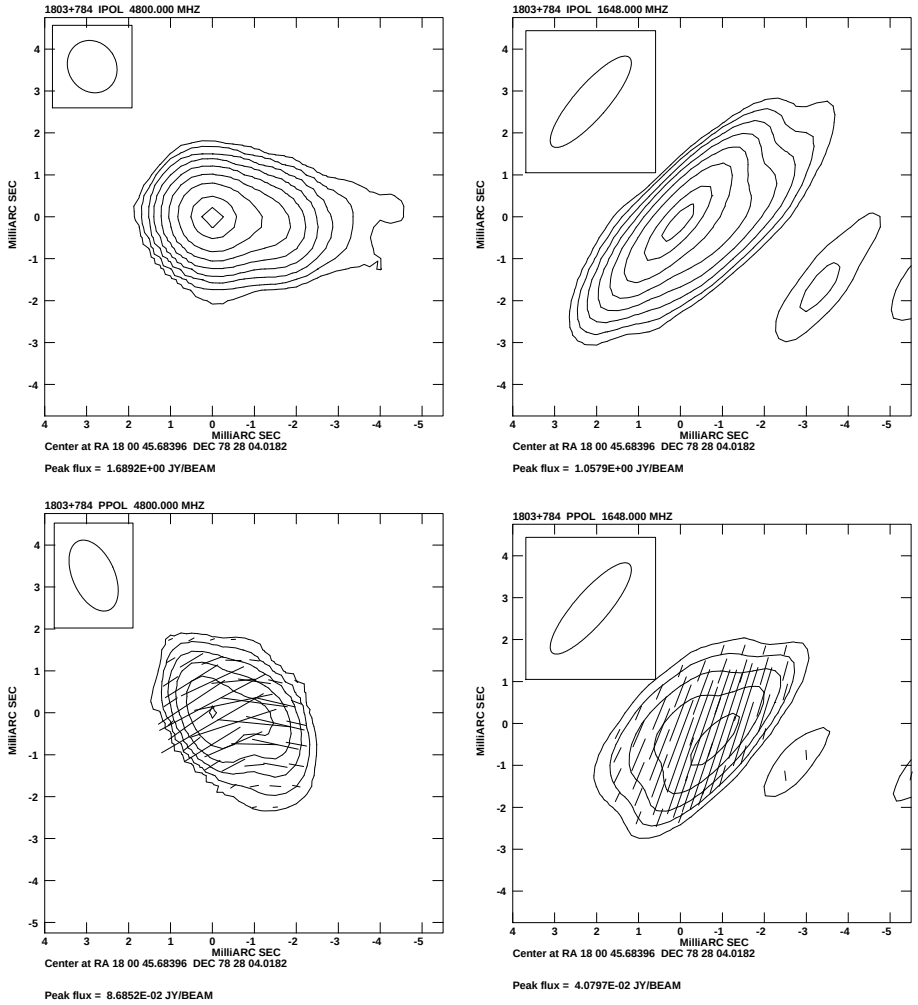


Figure 3: 5 GHz ground-only $I$ (top left) and $P$ (bottom left) images of the inner jet of 1803+784 on July 21, 1998 and 1.6 GHz VSOP $I$ (top right) and $P$ (bottom right) images of the same region on July 20, 1998. The bottom contours for the 5 GHz $I$ and $P$ images are $\pm 0.5$ and $\pm 3\%$ of the peak flux densities of 1689 and 87 mJy/beam; the bottom contours for the 1.6 GHz $I$ and $P$ images are $\pm 1\%$ and $\pm 5\%$ of the peak flux densities of 1058 and 41 mJy/beam. The contours for all images increase in multiples of 2. The sticks show superposed $\chi$ vectors.

the derotated $\chi$ vectors will be aligned nearly east–west, so that they will lie at an oblique angle to the local jet direction.

Formally, we cannot distinguish between these two possibilities. Since we cannot verify that the $\chi$ values for the two regions of emission obey a $\lambda^2$ law, we cannot exclude another physical origin for the frequency dependence of the polarization angles. One obvious possibility is the presence of polarized subcomponents that have different $\chi$'s and make different contributions to the total polarizations at 5 and 1.6 GHz. However, the high-resolution 5 GHz image in Figure 2 suggests that the polarized emission within each of the two regions in Figure 3 has fairly uniform $\chi$ values, making it unlikely that subcomponents with very different polarizations are giving rise to the anomalous frequency dependence of the $\chi$ values in Figure 3. We feel that the most natural explanation for our observations is that the two regions of emission experience different Faraday rotations, but we are unable to unambiguously determine the corresponding local rotation measures using our two-frequency data.

Due to this uncertainty, we have not applied any rotation measure corrections to the 5 GHz $\chi$ vectors in Figure 2. VLBA polarization images of 1803+784 at 1.3 cm and 7 mm, where we would expect the effects of the proposed rotation measures to be negligible, show that $\chi$ in the region of the stationary component clearly aligns with the direction of the jet channel curving downward from the north (Gabuzda and Chernetskii, in preparation; Marscher et al., in preparation). For this reason, we believe that our result, based on Figure 2, that the inferred **B** in the curved VLBI jet is everywhere transverse is on firm ground.

## 4 Conclusion

These first polarization images made from data obtained as part of VSOP General Observing Time have yielded two unexpected and potentially quite important results. The 5 GHz VSOP $I$ and $P$ images provide compelling evidence for a toroidal magnetic field in the curved VLBI jet of 1803+784 (Gabuzda 1999), as is, in fact, expected in many theoretical models of relativistic jet flows. Comparison of the 5 GHz ground-only and 1.6 GHz VSOP polarization images suggest that the rotation-measure distribution of this source is non-uniform on parsec scales. The implied rotation measures are not large – some tens of rad/m$^2$ – but it is surprising to find appreciable differences in the rota-

tion measures of regions separated by only $\sim 1-2$ mas ($\sim 5-10$ pc at the redshift of 1803+784). This indicates the presence of thermal plasma in the immediate vicinity of the BL Lacertae object, and demonstrates that applying integrated rotation measures equally to all VLBI components can lead to erroneous results in some cases.

A more complete analysis of these data is in progress. We are also in the process of analyzing multi-frequency VLBA data for 1803+784, which we hope will enable us to study the toroidal **B** field in this source in more detail and better constrain values for the local rotation measures on parsec scales.

**Acknowledgements.** This work was supported by the European Commission under TMR contract No. ERBFMGECT950012. I would like to thank the National Astronomical Observatory in Mitaka for hospitality during my stay in the last months of 1998. I also gratefully acknowledge the VSOP Project, which is led by the Japanese Institute of Space and Astronautical Science in cooperation with many organizations and radio telescopes around the world.

## References

Gabuzda, D.C., 1999, *New Astronomy Reviews*, **43**, 691

Gabuzda, D.C. & Cawthorne, T.V., 1996, *MNRAS*, **283**, 759

Gabuzda, D.C., Cawthorne, T.V., Roberts, D.H. & Wardle, J.F.C. 1992, *ApJ*, **388**, 40

Gabuzda, D.C., Mullan, C.M., Cawthorne, T.V., Roberts, D.H. & Wardle, J.F.C., 1994, *ApJ*, **435**, 140

Gabuzda, D.C., Pushkarev, A.B., & Cawthorne, T.V., 1999, *MNRAS*, **307**, 725

Gabuzda, D.C., Pushkarev, A.B., & Cawthorne, T.V., 2000, *MNRAS*, submitted

Hughes, P.A., Aller, H.D. & Aller, M.F., 1989, *ApJ*, **341**, 69

Laing, R., 1980, *MNRAS*, **193**, 439

Witzel, A., Schalinski, C.J., Johnston, K.J., et al. 1988, *A&A*, **206**, 245

*Astrophysical Phenomena Revealed by Space VLBI*
*H. Hirabayashi, P.G. Edwards and D.W. Murphy (eds.)*

# Polarization-Sensitive VSOP Observations of Bright Quasars and $\gamma$-Ray AGN

G.A. Moellenbrock[1], D.H. Roberts[2] & J.F.C. Wardle[2]

[1] *NRAO, Green Bank, WV, USA*
[2] *Brandeis University, Waltham, MA, USA*

**Abstract**

Polarization-sensitive VLBI is an effective probe of local jet flow and pattern structure via compression or stretching of tangled field lines in shocked or boundary regions in the synchrotron plasma. In sources thought to have jets most closely aligned with our line of sight, projection effects can exaggerate 3-dimensional bending and when combined with aberration, yield complex apparent polarization structure in VLBI images. HALCA represents a unique opportunity to better resolve and model this complex structure at lower frequencies where the jet material remains strong, yet where ground-only VLBI hasn't sufficient resolution. We present some initial results of polarization-sensitive 5 GHz VSOP observations of the bright quasar 3C 345 and the $\gamma$-ray blazar 0234+285. Both sources reveal interesting polarization structure which is relevant to jet models.

## 1 3C 345

The bright quasar 3C 345 has been regularly monitored with VLBI for more than 2 decades (e.g., Lobanov 1996, and references therein), revealing a succession of apparently superluminal components emerging along curved (and different) trajectories. It was one of the first superluminal sources to be monitored in detail with polarization-sensitive VLBI (at 5 GHz, Brown et al. 1994). The 5 GHz VSOP observation presented here was made on July 28, 1998 using HALCA, the VLBA, the phased VLA, and Effelsberg. The total intensity data was shared with the MPIfR collaboration and is described in detail by Klare et al. 2000 (these proceedings). Figure 1 shows our full-resolution total intensity image and the corresponding polarization image. Remarkably consistent with the higher frequency results of Ros et al. (2000), the polarization position angle changes rapidly over inner 2 milliarcseconds, and there

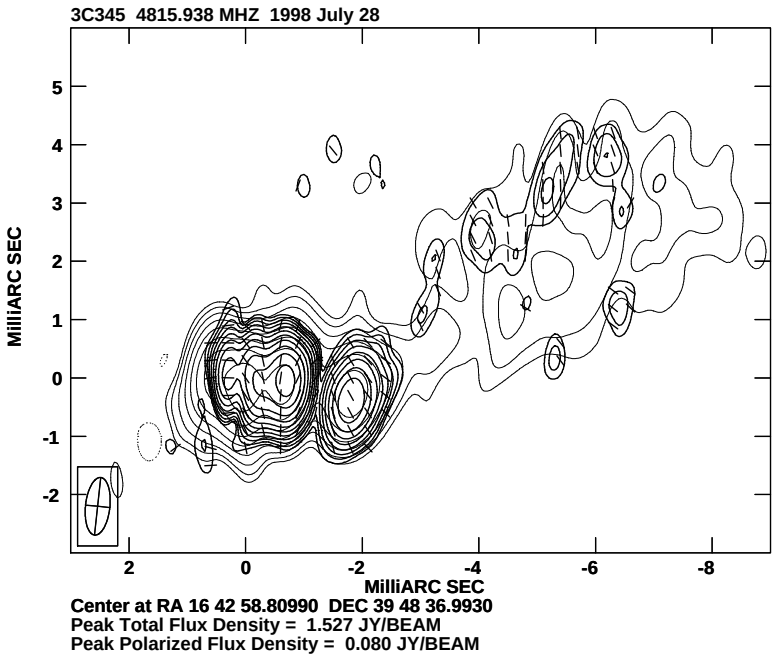


Figure 1: Total intensity (I) and polarization (P) VSOP image of 3C 345. The I contours are spaced by factors of 2, beginning at 7.5 mJy/beam. The P contours (bold) are spaced by factors of $\sqrt{2}$, beginning at 2.1 mJy/beam and the electric vectors are of constant length for clarity.

is significant depolarization within the beam just east of the western-most compact component. The eastern-most polarized component has a transverse inferred magnetic field (assuming the emission is optically thin), consistent with it being a shock newly emerged from the unresolved core. The peak in total intensity does not coincide with a peak in the polarized image, and the fractional polarization increases just downstream of it. An interpretation similar to that of Wardle et al. (1994) for this source, where transverse shocks are postulated to dilute an underlying longitudinal magnetic field, may be applicable. However, the detailed polarization position angle distribution within this region (often oblique), suggests that interpretation exclusively in terms of shocks must invoke the existence of highly projected curvature (observed in the component trajectories), opacity effects, or Faraday rotation (Taylor 1998 measures integrated rotation measures in this region consistent

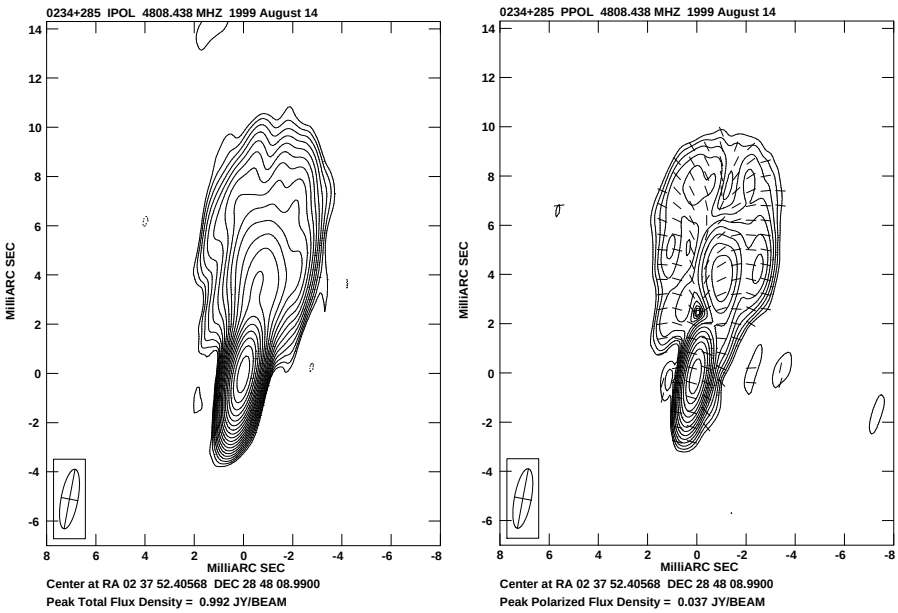


Figure 2: Total (left) and polarized (right) intensity images of 0234+285. The minimum contours are 1.5 mJy/beam and 0.45 mJy/beam for I and P, respectively, and are spaced by factors of $\sqrt{2}$ in both. The polarization E vectors are of constant length.

with rotation $\leq 30^\circ$). Contemporaneous high-frequency observations at matched resolution (being reduced) will help resolve this issue.

## 2 0234+285

The HPQ 0234+285, detected in $\gamma$-rays by EGRET (Mattox et al. 1997), is a challenging target for studies of projection effects since its jet (at least where the $\gamma$-rays originate, assuming current models for their emission) must be very well aligned with our line of sight. Our 5 GHz VSOP observation took place on August 14, 1999 and used HALCA, the VLBA, and Effelsberg. The space-VLBI image (Figure 2) reveals a diffuse, edge-brightened jet with inferred magnetic field running longitudinally along each limb, suggesting that field lines are stretched out along the jet boundary. Between the limbs, the inferred field is largely transverse. Combined with our finite resolution, this creates a spine of beam depolarization beginning $\sim$2 milliarcseconds north of the core. Except for the

core and a rather diffuse (and obliquely polarized) knot, the polarized emission is weakest between the limbs of the jet over the entire visible length. While still rather diffuse, the jet resolves into more concentrated components at higher observing frequencies (Moellenbrock 1999) and the overall jet structure oscillates from limb to limb. Due to the elongation and orientation of the beam, this effected is only marginally detected in the VSOP observation, but is consistent with the jet being highly projected.

**Acknowledgements.** We gratefully acknowledge the VSOP Project, which is led by the Japanese Institute of Space and Astronautical Science in cooperation with many organizations and radio telescopes around the world. The National Radio Astronomy Observatory is a facility of the National Science Foundation operated under cooperative agreement by Associated Universities, Inc.

## References

Brown, L.F., Roberts, D.H., & Wardle, J.F.C. 1994 *ApJ*, **437**, 108

Klare, J. et al. 2000, *these Proceedings*

Lobanov, A.P. 1996, PhD Thesis, New Mexico Institute of Mining and Technology

Mattox, J.R., Schachter, J., Molnar, L., Hartman, R.C., Patnaik, A.R. 1997 *ApJ*, **481**, 95

Moellenbrock, G.A. 1999, PhD Thesis, Brandeis University

Ros, E., Zensus, J.A., Lobanov, A.P. 2000, *A&A*, *in press*

Taylor, G.B. 1998, *ApJ*, **506**, 637

Wardle, J.F.C., Cawthorne, T.V., Roberts, D.H., & Brown, L.F. 1994, *ApJ*, **437**, 122

*Astrophysical Phenomena Revealed by Space VLBI*
*H. Hirabayashi, P.G. Edwards and D.W. Murphy (eds.)*

# Observations of Intraday Variable Sources

T.P. Krichbaum[1], C. Jin[1,2], A. Kraus[1], A. Witzel[1] & J.A. Zensus[1]

[1] *MPIfR, Auf dem Hügel 69, D-53121 Bonn, Germany*
[2] *Beijing Astronomical Observatory, Beijing 100012, China*

**Abstract**

Evidence is obtained for relatively rapid motion in an IDV source. We present first results from a VSOP monitoring of BL 2007+77, which reveals structural variability on a 3 week time scale.

## 1 Introduction

Since its discovery in the mid eighties (Witzel et al. 1986, Heeschen et al. 1987), Intraday Variability (IDV), which is common in about one third of compact flat spectrum radio sources, still poses the question of its physical origin. The variations in total intensity and polarization lead to apparent brightness temperatures of $T_B = 10^{15-21}$ K, largely exceeding the inverse Compton limit ($T_B = 10^{12}$ K). In order to avoid Doppler factors of $D > 100$, which would be required if bulk relativistic motion is the only cause for IDV, models invoking refractive interstellar scintillation (e.g. Rickett et al. 1995; Walker 1998; also Kedziora-Chudczer et al. and Jauncey et al. these proceedings), special shock-in-jet models (Qian et al. 1996a; Spada et al. 1999), and coherent emission mechanisms (Benford & Lesch 1998) are discussed.

In the last years it became clear that sources, which are intrinsically small, must show interstellar scattering effects (cf. Wagner & Witzel, 1995) and that the IDV phenomenon is probably a (frequency dependent) mixture of source intrinsic and propagation effects. However, even if refractive interstellar scintillation is adopted as the main cause of IDV in radio bands, the problem of the small source sizes, which lead to intrinsic brightness temperatures of $> 10^{14}$ K and Doppler factors of $D \geq 100$ remains[1], at least for the more rapid sources like e.g. PKS 0405−38 (Kedziora-Chudczer et al. 1997). Recently, it was suggested that this brightness temperature and Doppler factor could be a factor

[1] In this case $T_B$ scales with $D$ and not with $D^3$.

Table 1: The Experiments on 2007+77 at 5 GHz

| Code | Date | Epoch | Stations | Polarization |
|---|---|---|---|---|
| V053F1 | 1998 Mar.10 | 1998.19 | VLBA+Y+HALCA(1) | no |
| V053F3 | 1998 Apr. 1 | 1998.25 | VLBA+Y, no HALCA | no |
| V053F4 | 1998 Apr. 5 | 1998.26 | VLBA(8)+HALCA(3) | no |
| | | | | |
| W044F1 | 1999 Sep. 5 | | VLBA+EB+HALCA | yes |
| W044F2 | 1999 Sep. 7 | | VLBA+EB+HALCA | yes |
| W044F3 | 1999 Oct. 2 | 1999.75 | VLBA+EB+HALCA(3) | yes |
| W044F4 | 1999 Oct. 4 | | VLBA+EB+HALCA | yes |

Note: HALCA(n) mean data from HALCA with n tracking stations. Y denotes for the VLA, EB for Effelsberg. A missing entry in the third column means not yet fully analyzed.

of 10 lower, if the distance of the scattering screen is reduced (to 25 pc in the case of J1819+38, Dennett-Thorpe & de Bruyn, 2000). However, interstellar scintillation cannot explain the correlated radio-optical IDV, observed in 0954+65 (Wagner et al. 1993) and 0716+71 (Wagner et al. 1996; Qian et al. 1996b).

Evidence for large Doppler factors also comes from the standard synchrotron theory. Homogeneous synchrotron sources with sizes $\theta$ of a few to a few ten micro-arcseconds cannot be in equipartition, unless the Doppler factors are larger than $D > 50$ for $\nu_m \leq 22\,\mathrm{GHz}$. Another argument comes from the magnetic field, which should not decrease below the field induced by the cosmic background radiation. The sources have to be Doppler boosted with $D > 12$ for $\theta < 10\,\mu$as, but with $D > 192$ for $\theta < 5\,\mu$as ! In the frame of incoherent synchrotron theory, this dilemma might be solved, if one either allows a violation of the brightness temperature limit (cf. Kellermann et al. these proceedings) or just higher jet velocities. The latter seem to be detected in at least some sources (e.g. Marscher et al. these proceedings; Kraus et al. 1999).

## 2 VSOP Observations of IDV Sources

Owing to their high brightness temperature and intrinsic compactness, IDV sources are promising targets for present and future space VLBI observations. The observations of IDV sources therefore got the status of a 'key project' for VSOP. So far, data were obtained for 1803+78

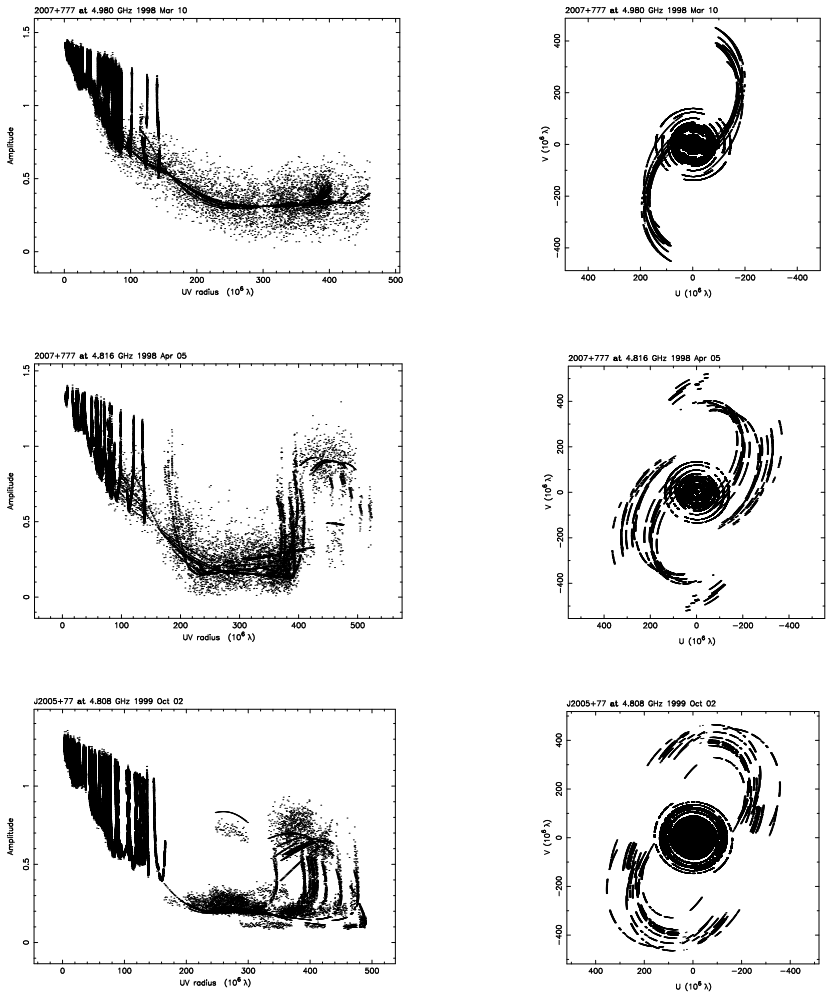


Figure 1: Visibility amplitudes (left) and $(u, v)$-coverages (right) for the experiments V053F1 (top), V053F4 (center) and W044F3 (bottom). Differences in the $(u, v)$-coverage could cause differences in the final images or model fits, which could be misinterpreted as structural variability. These uncertainties are reduced, if the data from the ground array are imaged/model fitted first. Although HALCA provides the higher angular resolution and therefore allows to determine positions within the source more accurately, the basic changes of the source structure already became obvious, when only the ground array data were analyzed.

(V053E) and 2007+77 (V053F & W044F). Here we report on VSOP observations of the BL Lac object 2007+77 ($z = 0.342$) during 1998–1999 at 5 GHz. This IDV sources is relatively slow and varies on time scales of a few days (Quirrenbach et al. 2000). The variability amplitudes increase with frequency and in the infrared/optical are by a factor of 5/10 larger than in the radio (Peng et al. 2000a). Table 1 summarizes the observational details. In addition to total intensity (3 epochs during AO1), the source was observed also in polarization and with a more uniform $(u, v)$-coverage in 1999 (4 epochs in AO2). From AO2, only W044F3 is analyzed so far. Whereas V053F covers timescales of 4, 21 & 26 days, the comparison of these data with W044F3 probes a time scale of 1.6 years. In Figure 1 we show the visibility amplitudes (left) and the $(u, v)$-coverages (right) for the 3 experiments with HALCA. We note that during March/April 1998 flux density measurements with the 100 m RT at Effelsberg revealed no significant flux density variations of 2007+77 on timescales of days. Between 1998.2 and 1999.8, however, the total flux density decreased by 30 %. During this period, the position angle of the total polarization vector increased from $-40°$ to $-10°$. A change probably corresponding to this, is seen in the ground array maps, which show an increase of the position angle of the axis in the central 1 mas region of the jet. This indicates that the direction of the magnetic field, or the inner jet itself, is slowly rotating towards north. In Figure 2 we show the polarization image obtained from W044F3. The comparison with the remaining 3 polarization observations from AO2 (see Table 1) will clarify, if and how the jet emission evolves in polarization.

The data set of 1998 allows to search for structural variations on timescales of 4 days to $\sim 3$ weeks. After fringe fitting and careful checks of the amplitude calibration, using two calibrators observed with the ground array, we imaged the sources in basically two ways, with and without HALCA baselines. The source structure was parameterized by circular Gaussian component fitted to the visibilities. Figure 3 shows the high angular resolution maps (beam: 0.4 mas) which include the HALCA baselines. The positions of the Gaussian components are superimposed. The brightest component at the map center ($r = 0$ mas) is used as a reference. We note that between the two maps on top (V053F1 and V053F4), the relative alignment of the 3 western components (the component at $r = 0$ mas, and the two components east and west from it, see Figure 4) has changed on a timescale of only 26 days. Further evidence for structural variability on such timescales comes from the

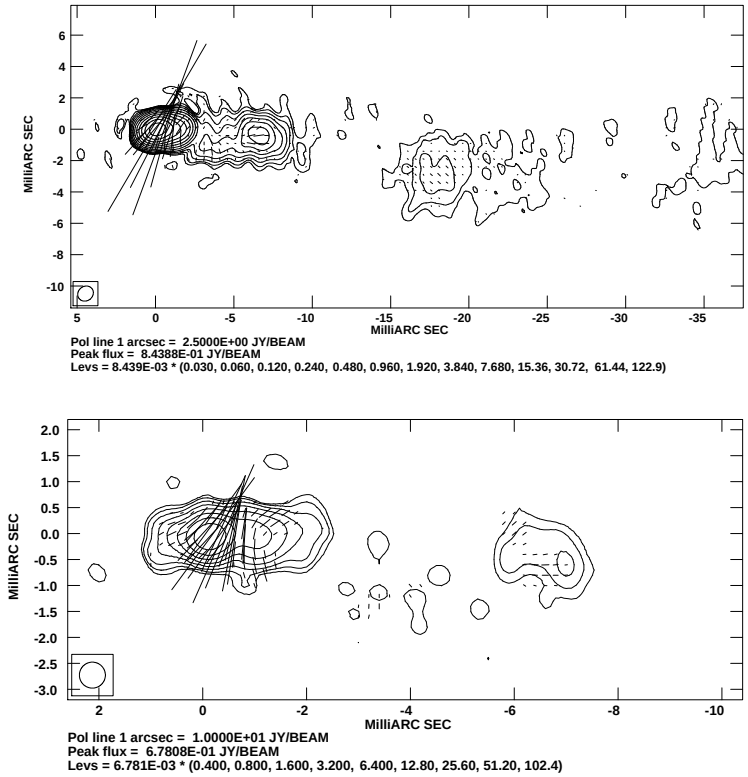


Figure 2: Polarization maps of 2007+77 obtained in 1999.75 at 5 GHz. Top: ground array only. Bottom: including baselines to HALCA.

comparison of the residual images (Figure 5).

In addition to the north-south 'displacement' of the core, the east-west separation of the 2 outer components has increased by 0.11 mas, which corresponds to an angular separation rate of $1.6 \pm 0.6$ mas/yr or an apparent velocity of $\beta_{app} = 40 \pm 15$ c (for $H_0 = 50$ km s$^{-1}$ Mpc$^{-1}$, $q_0 = 0.05$). Between 1998 and 1999, a new component appeared near the brightest component (see Figure 3, bottom, and Figure 4). This ejection of a new component was accompanied by a small flux density outburst observed at 5 GHz (Peng et al. 2000b). Using either the beginning (1998.7) or the peak of the flare (1999.2) as time of ejection of this component, a velocity between 7 and 13 c is obtained, consistent with velocities measured earlier (Witzel et al. 1988).

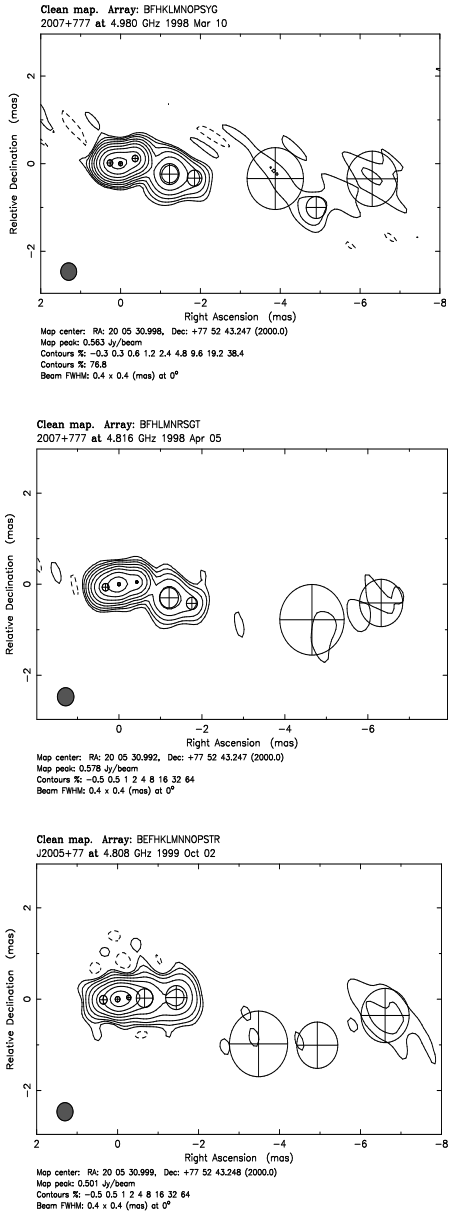


Figure 3: Maps of the Gaussian model fits. All maps are convolved with a circular beam of 0.4 mas size. The observing dates from top to bottom are March 10, 1998, April 5, 1998, and October 2, 1999.

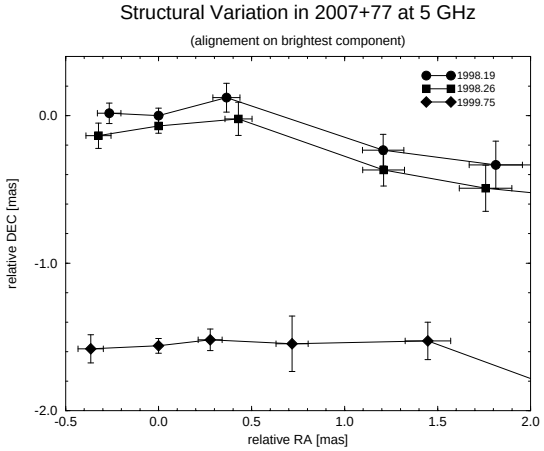


Figure 4: Positions of components in the inner jet region from the 3 VLBI observations. The vertical shifts in declination are proportional to the observing times. The relative alignment in right ascension is arbitrary, with the brightest component located at the map center at $r = 0$.

In Figure 6 we plot the brightness temperature along the jet axis, derived from the Gaussian model fits. For the brightest component ('the core'), which remained unresolved on ground-to-space baselines, the lower limit to the brightness temperature varied between $T_B \geq 7.7 \cdot 10^{12}$ K in 1998.19 and $T_B \geq 2.1 \cdot 10^{12}$ K in 1999.75. This clearly indicates time variable bulk relativistic motion with Doppler factors $D > 2.1$, respectively $D > 7.7$. An order of magnitude larger values of $D$ would be obtained, if the brightness temperature limit is not $10^{12}$ K, but is lower, e.g. $\sim 10^{11}$ K as required from energy equipartition. We note that the component 0.3 mas east of 'the core' has a brightness temperature below $10^{12}$ K, either indicative of synchrotron self-absorption at the jet base (likely), or presence of a counter-jet (unlikely).

The determination of the jet velocity depends on the component registration at different epochs and on the assumption of the stationarity of the reference point. At present, it is difficult to determine the source kinematics unambiguously. Scenarios in which the assumption of the stationarity of the core component is dropped lead to a different component identifications and to velocities in the range of $4 \leq \beta_{app} \leq 21$. The higher velocity values are obtained, if the most eastern jet component is regarded as the 'self-absorbed' core.

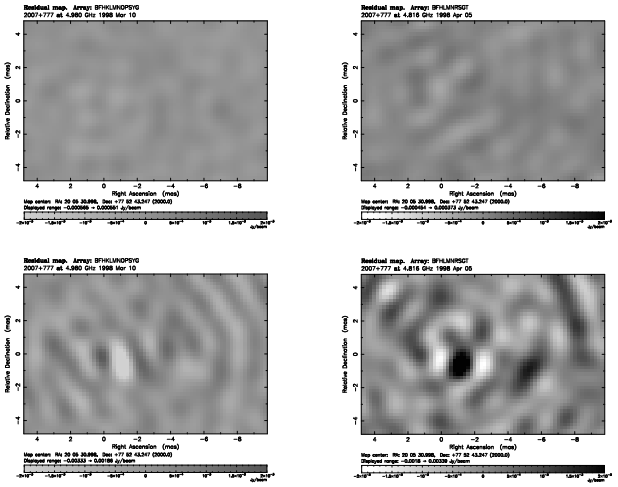

model versus own data

model versus other data

Figure 5: Comparison of the residual maps from epochs 1998.19 (V053F1, data set 1) and 1998.26 (V053F4, data set 3). The maps on top show the residuals between data and model set 1 (left) and data and model set 3 (right). Below the residuals are shown after data and model were exchanged. Plotted are data set 1 versus model set 3 (left) and data set 3 versus model set 1 (right). Structural variability between the two epochs show up as enhancements or depressions of the residual flux.

## 3 Summary

As a tentative result we conclude, that in 2007+77 structural variations on time scales of a few weeks, are detected. So far, no variations are detected on a timescale of a few days, which is consistent with the stationarity of the total flux during the observations. Variations appear in flux and position, position variations are along and transverse to the jet axis. The brightest component (core) is probably not stationary. The analysis of the other VSOP observations of 1999 (see Table 1) will resolve the remaining ambiguities for the component identification and will answer the question, if the velocities in 2007+77 are higher than previously thought. Of particular interest will be the search for changes of the orientation of the polarization vector on mas-scales. The rotation of the jet axis to the north, which was accompanied by a rotation of the polarization vector of the total flux, let us expect to detect polarization changes on mas-scale, also on short times scales.

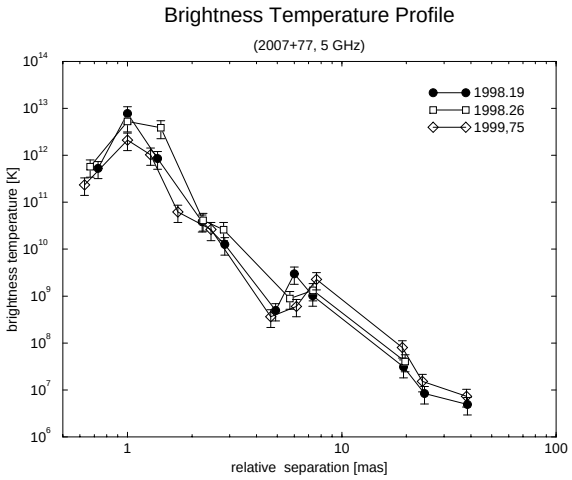


Figure 6: The brightness temperature profile along the jet axis. The individual values of the brightness temperatures of the components were calculated from the parameters of the Gaussian component model fits.

**Acknowledgements.** We gratefully acknowledge the VSOP Project, which is led by the Japanese Institute of Space and Astronautical Science in cooperation with many organizations and radio telescopes around the world.

## References

Benford, G. & Lesch, H., 1998, *MNRAS*, **301**, 414

Dennett-Thorpe, J. & de Bruyn, A.G., 2000, *ApJ*, **529**, L65

Heeschen, D.S., Krichbaum, T., Schalinski, C. J., Witzel, A., 1987, *AJ*, **94**, 1493

Kedziora-Chudczer, L., Jauncey, D.L., Wieringa, M.H., et al., 1997 *ApJ*, **490**, L9

Kraus, A., Quirrenbach, A., Lobanov, A.P., et al., 1999, *A&A*, **344**, 807

Peng, B., Kraus, A., Krichbaum, T.P., et al., 2000a, *A&A*, **353**, 937

Peng, B., Kraus, A., Krichbaum, T.P., & Witzel, A., 2000b, *A&A*, submitted

Qian, S.J., Witzel, A., Kraus, A., et al., 1996a, in: *Energy Transport in*

*Radio Galaxies and Quasars*, eds. P.E. Hardee, A. Bridle, & J.A. Zensus, ASP Conf. Ser. **100**, 55

Qian, S.J., Li, X.C., Wegner, R., et al., 1996b, *Chin. Astron. Astrophys.*, **20**, 15

Quirrenbach, A., Kraus, A., Witzel, A., et al., 2000, *A&AS*, **141**, 221

Rickett, B.J., Quirrenbach, A., Wegner, R., et al., 1995, *A&A*, **293**, 479

Spada, M., Salvati, M., & Pacini, F., 1999, *ApJ*, **511**, 136

Wagner, S.J., Witzel, A., Krichbaum, T.P., et al., 1993, *A&A*, **271**, 344

Wagner, S.J., & Witzel, A., 1995, *ARA&A*, **33**, 163

Wagner, S.J., Witzel, A., Heidt, J., et al., 1996, *AJ*, **111**, 2187

Walker, M.A., 1998, *MNRAS*, **294**, 307

Witzel, A., Heeschen, D.S., Schalinski, C.J., Krichbaum, T.P., 1986, *MitAG*, **65**, 239

Witzel, A., Schalinski, C.J., Johnston, K.J., et al., 1988, *A&A*, **206**, 245

*Astrophysical Phenomena Revealed by Space VLBI*
*H. Hirabayashi, P.G. Edwards and D.W. Murphy (eds.)*

# Circular Polarization of Intraday Variable Sources

L.L. Kedziora-Chudczer[1,2], J-P. Macquart[3],
D.L. Jauncey[2] & D.P. Rayner[4]

[1] *AAO, P.O. Box 296, Epping NSW 1710, Australia*
[2] *ATNF, PO Box 76, Epping NSW 1710, Australia*
[3] *SRCfTA, University of Sydney, NSW 2006, Australia*
[4] *University of Tasmania, Hobart, 7001, Tasmania, Australia*

**Abstract**

We present circular polarization observations of the intraday variable sources PKS 0405−385 and PKS 1519−273. We find strong ($> 1\%$) and variable circular polarization for PKS 1519−273, well correlated with fluctuations in the total flux density at 4.8 and 8.6 GHz. The circular polarization of PKS 0405−385 is weaker and less correlated with the total intensity, but shows fast variability on a timescale similar to the total flux density changes. We find no simple explanation for the origin of the circular polarization.

## 1 Introduction

Circular polarization (CP) in extragalactic sources is weak and has been difficult to measure reliably. The Australia Telescope Compact Array (ATCA) was designed with the ability to measure low levels of circular polarization and is now providing excellent results. In this paper we present ATCA polarimetric data for two compact intraday variable (IDV) sources PKS 0405−385 and PKS 1519−273.

PKS 0405−385 is a $m_V = 18.5$, $z = 1.285$ quasar in which we discovered extreme IDV in the total intensity in June 1996 (Kedziora-Chudczer et al. 1997). This IDV episode lasted only two months and IDV did not recur until two years later, from November 1998 to April 1999. PKS 1519−273 is a $m_V = 18.5$, $z > 0.2$ BL Lac in which total and polarized flux density IDV was discovered during our ATCA IDV Survey (Kedziora-Chudczer et al. 1998).

## 2 Observations

Total and polarized flux density measurements of **PKS 0405−385** from 1999 January 15 are shown in Figure 1. The start of the November 1998 IDV episode was characterized by rapid, weak fluctuations, but by January the variability timescale had doubled and the amplitude increased. The modulation indices of the total flux density at 8.4 and 4.8 GHz were 2.3% and 3.1%, respectively in November 1998, and 11.1% and 9.8% in January 1999. The mean CP over this second period was $\langle V \rangle / \langle I \rangle \approx 0.2\%$, however the CP was variable with no significant correlation with the total flux density.

The amplitude of the variations in **PKS 1519−273** is comparable to that in PKS 0405−385 but its timescale is slower (cf. Figs. 1 & 2). Figure 2 illustrates the high CP and its strong correlation with the fluctuations in total intensity, indicating an identical origin for their variability (Macquart et al. 2000). From this we can derive the degree of CP of the variable component: $-2.6 \pm 0.5\%$, $-3.8 \pm 0.4\%$ and $-2.4 \pm 1.3\%$ at 8.6, 4.8 and 2.5 GHz respectively.

## 3 Discussion

We argue that the IDV of PKS 0405−385 is caused by interstellar scintillation (ISS) of a microarcsecond component (Kedziora-Chudczer et al. 1997). Our measurement of the time-delay in the arrival of the variability pattern of this source between the VLA and the ATCA is a persuasive argument (Jauncey et al., this Symposium) that IDV in general is caused by ISS. The characteristics of the variability in PKS 1519−273 also favour ISS (Macquart et al. 2000). Scintillation-based size estimates imply $T_B \approx 2 \times 10^{14}$ K for PKS 1519−273 and $T_B \approx 5 \times 10^{14}$ K for PKS 0405−385.

The characteristics and degree of CP detected in the variable component of PKS 1519−273 are difficult to reconcile with theory. The high fractional CP observed in the variable component decreases sharply between 4.8 and 1.4 GHz, in disagreement with $\nu^{-1/2}$ dependence expected from the synchrotron theory.

CP may arise due to conversion of linear polarization to CP (circular repolarization) in a relativistic pair plasma, analogous to the effect of Faraday rotation. Such conversion is characterized by a strong frequency dependence on the sign of the CP. However, we detect no changes in the

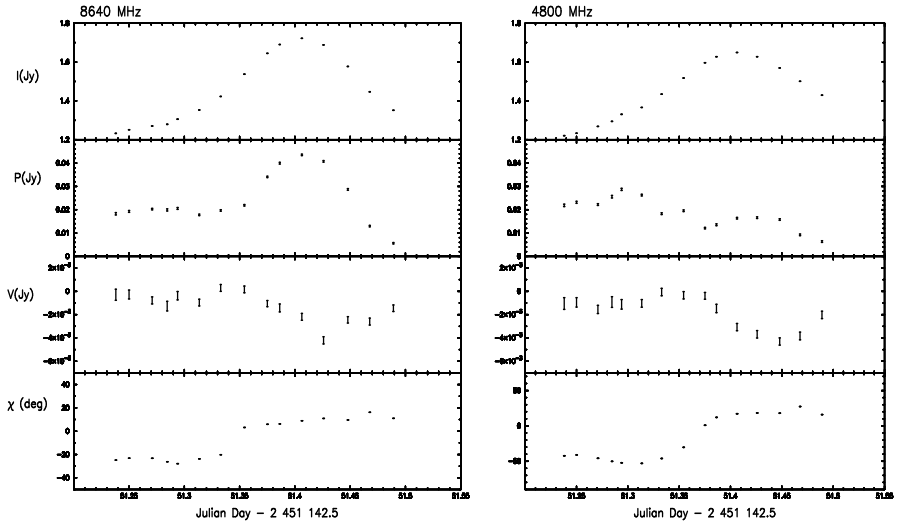


Figure 1: Variability of PKS 0405−385 in the total intensity ($I$), CP ($V$), and magnitude and position angle of the linear polarization ($P$ and $\chi$) at 4.80 and 8.64 GHz over 12 hours on 15 Jan 99. Each point represents a 20 min average, and is plotted with $1\,\sigma$ error bars.

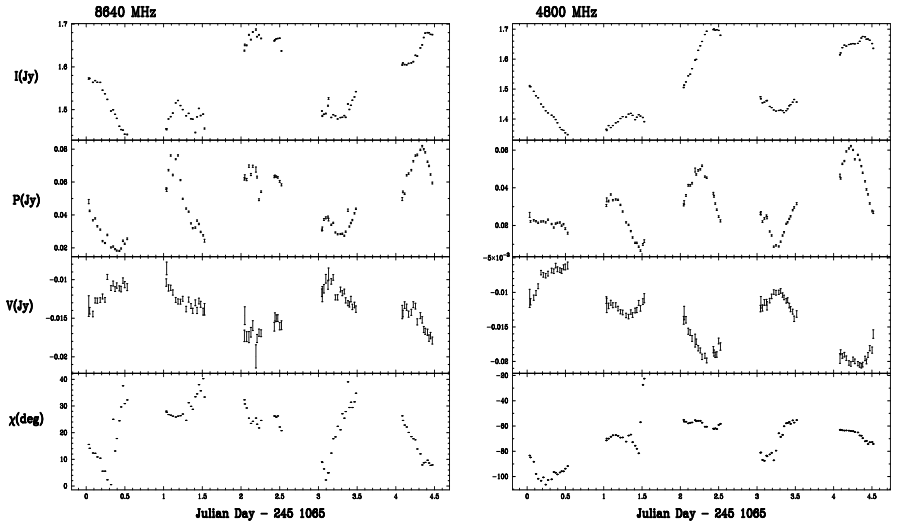


Figure 2: Variability of PKS 1519−273 at 4.80 and 8.64 GHz over 5 days. Each point represents a 10 min average, and is plotted with $1\,\sigma$ error bars.

sign of the CP between 8.6 and 1.4 GHz.

Inhomogeneity and optical depth effects in a pair plasma (Jones & O'Dell 1977) may account for CP *provided that* the self-absorption frequency is between $\approx$ 3.4 and 6.7 GHz. This is difficult to confirm since the intrinsic spectrum of the variable component is unknown.

## 4 Conclusion

The observed variability of PKS 0405−385 and PKS 1519−273 are both well explained by scintillation theory. The associated variability in the CP is also likely due to ISS but the two sources differ substantially in their degree of CP and its correlation with the total intensity. The exceptionally high CP in PKS 1519−273 is difficult to account for with simple existing models (Macquart et al. 2000).

If an explanation of the origin of the high brightness temperatures of these sources demands we abandon the hypothesis that their emission is due to synchrotron radiation, it is tempting to speculate on its connection with the CP.

**Acknowledgements.** The Australia Telescope is funded by the Commonwealth Government for operation as a national facility by the CSIRO. The Special Research Centre for Theoretical Astrophysics was funded by the Australian Research Council under its Special Research Centres programme.

## References

Jones, T.W. & O'Dell, S.L., 1977, *ApJ*, **215**, 236

Kedziora-Chudczer, L. et al. 1997, *ApJ*, **490**, L9

Kedziora-Chudczer, L. et al. 1998 in *ASP Conf. Ser.* **144***: IAU Coll. 164: Radio Emission from Galactic and Extragalactic Compact Sources*, eds. J.A. Zensus, G.B. Taylor & J.M. Wrobel (San Francisco: Astron. Soc. Pac.), 271

Macquart, J.-P. et al. 2000, *ApJ*, *in press*

*Astrophysical Phenomena Revealed by Space VLBI*
*H. Hirabayashi, P.G. Edwards and D.W. Murphy (eds.)*

# The Origin of Intra-Day Variability

D.L. Jauncey[1], L.L. Kedziora-Chudczer[1,2], J.E.J. Lovell[1],
G.D. Nicolson[3], R.A. Perley[4], J.E. Reynolds[1],
A.K. Tzioumis[1] & M.H. Wieringa[1]

[1] *ATNF, PO Box 76, Epping NSW 1710, Australia*
[2] *AAO, PO Box 296. Epping NSW 1710, Australia*
[3] *HartRAO, Krugersdorp 1740, South Africa*
[4] *NRAO, Socorro NM 87801, USA*

**Abstract**

We report simultaneous flux density measurements at 4.86 GHz of the Intra-Day Variable (IDV) source PKS 0405−385 made with the VLA and the ATCA. These show a significant time difference between the arrival times of the variability patterns at the two telescopes, as expected if interstellar scintillation (ISS) is the origin of the IDV.

## 1 Introduction

Radio variability was discovered 35 years ago when the first quasar, 3C273, was found to double in intensity in 3 years at 8 GHz (Dent 1965). These observations led directly to the development of VLBI, to Space VLBI, to VSOP and to this Symposium. Super-luminal expansion was discovered and bulk relativistic motion (Rees 1966) found to explain the observed brightness temperatures of up to $\sim 10^{13}$ K, in excess of the inverse Compton limit (Kellermann and Pauliny-Toth 1969). And the variability proved to be intrinsic to the sources.

Twenty years later a new kind of variability, IDV, with a time-scale not of years, but of days, was discovered (Heeschen 1984). Recent observations find sources with time-scales from days to hours (Quirrenbach et al. 1989; Kedziora-Chudczer et al. 1997; Dennett-Thorpe and de Bruyn, 2000). If the variations are intrinsic, causality arguments imply nanoarcsecond sizes and brightness temperatures of $10^{18}$ K to $10^{21}$ K. While bulk relativistic motion was an acceptable explanation for brightness temperatures up to $10^{13}$ K, it is less so for $10^{21}$ K. Interstellar scintillation (ISS) was proposed as an alternative to avoid such extreme conditions (Heeschen and Rickett 1987).

If the variations are intrinsic, the pattern of variations should be the same when seen at two widely spaced radio telescopes. However,

if ISS is the cause, the motion of the irregularities in the interstellar medium (ISM) can cause the patterns to arrive at different times at the two telescopes.

## 2 Observations

The source PKS 0405−385 was chosen since it shows large amplitude variations on a time-scale as short as an hour (Kedziora-Chudczer et al. 1997). In November 1998 it returned to an active state (Kedziora-Chudczer et al. 1998), and the observations were made on December 9 as the source set at the VLA in the USA and rose at the ATCA in Australia. The observations were centred at 4.86 GHz where both telescopes offer optimum performance. The VLA was in C configuration and separate sub-arrays were used at 1.4, 8, 15, 22 and 43 GHz to determine the overall spectrum. The ATCA was in a 750 m configuration with antenna CA02 excluded because of shadowing at low elevations.

We saw strong variability with very similar patterns at both telescopes, and were fortunate to observe a clear minimum, since an inflection is essential for precise alignment of the patterns. Close examination of the flux density curves shows that the pattern arrived first at the VLA then, $\sim 2$ minutes later, at the ATCA. Using the time-delay analysis of Pelt et al. (1996) we find a time difference of 140 seconds. A series of Monte Carlo trials was made to estimate the uncertainty. After 1000 trials we estimate the time difference as $140 \pm 25$ seconds. Such a large time difference, much greater than the light travel time difference, shows that the variations are not intrinsic to the source, and gives strong support to an ISS origin for IDV.

## 3 Discussion

A feature of the variability curves is that the flux density difference changes sign systematically before and after the inflection. Both the gain-elevation and atmospheric absorption corrections are such that they serve to increase the ATCA measured flux densities before the inflection and to also increase the VLA flux densities after the inflection. Thus, if the observations show a time delay *before* these corrections are applied, this delay can only *increase* after application of gain-elevation and atmospheric absorption corrections. Re-analysis of the observations, but without these corrections, yielded the smaller difference of $96 \pm 25$

seconds, and with the same sign. The Monte Carlo histogram is shown in Figure 1, where the strong peak around 100 seconds can be seen, with no differences smaller than 50 seconds.

Thus the observed time difference is clearly real. For the 10,000 km telescope separation the time difference of $140 \pm 25$ seconds corresponds to a velocity of $75 \pm 15$ km s$^{-1}$, in good agreement with the $\sim$50 km s$^{-1}$ typical of the ISM.

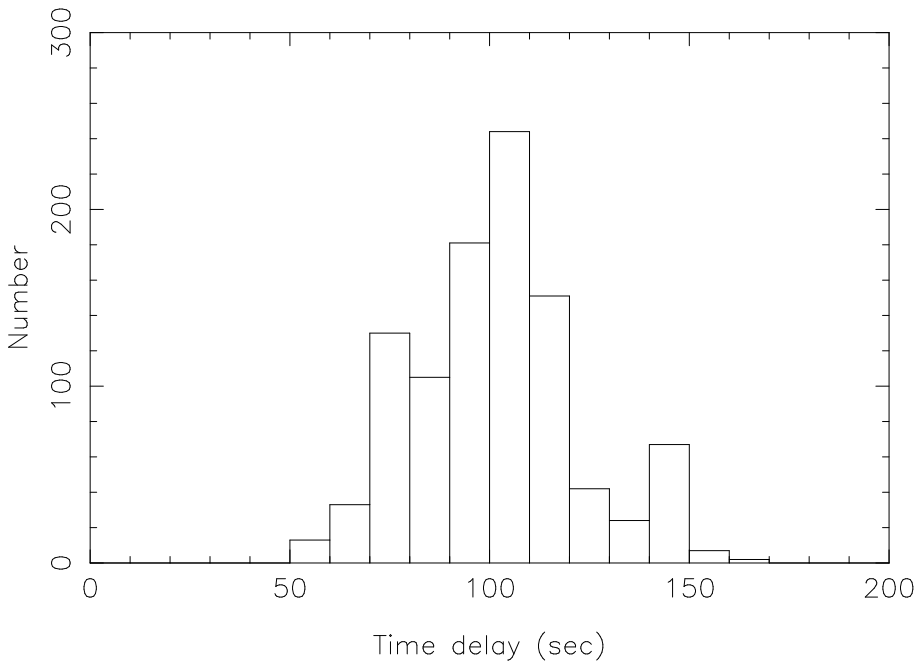


Figure 1: Plot of the VLA − ATCA Monte Carlo time difference, with no flux density corrections

## 4 Conclusions

The measured time difference shows that the intra-day variability observed in PKS 0405−385 is not intrinsic to the source, but rather is best explained by interstellar scintillation. A microarcsecond source angular size component is implied with brightness temperatures of $\sim 5 \times 10^{14}$ K. It seems natural, following these results for PKS 0405−385, to assume an ISS origin for IDV in general.

These results have significant implications for future Space VLBI missions, since IDV studies show that many sources possess microarcsecond angular size components at cm wavelengths. These components are generally weak, so that high sensitivity will be necessary on the space telescope, along with full polarization capability, since several IDV sources show both strong linear and circular polarization (Macquart et al. 2000; Kedziora-Chudczer et al. these proceedings). Retaining an 18 cm capability will be an important tool to investigate both source structure as well as properties of the ISM. Finally, ISS will ultimately limit achievable angular resolution at cm wavelengths.

**Acknowledgements.** We gratefully acknowledge the VSOP Project, which is led by the Japanese Institute of Space and Astronautical Science in cooperation with many organizations and radio telescopes around the world. The Australia Telescope is funded by the Commonwealth Government for operation as a national facility by CSIRO.

## References

Dennett-Thorpe, J. & de Bruyn, A.G. 2000, *ApJ*, **529**, L65

Dent, W.A. 1965, *Science*, **148**, 1458

Heeschen, D.S. 1984, *AJ*, **89**, 1111

Heeschen, D.S. & Rickett, B.J. 1987, *AJ*, **93**, 589

Kedziora-Chudczer, L. et al., 1997, *ApJ*, **490** L9

Kedziora-Chudczer, L. et al., 1998, IAU Circular 7066

Kellermann, K.I. & Pauliny-Toth, I.I.K. 1969, *ApJ*, **155** L71

Macquart, J.-P. et al., 2000, *ApJ*, *in press*

Pelt, J. et al., 1996, *MNRAS*, **231**, 229

Quirrenbach, A. et al., 1989, *A&A*, **226** L1

Rees, M.J. 1966, *Nature*, **211** 468

*Astrophysical Phenomena Revealed by Space VLBI*
*H. Hirabayashi, P.G. Edwards and D.W. Murphy (eds.)*

# Why Space VLBI is of Special Value for Studies of High-Redshift Radio Sources

L.I. Gurvits

*JIVE, P.O.Box 2, 7990 AA, Dwingeloo, The Netherlands*

**Abstract**

Space VLBI brings a special benefit in the studies of milliarcsecond radio structures of extremely high redshift sources. This property is illustrated by the simulated SVLBI and real VSOP data.

## 1 Introduction

Dual frequency VSOP studies of a sample of high redshift quasars constitute one of the General Observing Time (GOT) projects of the mission. At the time of this Symposium the project is not yet completed. Some preliminary results of the high-$z$ VSOP project have been or will be soon presented by Hirabayashi et al. (1998), Gurvits et al. (2000a; 2000b) and Lobanov et al. (2000). The project is aimed at two goals: *(i)* to search for potential evolutionary effects intrinsic to the quasars in the milliarcsecond scale radio structures, and *(ii)* to investigate possible imprints of the cosmological model by studying the milliarcsecond scale structural properties as a function of redshift.

VSOP, as the first dedicated Space VLBI (SVLBI) mission, in addition to its self-standing scientific value, provides the most important practical experience and experimental basis for planning future SVLBI missions, in particular those described in these proceedings by Marscher (ARISE), Hirabayashi (VSOP-2) and Gurvits (SVLBI observatory assembled in space). It is expected that the next generation SVLBI mission will operate in a significantly broader range of frequencies than VSOP. There is a strong and well motivated move toward as high observing frequencies as feasible: all next generation SVLBI missions include 43 GHz as a nominal band, and some aim at the challenging 87 GHz. However, as stressed in several presentations at this symposium, frequencies of 5 GHz and lower could be of high importance for the future SVLBI studies of pulsars (Gwinn, these proceedings), Galactic OH masers (Diamond, these proceedings) and radio stars (Taylor et al. these proceedings).

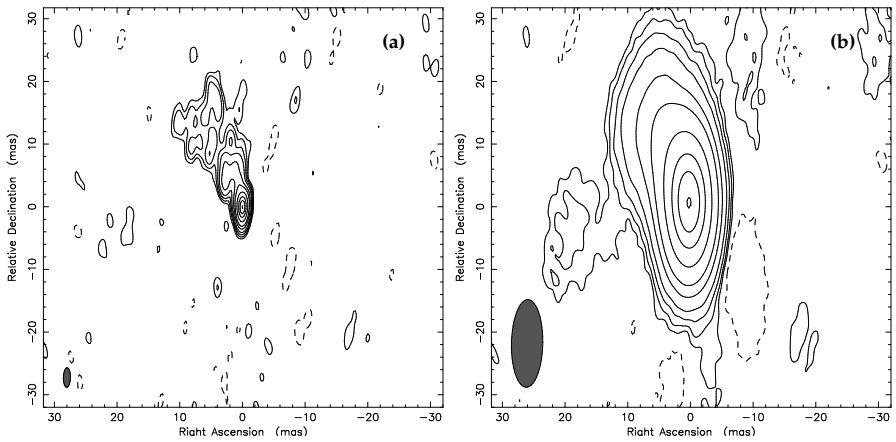


Figure 1: A simulated source as seen by the global ground-based VLBI array at **(a)** $z = 0.1$ and $\nu = 8$ GHz and **(b)** $z = 3.6$ and $8/(1+z) = 1.6$ GHz. Both images have noise close to the expected thermal limit.

High redshift quasars (and other types of AGN) also represent a class of targets for future SVLBI missions, for which the lower end of the overall frequency coverage is promising to be very productive.

## 2 What is Special About High Redshift Targets for SVLBI

It is a well established fact that the most compact components in milliarcsecond scale radio structures of AGN have flatter spectra than the extended features. In fact, this spectral difference is widely accepted as the most reliable criterion which makes it possible to distinguish "core" components which are believed to be close to the central engine and the "jets". As shown recently by Frey et al. (1997) and Paragi et al. (1999), the average difference between the spectral indices of compact "jets" and "cores" in quasars is $\alpha_j - \alpha_c = -0.62 \pm 0.45$. Due to this difference, the extended "jets" fade faster with growing emitting frequency than the flatter spectrum "cores". Not surprisingly, on average, at any fixed receiving frequency, sources at a higher redshift appear more compact than their lower redshift counterparts. Thus, in order to study milliarcsecond scale "core–jet" structures in high-redshift quasars it is beneficial to operate at a lower observing frequency. However, this comes at a high cost in terms of angular resolution which is proportional to the observing wavelength. It is virtually impossible to match in angular resolution and

emitting frequency observations of high and low redshift sources on the milliarcsecond scale while using ground-based VLBI networks only.

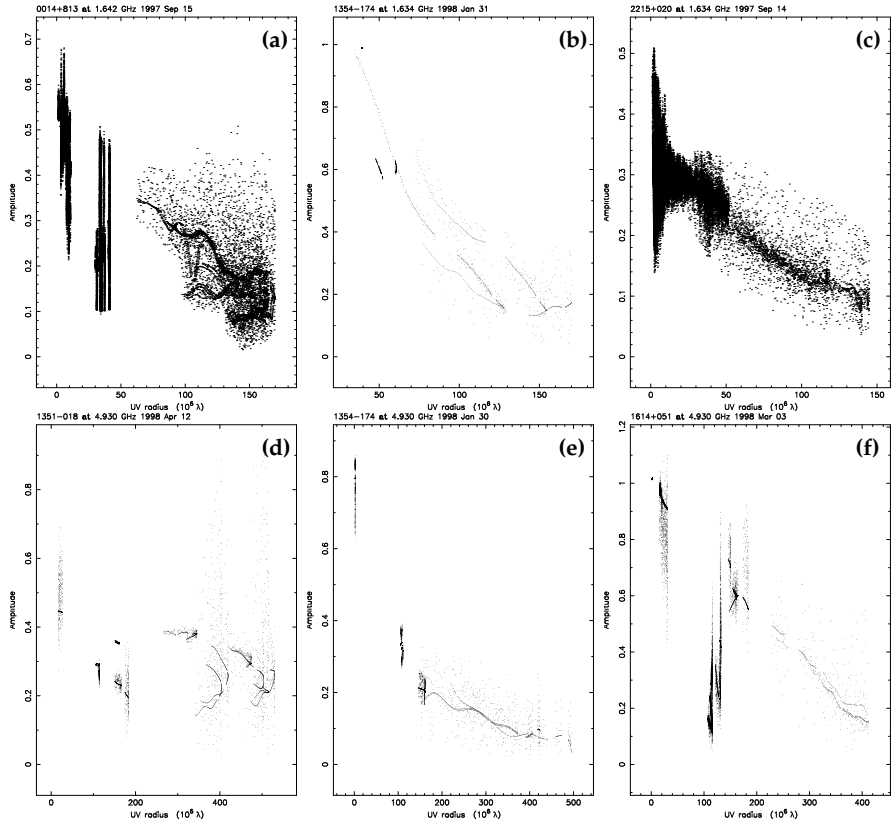


Figure 2: Correlated flux density (amplitude, Jy) versus projected baseline (mega-wavelengths) from VSOP observations of quasars **(a)** 0014+813, **(b)** 1354−174, **(c)** 2215+020 at 1.6 GHz and **(d)** 1351−018, **(e)** 1354−174 and **(f)** 1614+051 at 5 GHz.

Figure 1 illustrates this problem (see Gurvits 2000 for details). It shows simulated images of two similar sources, both observed with the global ground-based VLBI arrays. The left image corresponds to the source at $z = 0.1$ and observed at 8 GHz, while the right image corresponds to the source "moved away" to $z = 3.6$ and observed at the source-frame-matched frequency $8/(1 + z) = 1.6$ GHz. The insufficient sharpness of the image on the right is obvious. The only cure for this problem is to extend the baselines beyond the Earth's diameter as VSOP does.

## 3 VSOP High Redshift Project: Status and Conclusion

The high redshift VSOP project includes observations of 21 quasars at $z \geq 3$ at either one or both VSOP frequencies, 1.6 and 5 GHz. The sources included have total flux density $\gtrsim 400$ mJy at the frequency of observation. To date, the VSOP high-redshift observing project is $\approx 50\%$ complete. Its preliminary results do prove the expectation on the efficiency of SVLBI observations of high-redshift targets. All sources observed so far are resolved (Figure 2), with the typical correlated flux densities $\lesssim 200$ mJy at the longest VSOP projected baselines ($\approx 170$ M$\lambda$ at 1.6 GHz and $\approx 500$ M$\lambda$ at 5 GHz). Qualitatively, this result is in agreement with the statistical result of the VSOP Survey Programme (Lovell et al. these proceedings).

The high angular resolution of SVLBI at lower frequencies is of special importance for studies of extremely high redshift sources. For steeper spectrum components, this property of SVLBI cannot be matched by ground-based VLBI at a higher frequency. From this perspective, it is important not to exclude lower frequencies $\leq 5$ GHz from the ongoing studies of the next generation SVLBI missions.

**Acknowledgements.** I gratefully acknowledge the VSOP Project, led by ISAS in cooperation with many agencies, institutes and observatories around the world. I express my gratitude to the co-investigators of the high-redshift VSOP project S. Frey, N. Kawaguchi, K.I. Kellermann, A.P. Lobanov, I.I.K. Pauliny-Toth and R.T. Schilizzi.

### References

Frey, S., Gurvits, L.I., Kellermann, K.I. et al. 1997, *A&A*, **325**, 511

Gurvits, L.I. 2000, in *Perspectives on Radio Astronomy*, eds. M.P. van Haarlem and J.M. van der Hulst, in press

Gurvits, L.I., Frey, S., Schilizzi R.T. et al. 2000a, *Adv. Sp. Res.*, **26**, No. 4, 719

Gurvits, L.I., Frey, S., Schilizzi R.T. et al. 2000b, in preparation

Hirabayashi, H., Hirosawa, H., Kobayashi, H. et al. 1998, *Science*, **281**, 1825 and erratum **282**, 1995

Lobanov, A.P., Gurvits, L.I., Frey, S. et al. 2000, in preparation

Paragi, Z., Frey, S., Gurvits, L.I. et al. 1999, *A&A*, **344**, 51

*Astrophysical Phenomena Revealed by Space VLBI*
*H. Hirabayashi, P.G. Edwards and D.W. Murphy (eds.)*

# VSOP Studies of the Bright Radio Source PKS 1921−293

Zhi-Qiang Shen[1], P.G. Edwards[2], J.E.J. Lovell[3] & S. Kameno[1]

[1] *NAO, Osawa 2-21-1, Mitaka, Tokyo 181-8588, Japan*
[2] *ISAS, Yoshinodai 3-1-1, Sagamihara, Kanagawa 229-8510, Japan*
[3] *ATNF, CSIRO, P.O. Box 76, Epping, NSW 2121, Australia*

**Abstract**

We (for collaborators see acknowledgements) present a preliminary report on VLBI Space Observatory Programme (VSOP) observations of one of the brightest radio sources, PKS 1921−293, at both 1.6 and 5.0 GHz. With the high-resolution provided by HALCA, we are able to look deeper into the core region. An inner jet component about 1.5 mas to the core is revealed for the first time. The core brightness temperature (in the rest frame of the quasar) is estimated of $3.0 \times 10^{12}$ K.

## 1 Introduction

The quasar PKS 1921−293 (OV−236) is a relatively nearby radio-loud blazar with $m_v = 17.5$. It is one of the strongest radio sources in the sky. Figure 1 shows a composite spectrum of PKS 1921−293. Despite its dramatic variability over a wide range of wavelengths from radio to X-ray, its spectrum is quite simple: a flat radio spectrum over 3 orders of magnitude (from ∼300 MHz to ∼300 GHz) plus a power-law spectrum with a slope of −1.3 from infrared to X-ray. If this power law spectrum extends to $\gamma-$ray band, the extrapolated flux at 100 MeV is about $1.1 \times 10^{-13}$ Jy. This is lower than those of EGRET sources (see Figure 5 in von Montigny et al. 1995), which might be the simplest explanation to the non-detection of $\gamma-$ray emission from the source.

The compactness of PKS 1921−293, implied by its flat radio spectrum, has been confirmed by existing VLBI measurements. It is not resolved on arcsecond scales with VLA observations (de Pater et al. 1985). Previous VLBI observations suggest a very compact bright core with a brightness temperature ($T_b$) measured in the rest frame of the quasar, in excess of $10^{12}$ K, which is among the highest measured for any blazar (cf., Linfield et al. 1989; Moellenbrock et al. 1996).

At a redshift of only 0.352 (Wills and Wills 1981), an angular resolution of 1 mas corresponds to a linear resolution of 4.6 pc (assuming $H_0 = 65\,\mathrm{km\,s^{-1}\,Mpc^{-1}}$ and $q_0 = 0.5$).

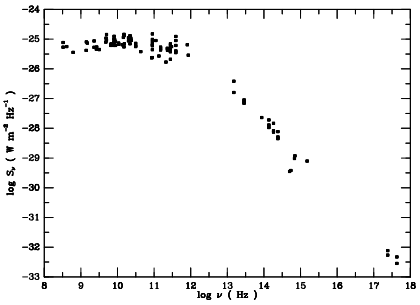


Figure 1: The composite spectrum of PKS 1921−293 obtained from various published and unpublished measurements.

## 2 VSOP Observations

VSOP observations of PKS 1921−293 have been performed at two epochs. On 1997 July 18, VSOP in-orbit checkout observations of PKS 1921−293 were made with interleaved 1.6 and 5.0 GHz scans. The data were recorded in standard VLBA format, but with only one intermediate-frequency (IF) band of 16 MHz for each frequency. On 1998 June 19, PKS 1921−293 was observed at a frequency of 5.0 GHz with a recording bandwidth of 32 MHz (two IFs). NRAO's VLBA and phased VLA provided the ground array for these observations. These data were correlated in Socorro. The total durations of these observations were about 3.0 hr in 1997 (1.5 hr for each frequency) and 7.5 hr in 1998 (at 5.0 GHz). Figure 2 shows the $(u, v)$ coverage for each epoch.

Post-correlation data reduction was performed within AIPS and Difmap. Strong fringes were consistently detected on all space baselines to HALCA. In order to explore the compact core region, uniform weighting was adopted for the VSOP images.

## 3 Results

The details of 1.6 GHz VSOP imaging are given in Shen et al. (1999). The analysis of the 5.0 GHz data is still ongoing. We show preliminary images from two-epoch 5.0 GHz VSOP observations in Figure 3 along with the plots of visibility amplitude versus $(u, v)$ distance.

The core-jet morphology of VSOP images is consistent with ground-based VLBI images, consisting of a very strong and compact core with some extended jet emissions (cf. Kellermann et al. 1998). Moreover,

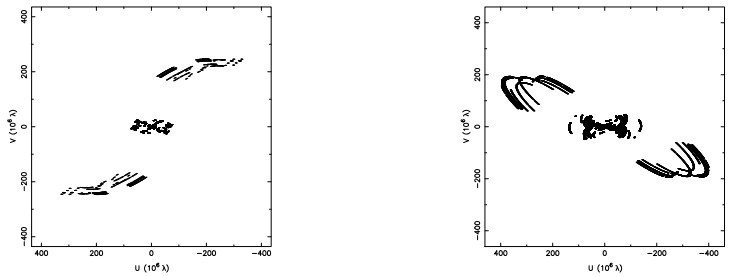

Figure 2: The $(u, v)$ coverage corresponding to VSOP observations of PKS 1921−293 on 1997 July 18 (*left*) and 1998 June 19 (*right*).

the addition of data from HALCA has greatly improved the angular resolution, especially along the north-south direction for this southern source (7-times better at the first epoch, see Figure 2). As a result, we are able to look deeper into the core region than ever before at 1.6 and 5.0 GHz. For the first time, a new inner jet component was revealed at about 1.5 mas north to the 1.6 GHz core. This feature is also seen in the 1998 5.0 GHz image with a little shift to the east. So, it may be moving on a common curved path connecting the jet within a few parsecs to the 10-parsec-scale jet seen in VLBA images (Shen et al. 2000, in preparation).

The distribution of the correlated flux density versus $(u, v)$ distance indicates that the core is partially resolved on space baselines. A dip seen in 1997 5.0 GHz data at ∼250 M$\lambda$ (Figure 3 top) may suggest the existence of the compact double separated by ∼0.4 mas along the position angle of HALCA baselines within the core. Unfortunately, there was a ∼90° change in the position angle for the 1998 observations (see Figure 2), which made it difficult to discern any double structure. But the non-monotonic decrease in the correlated flux density (Figure 3 bottom) implies that the central region cannot be fitted with a single circular component. The derived core $T_b$ from both 1.6 and 5.0 GHz images is about $3.0 \times 10^{12}$ K, an indication of relativistic beaming.

**Acknowledgements.** We gratefully acknowledge the VSOP Project, which is led by ISAS in cooperation with many organizations and radio telescopes around the world. In addition to the authors, people who are involved in the project are M. Inoue, K. Fujisawa (NAO), D. Jauncey, S. Tingay, J. Reynolds, A. Tzioumis, E. King (ATNF), J. Moran (CfA), R. Preston, D. Murphy, D. Meier, D. Jones (JPL), G. Nicolson (HartRAO), P. McCulloch and M. Costa (Univ. of Tasmania).

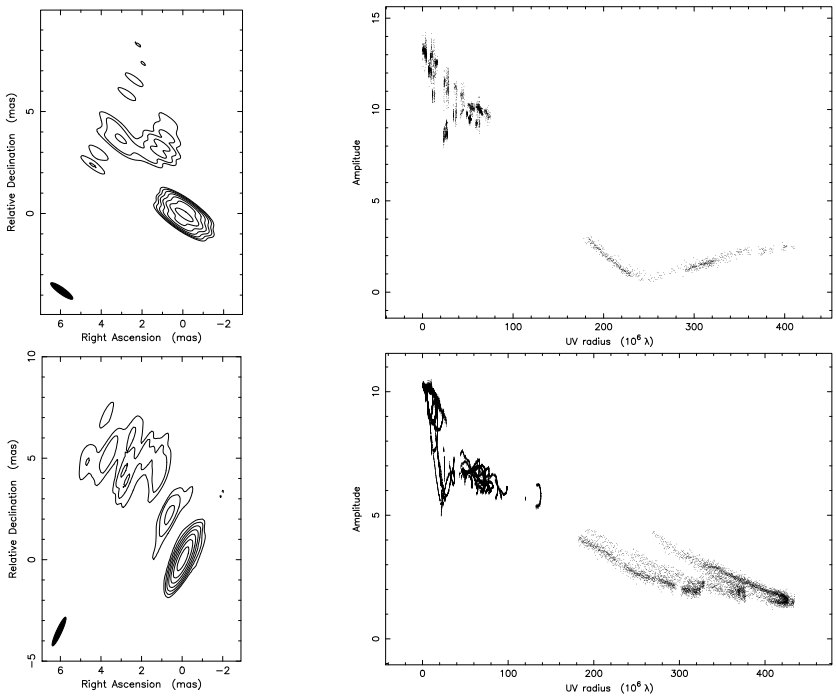


Figure 3: 5.0 GHz VSOP images and plots of visibility amplitude vs. $(u, v)$ distance from the two epochs (Top: 1997 July 18; Bottom: 1998 June 19). Contour levels are at $-1$, 1, 2, 4, 8 and 64% of the peak flux densities, which are 5.3 Jy/beam and 4.1 Jy/beam for the two images respectively. The synthesized beams are $1.32 \times 0.32$ (mas) at $54.3°$ and $1.55 \times 0.26$ (mas) at $-24.7°$, respectively.

## References

de Pater, I., Schloerb, F.P. & Johnson, A.H. 1985, *AJ*, **90**, 846

Kellermann, K.I., Vermeulen, R.C., Zensus, J.A. & Cohen, M.H. 1998, *AJ*, **115**, 1295

Linfield, R.P., Levy, G.S. & Ulvestad, J.S. et al. 1989, *ApJ*, **336**, 1105

Moellenbrock, G.A., Fujisawa, K. & Preston, R.A. et al. 1996, *AJ*, **111**, 2174

Shen, Z.-Q., Edwards, P.G. & Lovell, J.E.J. et al. 1999, *PASJ*, **51**, 513

von Montigny, C., Bertsch, D.L. & Chiang, J. et al. 1995, *ApJ*, **440**, 525

Wills, D. & Wills, B.J. 1981, *Nature*, **289**, 384

*Astrophysical Phenomena Revealed by Space VLBI*
*H. Hirabayashi, P.G. Edwards and D.W. Murphy (eds.)*

# Observations of Relativistic Outflow in AGN and the Brightness Temperature of Synchrotron Sources

K.I. Kellermann [1], R.C. Vermeulen [2], J.A. Zensus[3,1], & M.H. Cohen[4]

[1] *NRAO, 520 Edgemont Rd., Charlottesville, VA 22903, USA*
[2] *NFRA, Oude Hoogeveensedijk 4, 7991 PD Dwingeloo, The Netherlands*
[3] *MPIfR, Auf dem Hügel 69, D53121 Bonn, Germany*
[4] *Dept. of Astronomy, MS 105-24, Caltech, Pasadena, CA 91125, USA*

**Abstract**

VLBA observations over a five year period are used to discuss the outflow of relativistic plasma from the center of quasars and AGN. The distribution of apparent linear velocity has a tail indicating pattern velocities up to 20$c$, but there is little evidence for corresponding Doppler boosting of the flux density.

## 1 Introduction

We are using the VLBA to investigate the flow of relativistic plasma from the center of quasars and AGN. Our goals are to describe and understand source kinematics. We wish to know: a) Do components move along straight or curved trajectories? b) Do all components in an individual source follow the same trajectory or have the same velocity? c) Are there accelerations or decelerations of individual components? d) Does the apparent velocity depend on luminosity or other parameters? e) Can the time of component ejection be related to flux density changes at radio, optical, or high-energy wavelengths? We also wish to compare the kinematic properties of AGN, quasars, and BL Lac objects with the systematic differences expected from unified models, and we also want to compare the observed motions of strong gamma-ray sources with those that are not.

We interpret our observations in terms of relativistic beaming models with the ultimate goal of understanding the process of acceleration and collimation of relativistic jets. We want to know if simple ballistic models are correct or whether there are differences between the bulk flow velocity and the pattern velocity. Finally, we are interested in exploring the use of the angular velocity–redshift ($\mu$–$z$) relation to test

world models. We are mainly interested in statistical properties, so our investigation complements other programs designed to study individual sources in more detail including multiwavelength polarization observations (e.g., Marscher, these proceedings) or studies of particular classes of source such as BL Lac objects.

We have chosen to observe at a wavelength of 2 cm as a compromise between getting the best angular resolution and good image quality. At shorter wavelengths the resolution is better, but the sensitivity is worse; individual features may decay with time before their motion can be determined, and tropospheric fluctuations degrade the image quality. At longer wavelengths the data are more robust, but the resolution is often inadequate to separate closely spaced components.

We have observed approximately 150 sources over a period of five years. Two to three 48-hour observing runs per year allow 60 sources to be observed in each session. There are 4–18 month intervals between observations of individual sources, depending on the apparent rate of change in the structure. Up to ten epochs have been obtained for the fastest sources. The observing procedure is described in more detail by Kellermann et al. (1998). Typically each image has an rms noise of 200 to 300 $\mu$Jy and the resolution is $0.5 \times 1$ mas. Assuming a minimum SNR of 10:1 for individual components, we should be able to measure component locations to within about 0.1 mas; therefore, after 5 years we might expect to determine the rate of motion with an accuracy of only a few hundredths of a mas/yr. However, in practice our accuracy is considerably poorer, owing in part to changes in component structure and/or changes in the synthesized beam shape resulting from the loss of one or more antennas.

Single-epoch images for 132 sources have already been published (Kellermann et al. 1998). Images from other epochs are available at http://www.cv.nrao.edu/2cmsurvey. As our resolution at 2 cm is similar to that of VSOP at 6 cm, our program provides good matched resolution images for studies of the spectral distribution across compact sources.

## 2 The Distribution of Apparent Velocity

We interpret our observations in terms of relativistic twin-ejection models. For a given intrinsic value of velocity, $v$, $\beta = (v/c)$ where $c$ is the velocity of light; $\gamma = (1 - \beta^2)^{-1/2}$; and the Doppler factor, $\delta = 1/(1 - \beta_b \cos\theta)$; and where $\theta$ is the angle between the beam and the

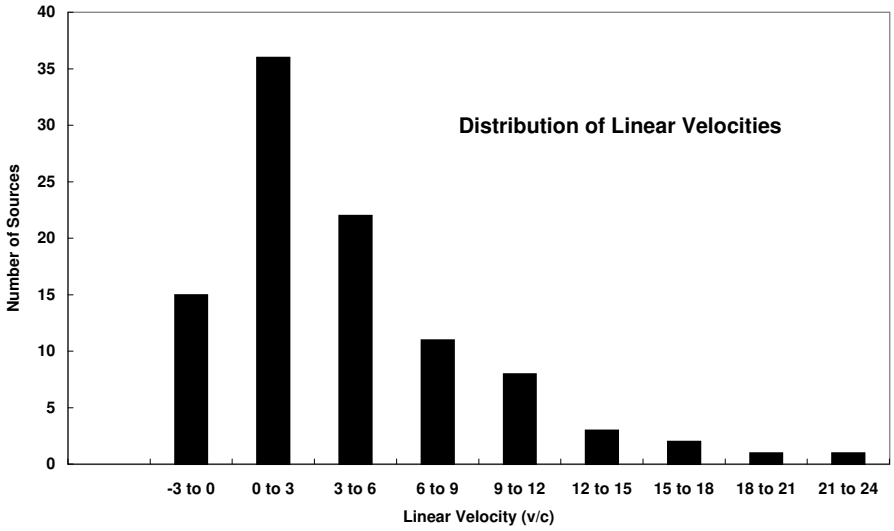


Figure 1: The observed apparent velocity distribution

line of sight and $\beta_b$ is the bulk velocity of the plasma flow. For numerical calculations we assume $H_0 = 65\,\mathrm{km\,s^{-1}\,Mpc^{-1}}$ and $q_0 = 1/2$.
There are three observable effects of relativistic motion.

a) The Doppler shift, which moves the rest frame frequency, $\nu_r$, to $\nu_{obs} = \delta\nu_r$ in the observer's frame.

b) The apparent transverse motion $\beta_a = \sin\theta/(1 - \beta_p \cos\theta)$ where $\beta_p$ is the intrinsic velocity of the pattern flow.

c) Relativistic or Doppler boosting of the intrinsic luminosity, $S_i$ to give an observed luminosity, $S_{obs} = S_i\delta^3$.

Assuming that the ejection of relativistic beams is randomly oriented in space, in the absence of Doppler boosting the probability, that a source lies within an angle $\theta$ to the line of sight is proportional to $1/(1 - \cos\theta)$ and most sources will lie close to the plane of the sky. However, due to Doppler boosting, flux-limited samples are dominated by sources oriented close to the critical angle $1/\gamma$.

Figure 1 shows the observed distribution of $\beta_a$, defined as the separation rate of the two brightest components for each source in our sample where we have adequate data to define the apparent velocity. In every

case where the core can be unambiguously identified at the end of a one-sided structure, the observed flow is outward. The few cases shown in Fig. 1 with negative velocity are not significant, or occur in complex, often symmetric sources, where we have probably not properly identified the core. The distribution of observed velocity is concentrated at low velocities, with a median value of $\beta_a = 2.9$. This is in sharp contrast to early studies which appear to have been biased by observers' selection to study and report only sources with large apparent velocity, but it is consistent with the more recent studies reported by Vermeulen (1995) based on observations at 6 cm. The observed distribution appears to require either a large spread in $\gamma$ (Lister and Marsher 1997) or that the bulk velocity is much less than the pattern velocity so that there is little or no Doppler bias toward observing sources near the critical orientation $\theta = 1/\gamma$. Indeed the observed distribution is not unlike the simple *light echo model* discussed by Ekers & Laing (1990).

It is tempting to consider interpretations which do not invoke the usual Doppler bias. However, it is then hard to understand the apparent one-sidedness of the observed structures (e.g., Kellermann et al. 1998). The low-luminosity sources, which often have two-sided jets, appear to move more slowly, consistent with the simple Doppler boosting picture. It will be important, in future observations of the more rapidly moving sources, to obtain sufficient dynamic range and sensitivity to detect any counter-jet, thus providing additional constraints on models which invoke Doppler boosting. Interestingly, we find a very slow velocity in the jet of M87 where the brightest jet component located about one parsec from the core has an apparent velocity of only $0.1c$, although HST and VLA observations further along the jet show velocities closer to $c$ (Junor, these proceedings). In other sources as well, such as 3C84 (Dhawan et al. 1998), where there is a clear observed difference between the flow velocity and pattern velocity, there is an apparent increase in velocity along the jet.

Of course, this does not necessarily mean that components actually accelerate as they move outward from the core. In fact, we do not find significant evidence for changes in the speed or direction of any individual component. Instead, the observed increase in apparent velocity may be the result of bending, although this should produce apparent decelerations in addition to accelerations. Alternately, we may simply be seeing the consequence of the fact that the faster components have propagated further from the core. This may be tested by checking if the

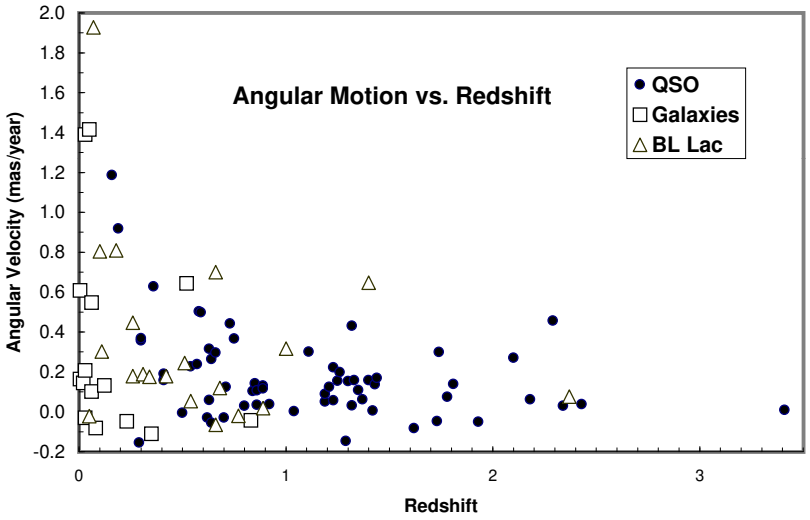


Figure 2: Apparent angular velocity for quasars, BL Lacs and radio galaxies as a function of redshift.

observed velocities are proportional to their distance from the core.

In sources with multiple components, the apparent velocities are similar, but not identical. In those cases where we have been able to follow the two-dimensional trajectory, there is some evidence that the different components do not follow the same trajectories, but further observations will be required to confirm this (e.g., Zensus et al. 1995)

It is widely assumed that the observed gamma-ray emission from quasars originates at the base of the jet, close to the accretion disk of a supermassive black hole. Radio VLBI observations image the region closer to the central engine than is possible in any other wavelength band and may provide some insight into the generation of the gamma-ray emission. We have examined the distribution of apparent velocities for sources which have been detected by the EGRET facility aboard GRO. Taking only radio loud quasars with $P_{5GHz} \geq 10^{25.5}\ W/Hz$, the EGRET sources appear to have a median value of $\beta = 5.7 \pm 0.6$ compared with the non EGRET sources of $3.9 \pm 0.4$. We note however, that unlike the radio observations of QSO's which have a well defined radio-loud and radio-quiet population, the range of gamma-ray flux sensitivity is currently

very limited so that there is not a well defined class of gamma-ray loud and gamma-ray quiet quasars. Future observations with GLAST will better define the relationship, if any, between gamma-ray luminosity and apparent velocity as well as determine if the onset of a component ejection corresponds to a gamma-ray flare.

## 3 Applications To Unified Models and Cosmology

Figure 2 shows the dependence of apparent angular velocity on redshift for the brightest jet component in each source. We note two important things. First, there appears to be no obvious difference in observed velocity among quasars, the cores of FR II radio galaxies, and BL Lacs, contrary to what might be expected from unified models which predict systematic differences in orientation among sources classified as quasars, radio galaxies, or BL Lacs. In particular, we confirm the previously reported superluminal motion for the cores of the FR II radio galaxies, 3C 111 (Preuss et al. 1990) and 3C 390.3 (Alef et al. 1996).

Second, we note the apparent angular velocity is greatest for sources at low redshift, as expected if the redshift is a measure of distance. Vermeulen & Cohen (1994) have discussed the use of the angular velocity–redshift, or $\mu$–$z$, relation to distinguish among cosmological models. Unlike these earlier studies which considered the upper envelope of the distribution appropriate to a Doppler-boosted sample, we have considered the binned median velocity distribution which may be more appropriate to the apparent lack of Doppler induced bias in our sample. While the dispersion is too great to meaningfully distinguish among world models, it is encouraging that the median angular velocity does appear to decrease with increasing redshift in a manner consistent with standard world models. Future observations of component motions for high-redshift quasars may offer the possibility of better defining the cosmological parameters.

## 4 Inverse Compton Limits and Brightness Temperature

Although there are no unresolved sources in our sample, there are ten sources, 0007+106, 0048−097, 0235+164, 0642+449, 0808+019, 1308+326, 1638+398, 1741−038, 1758+388, and 2145+067 which consist of a single barely resolved component with apparent brightness temperatures in the range $10^{11-12}$ K. These sources will be useful as

calibrators for centimeter wavelength VLBI. In addition, the strong millimeter source 1921−293 which has a diffuse cocoon-like extended feature is dominated by a single component with brightness temperature comparable to the above sources. Kellermann and Pauliny-Toth (1969) have pointed out that owing to inverse Compton cooling, brightness temperatures in excess of $10^{11-12}$ K cannot be maintained for long periods. However, Readhead (1994) has argued that if there is equipartition between the magnetic energy density and relativistic particle density, then the peak brightness temperatures are nearly an order of magnitude lower. It seems to us, however, that it is unlikely that such equipartition conditions will exist in sources where there is clearly a sudden highly collimated violent release of relativistic plasma.

These sources, therefore, do not necessarily require a Doppler boosting factor to reduce the rest frame brightness temperature to the equipartition value. Moreover, Slysh (1992) has argued that a non-equilibrium situation may exist for months to years following the turn-on of an electron energy distribution initially extending to very high energy. This is consistent with the observed variability time scales, even in the case of the rapid intraday variables (e.g., Wagner 1998). However, it is not clear if the analysis of Slysh properly includes the effect of second order scattering which greatly reduces the lifetime to inverse compton cooling.

Thus, Doppler factors deduced from observed brightness temperatures and measurements of inverse Compton scattered X-ray emission, may not be as large as previously discussed, consistent with the low apparent velocities which we have observed, and the apparent absence of strong Doppler boosting.

## 5 Summary

Although most theoretical models of AGN and jets involve infall on a massive central engine, only outflows are observed. The typical apparent observed velocity is about $3c$ and ranges up to about $20c$ corresponding to real velocities of 95 and 99.7 percent of the speed of light, respectively. As previously reported in other studies, low-luminosity sources, lobe dominated quasars, and compact symmetric objects appear to show smaller velocities. Quasars associated with powerful gamma-ray emission appear to have somewhat faster ejection velocities.

Individual components appear to move with constant velocity. We find no convincing evidence for acceleration or deceleration of individual

components, although more detailed studies of some strong sources do show changes in component velocity (e.g. Zensus et al. 1995). In any individual source, different components appear to move with similar velocity possibly along somewhat different trajectories. The distribution of linear velocity shows surprising little evidence for Doppler bias.

There is no clear difference in the kinematics of quasars, BL Lacs and AGN. The median angular velocity decreases with increasing redshift consistent with standard cosmological models, but the data are not yet sufficiently precise to distinguish among currently discussed models.

**Acknowledgements.** The VLBA is a facility of the National Radio Astronomy operated by Associated Universities, Inc. under a cooperative agreement with the U.S. National Science Foundation.

## References

Alef, W. et al. 1996, *A&A*, **308**, 376

Dhawan, V., Kellermann, K.I., & Romney, J.D. 1998, *ApJ*, **498**, L111

Ekers, R. & Liang, H. 1990, in *Parsec Scale Radio Jets* eds. J.A. Zensus & T.J. Pearson (San Francisco: Astron. Soc. Pac.), 333

Kellermann, K.I. & Pauliny-Toth, I.I.K. 1969, *ApJ*, **155**, L71

Kellermann, K.I., Vermeulen, R.C., Zensus, A.J., & Cohen, M.H. 1998, *AJ*, **115**, 1295

Lister, M.L., & Marsher, A.P. 1997, *ApJ*, **476**, 572

Preuss, E. et al. 1990, in *Parsec Scale Radio Jets*, eds. J.A. Zensus & T.J. Pearson (San Francisco: Astron. Soc. Pac.), 120

Readhead, A.C.S 1994, *ApJ*, **426**, 51

Slysh, V.I. 1992, *ApJ*, **391**, 453

Vermeulen, R.C. 1995, *PNAS*, **92**, 11385

Vermeulen, R.C & Cohen, M.H. 1994, *ApJ*, **430**, 467

Wagner, S.J. 1998, in *ASP Conf. Ser.* **144***: IAU Coll. 164: Radio Emission from Galactic and Extragalactic Compact Sources*, eds. J.A. Zensus, G.B. Taylor & J.M. Wrobel (Astron. Soc. Pac.), 257

Zensus, J.A., Cohen, M.H., & Unwin, S.C. 1995, *ApJ*, **443**, 35

*Astrophysical Phenomena Revealed by Space VLBI*
*H. Hirabayashi, P.G. Edwards and D.W. Murphy (eds.)*

# The VSOP Survey I: Description and Participation

E. Fomalont[1,2], H. Hirabayashi[2], Y. Murata[2], H. Kobayashi[2], M. Inoue[3], B. Burke[4], P. Dewdney[5], L. Gurvits[6], D. Jauncey[7], P. McCulloch[8], R. Preston[9], S. Horiuchi[3], J. Lovell[7,2], G. Moellenbrock[10,2], P. Edwards[2], Y. Asaki[2], I. Avruch[2], G. Nicolson[11], J. Quick[11], M. Costa[8], R. Dodson[8], J. Reynolds[7], A. Tzioumis[7], S. Tingay[7], X. Hong[12], S. Liang[12], C. Trigilio[13], G. Tuccari[13], J. Nakajima[14], E. Kawai[14], K. Fujisawa[3], N. Kawaguchi[3], T. Miyaji[3], A. Kus[15], F. Ghigo[10], C. Salter[16], V. Slysh[17], W. Cannon[18], B. Carlson[5], S. Dougherty[5], D. Del Rizzo[5], W. Scott[19], R. Taylor[19], S. Kameno[3], K. Shibata[3], T. Umemoto[3], J. Benson[20], C. Flatters[20], A. Hale[20], C. Lewis[20], J. Romney[20], K. Miller[9], J. Smith[9], R. Wietfeldt[9], D. Meier[9], D. Murphy[9,2], G. Langston[10,2], A. Minter[10], M. Popov[17,2], R. Schilizzi[6] and Z.-Q. Shen[3]

[1] *NRAO, Charlottesville, VA, USA*
[2] *ISAS, Sagamihara, Kanagawa, Japan*
[3] *NAO, Mitaka, Tokyo, Japan*
[4] *MIT, Cambridge, MA, USA*
[5] *DRAO, Penticton, BC, Canada*
[6] *JIVE, Dwingeloo, Netherlands*
[7] *ATNF, Epping, NSW, Australia*
[8] *University of Tasmania, Hobart, Tasmania, Australia*
[9] *JPL, California Inst. of Tech., Pasadena, CA, USA*
[10] *NRAO, Green Bank, WV, USA*
[11] *HartRAO, Krugersdorp, Transvaal, South Africa*
[12] *Sheshan Observatory, Shanghai, China*
[13] *Instituto di Radioastronomia del CNR, Noto, Italy*
[14] *Communications Research Lab., Kashima, Ibaraki, Japan*
[15] *Nicolas Copernicus University, Torun, Poland*
[16] *NAIC, Arecibo Observatory, Arecibo, Puerto Rico*
[17] *Astro Space Center, Lebedev PI, Moscow, Russia*
[18] *York University, Toronto, ON, Canada*
[19] *University of Calgary, Calgary, AB ,Canada*
[20] *NRAO, Socorro, NM, USA*

**Abstract**

The VSOP mission is a Japanese-led project to image radio sources with sub-milliarcsec resolution by correlating the signal from the orbiting 8-m telescope, HALCA, with a global array of telescopes. Twenty-five percent of the scientific time of this mission is devoted to a survey of the 400 brightest, small-diameter extra-galactic radio sources at 5 GHz. The major goals of the VSOP survey are statistical in nature: to determine the brightness temperature and approximate structure; to provide a source list for use with future VLBI space missions; and to compare radio properties with other data throughout the EM spectrum. This paper describes: The compilation of the entire source list; the selection of sources to be observed with VSOP; the extensive ground resources; and the status of the observations as of March 2000. In these proceedings Paper II describes the reduction methods and Paper III gives initial statistical results.

## 1 Introduction

On February 12, 1997 the Institute of Space and Astronautical Science (ISAS) launched an 8-m radio telescope, called HALCA, into orbit as one element of a global array of radio telescopes. With an apogee height of 22,000 km and an orbital period of six hours, radio sources at 1.6 and 5 GHz can be imaged with a linear resolution three times greater than with ground arrays at these frequencies (Hirabayashi et al. 1998). One of the main scientific goals of the mission is the study the radio properties of AGN at sub-milliarcsec resolution, corresponding to brightness temperatures near $10^{12}$K.

The majority of HALCA observing time is given to peer-reviewed proposals which are solicited from the world-wide astronomical community and designated as GOT (General Observing Time) proposals. Most of these projects study the source properties by obtaining high-quality images, often at several epochs separated by days to years. However, with a detection sensitivity of 0.1 Jy, hundreds of radio sources, many of which are not in the GOT proposals, can be detected with HALCA to provide a systematic study of a large sample of sources. This project was undertaken, under Japanese leadership with H. Hirabayashi as the Principle Investigator (PI), and it is called the VSOP Survey Program.

This paper concentrates on the following aspects of the VSOP Survey Program: (1) the compilation of the all-sky 5-GHz sample; (2) the

selection of sources observed with HALCA; (3) the listing of the ground resources used for the survey; and (4) the description of a typical experiment and the observational progress to date. Two additional papers in these proceedings describe the data reduction techniques (Moellenbrock et al. 2000) and results from an analysis of the sample (Lovell et al. 2000). A more complete description of the VSOP survey and the full source list will be given elsewhere (Hirabayashi et al. 2000).

## 2 The VSOP All-Sky 5 GHz Sample

The VSOP survey sample was defined to include all cataloged extra-galactic radio sources in the sky with: a total cataloged flux density at 5 GHz $S > 0.95$ Jy; a spectral index $\alpha > -0.45$ (where $S \propto \nu^{\alpha}$); a galactic latitude $|b| > 10^{\circ}$. Such a sample definition is relatively unbiased. The sample also included *all* extra-galactic sources with $S > 5$ Jy, regardless of spectral index and galactic latitude.

The existing surveys from which the 5-GHz sample were compiled were the Green Bank *GB6 Catalog* (Gregory et al. 1996) and the Parkes-MIT-NRAO *PMN Survey* (Lawrence et al. 1986, Griffith & Wright 1993). These surveys were observed with several large telescopes and covered most of the sky to a flux density level of $< 0.3$ Jy. Spectral information was determined from the above catalogs or from other, more recent observations, as needed. The NASA/IPAC Extra-galactic Database (NED; http://nedwww.ipac.caltech.edu) provided the most convenient location for additional information. Additional sources were found in the *S5 survey* near the North Galactic Pole (Kühr et al. 1981), and from the VLA calibrator list.

Since the survey observations used to compile the VSOP sample spanned a period between 1985 and 1996, source variability clearly affected the source membership in the sample. The only way to avoid such ambiguities would be to observe approximately the brightest 1000 sources in the sky at several frequencies within a short period of time: this effort was not possible. A source was included in the sample if the flux density at 5 GHz for *any* of the finding survey was $> 0.95$ Jy, or there was indication from other VLBI observations of a flat radio spectrum component within the source.

The VSOP 5 GHz survey sample, compiled as described above, contains 404 sources. This number accounts for about 60% of all sources above 1 Jy (Kühr et al. 1981). The source list is available from the

VSOP website (http://www.vsop.isas.ac.jp, click on VSOP Survey Program). The original plan for the VSOP survey was to observe all 404 sources at 5 GHz, the highest frequency and resolution of VSOP. If time permitted, an additional observation at 5 GHz or one at 1.6 GHz would be considered.

## 3 The VSOP Survey Observing Sample

In order to maximize the return from the HALCA observations, those sources with correlated flux density $< 0.32$ Jy at 5 GHz on the largest earth baselines were not included in the observing list. These sources would be very resolved with space baselines and many would likely be undetected. This filtering was accomplished in 1996 with a pre-launch 5 GHz VLBA snap-shot survey of all sources in the complete catalog north of declination $-43°$. A detailed presentation of these results are given elsewhere (Fomalont et al. 2000). Additional information was obtained from: the VLBA calibrator list (Peck and Beasley 1998); the USNO geodetic catalog and the International Celestial Reference Frame (ICRF) information (http://maia.usno.navy.mil/rorf/rrfid.html); the 15 GHz VLBA survey (Kellermann et al. 1998); two trans-continental surveys at 2.6 and 22 GHz (Preston et al. 1985, Moellenbrock et al. 1996); and from SHEVE observations (Tingay et al. 2000)

Using the above ground observations 115 of the 404 sources in the VSOP all-sky sample were found to be sufficiently resolved on ground baselines and would probably not be detected with HALCA observations. The remaining 289 sources formed the VSOP Survey Observing Sample and these sources formed the basic source list for the HALCA observations during the mission. These sources are also listed in the ISAS website. Although observations are being made only for this subsample, all 404 sources in the complete sample should included in any statistical studies of these AGN.

After six months of observing it was apparent that not even this reduced sample of 289 source could be observed within the expected mission lifetime. Thus, for those GOT observations which looked at sources also found in the VSOP observing list, permission was requested from the relevant PI's to extract part of their observations for the use in the Survey Program, but only for statistical purposes. The PI's were unanimous in giving permission for such GOT/Survey extractions.

## 4 The VSOP Survey Ground Resources

The HALCA on-board hardware, telemetry and tracking station systems, and the data correlation are described elsewhere (Hirabayashi et al. 1998). Both the GOT and the VSOP Survey observations require a large effort and cooperation of numerous ground resources and these will be acknowledged and described in this paper, with emphasis on the VSOP survey.

### 4.1 The Ground Telescopes

A typical GOT array consists of HALCA with six to nineteen ground telescopes, observing for a duration of about 10 hours, or about two orbits of the spacecraft. These data generally produce images of high quality. The ground telescope time for these observations were arranged before the mission by the Global VLBI Working Group (GVWG). The VSOP Survey, on the other hand, was designed to observe using three telescopes with observation length of about one orbit. These more minimal resources made it possible for the survey to negotiate for sufficient additional ground resources *after* telescope allocations were made for the GOT experiments.

The telescopes (with supporting institution, country and total survey observing time in days in 1998–1999) are as follows: Arecibo (NAIC, Puerto Rico, 1.7d); Ceduna and Hobart (University of Tasmania, Australia, 1.2d, 10.8d); Green Bank 140-ft (NRAO, USA, 3.7d); Hartebeesthoek (HartRAO, South Africa, 12.5d); Kalyazin (Lebedev Institute, Russia, 1.4d); Kashima (CRL, Japan, 4.0d); Mopra (ATNF, Australia, 10.5d); Noto (CNR, Italy, 5.0d); Sheshan (Shanghai Univ., China, 9.7d); Torun (Copernicus University, Poland; 3.7d); Usuda (ISAS, Japan, 3.8d). Telescopes participating only in GOT observations, indirectly contributing to the survey program via data extractions, are: ATCA (ATNF, Australia, 1.5d); Effelsberg (MPIfR, Germany, 2.7d); Jodrell MKII (MERLIN/VLBI NF, UK, 0.5d); VLBA (NRAO, USA, 7.0d using three of ten telescopes).

### 4.2 The Tracking Stations

The ISAS Space Center facility near Kagoshima, Japan is the command and control center of HALCA. For telemetry between the ground and HALCA, five tracking stations are used: one tracking station is operated by ISAS at Usuda, Japan; three stations by the NASA Deep Space

Network (DSN) at Goldstone, CA, USA, Robledo, Spain, and Tidbinbilla, Australia; and one station in Green Bank, WV, USA, operated by NRAO and supported by NASA.

The main responsibilities of each tracking station are: (1) To transmit a high-purity carrier signal to the spacecraft in order to convert the radio signals to a lower frequency; (2) to receive the HALCA data on a 15 GHz down-link; (3) to determine the time of flight of the round-trip signal to HALCA; and (4) to record the data on video tape which is subsequently sent to one of the data correlation centers. The length of time when HALCA is visible for each tracking pass varies from a few minutes to four hours.

Three data recording formats are used for the VSOP mission: VSOP-format, developed in Japan; S2-format, developed in Canada; and VLBA-format, developed in the USA. The MKIV recording format, developed in the USA and used mostly for European telescopes, is compatible with the VLBA-format. When necessary, data among the three formats are translated with copying facilities in Mitaka and Usuda, Japan.

### 4.3 The Correlators

The HALCA data, which is recorded at each of the tracking stations, is shipped to one of the three correlation centers where it is correlated with ground-telescope data, approximately one month after the observations. An updated HALCA orbit, determined by JPL and by ISAS, is also supplied. The three correlators are: The VSOP correlator in Mitaka, Japan (Shibata et al. 1998); the S2 correlator in Penticton, BC, Canada (Carlson et al. 1999); and the VLBA correlator in Socorro, NM, USA (Napier et al. 1994).

Because the VSOP Survey Program was designed to use telescopes with S2- or VSOP-recording systems, most survey observations were correlated in Penticton or in Mitaka. However, the VLBA correlator is also used for data extracted from GOT experiments.

## 5 The VSOP Survey Observations

Sources in the VSOP survey observing list are observed in the following way. The GOT observations are first scheduled and then survey observations are placed to make the HALCA relatively efficient. About one in three HALCA observations (including GOT extractions) is a survey observation, and these account for about 25% of the total on-source ob-

serving time. A typical survey observation consists of five hours of data, about one HALCA orbit, with three well-separated ground telescopes. More than 100 of the 289 sources are also in GOT proposals, and a typical amount of survey data (three ground telescopes over five hours) are extracted at the correlator from these observations. The priority in the scheduling of the survey observations is from the strongest sources to the weakest sources. However, constraints of when a source can be observed with HALCA somewhat randomizes the selection process.

The survey ground array that is scheduled depends on source declination. Sources south of $-30^\circ$ use telescopes in Australia (Mopra, Hobart, Ceduna) and Hartebeesthoek in South Africa. For more Northern declinations telescopes in Eastern Asia (Shanghai, Usuda, Kashima) or telescopes in the Europe-Atlantic region (Hartebeesthoek, Noto, Torun, Green Bank 140-ft, Arecibo) are also included. Generally four ground telescopes are scheduled for each experiment, although only three (and sometimes two) telescopes are available for the observations.

After correlation of a survey observation the data are edited, fringed and calibrated. Images of the radio sources and model-fits to the visibility data are used to determine flux densities, angular sizes and brightness temperatures of the radio components. A description of the reduction and imaging techniques (Moellenbrock et al. 2000) and initial results (Lovell et al. 2000) are given elsewhere in these proceedings.

As of March 2000, 194 of the 289 sources (67%) were observed. For about 40 of the observations only two ground telescopes were available; nonetheless, most of these have produced satisfactory images and models. About 10% of the observations appear faulty (no signal was detected from HALCA although there were strong fringes from ground baselines) and these will be rescheduled if possible.

The results from the VSOP Survey Program will be enhanced by comparison with other ground observational results, across the entire EM spectrum. Some of these ground observations have been proposed specifically for support of the VSOP survey. Additional information are: (1) radio source variability; (2) the arcsec radio structure of the sources; (3) VLBA 15 GHz observations nearly contemporaneous with the VSOP survey observations; (4) compilation of relevant radio/optical/X-ray data associated with each source in a convenient data base.

## 6 Summary

The informal agreements made by ISAS with global observatories, with tracking stations, with correlator centers, and with a host of other supporting personnel and organizations have formed the basis for the successful VSOP Survey Program. Over two-thirds of the 289 sources in the observing sample have been observed through March 2000 and the reduction and imaging are complete for more than half of these sources.

Preliminary results are given elsewhere (Lovell et al. 2000). Many interesting sources (e.g. those with extremely compact or with peculiar radio structure) have been found, and a surprisingly large number of radio sources have significant emission unresolved at the longest HALCA baselines, corresponding to an angular size $< 0.15$ mas with a brightness temperature in excess of $10^{12}$K. The VSOP survey program has demonstrated that hundreds of sources can be studied in future space missions at even higher resolution.

**Acknowledgements.** We gratefully acknowledge the VSOP Project, which is led by the Japanese Institute of Space and Astronautical Science in cooperation with many organizations and radio telescopes around the world.

Institutional acknowledgements are: The National Radio Astronomy Observatory is a facility of the National Science Foundation operated under cooperative agreement by Associated Universities, Inc. The Australia Telescope is funded by the Commonwealth Government for operation as a national facility by CSIRO. We also thank Ron Ekers for his support. The Canadian S2 Space-VLBI correlator is supported by funding from the Canadian Space Agency and the National Research Council of Canada. Part of the research was carried out at the Jet Propulsion Laboratory, California Institute of Technology under contract to NASA. The Nicolas Copernicus University in Torun, Poland is supported by the Polish Government through the State Committee for Scientific Research under the annual grant SPUB. The Noto Observatory thanks the Italian Space Agency for financial support. HartRAO wishes to thank the Canadian Space Agency, the Dominion Radio Observatory at Penticton and the Space Geodynamics Laboratory of the Centre for Research in Earth and Space Technology for the loan of an S2 Recording terminal. The Australia Telescope National Facility is also thanked for providing one of their Data Acquisition Systems. The Green Bank Tracking Station is operated by the National Astronomy Observatory with funding

provided by NASA.

Personal acknowledgements are: The Operations at Torun were supported by Messrs. Borkowsky, Pazderski, Jakubowicz and Kepa. For the Kalyazin operations, we thank B. Kanevsky (ASC), Y. Ilyasov (Pushchino Observatory) and B. Poperechenko (Special Research Bureau of Moscow Power Engineering Institute), and the staff of the Kalyazin Observatory for providing operational and logistical support. HartRAO thanks M. Khumalo for assistance with the HALCA observations. Also gratefully acknowledged are the efforts of R. Jenkins, J. Border and J. Gimeno at the DSN tracking stations, and the contributions of Yu. Kovalev, R. Linfield, J. Ulvestad and E. Valtaoja to early planning for the VSOP Survey Program.

## References

Carlson, B.R., Dewdney, P.E., Burgess, T.A., et al. 1999, *PASP*, **111** 1025

Fomalont, E. B., Edwards, P. G., Hirabayashi, H., Frey, S., Paragi, Z., Gurvits, L. I. & Scott, W. K., 2000, *AJ*, submitted

Gregory, P. C., Scott, W. K., Douglas, K. & Condon, J. J., 1996, *ApJS*, **103**, 427

Griffith, M. R. & Wright, A. E., 1993, *AJ*, **105**, 1066

Hirabayashi, H., Hirosawa, H., Kobayashi, H., Murata, Y, et al. 1998, *Science*, **281**, 1825 and erratum **282**, 1995

Hirabayashi, H., Fomalont, E., et al., 2000, in preparation

Kellermann, K. I., Vermeulen, R. C., Zensus, J. A & Cohen, M. H., 1998, *AJ*, **115**, 1295.

Kühr, H., Witzel, A., Pauliny-Toth, I. I. K. & Nauber, U., 1981, *A&A*, **45**, 367.

Lawrence, C.R., Bennett, J.N., Hewitt, J.N., et al. *ApJS*, **61**, 105

Lovell, J. E. J., et al., 2000, *these Proceedings*

Moellenbrock, G. A., Fujisawa, K., Preston, R. A., et al., 1996, *AJ*, **111**, 2174

Moellenbrock, G. A., et al., 2000, *these Proceedings*

Napier, P.J., Bagri, D.S, Clark, B.G. et al. 1994, *IEEE Proc.*, **82**, 658

Peck, A.B & Beasley, A.J. 1998, in *ASP Conf. Ser.* **144***: IAU Coll. 164: Radio Emission from Galactic and Extragalactic Compact*

*Sources*, eds. J.A. Zensus, G.B. Taylor & J.M. Wrobel (San Francisco: Astron. Soc. Pac.), 155

Preston, R.A., Morabito, D.D., Williams, G. et al. 1985, *AJ*, **90**, 1599

Shibata, K. M., Kameno, S., Inoue, M., Kobayashi, H., 1988 in *ASP Conf. Ser.* **144***: IAU Coll. 164: Radio Emission from Galactic and Extragalactic Compact Sources*, eds. J.A. Zensus, G.B. Taylor & J.M. Wrobel (San Francisco: Astron. Soc. Pac.), 413

Tingay. S., Jauncey, D., King, E, et al. 2000, in preparation.

*Astrophysical Phenomena Revealed by Space VLBI*
*H. Hirabayashi, P.G. Edwards and D.W. Murphy (eds.)*

# The VSOP Survey II:

# Reduction Methods

G.A. Moellenbrock[1], J. Lovell[2], S. Horiuchi[3],
E. Fomalont[4], H. Hirabayashi[5],
R. Dodson[6], S. Dougherty[7], P. Edwards[5], S. Frey[8],
L. Gurvits[9], M. Lister[10], D. Murphy[10,5], Z. Paragi[8],
G. Piner[10], W. Scott[11], Z. Shen[3], S. Tingay[2],
Y. Asaki[5], D. Jauncey[2], G. Langston[1], D. Meier[10],
D. Moffet[12], Y. Murata[5], R. Preston[10],
R. Taylor[11], K. Wajima[5]

[1]*NRAO, Green Bank, WV, USA*
[2]*ATNF, Epping, NSW, Australia*
[3]*NAO, Mitaka, Tokyo, Japan*
[4]*NRAO, Charlottesville, VA, USA*
[5]*ISAS, Sagamihara, Kanagawa, Japan*
[6]*University of Tasmania, Hobart, Tasmania, Australia*
[7]*DRAO, Penticton, BC, Canada*
[8]*FÖMI, Penc, Hungary*
[9]*JIVE, Dwingeloo, The Netherlands*
[10]*JPL, Pasadena, CA, USA*
[11]*University of Calgary, Calgary, AB, Canada*
[12]*Furman University, Greenville, SC, USA*

**Abstract**

This second paper on the VSOP Continuum Survey describes the data reduction procedures and gives a sampling of Survey results for individual sources.

## 1 Data Reduction Procedures

The reduction of VSOP Survey observations is being undertaken by a group of analysts located world-wide. This group has met at ISAS on three occasions and meets regularly via telephone to discuss and formulate procedures for VSOP Survey data reduction and analysis. This section summarizes the data reduction scheme devised for the Survey in these meetings.

### 1.1 Preliminaries and *a Priori* calibrations.

The Survey observations are undertaken in the standard VSOP observing mode (two 16 MHz two-bit sampled IFs) at sky frequencies in the range 4800–5000 MHz. For initial calibrations and detection of fringes, the correlator distribution data for each experiment is imported into NRAO-AIPS using the task FITLD. The datasets are large: typically 128 frequency channels in each IF, with temporal averaging to 0.5 seconds and 2.0 seconds for space- and ground-baselines, respectively. The datasets are sorted, indexed, and documented using standard AIPS tasks (MSORT, INDXR, LISTR, PRTAN, DTSUM). Except for datasets correlated in Penticton, it is necessary to run ACCOR to remove fringe normalization errors. The *a priori* amplitude calibration is applied using ANTAB to load system temperature and gain values into AIPS tables attached to the dataset, and APCAL to form the $\sqrt{SEFD}$ calibration factors required for each antenna.[1] For HALCA, the nominal 5 GHz system temperature is $\sim$ 90 K and stable. The 5 GHz gain is 0.0062 K/Jy and this yields an $SEFD \sim 14,500$ Jy, which is more than an order of magnitude larger than most ground telescopes. The *a priori* amplitude calibration is thought to be uncertain by 10–20%.

### 1.2 Fringe-Fitting

Fringe-fitting, where the visibilities are detected, is the most important part of the Survey reductions. Unlike ground-only VLBI, fringe detection for HALCA observations is difficult due to the limited sensitivity of the orbiting station, the generally lower expected correlated flux density and the larger uncertainty in the spacecraft's location and clock. This combination of conditions requires weak-signal fringe searches over large ranges of delay and fringe rate, hence the extremely fine time and frequency sampling. The small number of ground telescopes limits the sensitivity of global fringe-fitting, as well. It is highly desirable to limit as much as possible the range of the search in delay and fringe rate in order to keep the fringe searching efficient, and to avoid false detections. For many Survey datasets, high confidence delay and fringe rate solutions are available from baseline-based fringe searches performed at the correlators for data quality analysis. Application of these solutions

[1] The *System Equivalent Flux Density (SEFD)* is the ratio of the system temperature (K) and telescope gain (K/Jy). It concisely describes the sensitivity of a radio telescope and the geometric mean of $SEFD$ for two telescopes provides the proper scaling factor to convert normalized correlation coefficients to janskys.

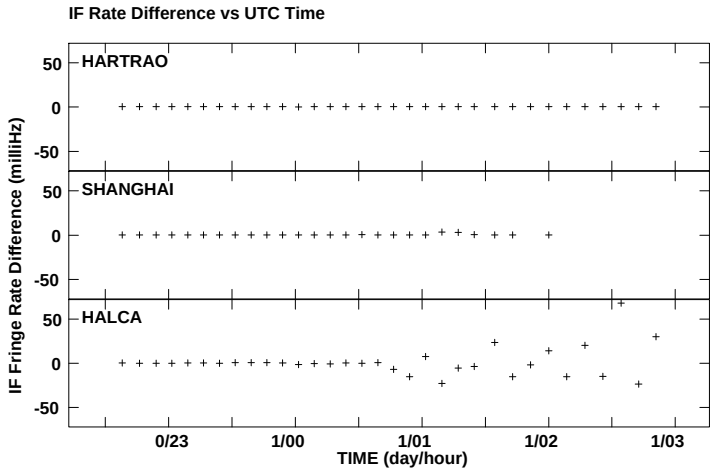


Figure 1: An example of the difference in fringe rate solutions between the two IFs for a typical Survey experiment. Fringes to HALCA are detected until nearly 1/01 at which time the differences become randomly distributed on a scale exceeding the fringe rate resolution ($\sim$3 mHz FWHM).

using CLCOR allows significant data averaging and smaller fringe-search windows. For datasets with strong fringes for only a portion of the observation, the resulting narrower search should in principle allow detection of the weaker fringes. In practice, the gains have been modest.

For most observations, the AIPS task FRING is used for fringe-fitting. Solution intervals of at least 10 minutes (approaching the coherence time) are attempted to maximize SNR. Detections are best gauged by consistency in the delay and fringe rate solutions between the two independent IF channels (see Figure 1). For the weakest sources (few or no detections in the correlator's data quality search), the AIPS task KRING may be attempted since it allows larger searches and longer integrations than FRING for the same CPU.

### 1.3 Imaging and Modelfitting

With limited $(u, v)$-coverages, the imaging and modelfitting of Survey observations recall the early days of ground-based VLBI imaging. With its simple and efficient implementation, Difmap (Shepherd et al. 1994) has been chosen for post-detection editing, imaging, and modelfitting.

Upon importing the frequency-averaged (each IF) data to Difmap, it is averaged in time to 30-second samples and point-source phase self-

calibration solutions are determined on a 10 minute timescale and applied. Manual flags are then applied to obviously discrepant and undetected data, the latter based on lack of continuity in the IF phase solution differences. At this point, the *a priori* amplitude calibration may be checked for consistency using crossing points in the $(u, v)$-plane (if available) and by comparison with similar baselines from a pre-launch survey (Fomalont et al. 2000). Allowance for source variability is made by assuming the varying part of the source is what dominates the visibilities we measure. The ground array typically observes several calibrator sources (for fringe searching at the correlator), and these provide an amplitude calibration consistency check as well.

Imaging proceeds with incremental and iterative CLEAN deconvolution and phase-only self-calibration. So that the full resolution of the space-VLBI dataset is realized, the HALCA data must be up-weighted by a factor ∼20–100 to compensate for their lower sensitivity. The timescale for the self-calibration solutions is limited to the minimum required to maintain clear continuity in the difference of the IF phase solutions. When satisfied with convergence, and if at least four stations are available, constant amplitude self-calibration factors are determined. If the station-based amplitude corrections are less than 10%, the phase-self-calibration imaging is repeated with the new amplitudes and a final image obtained; if not, and if such large discrepancies cannot be accounted for by obvious (if subtle) problems in the *a priori* amplitude calibration, then the phase-only self-calibrated dataset is accepted as the final result. The final calibrated dataset is then modelled with a small number of point and/or Gaussian components. As in the imaging, the HALCA baselines must be up-weighted so that they have a significant influence on the modelfitting solutions.

## 2 Sample Results

Figure 2 shows the $(u, v)$-coverages, visibility functions, and images for two typical Survey observations: a northern source (0745+241) observed with the ground telescopes at Mopra, Kashima, and Shanghai and correlated at Mitaka, and a southern source (J0106−4034) observed with Hartebeesthoek and Mopra and correlated at Penticton. The compact component in 0745+241 has a brightness temperature in excess of $0.8 \times 10^{12}$ K. J0106−4034 is resolved with a peak brightness temperature of $\sim 2.8 \times 10^{12}$ K.

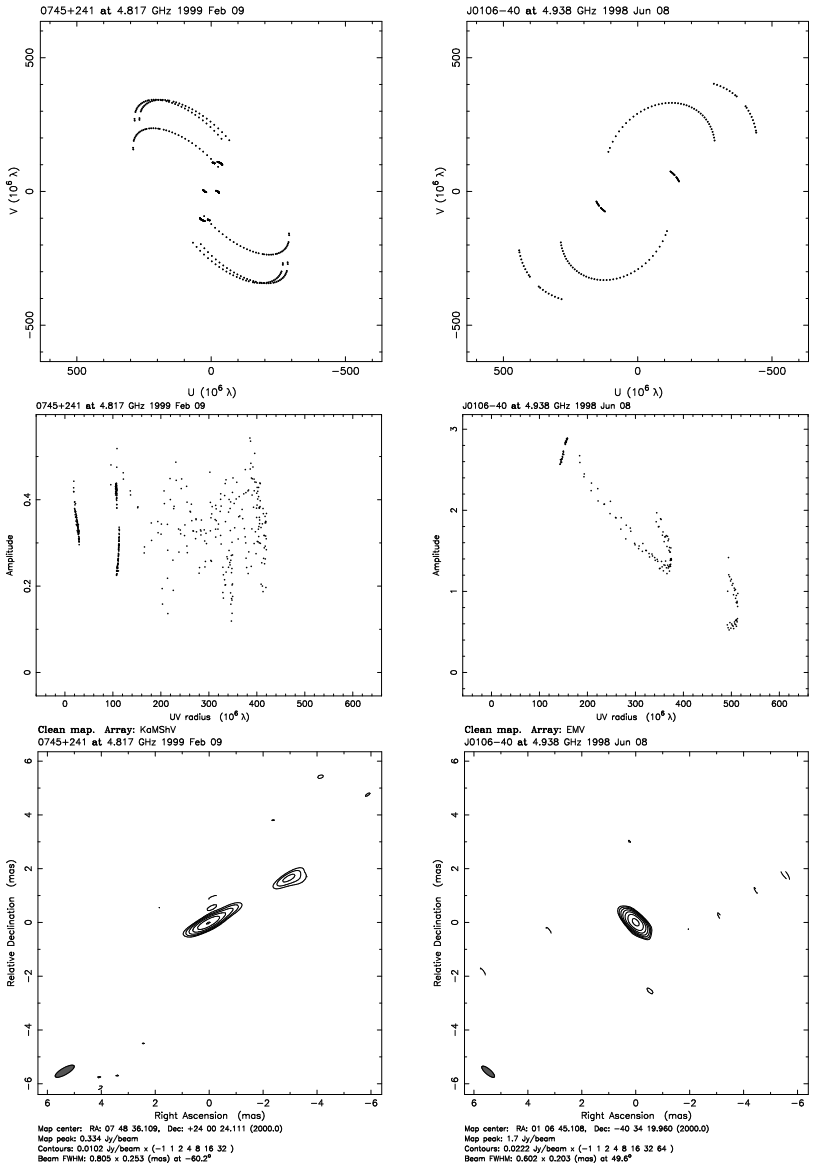


Figure 2: $(u, v)$-coverages (top), visibility plots (middle) and images for two typical Survey observations: 0745+241 at epoch 1999.11 (left) and and J0106−4034 at epoch 1998.43 (right). For the images, the contour intervals are factors of 2, beginning at $\sim 3$ times the off-source rms noise (typically 5 mJy/beam) and the full-resolution restoring beam is at the bottom left.

In general, the quality of imaging results rarely approach that which is possible with a full GOT dataset, especially for complex sources; see Lister et al. (these proceedings) for a detailed analysis of the difference between Survey and full GOT datasets. While the Difmap imaging/modelfitting results generally represent the qualitative structure acceptably (familiar sources look familiar), detailed interpretation remains limited. In general, the flux densities and positions of image features below $\sim$15% of the peak carry considerable uncertainty due to the limited $(u, v)$-coverage. Also, most central modelfitting components are consistent with zero size in at least one dimension, and so a more careful analysis is required to derive robust brightness temperature limits. This issue is discussed in greater detail in Lovell et al. (these proceedings).

**Acknowledgements.** We gratefully acknowledge the VSOP Project, which is led by the Japanese Institute of Space and Astronautical Science in cooperation with many organizations and radio telescopes around the world. The Australia Telescope National Facility (ATNF) is funded by the Commonwealth of Australia for operation as a National Facility managed by CSIRO. The National Radio Astronomy Observatory is a facility of the U.S. National Science Foundation operated under cooperative agreement by Associated Universities, Inc.

## References

Fomalont, E.B. et al., 2000, to be submitted to *AJ*

Shepherd, M.C., Pearson, T.J., & Taylor, G.B. 1994, *BAAS*, **26**, 987

*Astrophysical Phenomena Revealed by Space VLBI*
*H. Hirabayashi, P.G. Edwards and D.W. Murphy (eds.)*

# The VSOP Survey III: Statistical Results

J.E.J. Lovell[1,4], S. Horiuchi[2], G. Moellenbrock[3,4], H. Hirabayashi[4], E. Fomalont[5,4], R. Dodson[6], S. Dougherty[7], P. Edwards[4], S. Frey[8], L. Gurvits[9], M. Lister[10], D. Murphy[10,4], Z. Paragi[8], B. Piner[10], W. Scott[11], Z.-Q. Shen[2], S. Tingay[1], M. Inoue[2], Y. Murata[4], K. Wajima[4], B. Carlson[7], K.M. Shibata[2], J. Quick[12], M. Costa[6], A. Tzioumis[1], C. Trigilio[13], J. Nakajima[14], H. Xinyong[15] and W. Wei[15]

[1] *ATNF, Epping, NSW, Australia*
[2] *NAO, Mitaka, Tokyo, Japan*
[3] *NRAO, Green Bank, WV, USA*
[4] *ISAS, Sagamihara, Kanagawa, Japan*
[5] *NRAO, Charlottesville, VA, USA*
[6] *University of Tasmania, Hobart, Tasmania, Australia*
[7] *DRAO, Penticton, BC, Canada*
[8] *FÖMI, Penc, Hungary*
[9] *JIVE, Dwingeloo, The Netherlands*
[10] *JPL, Pasadena, CA, USA*
[11] *University of Calgary, Calgary, Alberta, Canada*
[12] *HartRAO, Krugersdorp, Transvaal, South Africa*
[13] *Instituto di Radioastronomia del CNR, Noto, Italy*
[14] *Communications Research Lab., Kashima, Ibaraki, Japan*
[15] *Sheshan Observatory, Shanghai, China*

**Abstract**

In the third paper on the VSOP Continuum Survey, we present an initial statistical analysis of the data reduced to date. We find that nearly all sources are resolved to some degree with the BL Lac sources being more compact than quasars. We also find that 51% of the sources have source-frame brightness temperatures in excess of $10^{12}$ K.

## 1 Introduction

This is the third paper in this proceedings that describes the VSOP Continuum Survey. In Paper I (Fomalont et al., these proceedings) the

organisation of the survey is presented and in Paper II (Moellenbrock et al., these proceedings) a description of the data reduction is given. This paper presents a statistical analysis of the results from the first 67 sources to be reduced and analysed.

We stress however that this is not a random sample of the sources being observed by the VSOP for the Survey. Most of the data reduced to date consists of sources with strong ground-space fringe detections as many observations where these fringes are weak or absent are still under investigation by the Survey data analysts or are being scheduled for re-observation.

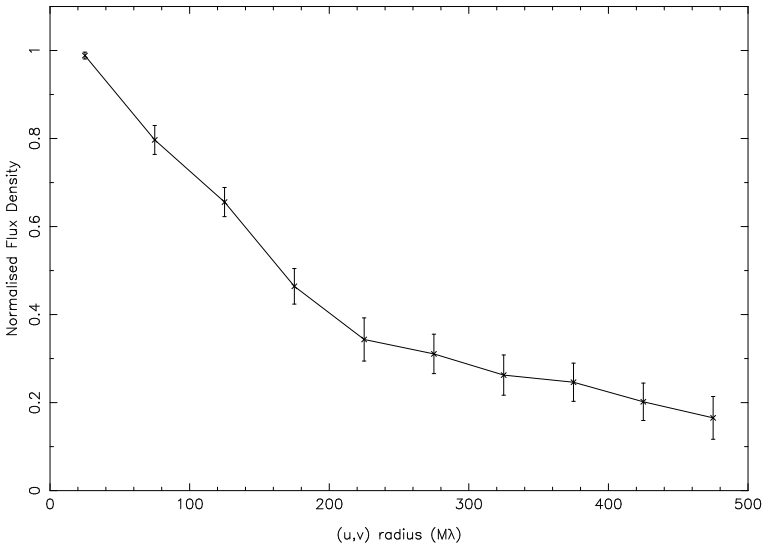


Figure 1: The weighted mean of the normalised flux density distribution for the survey sources so far analysed.

## 2 Flux Density Measurements

For the purposes of a statistical analysis, the visibility amplitudes for each source have been divided into 50 M$\lambda$ bins from 0 to 500 M$\lambda$. The average visibility function (normalized to the 0–50 M$\lambda$ bin[1]) for the currently reduced sample is shown in Figure 1. At 200–250 M$\lambda$, the

[1]Note: The 0–50 M$\lambda$ fluxes used in this analysis represent the flux density on the shortest VLBI baselines and not the total, zero-baseline, flux density.

visibility functions clearly flatten significantly, indicating a less-resolved component tends to dominate on the space-VLBI scale at 5 GHz.

The normalised long baseline (400–500 M$\lambda$) flux density plotted as a function of short baseline (0–50 M$\lambda$) flux density is shown in Figure 2. This figure clearly shows that nearly all survey sources are resolved significantly. It is also apparent that there is some division between source types, with the BL Lac objects (albeit few in number) generally more compact than the quasars at the 1% significance level.

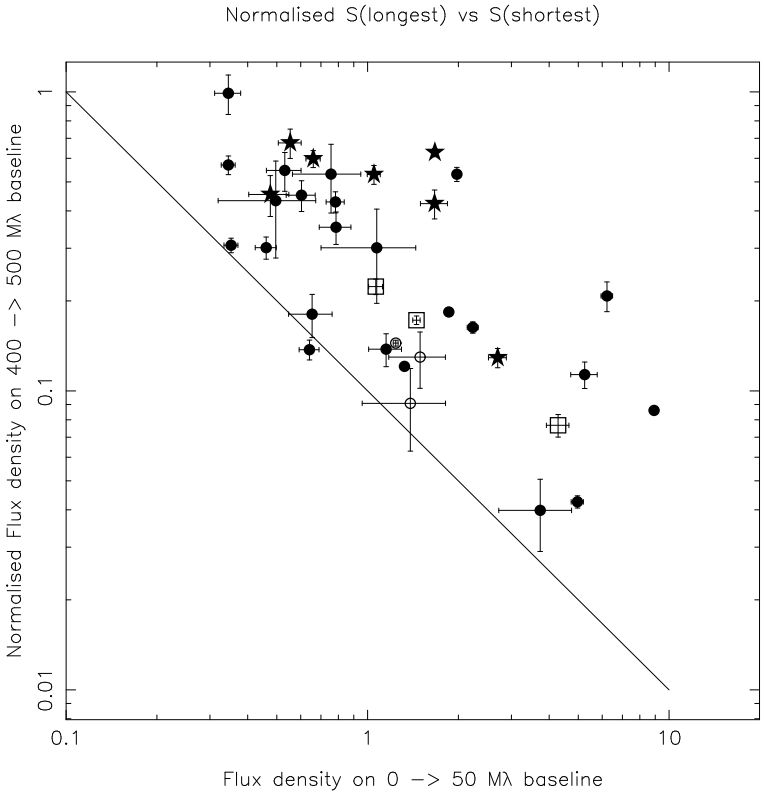


Figure 2: Normalised long baseline flux density plotted against short baseline flux density. The star-shaped symbols represent BL-Lacs, filled circles represent quasars, open circles represent galaxies and open boxes represent unidentified sources. The solid lines indicates the nominal detection limit on ground-space baselines of 0.1 Jy.

## 3 Brightness Temperature Measurements

As described in Paper II, the angular size of the components in all sources is determined using the Difmap software package (Shepherd et al. 1994) which fits one or several Gaussian components directly to the measured visibility data. However, whether a component is consistent with a point source, within the data errors, can not be ascertained from the algorithm because no errors are estimated and the algorithm rarely converges on a point source. This problem is exacerbated by the elliptical $(u, v)$-coverage for most survey observations.

A estimate of the minimum detectable angular size, $A$, that can be measured for an isolated small-diameter component of flux density $S$, with observations with an integrated rms noise $N$, and the maximum baseline length $U$ is

$$A < \frac{2.4\sqrt{\frac{N}{S}}}{U}$$

where $A$ is in milliarcsec and $U$ is in units of 100 M$\lambda$. The constant 2.4 depends on the details of the $(u, v)$-coverage and weighting of the data and was chosen to represent that used for the typical survey dataset. For $S = 0.5$, $N = 0.005$ and $U = 5$, the expected minimum detectable angular size is 0.05 mas. Using the above algorithm we determined the angular size limit in the major and minor axis direction of the $(u, v)$-coverage and compared these limits to the angular sizes produced by Difmap. If the modelfit size was more than 50% greater than the derived limits, it was taken as a robust measurement of the angular size. Otherwise, the limiting size was adopted and used as a lower limit to the brightness temperature.

Figure 3 shows the brightness temperatures measured with VSOP for the Survey, in the observers' frame and in the source frame (at source emitted frequency) respectively. Each plot is divided into sources for which only a lower limit was possible (which accounts for $\sim 2/3$ of the sources so far analysed) and those for which a core size could be reliably measured.

The highest observer-frame brightness temperature so far measured in the survey is $2.8 \times 10^{12}$ K and the highest lower-limit brightness temperatures observed is $6 \times 10^{12}$ K. We find that 30% of the 67 sources have observers'-frame brightness temperatures in excess of $10^{12}$ K and of the 59 sources for which redshifts are available, 51% have source-frame brightness temperatures greater than $10^{12}$ K.

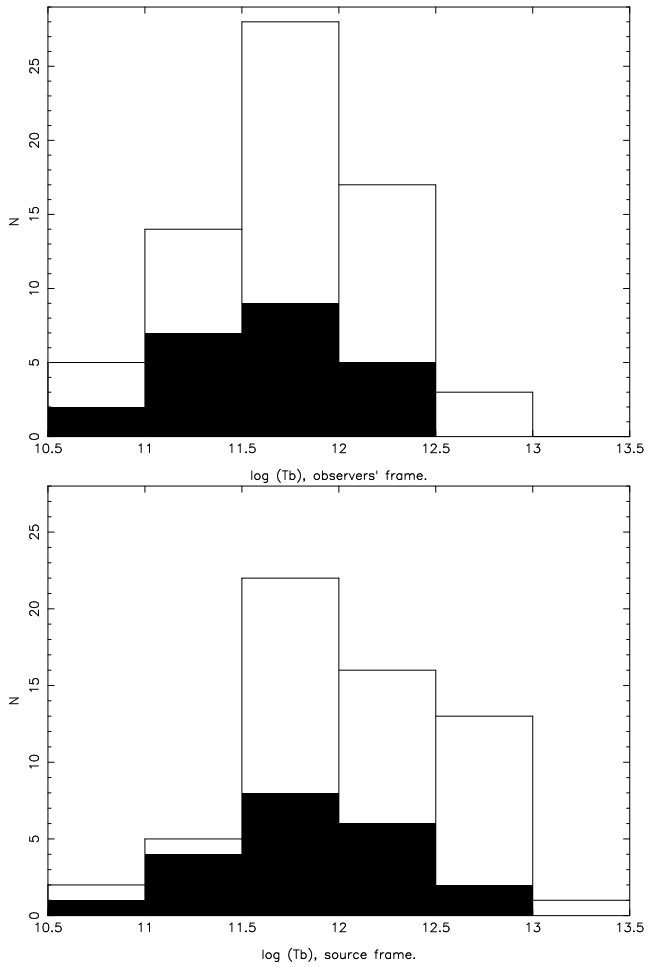


Figure 3: Brightness temperature distributions in the observers' frame (top) and in the source frame at the source emitted frequency (bottom). The filled blocks represent sources where a compact component size was measured while open blocks represent sources where only an upper limit on size and hence a lower limit on brightness temperature was possible.

**Acknowledgements.** We gratefully acknowledge the VSOP Project, which is led by the Japanese Institute of Space and Astronautical Science in cooperation with many organizations and radio telescopes around the world. Special thanks to the VSOP PIs for making extractions from their GOT observations available to the Survey program.

## References

Shepherd, M.C., Pearson, T.J., & Taylor, G.B. 1994, *BAAS*, **26**, 987

*Astrophysical Phenomena Revealed by Space VLBI*
*H. Hirabayashi, P.G. Edwards and D.W. Murphy (eds.)*

# The Impact of Minimal Ground Antenna Coverage on the VSOP Survey

Matthew L. Lister[1], B. Glenn Piner[1] & S. J. Tingay[2]

[1] *Jet Propulsion Laboratory, California Institute of Technology*
[2] *Australia Telescope National Facility*

**Abstract**

The VSOP survey consists of 5 GHz space-VLBI observations of over two hundred active galactic nuclei using the HALCA satellite and various telescopes located around the world. Generally only a few ground telescopes participate in any given observation, which results in poor coverage of the $(u, v)$ plane. By making comparisons with datasets using a full array of ground antennas, we find that the VSOP survey data can be used to obtain reliable brightness temperature measurements of strong components in AGN jets. The images, however, are of low dynamic range, and are not well-suited for detailed statistical studies of jet morphology.

## 1 Introduction

One of the key projects of the VLBI Space Observatory Programme (VSOP) is a survey of several hundred active galactic nuclei at 5 GHz (Fomalont et al. these Proceedings). The individual observations for the survey are carried out with a minimal number (i.e., less than four) ground telescopes, plus the spacecraft, which results in poor quality images and a sparse sampling of the $(u, v)$ plane. In this paper we examine what source information is lost when one goes from a ground array of ten telescopes used in a typical general observing time (GOT) experiment, to just three telescopes for a survey experiment. Such a study is necessary to determine what properties of AGNs can be reliably measured by the survey program, and to identify possible biases that may affect the results.

## 2 Method

In order to minimize observing time requirements, some data for the VSOP survey are "extracted" from GOT observations by keeping data from only three ground antennas and one spacecraft orbit. We have

performed these data extractions on nineteen survey sources that are also members of our Pearson-Readhead GOT survey (Preston et al. these Proceedings). The extractions were made following the fringe-fitting and amplitude calibration stage, giving us a "full" and "extracted" dataset for each source. We reduced these datasets independently using the Caltech Difmap package, and compared the resulting images and model fits. It is important to note that most of the observations in the VSOP survey are of weaker objects than those in our sample, and are generally of poorer data quality. Our results should therefore be interpreted as a "best-case" scenario for the amount of information that can be reliably drawn from survey data.

## 3 Imaging

There are three main aspects of VLBI images that are highly sensitive to the loss of ground antennas. These are: i) on-source errors, caused by holes in the $(u, v)$ plane, ii) a loss of dynamic range, due to increased image noise, and iii) a lack of sensitivity to diffuse, extended emission, due to the loss of short baselines.

The issue of on-source errors is especially complicated for space-VLBI images, since the $(u, v)$-coverages are generally elongated in one direction, and contain significant holes at spacings slightly larger than an earth diameter. These tend to create large side-lobes and sinusoidal ripples in space-VLBI images that can mimic oscillations in brightness along the jet. A full quantitative description of the effects of $(u, v)$-holes on the true dynamic range of an image (i.e., peak flux / maximum flux error) has yet to be formulated. It is possible to obtain an upper limit on this quantity, however, by taking the ratio of peak flux in a map to the off-source rms noise level.

In the top panel of Fig. 1 we show the percentage difference in peak/rms noise level between the full and survey images for nineteen AGNs in the Pearson-Readhead sample. Given that the system equivalent flux density of HALCA at 5 GHz is roughly 50 times that of a typical VLBA antenna, the drop from 10 to 3 ground antennas implies a theoretical rms thermal noise roughly twice that of an image made with the full dataset. This prediction is verified in Fig. 1.

Another consequence of limited ground antenna coverage is the potential lack of short baselines, which are sensitive to extended structure in the source. In the bottom panel of Fig. 1 we plot the percentage dif-

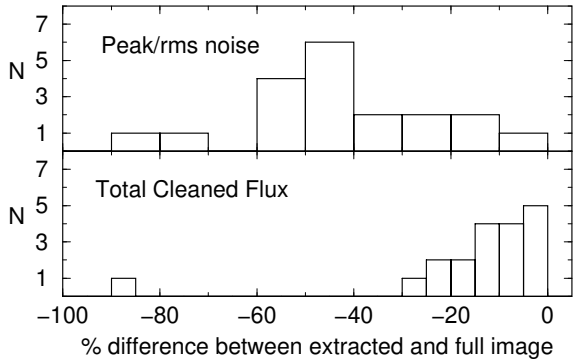


Figure 1: *Top*: Distribution of percentage difference in image dynamic range between full and extracted datasets of Pearson-Readhead AGNs. *Bottom*: Same as top panel, for total cleaned flux density.

ferences in total cleaned flux density for the two types of image. In the majority of cases, over $\sim 85\%$ of the parsec-scale emission is recovered in the survey image. One notable exception is 3C 84, a nearby radio galaxy with a large amount of extended emission on milliarcsecond scales. The fact that the survey and full dataset images recover similar amounts of flux is likely due to the nature of our sample, which was selected on the basis of sufficient flux ($> 0.4$ Jy) on baselines $> 6000$ km. As such, it is heavily biased towards objects that have bright cores and little extended structure. The VSOP survey should contain a similar bias, as most of its members are also flat-spectrum, core-dominated AGNs.

## 4 Model Fitting

We used the model fitting routine in Difmap to fit Gaussian components to the bright core features in our survey and full datasets. The survey data gave reliable core fluxes (top panel of Fig. 2), but less reliable sizes (middle panel). In two cases, the core components dropped below the noise level in the survey images, and could not be model fit. In terms of brightness temperature, which is proportional to core flux divided by component area, the survey data reproduced the values from the full datasets to within approximately a factor of two (bottom panel).

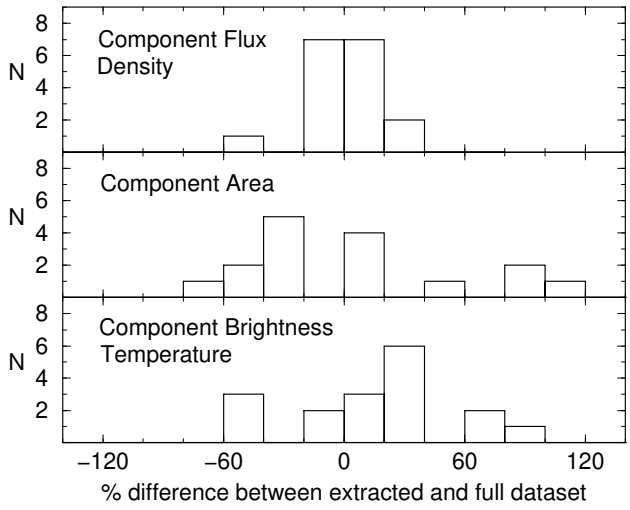


Figure 2: *Top*: Distribution of percentage difference in fitted core component flux density between full and extracted datasets of Pearson-Readhead AGNs. *Middle*: Same as top panel, for component area. *Bottom*: Percentage difference distribution for brightness temperature.

## 5 Conclusions

Our comparison experiments have shown that the images from the VSOP survey are likely to have very poor dynamic range due to minimal ground antenna coverage and large $(u, v)$ holes. As such, they are not well-suited for statistical studies of jet morphology, with perhaps the exception of crude estimates of jet position angle on parsec scales. The absence of short-baselines should not have a large impact on the survey results, as most of the sources are intrinsically core-dominated. However, the total cleaned flux density (and in turn, the measured flux on shortest baselines) are subject to strong biases, depending on the properties of each individual source. Our model fitting tests have shown that reliable brightness temperatures can be obtained with the survey data, although in some cases the identification of the true core component may be difficult due to the high thermal noise level in the image.

**Acknowledgements.** This research was performed at the Jet Propulsion Laboratory, California Institute of Technology, under contract to NASA. We gratefully acknowledge the VSOP Project, which is led by Japanese Institute of Space and Astronautical Science in cooperation with many organizations and radio telescopes around the world.

*Astrophysical Phenomena Revealed by Space VLBI*
*H. Hirabayashi, P.G. Edwards and D.W. Murphy (eds.)*

# Instantaneous 1–22 GHz Spectra of 214 VSOP Survey Sources

Yu.A. Kovalev[1], Y.Y. Kovalev[1] and N.A. Nizhelsky[2]

[1] *ASC, Profsoyuznaya 84/32, Moscow, 117810 Russia*
[2] *SAO, Nizhny Arkhyz, Karachaevo–Cherkessia, 357147 Russia*

**Abstract**

We present selected results of our monitoring, which form the basis of a ground spectra support for a space VLBI survey in the framework of the VSOP work team project. The 214 sources were selected from the HALCA continuum survey list, containing 230 sources with declinations north of $-30^\circ$ (Fomalont et al., these proceedings). Every 1–22 GHz spectrum was measured with the RATAN–600 radio telescope at six wavelengths of 1.4, 2.7, 3.9, 7.7, 13, and 31 cm, over a period of a few minutes (ten minutes or more near the pole). Almost all sources are suggested to have continuous jets at milliarcsecond scales. This conclusion is supported by the analysis of the 214 individual spectra, their mean normalized statistical shape in the local frame, and the long-term variable spectra of 23 objects. Model and statistical analysis suggest the common physical origin of various radio sources in the studied sample.

## 1 Results of Observations

We carried out three following sets of six frequency 1–22 GHz spectra observations of the HALCA survey sources: from 1 to 22 December, 1997 (sources with declinations $-30^\circ < \delta < +43^\circ$), from 11 to 25 July, 1998, and from 15 September to 1 October, 1998 (sources with $\delta > +49^\circ$). We used the 600 meter ring radio telescope RATAN–600 (Korolkov and Parijskij 1979; Parijskij 1993), located at the North Caucasus. The parameters of broad band receivers, the RATAN–600 beam widths, the details of the observational procedure, data processing, and calibration, as well as the spectra of 170 of 214 VSOP/HALCA sources are recently published in Kovalev et al. (1999). The spectra of the other 44 of 214 sources from our list are presented in Fig. 2 (flux density calibration is preliminary for the sources with $\delta > +49^\circ$). In addition, the results of the long-term spectra monitoring program (Kovalev 1997) for the

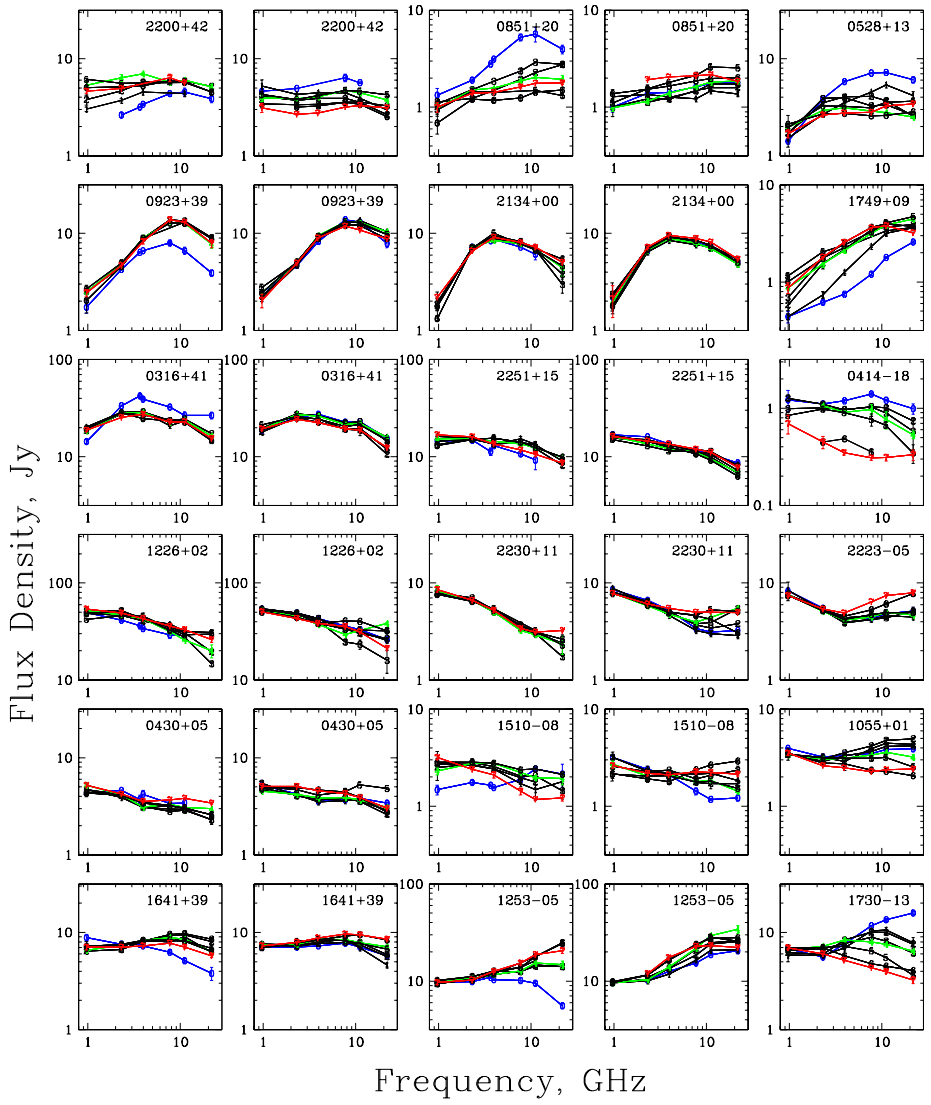


Figure 1: Multi-epoch instantaneous spectra for 18 well-known strong variable sources. Epochs for each of the columns 1 and 3 from the left: 1989, November; 1995, August, October, December; 1996, March, June, July, December (eight epochs, labeled 0–7, respectively). Epochs for each of the columns 2, 4 and 5: 1996, December; 1997, March, June, September, December; 1998, March; 1999, April, September (eight epochs, labeled 0–7).

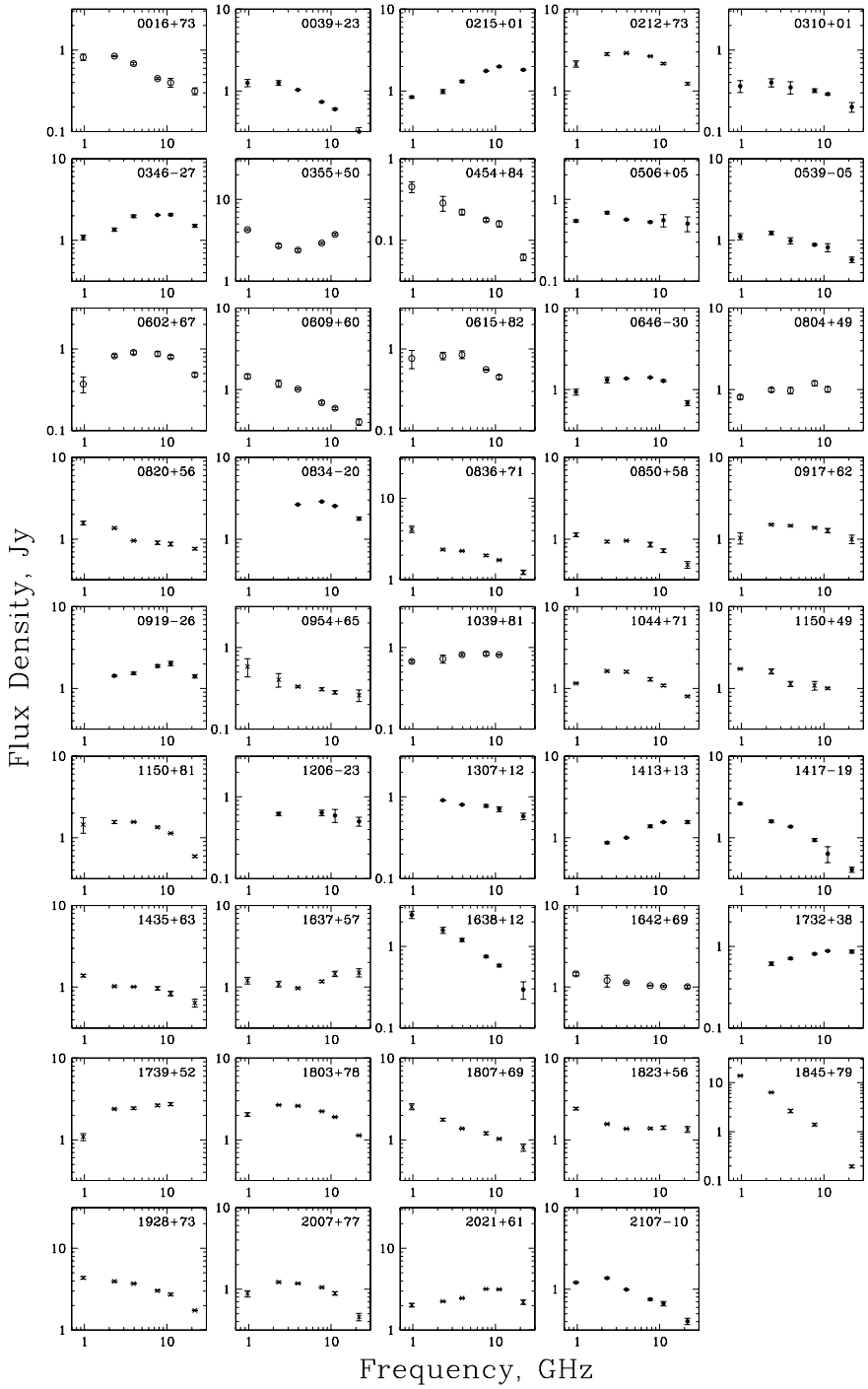


Figure 2: One epoch spectra of 44 sources in 1997–1998.

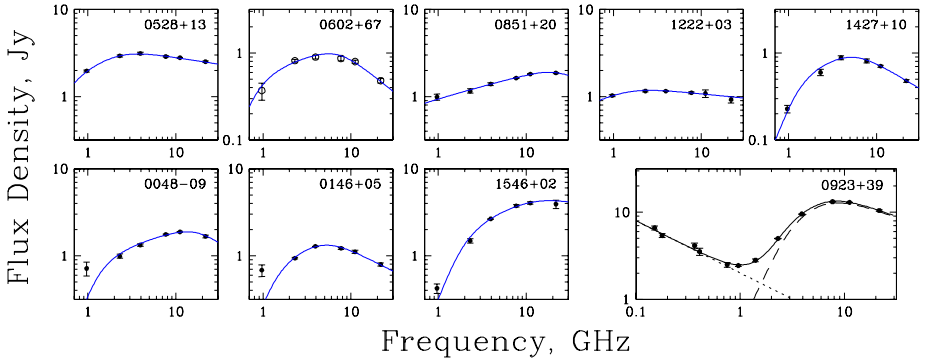


Figure 3: Examples of fitting (solid lines) by the Hedgehog jet model. $\chi^2$-criterion is satisfied at 0.05 significance level. Only for 0923+39 the low frequency component of the spectrum is modeled. Additional low frequency data for 0923+39 are from CATS data base.

18 strong HALCA sources in 1989, 1995–1999 (up to 15 epochs) are presented in Fig. 1. The IAU B1950 names of the sources are adopted.

## 2 Results of Analysis

The jet model analysis of the spectra is similar to the one by Kovalev and Larionov (1994), Kovalev and Kovalev (1997). It is based on the Hedgehog jet model of an active galactic nucleus with quasi radial magnetic field, suggested by Kardashev (1969) and developed by Kovalev and Mikhailutsa (1980). The one epoch spectra for all observed HALCA sources have been analyzed (see examples in Fig. 3). The analysis allows distinguishing a broad band emission of a continuous jet with quasi-stationary ejection at milliarcsecond scales for almost all objects of the sample. In addition, a second component at lower frequencies with a steep spectrum is visible in a part of the sources (e.g. lower boxes in Fig. 3). The second component can be explained by the emission of an extended magnetized envelope/lobe which accumulates the relativistic particles from the jet.

Using the calculated distributions of 214 sources over the red shift and the two points spectral indices (Fig. 4), we obtain the mean normalized statistical spectrum in the local frame. The mean spectral shape can also be interpreted by the combined emission from the jet and the envelope/lobe (Fig. 5).

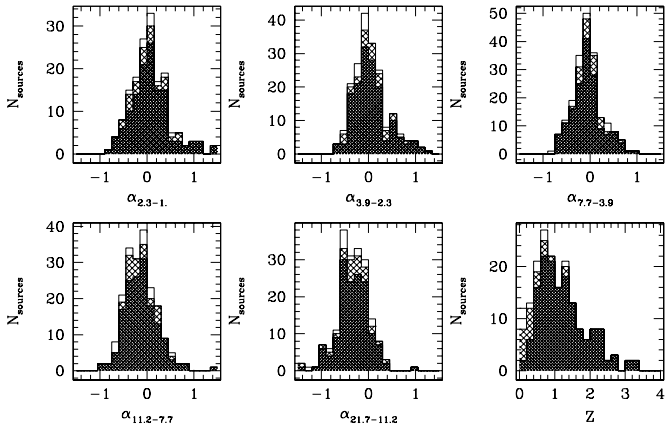


Figure 4: The distributions of 214 sources over the two-point spectral indices $\alpha_{\nu_2-\nu_1}$ and the red shift $z$ (strong hatched for quasars, hatched for BL Lacs, open for galaxies).

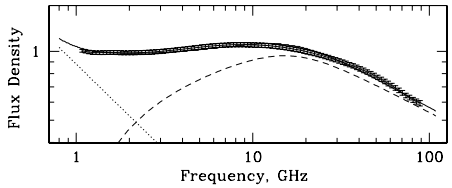


Figure 5: Mean statistical normalized spectrum with errors for the full sample in the local frame and the model fit. The thin solid line curve is the sum of dashed line curves for two spectral components, similar to 0923+39 model in Fig. 3.

The strong long term variability of the instantaneous spectra, which is seen in Fig. 1, can be explained in the same jet model by the variability of a flow of relativistic particles ejecting from an active core. Evolution of multi-epoch instantaneous spectra demonstrates such variability, at least, for the following 23 objects: 0316+41, 0430+05, 0851+20, 0923+39, 1226+02, 1253−05, 1510−08, 1641+39, 2134+00, 2200+42, 2251+15 (for up to 20 years), and for 0458−02, 0414−18, 0528+13, 1055+01, 1124−18, 1156+29, 1730−13, 1749+09, 2209+23, 2223−05, 2230+11, 2355−10 (for up to 10 years).

In the framework of our model, all strong VLBI structure components are interpreted as the maximums of a quasi-stationary or evolving distribution of the brightness along a continuous jet, rather than as a set of separate clouds of a structure. It is interesting to note that the

radio emission of an active core is not visible in these spectra. On this reason, a bright region in VLBI maps, which is sometimes interpreted as a strong compact core, may actually be the local brightest part of a jet (not a real active core of a source). If this region is the real active core and its flux density is greater than $3\sigma$ level or (5–10)% of the total flux density, the spectrum of the core would have to be well recognized as an additional spectral component.

Presented model calculations of the spectra yield the same results for both straight line jets and a class of twisted jets, which is characterized by a constant angle between a curved axis of a jet and the direction to an observer. Thus, the VLBI images with high resolution are required also to decide between two these types of the jet and predictions of other models.

**Acknowledgements.** We gratefully acknowledge the VSOP Project, which is led by the Japanese Institute of Space and Astronautical Science in cooperation with many organizations and radio telescopes around the world. YAK thanks the LOC and the RFBR for partly supporting the travel to the Symposium. The work has been supported in part by the Russian State Program "Astronomy" (grant 1.2.5.1) in 1997–1999 and by the NASA JURRISS Program (Project W–19,611). We have made use of the data base CATS (Verkhodanov et al. 1997) of the Special Astrophysical Observatory.

## References

Kardashev, N.S. 1969, Epilogue to Russian edition of Burbidge, G.R., & Burbidge, E.M., Quasars, Freeman (1967), Mir, Moscow

Korolkov, D.V. & Parijskij, Yu.N. 1979, *Sky & Telescope*, **57**, 324

Kovalev, Yu.A. & Mikhailutsa, V.M. 1980, *Sov. Astron.*, **24**, 400

Kovalev, Yu.A. 1997, *Bull. Spec. Astr. Obs*, **44**, 50

Kovalev, Yu.A. & Kovalev, Y.Y. 1997, *Ap&SS*, **252**, 133

Kovalev, Y.Y. & Larionov, G.M. 1994, *AstL*, **20**, 3

Kovalev, Y.Y., Nizhelsky, N.A., et al. 1999, *A&AS*, **139**, 545

Parijskij, Yu.N. 1993, *IEEE Antennas and Propagation Magazine*, **35**, 7

Verkhodanov, O.V., et al. 1997, *ASP Conf. Ser.*, **125**, 322

*Astrophysical Phenomena Revealed by Space VLBI*
*H. Hirabayashi, P.G. Edwards and D.W. Murphy (eds.)*

# The Pearson-Readhead Survey From Space

R.A. Preston[1], M.L. Lister[1], S.J. Tingay[2], B.G. Piner[1], D.W. Murphy[1], D.L. Meier[1], T.J. Pearson[3], A.C.S. Readhead[3], H. Hirabayashi[4], H. Kobayashi[5], M. Inoue[6]

[1] *Jet Propulsion Laboratory, California Institute of Technology, USA*
[2] *Australia Telescope National Facility, Narrabri, Australia*
[3] *California Institute of Technology, Pasadena, USA*
[4] *Institute of Space and Astronautical Science, Sagamihara, Japan*
[5] *National Astronomical Observatory, Mitaka, Tokyo, Japan*
[6] *Nobeyama Radio Observatory, Minamisaku, Nagano, Japan*

**Abstract**

We are using the VSOP mission to observe a complete sample of Pearson-Readhead survey sources at 4.8 GHz to determine core brightness temperatures and pc-scale jet properties. To date we have imaged 27 of the 31 objects in our sample. Preliminary results show that the majority of objects contain strong core components that remain unresolved on baselines of ∼30,000 km. The brightness temperatures of several cores significantly exceed $10^{12}$ K, which is indicative of highly relativistically beamed emission.

## 1 Introduction

Ground-based VLBI imaging surveys have been of critical importance in determining the general morphological and dynamical properties of the nuclear regions of active galaxies. Studies of individual sources alone leave many questions unanswered, and can even provide a biased view of nuclear activity. The statistical results obtained from imaging surveys have been key in providing constraints and insights for theoretical models of nuclear jets and environments. The same can be true for space-based VLBI imaging surveys.

The VSOP imaging survey we are undertaking is aimed at studying the nuclear regions of a complete sample of active galaxies. In addition to exploring the menagerie of source morphologies and dynamics, we will address a number of issues aimed ultimately at elucidating the fundamental characteristics of galactic nuclear activity and the physical conditions in these regions. These include the brightness temperature ($T_b$) distribution of the nuclei and the inner jet components, jet Doppler factors, and curvature.

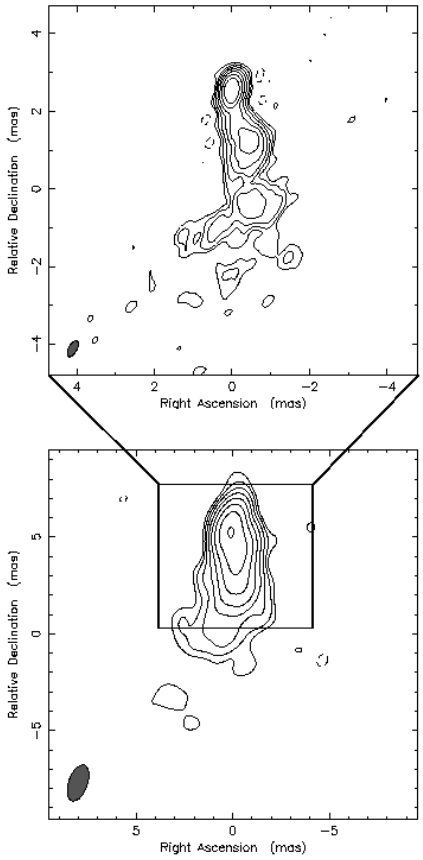


Figure 1: Images of 2200+420 (BL Lac) at 5 GHz as seen with VSOP (top panel), and with space-baselines removed (bottom).

## 2 The Sample

The complete sample from which we have drawn our sources is the Pearson-Readhead sample, which is defined by the following criteria: (1) $\delta > 35°$; (2) $|b| > 10°$; and total flux density at 5 GHz $> 1.3$ Jy (Pearson & Readhead 1988). This sample is ideal for a VSOP survey because the sources are strong, the VSOP $(u, v)$ coverages are especially good above $+35°$ declination, and multi-epoch ground-based VLBI data and other existing supporting data on these sources exceeds that of any other possible sample. Based on the multi-epoch ground-based VLBI observations at 5 GHz of this sample involving two of us (TJP and

ACSR), we have been able to carefully choose a complete subset of this sample having compact emission that is most likely to show fringes on VSOP baselines.

## 3 Results

To date we have imaged 27 of the 31 sources in the sample. In Fig. 1 we show a 5 GHz of 2200+42 (BL Lac). In the bottom panel, we also show the image of the source that can be made with the same data set if the baselines to the HALCA spacecraft are removed, and only the VLBA data are used. The box superimposed on the ground-only image shows the area of the map that is shown in the VSOP image. Note the significant increase in fine-scale detail that is apparent in the VSOP image compared to the ground VLBI image.

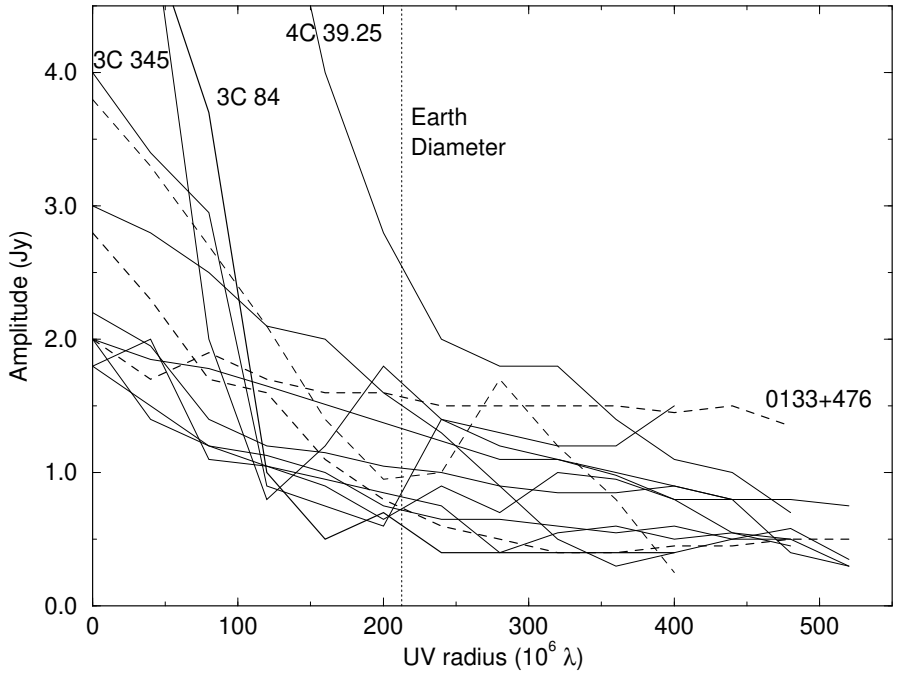


Figure 2: Upper envelope of visibility amplitude distribution plotted against $(u, v)$ distance for strong sources in our Pearson-Readhead sample.

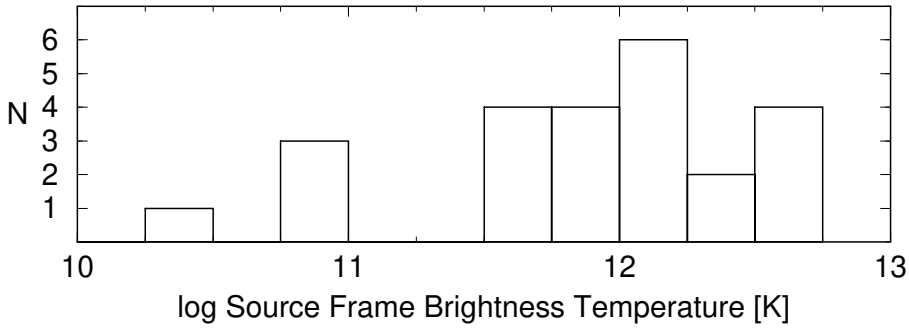


Figure 3: Distribution of source-frame core brightness temperature for fitted Gaussian components in our Pearson-Readhead sample. Most of these values may represent lower limits.

The fine-scale structure of nearly all of our sources is dominated by a bright, unresolved core component, as is revealed in plots of visibility amplitude versus $(u, v)$ distance (Fig. 2). The curves show a pronounced flattening at baselines greater than an earth diameter, instead of dropping smoothly to zero. The brightness temperatures of many of these core components exceed $10^{12}$ K in the source rest frame (Fig. 3). For $T_b$'s this high, the simplest way to alleviate problems associated with an inverse-Compton catastrophe (e.g., Kellermann & Pauliny-Toth 1969) is to assume that the emission is highly relativistically beamed. A preliminary analysis has shown that our brightness temperatures are positively correlated with 15 GHz variability amplitude, 5 GHz core-to-extended flux ratio, and fractional optical polarization, which are all known beaming indicators.

**Acknowledgements.** We gratefully acknowledge the VSOP Project, which is led by the Japanese Institute of Space and Astronautical Science in cooperation with many organizations and radio telescopes around the world. This research was performed in part at the Jet Propulsion Laboratory, California Institute of Technology, under contract to NASA.

## References

Pearson, T. J. & Readhead, A. C. S. 1988, *ApJ*, **328**, 114

Kellermann, K. I. & Pauliny-Toth, I. I. K. 1969, *ApJ*, **155**, L71

*Astrophysical Phenomena Revealed by Space VLBI*
*H. Hirabayashi, P.G. Edwards and D.W. Murphy (eds.)*

# The Pearson-Readhead Survey at 43 GHz

Matthew L. Lister[1], R.A. Preston[1], B. Glenn Piner[1]
& S.J. Tingay[2]

[1] *Jet Propulsion Laboratory, California Institute of Technology*
[2] *Australia Telescope National Facility*

**Abstract**

We present results of a program to obtain 43 GHz ground VLBI polarization images of a sample of AGNs from the Pearson-Readhead survey that we are also observing with HALCA at 5 GHz. The sources analyzed so far display bright, weakly polarized cores with magnetic fields predominantly perpendicular to the inner jet direction. The polarizations of components in the jets increase with distance from the core, and have magnetic field orientations that are consistent with oblique relativistic shocks.

## 1 Introduction

In this paper we present preliminary results of a VLBA polarization study at 43 GHz of flat-spectrum AGNs in the Pearson-Readhead (PR) survey. This work complements our 5 GHz space-VLBI observations of this sample (Preston et al. 2000), with the goal of better understanding the physics and dynamics of the core regions of AGNs.

The original VLBI polarization study of the PR sample was carried out at 5 GHz (Cawthorne et al. 1993), and revealed that quasars tend to have magnetic fields that are parallel to the jet, while in the jets of BL Lacertae objects, the orientations are mostly perpendicular. Observations at higher frequencies (e.g., Nartallo et al. 1998, Lister et al. 1998) indicate that this dichotomy might not hold for jet regions closer to the core, however. This may be related to the nature of the underlying longitudinal field component and/or relativistic shocks in these regions. Our 43 GHz polarization study represents the first high-resolution survey of a complete sample of objects with which to investigate these issues.

## 2 Observations

To date we have obtained VLBA 43 GHz polarization snapshot observations of 25 of 34 flat-spectrum ($\alpha_{5-15\,\mathrm{GHz}} > -0.5$) PR objects that

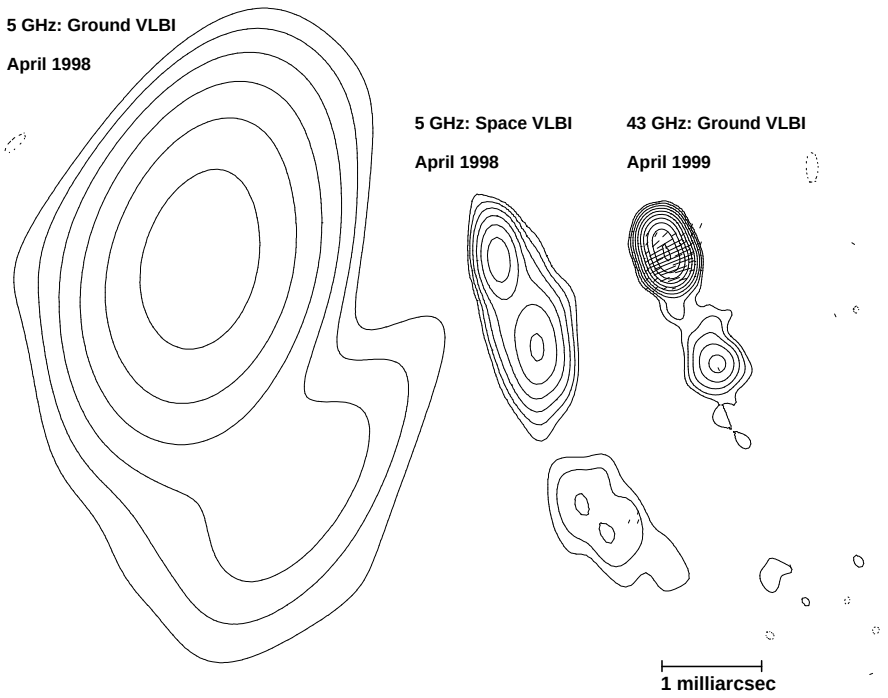


Figure 1: Images of the quasar 1637+574, taken with space and ground VLBI at two epochs. Electric polarization vectors are shown in the 43 GHz image.

have total 43 GHz flux densities $> 300$ mJy. Nearly all of the 19 objects that we have imaged so far are highly core-dominated, with the exception of the two radio galaxies in the sample: 2021+614 and 3C 84. In three sources (0016+731, 0804+499, and 0954+658), the core accounts for over 92% of the total cleaned flux, which illustrates the usefulness of this sample for identifying good targets for future high-frequency space VLBI. In Fig. 1 we show the improvements in resolution obtained with various VLBI techniques for the quasar 1637+574.

## 3 Polarization Properties

The core components of our sources are generally weakly linearly polarized ($< 3\%$), with more than half displaying magnetic fields that

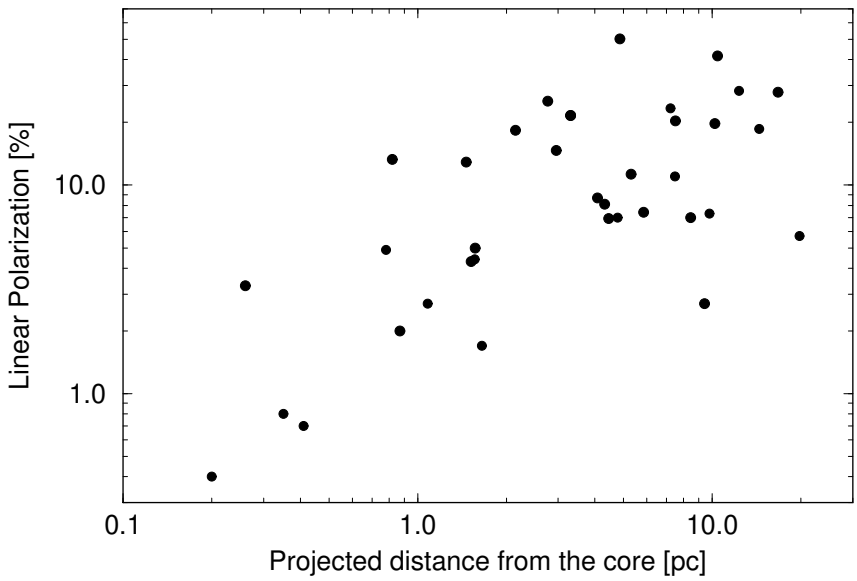


Figure 2: Fractional polarization of jet components versus projected distance from the core in parsecs.

are nearly perpendicular to the innermost jet direction. We find no strong correlations between the measured core brightness temperatures at 5 GHz and the polarization properties of the core components.

The components found in the jets are generally more polarized than the cores, and follow an exponential trend of increasing polarization with distance from the core (Fig. 2). This may be due to a general increase in shock strength, or relativistic aberration as the jets bend away from the line of sight (Lister & Smith 2000).

The electric vectors of the jet components are predominantly parallel to the upstream jet direction (Fig. 3), as would be expected from transverse shocks that amplify the component of the magnetic field perpendicular to the jet (e.g., Hughes et al. 1985). However, the distribution also contains many components at oblique angles, and is more consistent with a family of oblique shocks moving at various speeds down the jet (e.g., Lister et al. 1998). Those components with electric vectors nearly perpendicular to the jet are more weakly polarized, which also supports this interpretation. Finally, we find no significant difference in the **B** field orientations of the BL Lac objects and quasars in our sample.

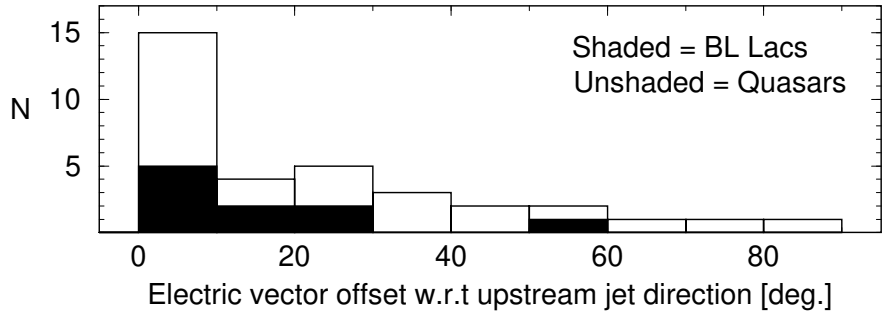


Figure 3: Distribution of electric polarization vector offset with respect to the upstream jet direction, for polarized jet components.

## 4 Conclusions

We have undertaken the first detailed polarization study of a complete sample of AGNs at 43 GHz, which is also being observed by HALCA at 5 GHz. Our preliminary results show the objects to be dominated by strong, unresolved cores at 43 GHz, which are weakly polarized and have magnetic fields mostly perpendicular to the inner jet direction. The fractional polarization of the jets increases exponentially with distance from the core, and their polarization orientations are consistent with those of a family of oblique shocks that are moving with various speeds down the jet.

**Acknowledgements.** This research was performed at the Jet Propulsion Laboratory, California Institute of Technology, under contract to NASA. We gratefully acknowledge the VSOP Project, which is led by Japanese Institute of Space and Astronautical Science in cooperation with many organizations and radio telescopes around the world.

## References

Cawthorne, T. V. et al. 1993, *ApJ*, **416**, 519

Hughes, P. A., Aller, H. D., & Aller, M. F. 1985, *ApJ*, **298**, 301

Lister, M. L., Marscher, A. P., & Gear, W. K. 1998, *ApJ*, **504**, 702

Lister, M. L. & Smith, P. S. 2000, *ApJ*, submitted

Nartallo, R. et al. 1998, *MNRAS*, **297**, 667

Preston, R. A., et al. 2000, *these Proceedings*

*Astrophysical Phenomena Revealed by Space VLBI*
*H. Hirabayashi, P.G. Edwards and D.W. Murphy (eds.)*

# High Resolution X-Ray Imaging and Spectroscopy of AGN and SS 433 with the Chandra X-Ray Observatory

Herman L. Marshall

*Center for Space Research, MIT, Cambridge, MA 02139, USA*

**Abstract**

We present some early results on AGN and jets with the Chandra X-ray Observatory, highlighting high resolution spectroscopy using the High Energy Transmission Grating Spectrometer (HETGS). The quasar PKS 0637–752 was found to have a very bright X-ray jet whose shape is remarkably similar to that of the radio jet on a size scale of 100 kpc but the X-ray emission is still unexplainably bright. Two BL Lac objects, PKS 2155–304 and Mk 421, were observed with the spectrometer and found to have no strong absorption or emission features. Other radio loud AGN observed with the HETGS show simple power law spectra without obvious features. These AGN results stand in marked contrast to the line-rich spectrum of SS 433, a Galactic X-ray binary which has relativistic jets. Broadened X-ray emission lines of H- and He-like S and Si are used to show that the characteristic temperature of the jet is near 2.5 keV at its base.

## 1 Introduction

The Chandra X-ray Observatory (CXO, or Chandra) was launched in July, 1999 into high Earth orbit. Although there has been some degradation of the spectral resolution of the Advanced CCD Imaging Spectrometer (ACIS), all instruments are performing extremely well.

The main scientific feature of Chandra is the mirror performance: the half-power radius is about $0.4''$. In addition, there are two objective grating spectrometers, providing a spectral resolution, $E/dE$, of 200–2000 in the 0.1–10 keV range. The ACIS detector provides $\sim$ 100 eV resolution over the energy range from 0.5-10 keV and the High Resolution Camera gives higher timing resolution and the best spatial resolution.

We will focus on data from ACIS and the HETGS here in order to demonstrate the overall performance of the telescope and some of

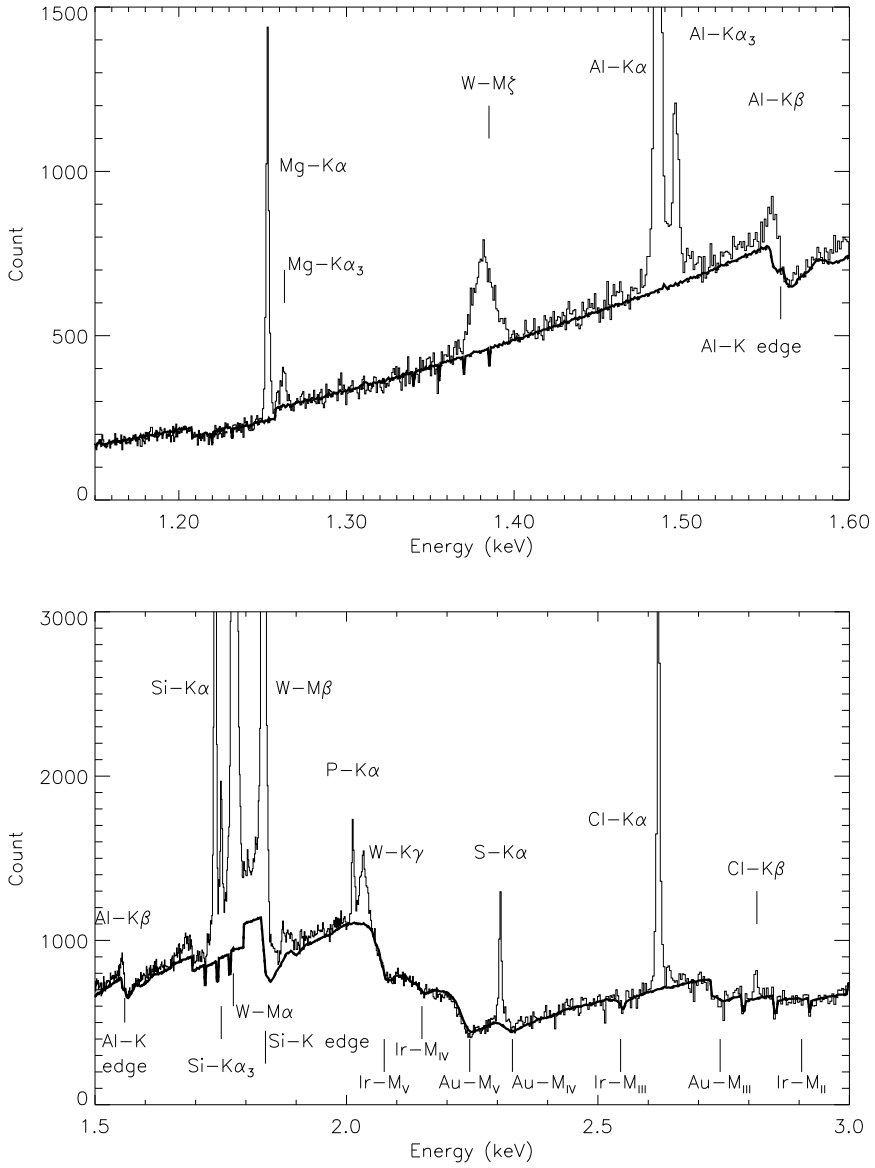


Figure 1: A portion of the calibration spectrum of a carbon source using the HEG portion of the HETGS. Note the emission lines from contaminant elements are quite narrow and are readily identified. The solid line is a model of a 5-parameter model of the source continuum folded with the effective area of the spectrometer and the exposure function.

the ways that Chandra will contribute to the understanding of jets in active galactic nuclei (AGN) and Galactic sources. Briefly, the HETGS consists of two different types of grating facets that tile the annular exit apertures of the telescope mirror shells. The outer mirror pairs focus X-rays through the medium energy gratings (MEG) while the outer pair, with much higher reflectivity at high energies, focusses X-rays through the high energy gratings (HEG). The HEG and MEG spectra are independently measured by the spectroscopic array of ACIS. Canizares et al. (2000) give a somewhat more detailed description.

## 2 Ground Calibration

In Figure 1, we show ground calibration data that demonstrate the overall performance of the pre-flight HETGS. The HEG portion of the continuum spectrum is well modelled from pre-flight effective areas; the edges near 2.1 keV due to the Ir coating on the mirror and the edges near 2.3 keV due to the Au in the grating do not show residuals after source modelling. The emission lines arise from contaminant elements on the carbon anode in the electron impact source and are readily identified. The spectral resolution of the HETGS is apparent; the narrow K-$\alpha$ lines stand in marked contrast to the broadened W-M$\zeta$ and W-M$\gamma$ lines at 1.38 and 2.03 keV, respectively.

## 3 Flight Calibration

The first target observed with Chandra was the quasar PKS 0637–752. It was rather surprising to find an X-ray jet extending 7-12$''$ from the quasar core because the target had been chosen for focus measurements. The core point response function is small enough, however, that the jet had no effect on determining the best detector focus position. New radio observations showed that the radio and X-ray jets were remarkably similar out to 12$''$ where there is a significant bend in the radio emission. The optical fluxes from Hubble data are so low that models of the jet X-ray emission are difficult to develop. See Lovell et al. (2000) for more discussion.

The HETGS flight calibration program includes observations of the Crab Nebula and pulsar in order to verify the absolute effective area of the system, an observations of the late type star Capella in order to verify the spectral resolution with emission lines, and observations of

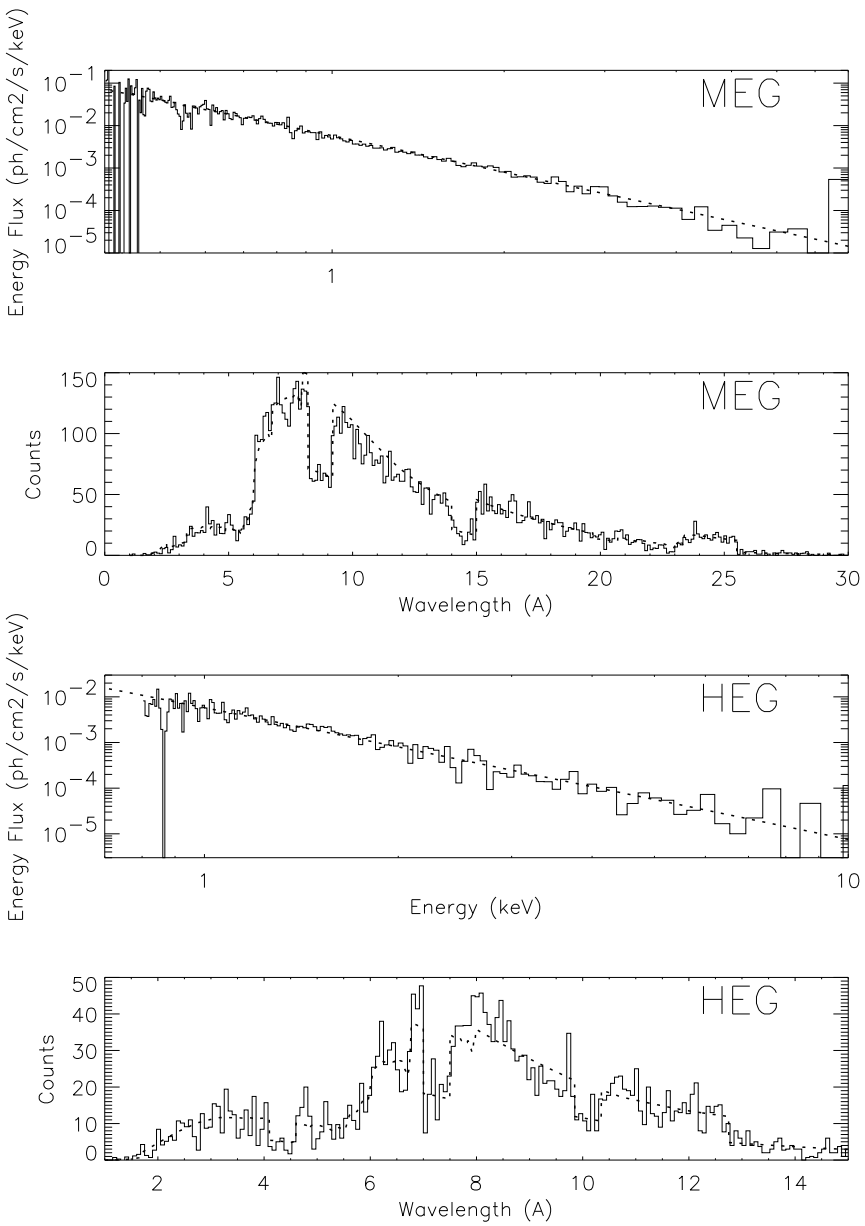


Figure 2: The spectra of Mk 421 with the Chandra HETGS. The top two are the flux and count spectra from the MEG grating data and the bottom two are from the HEG data. The count spectra are overlaid with well-fitting power law models with $\alpha = 1.9$, folded with the instrument effective area and exposure. The MEG and HEG spectra are consistent within 10-20% systematic uncertainties.

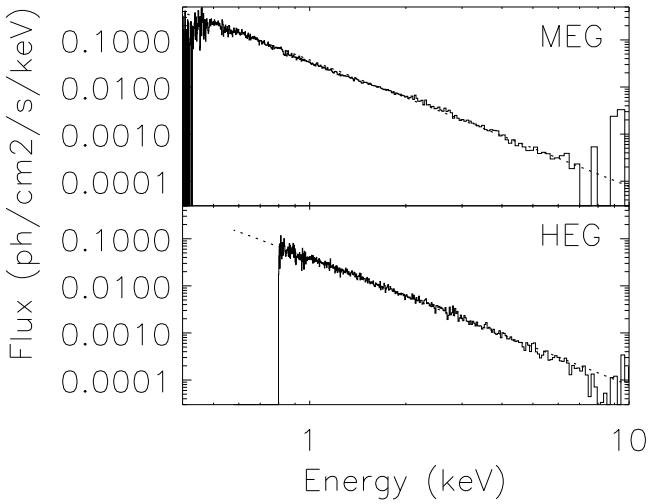


Figure 3: The spectrum of PKS 2155–304 with the Chandra HETGS. As with Mk 421, the MEG and HEG spectra are consistent within 10-20% systematic uncertainties; the spectra are fitted very well by a simple power law $\Gamma = 2.7$.

extragalactic sources 3C 273 and Mk 421 in order to verify the effective area for point sources and cross calibrate with other X-ray spectrometers. The Capella observation (Canizares et al. 2000) shows that the spectral resolution achieved in ground calibration is matched by flight data. The Crab nebula (Weisskopf et al. 2000) shows that the 0th order image reveals significant fine structure that was not previously observed.

## 4 High Resolution X-Ray Spectra of AGN

The calibration spectra of Mk 421 are shown in Figure 2. The spectra from the MEG and the HEG are consistent with each other within the 10-20% systematic uncertainties. The spectra are well fitted with a simple power law with $\alpha = 1.9$ ($f_\nu \propto \nu^{-\alpha}$) and the only deviation from this fit appears near the O-K edge, which will be removed as the detector calibration is refined.

The BL Lac object PKS 2155–304 was observed as part of the HETGS guaranteed time observation program. Spectra are shown in Figure 3. Again, the HEG and MEG spectra are consistent within 10-20% systematic uncertainties and are well fitted with a simple, pure

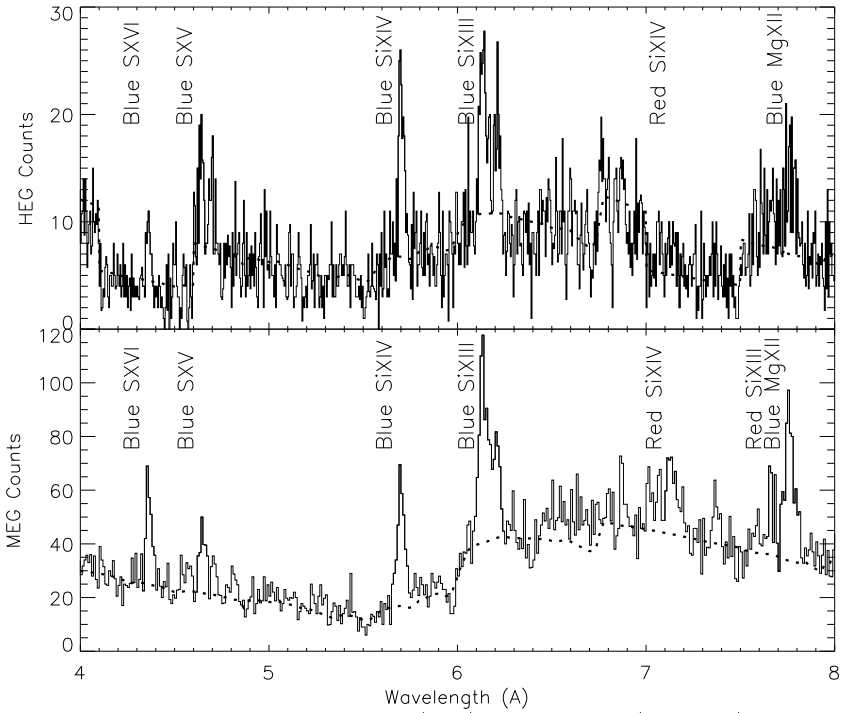


Figure 4: A portion of the HEG (top) and MEG (bottom) spectra of SS 433 observed with the Chandra HETGS, showing the blue-shifted H- and He-like lines of S (S XVI and S XV), the corresponding lines of Si (Si XIV and Si XIII) as well as the red-shifted counterparts to the Si lines. Note that the lines are broadened and that the He-like triplets of S and Si are resolved.

power law model. The spectral index is $1.70 + / - 0.02$ and there are no significant absorption features. A feature such as the one found by Canizares and Kruper (1984) would have been detected easily in the MEG portion of the Chandra HETGS spectrum, so we conclude that it must be variable.

Other AGN observed in the early phase of Chandra HETGS observations include NGC 1275, PKS 2149−305, and Q0836+710. Preliminary analyses indicates that these HETGS spectra are all well fitted by simple power law models with absorption by neutral interstellar material. The spectral indices are somewhat smaller: 0.8, 0.2, and 0.4, respectively. No Fe-K$\alpha$ lines are detected in any of their spectra.

## 5 SS 433

The Galactic X-ray binary SS 433 was observed in order to detect and measure X-ray lines from the opposing jets. As shown by Kotani et al. (1996) using ASCA, the blue-shifted lines are so much stronger than the red-shifted lines that Doppler boosting is insufficient to account for the line ratios, so absorption of the red-shifted lines is required. This absorption could arise in the accretion disk. Furthermore, Kotani et al. found that the temperature at the base of the jet must be of order 20 keV in order to give the observed ratio of the Fe XXVI and Fe XXV emission lines.

We observed SS 433 at very nearly the same precessional phase as Kotani et al.; portions of the MEG and HEG spectra are shown in Figure 4. We confirm the result of Kotani et al. that the red lines are systematically weaker than expected but now we can extend this result to the H-like and He-like ions of S and Si; the red-shifted lines are even weaker relative to the blue ones than for the Fe XXV lines. We also find that the lines are broadened significantly, with FWHM values of order 2000-5000 km/s, comparable to the broadening of the optical lines from the jets.

The base of the SS 433 jets, however, must be significantly cooler than found by Kotani et al.. We do not detect either the blue- or the red-shifted Fe XXVI lines at all with a limit that is more than a factor of 5 lower than derived from the ASCA data. The base temperature must be less than 3.5 keV, based on limits to the Fe XXV:Fe XXVI line ratios. We can get additional indications of the jet base temperature using the S XV and S XVI ratio as well as the Si XIII and Si XIV ratio. The S ratio is consistent with emission from a thin thermal plasma with a temperature of $2.3 + / - 0.1$ keV while the Si line ratio gives $1.8 + / - 0.1$ keV. Although these lines can be produced in cooler regions further out in the jet, the limit on the Fe line ratios indicates that the base temperature could be as low as 2.5 keV.

## 6 Summary

In general, Chandra is working very well and the newest results on AGN and astrophysical jets already promises to change our understanding of these phenomena.

**Acknowledgements.** I thank the PI of the HETGS, Prof. Claude R. Canizares for his support; Daniel Dewey and other members of the HETGS team with whom I worked during ground calibration; Norbert Schulz, Patrick Ogle, Mike Wise, and other members of the Chandra X-ray Center at MIT who have also contributed to the results presented here. I gratefully thank the VSOP Project, which is led by the Japanese Institute of Space and Astronautical Science in cooperation with many organizations and radio telescopes around the world, for inviting me to participate in this conference. This work was supported by contract SAO SV1-61010.

## References

Canizares, C.R. & Kruper, J. 1984, *ApJ*, **278**, L99

Canizares, C.R., Huenemoerder, D.P., Davis, D.S., et al., 2000, in preparation

Kotani, T., Kawai, N., Matsuoka, M., & Brinkmann, W. 1996, *PASJ*, **48**, 619

Lovell, J.E.J., Tingay S.J., Piner, B.G., et al. 2000, *these Proceedings*

Weisskopf, M., Hester, J.J., Tennant, A., et al., 2000, in preparation

*Astrophysical Phenomena Revealed by Space VLBI*
*H. Hirabayashi, P.G. Edwards and D.W. Murphy (eds.)*

# VSOP and ATCA Observations of PKS 0637−752

J.E.J. Lovell[1], S.J. Tingay[1], B.G. Piner[2], D.L. Jauncey[1], R.A. Preston[2], D.W. Murphy[2], P.M. McCulloch[3], M.E. Costa[3] G. Nicolson[4] H. Hirabayashi[5] J.E. Reynolds[1], A.K. Tzioumis[1], D.L. Jones[2], M.L. Lister[2], D.L. Meier[2], M. Birkinshaw[6], G. Chartas[7], E.D. Feigleson[7], G.P. Garmire[7], K.K. Ghosh[8], H.L. Marshall[9], S. Mathur[10], R.M. Sambruna[7], D.A. Schwartz[11], W.H. Tucker[11], B. Wilkes[11] & D.M. Worrall[6]

[1] *ATNF, PO Box 76, Epping NSW 1710, Australia*
[2] *JPL, California Institute of Technology, Pasadena, CA 91109, USA*
[3] *University of Tasmania, Hobart 7001, Tasmania, Australia*
[4] *Hartebeesthoek RAO, Krugersdorp 1740, South Africa*
[5] *ISAS, Yoshinodai 3-1-1, Sagamihara, Kanagawa 229-8510, Japan*
[6] *Department of Physics, University of Bristol, England, UK*
[7] *Astronomy Dept, Pennsylvania State University, PA 16802, USA*
[8] *NASA/MSFC, SD50, Huntsville, AL 35812, USA*
[9] *MIT Center for Space Research, Cambridge, MA 02139*
[10] *The Ohio State University*
[11] *Harvard-Smithsonian CfA, Cambridge, MA 02138, USA*

**Abstract**

In August 1999, the Chandra X-Ray Observatory detected an unexpectedly luminous $\sim$ 50 kpc jet in PKS 0637−752, coincident with the arcsecond-scale jet observed at radio wavelengths. Here we describe VSOP and ATCA observations of PKS 0637−752 and the important constraints that they provide for emission models.

## 1 Introduction

The bright ($\sim$ 7 Jy) quasar PKS 0637−752 ($z = 0.651$) was the first celestial object to be observed by the Chandra X-ray Observatory (Marshall et al. 2000) as a calibrator since it was thought to be unresolved. However, the first Chandra images discovered that the quasar hosts the most luminous X-ray jet yet known, at $L_X \approx 3 \times 10^{44}$ erg s$^{-1}$ (Schwartz et al. 2000)[1].

[1] $H_0 = 50\,\mathrm{km\,s^{-1}\,Mpc^{-1}}$, $q_0 = 0$

PKS 0637−752 is situated near the south ecliptic pole, making it an excellent target for an on-going VSOP experiment to monitor its milliarcsecond-scale structure (Tingay et al. 2000). Space-VLBI observations of this source were re-scheduled specifically to coincide with the Chandra observations in August 1999. These VLBI observations involved the Australia Telescope Compact Array (ATCA) from which we extracted ATCA-only images at 4.8 and 8.6 GHz. The ATCA at 8.6 GHz has the same resolution as Chandra and so provides a powerful structural comparison. A comparison of the X-ray and radio images is shown in Color Figure 8 on page xviii and reveals a striking coincidence. The arcsecond-scale western radio jet is clearly longer than the X-ray jet, and bends through a projected angle of about 60° at about 12 arcsec from the core. The eastern edges of the brightest knot in the radio and X-ray jets ($\sim 8''$ west of the nucleus) coincide, while the other edge of this knot extends farther west in the radio than in X-rays.

Follow-up ATCA observations were made in September 1999 to obtain linear polarization data at both 4.8 and 8.6 GHz. These data have revealed a strongly polarized jet with fractional polarizations of up to 30%. The polarization E-vectors remain perpendicular to the jet where X-rays are detected (Figure 1), but, as the X-ray flux decreases at the western end of the X-ray jet near the bend in the radio jet, the polarization position angle begins to change so that the E-vectors become parallel to the jet's centre line. Figure 1 and the figure on page X show that both the radio and X-ray jets are well entrained before the bend. The absence of X-ray emission past the bend in the radio jet suggests that whatever causes the bend may also be responsible for quenching the X-rays, or that having the E-field perpendicular to the flow is conducive to generating X-rays.

The lack of detectable rotation measure has been important in ruling out thermal Bremsstrahlung as a mechanism for the jet X-ray emission. The detection of very weak optical components in the jet by the HST is an important constraint on jet emission models. A simple synchrotron model extending from radio through to X-rays is not sufficient as the optical flux is two orders of magnitude weaker than required in such a model. Further, both Inverse-Compton and Synchrotron Self-Compton models have problems providing sufficient X-ray jet flux unless the jet plasma is far out of equipartition or the jet is Doppler boosted with $\delta \sim 0.3$, or the beaming and alignment of the core and kpc-scale jet are finely tuned to provide adequate seed photons from the inner region

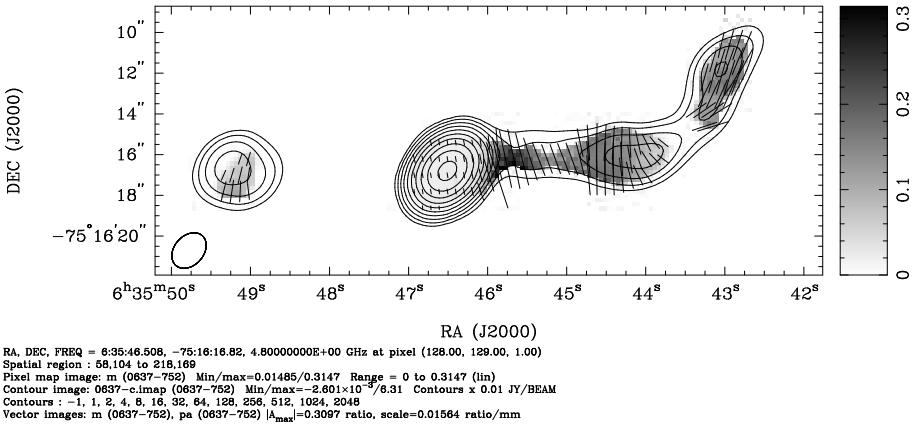


Figure 1: Our 4.8 GHz image of PKS 0637−752 (contours) together with the fractional polarization (greyscale) and polarization E-vectors.

of the source.

The VSOP and ground VLBI data provide key directional information. Analysis shows that the components near the milliarcsecond core are moving in the same projected direction as the arcsec-scale radio/X-ray jet (see figure on page X) at a mean apparent speed of $11.4 \pm 0.6\ c$ (Figure 2) which puts a lower limit on the Lorentz factor of 11.4 and an upper limit on the angle between the jet and the line of sight of 8.9°. If the arcsec-scale jet has a Doppler factor of 0.3, the jet angle to the line of sight would need to increase from $\sim 9°$ to $\sim 45°$ as one goes from the mas-scale to the arcsecond-scale. Under such conditions one would normally expect to see a large apparent bend in the jet which is not observed. The large required bending can only be explained by a geometry in which the mas-scale jet, arcsecond-scale jet and the observer-source line of sight all lie in the same plane which would be an unlikely special case for the first Chandra-observed quasar.

## 2 Conclusions

The serendipitous discovery of a luminous kpc-scale X-ray jet in PKS 0637−752 has raised many questions concerning its emission mechanism. Observations with VSOP and the ATCA have helped to rule out some models (such as thermal Bremsstrahlung and simple synchrotron models) and provided important constraints to others (such as Inverse-

Compton and Synchrotron Self-Compton models). We are continuing to monitor PKS 0637−752 and are also investigating similar sources to understand how common kpc-scale X-ray/radio jets are and under what conditions they occur.

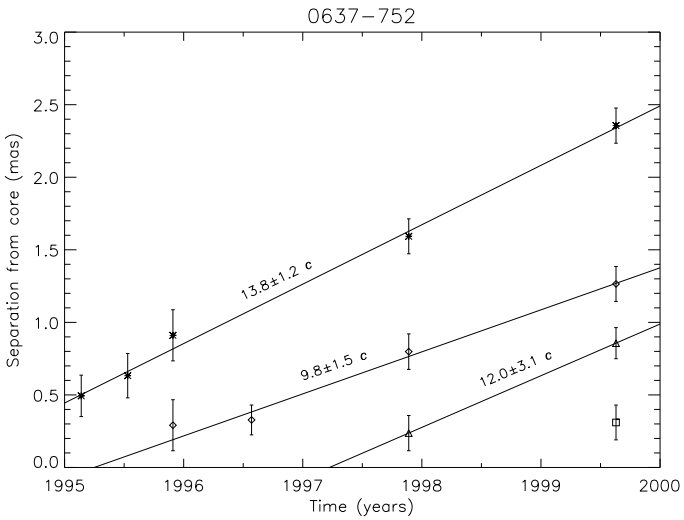


Figure 2: Positions of the milli-arcsecond-scale components as a function of time. The first four epochs are from ground-only VLBI observations and the last two epochs are from VSOP observations. The lines indicate the best fit speeds for each component. Component speeds have been calculated assuming $H_0 = 70\,\mathrm{km\,s^{-1}\,Mpc^{-1}}$ and $q_0 = 0.15$.

**Acknowledgements.** We gratefully acknowledge the VSOP Project, which is led by the Japanese Institute of Space and Astronautical Science in cooperation with many organizations and radio telescopes around the world. The Australia Telescope is funded by the Commonwealth of Australia for operation as a National Facility managed by CSIRO.

## References

Marshall, H. et al., 2000, *these Proceedings*

Schwartz, D. et al., 2000, in preparation

Tingay, S. et al., 2000, *Adv. Sp. Res.*, **26**, 677

*Astrophysical Phenomena Revealed by Space VLBI*
*H. Hirabayashi, P.G. Edwards and D.W. Murphy (eds.)*

# VSOP and Chandra Observations of 0836+710

D.W. Murphy [1], R.A. Preston [1], B.G. Piner [1], M.L. Lister [1],
H. Marshall [2] and P.G. Edwards [3]

[1] *JPL, 4800 Oak Grove Drive, Pasadena, CA*
[2] *Center for Space Research, MIT, Cambridge, MA 02139, USA*
[3] *ISAS, Yoshinodai 3-1-1, Sagamihara, Kanagawa 229-8510, Japan*

**Abstract**

In this paper we describe the radio observations that form part of co-ordinated Chandra, HALCA+VLBA, and VLBA-only observations of the gamma-ray loud quasar 0836+710. The radio observations were at 6 frequencies (1.6, 5, 8, 15, 22, and 43 GHz) with the two lower frequency observations being undertaken with HALCA co-observing with the VLBA. The aim of the radio observations is to determine the peak brightness temperature of each of the VLBI components and hence provide better constraints on predicted X-ray emission than has previously been possible.

## 1 Introduction

There is much interest in relating the radio properties of AGN with their high energy X-ray and gamma-ray properties. With the simultaneous operation of both the HALCA spacecraft and the Chandra mission it becomes feasible to test the popular Synchrotron-Self Compton (SSC) model with the current generation of both VLBI and X-ray facilities. We undertook co-ordinated observations of the high redshift ($z$=2.17) superluminal gamma-ray and X-ray loud, core-dominated radio quasar 0836+710, with the VLBI observations taking place on 7 October 1999 followed by the Chandra observations on 16 October 1999.

## 2 VLBI Observations of 0836+710

Our VLBI observations of 0836+710 were a target of opportunity proposal since the X-ray observations were scheduled earlier in the lifetime of the Chandra mission than we had previously envisioned. HALCA co-observed for about 11 hours with the VLBA at both 1.6 GHz and

5 GHz followed by 3 hours of VLBA-only data where several snapshots were undertaken at 8, 15, 22, and 43 GHz. The HALCA observations used the unusual observing mode with one 16 MHz channel observing at 1.6 GHz and the other at 5 GHz. During this time the VLBA switched between observing at 1.6 GHz or 5 GHz on a roughly 10-minute timescale. Figure 1 shows the $(u, v)$-coverages and images from our 1.6 and 5 GHz HALCA+VLBA observations. At 5 GHz, 0836+710 is the subject of a VSOP monitoring campaign by Lobanov and 5 GHz VSOP images have already been published (Lobanov et al. 1998).

## 3 X-Ray Flux Density and Radio Brightness Temperature

To a first approximation, the X-ray flux density (at $\nu_x$) due to SSC scattering in a VLBI component is given by:

$$\frac{S_x}{\mu Jy} \approx (\frac{S_m}{1Jy})(\frac{\nu_m}{1\,GHz})^{\alpha+2}(\frac{T_m}{2.6\times10^{12}K})^{2\alpha+3}(\frac{1+z}{\delta})^{2\alpha+4}(\frac{\nu_x}{1KeV})^{-\alpha}$$

where $S_m$, $T_m$, $\nu_m$ are the component's observed turnover flux density, brightness temperature, and frequency respectively. $\alpha$ and $\delta$ are the component's optically thin spectral index and Doppler factor while $z$ is the source redshift

X-ray observations give the overall source X-ray flux density and multi-frequency VLBI observations allow us to measure the properties of the individual VLBI components which make up the source (hopefully $S_m$, $T_m$, $\nu_m$, and $\alpha$ for every component). Combining the X-ray data with the VLBI data then allows the Doppler factor (or at least a lower limit on it) to be determined. From the above formula it can be seen that only those VLBI components with intrinsic brightness temperatures near $10^{12}$ K are able to produce substantial X-ray flux density.

In Figure 2 we show the observed brightness temperatures of the VLBI components which make up the VLBI jet on 0836+710. For this preliminary analysis we choose to consider the jet to be made up of 4 components which are labeled in Figure 1 (d). From Figure 2 it can be seen only components C0 and C1, i.e., the core and the strong jet component near the core (C1), have brightness temperatures which allow them to produce substantial X-ray emission. This result is similar to that found for the quasar 3C345 (Unwin et al. 1997) and indicates that there might be a universal mechanism which limits component brightness temperatures for components far away from the core i.e., strong shocks

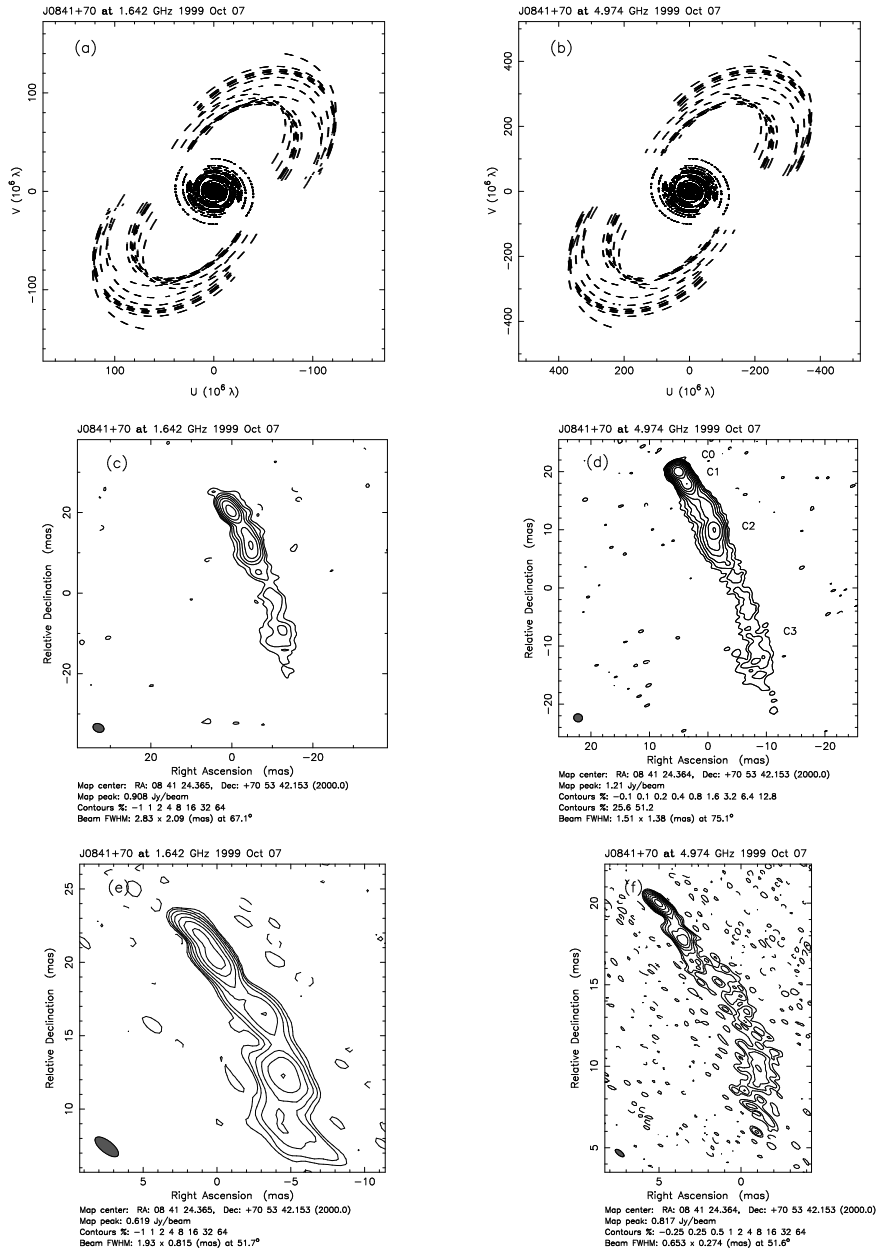


Figure 1: 1.6 GHz and 5 GHz HALCA+VLBA observations: (a) 1.6 GHz $(u, v)$-coverage (b) 5 GHz $(u, v)$-coverage (c) 1.6 GHz image (50 M$\lambda$ taper) (d) 5 GHz image (100 M$\lambda$ taper) (e) 1.6 GHz image (no taper) (f) 5 GHz image (no taper).

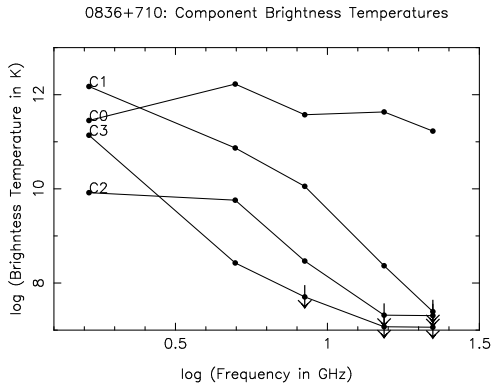


Figure 2: Component brightness temperatures

and *in situ* particle acceleration by themselves seem unable to produce substantial X-ray emission. In should be pointed out that only high resolution 1.6 GHz HALCA+VSOP observations enabled the C0 and C1 properties to be determined at this frequency since the VLBA-only image shows these two components blended into one.

## 4 Conclusions

The preliminary results above have shown that it is productive to undertake co-ordinated VSOP and Chandra observations. Furthermore the simultaneous 1.6/5 GHz HALCA observing mode with the VLBA switching frequencies is a very efficient mode for strong sources. A small extra amount of VLBA-only time also provides a large increase in the science return since multi-frequency analyses can be undertaken. So far, we have shown that the X-ray emission from 0836+710 is dominated by the emission from the core and 2-mas component. We will extend our analysis when the calibrated Chandra data becomes available.

**Acknowledgements.** We gratefully acknowledge the VSOP Project, which is led by ISAS in cooperation with many organizations and radio telescopes around the world.

## References

Lobanov, A.P., Krichbaum, T.P., Witzel, A. et al. 1998, *A&A*, **340**, L60
Unwin, S. C., Wehrle, A. E., Lobanov, A. P., et al. 1997, *ApJ*, **480**, 596

*Astrophysical Phenomena Revealed by Space VLBI*
*H. Hirabayashi, P.G. Edwards and D.W. Murphy (eds.)*

# VSOP Imaging of the Unusual X-Ray Binary Star LSI+61°303

A.R. Taylor[1], S.M. Dougherty[1], W.K. Scott[1],
M. Peracaula[2] & J.M. Paredes[2]

[1] *Physics and Astronomy, University of Calgary, Calgary, Alberta, T2N 1N4, Canada*
[2] *Departament d'Astronomia i Meteorologia, Universitat de Barcelona, E-08028 Barcelona, Spain*

**Abstract**

The HALCA spacecraft in combination with a large array of ground radio telescopes has been used to obtain multi-epoch images of a radio outburst of the radio emitting, X-ray binary star LSI+61°303. Preliminary results from two 6-hour segments separated by 28.6 hours are presented. The images reveal an apparently stationary pattern of symmetric emission extending about 2 mas on either side of a central source. The extended emission is reminiscent of the precessing radio jets seen in SS433. The central source is observed to expand at a rate of 0.2 mas/day. At the distance of LSI+61°303, this corresponds to ∼700 km s$^{-1}$.

## 1 Introduction

LSI+61°303 is one of the more unusual of known massive X-ray binary systems. It undergoes nonthermal radio outbursts every 26.5 days, that rise from quiescence to peak flux within 48 hours (Taylor & Gregory 1984). These are attributed to the eccentric orbit of a gravitationally collapsed object orbiting within the dense circumstellar envelope of a B0e star. In addition, the relative gamma-ray to X-ray luminosity of the system is far higher than in any other known X-ray binary system, indicating a fundamentally different energy production mechanism (Taylor et al. 1996).

Despite several ground-based VLBI observations of LSI+61°303, the properties of the radio emission region remain unclear. Observations near peak flux density a few days after onset of the outburst (Taylor et al. 1992, Massi et al. 1993) have shown a very compact source ∼1 mas in size, suggesting a low rate of expansion of a few hundred km s$^{-1}$. Observations at quiescence indicate a low level radio source with dimensions

of ∼4 mas (Lestrade 1988; Taylor et al. 1992). In contrast, observations of a small flare following a major outburst indicate initial expansion velocities of order $\sim 0.06c$, with deceleration upon reaching dimensions of 2mas (Peracaula et al. 1998). A clear picture of the evolving radio emission, linking these diverse results, remains elusive.

A primary difficulty with ground-based VLBI studies is that the variability time scale of the emission is short compared to the time required to obtain sufficient visibility coverage with a typical ground array. Because of the high northern declination of the source (+61°) joint VLBA/EVN observations provide reasonable 2-dimensional $(u, v)$ coverage in a few hours, and the addition of rapidly changing baselines to the HALCA spacecraft allows us, for the first time, to obtain an unambiguous picture of the dynamical evolution of the outburst ejecta from LSI +61°303 on sub-mas scales.

## 2 Observations and Analysis

LSI+61°303 was observed at 5 GHz with HALCA and a ground array of 18 radio telescopes, including the Very Long Baseline Array, the European VLBI Network and the Very Large Array. The observations were carried out for 48 hours, beginning 00:59 U.T. on 16 September, 1999. The source is almost circumpolar at most observatories, allowing for continuous ground array coverage over the observing period.

The light curve of total flux density over the course of the observations is shown in Figure 1. At the beginning of the observations, the flux density decayed on a time scale of several hours, from a peak of about 190 mJy to 140 mJy. Thereafter the mean flux density remained stable for approximately a day with variations of approximately 10%.

Initial images have been constructed from two segments of data separated by 28.6 hours. These two data segments, shown by the solid horizontal bars in Figure 1), are referred to respectively as epoch 1 (09:50 U.T., September 16) and epoch 2 (14:10 U.T., September 17). The images are shown in Figure 2. For comparison the data have been restored with the same beam, equal to the uniform weight beam of epoch 1. Both images show a central resolved source and symmetric extensions toward the northeast and southwest, out to a radius of approximately 2 mas. The maximum extent appears similar in the two images. However, the central intense source has obviously grown in the northeast-southwest direction between the two epochs.

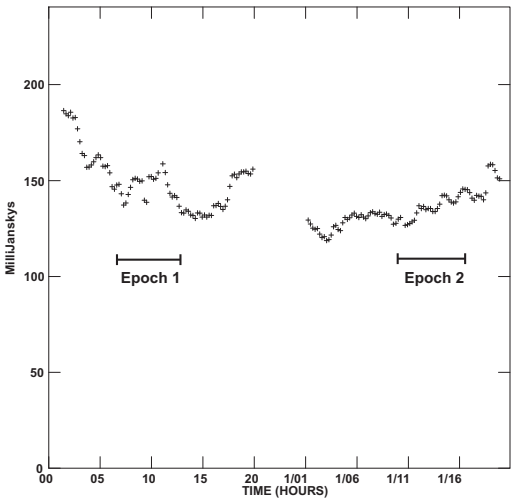


Figure 1: Radio light curve of LSI+61°303 during the VLBI observations obtained with the Very Large Array. The horizontal bars indicate the time ranges of the epoch 1 and 2 maps shown in Figure 2.

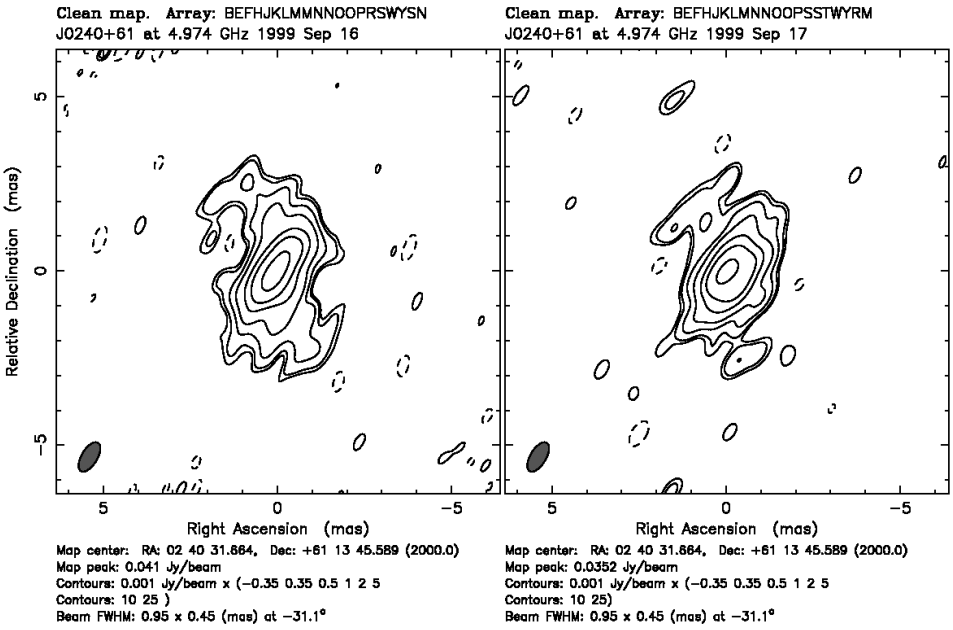


Figure 2: Two 5 GHz images of LSI+61°303 taken 28.6 hours apart. The epoch of each image is indicated in Figure 1. The map rms is $\sim 0.1$ mJy.

The change in angular size of the central source allows, for the first time, a direct measure the expansion rate of the outburst ejecta of LSI+61°303. Table 1 lists the results of an elliptical Gaussian fit to the central source. The minor axis has expanded by 50% from 0.52 to 0.77 mas, corresponding a change of 0.5 AU at the 2.0 kpc distance of LSI+61°303 (Frail and Hjellming 1991). The inferred expansion velocity is 730 km $s^{-1}$, along a direction pointing toward the extended lobes.

Table 1: Elliptical Gaussian model fits to the central source.

| | Flux Density (mJy) | Major Axis (mas) | Minor Axis (mas) | Position Angle (deg) |
|---|---|---|---|---|
| epoch 1 | 88 | 1.22 | 0.52 | -36.7 |
| epoch 2 | 89 | 1.06 | 0.77 | -36.2 |

The overall size of the radio emission, about 4 mas, is similar to that derived by Lestrade (1988) at quiescence. The radio extensions may represent a) a quasi-steady state emission region that is continually replenished in energetic particles by the recurring outbursts, or b) a high velocity component of the outburst ejecta that rapidly expands to radii of 2 mas and then decelerates, as inferred by Peracaula et al. (1998).

**Acknowledgements.** We gratefully acknowledge the VSOP Project, led by the Japanese Institute of Space and Astronautical Science in cooperation with many organizations and radio telescopes around the world.

## References

Frail, D. & Hjellming, R.M. 1991, *AJ*, **101**, 2126

Lestrade, J.-F. 1988, in *The Impact of VLBI on Astrophysics and Geophysics*, eds. M.J. Reid & J.M. Moran (Boston: Kluwer), 265

Massi, M., Paredes, J.M., Estalella, R. & Felli, M. 1993, *A&A*, **269**, 249

Peracaula, M., Gabuzda, D.C. & Taylor, A.R. 1998, *A&A*, **330**, 612

Taylor, A.R. & Gregory, P.C. 1984, *ApJ*, **283**, 273

Taylor, A.R., Kenny, H.T., Spencer, R.E. & Tzioumis, A. 1992, *ApJ*, **395**, 268

Taylor, A.R., Young, G., Peracaula, M., Kenny, H.T. & Gregory, P.C. 1996, *A&A*, **305**, 817

*Astrophysical Phenomena Revealed by Space VLBI*
*H. Hirabayashi, P.G. Edwards and D.W. Murphy (eds.)*

# Mapping Blazars' Inner Jets Through Multiwavelength Observations

Rita M. Sambruna

*Penn State University, 525 Davey Lab, University Park, PA 16802, USA*

**Abstract**

Being dominated by non-thermal emission from aligned relativistic jets, blazars allow us to elucidate the physics of extragalactic jets, and, ultimately, how energy is extracted from the central black hole in radio-loud AGNs. Crucial information is provided by blazars' spectral energy distributions from radio to gamma-rays, their trends with luminosity, and correlated multifrequency variability. I will review recent results from multiwavelength monitorings of blazars which provide us with a close look to jets' inner regions.

## 1 The Spectral Energy Distributions (SEDs) of Blazars

Blazars are radio-loud Active Galactic Nuclei characterized by polarized, highly luminous, and rapidly variable non-thermal continuum emission (Angel & Stockmann 1980) from a relativistic jet oriented close to the line of sight. The radio through gamma-ray spectral energy distributions (SEDs) of blazars exhibit two broad humps (Figure 1). The first component peaks at IR/optical in "red" blazars and at UV/X-rays in their "blue" counterparts, and is most likely due to synchrotron emission from relativistic electrons in the jet (e.g., Ulrich, Maraschi, & Urry 1997). The second component, extending from X-rays to gamma-rays, has less well understood origin. It could be due to inverse Compton (IC) scattering of ambient photons, either internal (synchrotron-self Compton, SSC; Tavecchio, Maraschi, & Ghisellini 1998) or external to the jet (external Compton, EC; e.g., Sikora 1994). In the following discussion I will assume the synchrotron and IC scenarios, keeping in mind, however, that a possible alternative for the production of gamma-rays is provided by the hadronic models (proton-induced cascades; e.g., Rachen 1999).

Red and blue blazars are just the extrema of a continuous distribution of SEDs. Recent multicolor surveys (Laurent-Muehleisen et al. 1998; Perlman et al. 1998) found sources with intermediate spectral shapes, and trends with bolometric luminosity were discovered (Sambruna, Maraschi, & Urry 1996; Fossati et al. 1998). In the more luminous red blazars the synchrotron and IC peak frequencies are lower, the

Compton dominance (ratio of the synchrotron to IC peak luminosities) is larger, and the luminosity of the optical emission lines/non-thermal blue bumps is larger than in their blue counterparts (Sambruna 1997). A possible interpretation is that the different types of blazars are due to the different predominant electrons' cooling mechanisms (Ghisellini et al. 1998). In this context, red blazars, where large external radiation fields are observed, are EC-dominated at $\gamma$-rays, while in blue blazars the higher energies are produced via SSC. While there are caveats to this picture (Urry 1999), it is clear that the spectral diversity of blazars' jets cannot be explained by beaming effects *only* (Sambruna et al. 1996; Georganopoulos & Marscher 1998), but require instead a change of physical parameters and/or a different jet environment.

## 2 Correlated Multiwavelength Variability: Testing the Blazar Paradigm

Correlated multiwavelength variability provides a way to test the cooling paradigm since the various synchrotron and IC models make different predictions for the relative flare amplitudes and shape, and the time lags (see Sambruna 1999 for a review). Here I summarize recent results for a few prototypical objects of both the red and blue types.

### 2.1 Results for Red Blazars

One of the best monitored red blazars is 3C279. From the simultaneous or contemporaneous SEDs in Figure 1a, it is apparent that the largest variations are observed above the synchrotron peak in IR/optical (not well defined) and the Compton peak at GeV energies, supporting the synchrotron and IC models. The GeV amplitude is roughly the square of the optical flux during the earlier campaigns, supporting an SSC interpretation (Maraschi et al. 1994) or a change of the beaming factor $\delta$ in the EC models, while in 1996 large variations were recorded at gamma-rays but not at lower energies (Wehrle et al. 1998). During the latter campaign, the rapid decay of the GeV flare (Figure 2a) favors the EC model (Wehrle et al. 1998). Note the good correlation, within one day, of the EGRET and RXTE flares, which provides the first evidence that the gamma-rays and X-rays are cospatial (Wehrle et al. 1998).

Another candidate for future gamma-ray monitorings is BL Lac itself. In 1997 July it underwent a strong flare at GeV and optical energies (Bloom et al. 1997). The gamma-ray light curve shows a strong

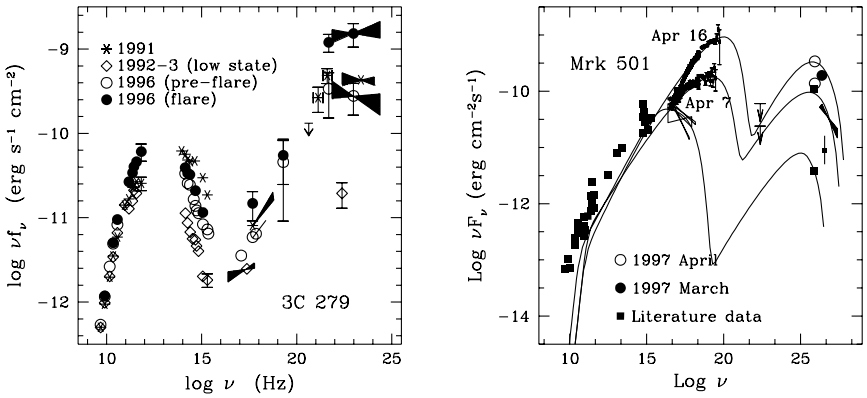


Figure 1: Spectral energy distributions (SEDs) of 3C279 [*(a), Left*] and Mrk 501 [*(b), Right*]. Data are from Maraschi et al. (1994), Wehrle et al. (1998), and Pian et al. (1998). Blazars' SEDs typically have two broad humps, the first peaking anywhere from IR/optical (in red blazars like 3C279) to hard X-rays (in blue blazars like Mrk 501) and due to synchrotron emission from a relativistic jet. The second component, extending to gamma-rays, is less well understood. A popular explanation is inverse Compton scattering of ambient seed photons off the jet's electrons.

flare possibly anticipating the optical by up to 0.5 days; however, the poor sampling does not allow firmer conclusions. The SED during the outburst is best modeled by the SSC model from radio to X-rays, while an EC contribution is required above a few MeV (Sambruna et al. 1999). A similar mix of SSC and EC is also required to fit the SEDs of PKS 0528+134 (e.g., Sambruna et al. 1997).

### 2.2 Results for Blue Blazars

Mrk 501, one of the two brightest TeV blazars, attracted much attention in 1997 April when it underwent a spectacular flare at TeV energies (Catanese et al. 1997; Aharonian et al. 1999; Djannati-Atai et al. 1999). This was correlated to a similarly-structured X-ray flare observed with RXTE, with no delay larger than one day (Krawczynski et al. 2000). These results are consistent with an SSC scenario where the most energetic electrons are responsible for both the hard X-rays (via synchrotron)

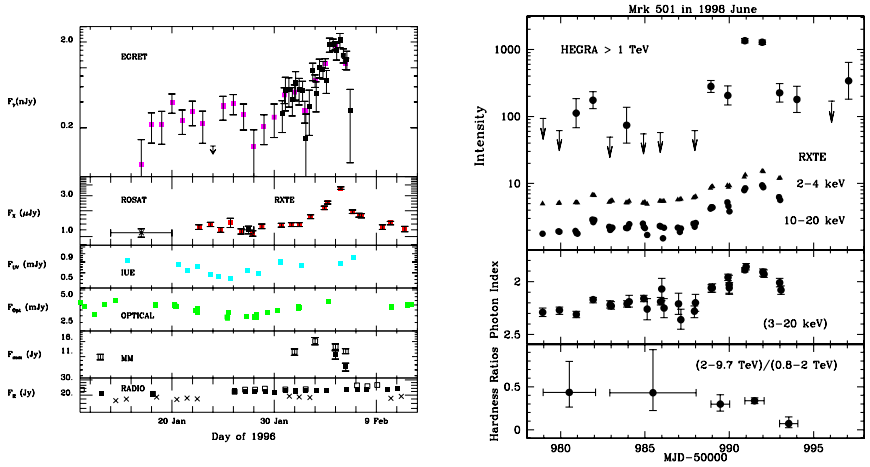


Figure 2: Multiwavelength light curves of 3C279 in 1996 January [*(a), Left*] and of Mrk 501 in 1998 June [*(b), Right*]. Data from Wehrle et al. (1998) and Sambruna et al. (2000).

and the TeV (via IC).

Figure 1b shows the SEDs of Mrk 501 during the 1997 April TeV activity, compared to the "quiescent" SED from the literature. An unusually flat (photon index, $\Gamma_X \sim 1.8$) X-ray continuum was measured by SAX and RXTE during the TeV flare ( Pian et al. 1998; Krawczynski et al. 2000), implying a shift of the synchrotron peak by more than two orders of magnitude. This almost certainly reflects a large increase of the electron energy (Pian et al. 1998), or the injection of a new electron population on top a quiescent one (Kataoka et al. 1999). Later RXTE observations in 1997 July found the source still in a high and hard X-ray state (Lamer & Wagner 1998), indicating a persistent energizing mechanism.

An interesting new behavior was observed during our latest 2-week RXTE-HEGRA monitoring of Mrk 501 in 1998 June (Sambruna et al. 2000), when 100% overlap between the X-rays and TeV light curves was achieved (Figure 2b). A strong short-lived ($\sim$ two days) TeV flare was detected, correlated to a flare in the X-rays, with energy-dependent amplitude. As in 1997, large X-ray spectral variations are observed, with the X-ray continuum flattening to $\Gamma_X = 1.9$ at the peak of the TeV flare, implying a similar shift to $\geq$ 50 keV of the synchrotron peak. However, while in 1997 the TeV spectrum hardened during the flare (Djannati-

Atai et al. 1999), as it did in the X-rays, we did not observe significant variability in the TeV hardness ratios during the flare (Figure 2b, bottom panel); instead the spectrum softens 1-2 days later. The correspondence between the X-ray and TeV spectra is no longer present during the 1998 June flare.

## 3 Acceleration and Cooling in Blue Blazars

X-ray monitorings of blue blazars are a powerful diagnostic of physical processes occurring in these sources. This is because in these objects the X-rays are the high-energy tail of the synchrotron component where rapid and complex flux and spectral variability is expected depending on the balance between escape, acceleration, and cooling of the emitting particles (Kirk et al. 1998).

An ideal target for X-ray monitorings is PKS 2155–304, one of the brightest X-ray blazars. Interest in this source was recently revived due to a TeV detection (Chadwick et al. 1999) during a high X-ray state (Chiappetti et al. 1999). ASCA and SAX observations detected strong X-ray variability, with the softer energies lagging the harder energies by one hour or less (Chiappetti et al. 1999; Kataoka et al. 2000; Zhang et al. 1999), and are consistent with a model where the electron cooling dominates the flares. This implies magnetic fields of $B \sim 0.1-0.2$ Gauss (for $\delta \sim 10$), similar to Mrk 421 (Takahashi et al. 1996).

A new mode of variability was discovered during our RXTE monitoring of PKS 2155–304 in 1996 May, as part of a larger multifrequency campaign. The sampling in the X-rays was excellent (Figure 3), and complex flux variations were observed, with short, symmetric flares superposed to a longer baseline trend. Inspection of the hardness ratios (the ratio of the counts in 6–20 keV over the counts in 2–6 keV) versus flux shows that different flares (separated by vertical dashed lines in Figure 3) exhibit hysteresis loops of opposite signs, both in a "clockwise" and "anti-clockwise" sense (labeled as C and A in Figure 3, respectively). Applying a correlation analysis to each flare separately, we find that the C loops corresponds to a soft lag (softer energies lagging) and the A loop corresponds to a hard lag (harder energies lagging), of the order of a few hours in both cases.

We interpreted the data using the acceleration model of Kirk et al. (1998). Here loops of both signs are expected depending on how fast the electrons are accelerated compared to their cooling time, $t_{cool}$. If

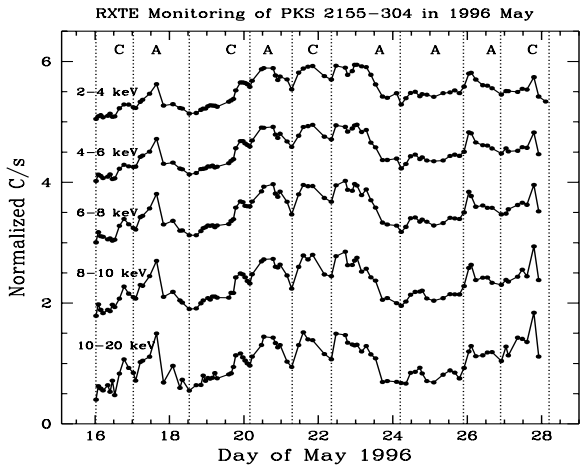


Figure 3: RXTE intensive monitoring of PKS 2155–304 in 1996 May. Energy-dependent X-ray light curves, normalized to their average intensity and arbitrarily shifted. The vertical dashed lines mark portions of the light curves characterized by "clockwise" (C) or "anti-clockwise" (A) hysteresis loops in the hardness ratio versus intensity diagrams. This complex spectral behavior is a powerful diagnostic of the acceleration and cooling processes in the jet.

the acceleration is instantaneous (i.e., $t_{acc} << t_{cool}$), cooling dominates variability and, because of its energy dependence, the harder energies are emitted first, with C loops. If instead the acceleration is slower ($t_{acc} \sim t_{cool}$), the electrons need to work their way up in energy and the softer energies are emitted first, with A loops. A close agreement between the RXTE light curve and the model is found by increasing $t_{acc}$ by a factor 100 going from a C to an A loop, when $t_{acc}$ becomes similar to the duration of the flare, and by steepening the electron energy distribution. Thus we reach the important conclusion that we are indeed observing electron acceleration, and together with cooling this is responsible for the observed X-ray variability properties of PKS 2155–304.

## 4 Summary and Future Work

Recent multiwavelength campaigns of blazars expanded the current available database, from which we are learning important new lessons. Detailed modeling of the SEDs of bright gamma-ray blazars of the red

and blue types tend to support the current cooling paradigm, where red sources are EC-dominated and blue sources are SSC-dominated at gamma-rays. However, several observational biases are present, including the limited EGRET sensitivity and currently small number of TeV blazars (5). A more definite test of the blazar paradigm awaits the higher sensitivities of future missions (GLAST, AGILE in GeV and HESS, VERITAS, MAGIC, CANGAROO II in TeV). Broader-band, higher quality gamma-ray spectra will also be available, allowing a better location of the IC peak, a more precise measure of the spectral shape at gamma-rays, and its variability. More correlated X-ray/TeV monitorings are necessary, in which RXTE and SAX have crucial roles, to add to the current knowledge of the variability modes of single sources.

**Acknowledgements.** This work was supported by NASA contract NAS–38252 and NASA grant NAG5–7276. I thank the local organizers for a stimulating meeting and partial support.

## References

Aharonian, F. et al. 1999, *A&A*, **342**, 69

Angel, J.R.P. & Stockman, H.S. 1980, *ARA&A*, **18**, 321

Bloom, S. et al. 1997, *ApJ*, **490**, 145

Catanese, M. 1999, in *ASP Conf. Ser.* **159***: BL Lac Phenomena*, 439 eds. L.O. Takalo & A. Sillanpää (San Francisco: Astron. Soc. Pac.), 243

Catanese, M. et al. 1997, *ApJ*, **487**, 143

Chadwick, P. et al. 1999, *AstroPart. Phys.*, **11**, 145

Chiappetti, L. et al. 1999, *ApJ*, **521**, 552

Djannati-Atai, A. et al. 1999, *A&A*, **350**, 17

Fossati, G. et al. 1998, *MNRAS*, **299**, 433

Georganopoulos, M. & Marscher, A. 1998, *ApJ*, **506**, 621

Ghisellini, G. et al. 1998, *MNRAS*, **301**, 451

Kataoka, J. et al. 1999, *ApJ*, **514**, 138

Kataoka, J. et al. 2000, *ApJ*, **528**, 243

Kirk, J.G., Riegler, F.M., & Mastichiadis, A. 1998, *A&A*, **333**, 452

Krawczynski, H. et al. 2000, *A&A*, **353**, 97

Lamer, G. & Wagner, S. 1998, *A&A*, **331**, L13

Laurent-Muehleisen, S. et al. 1998, *ApJS*, **118**, 127

Maraschi, L. et al. 1994, *ApJ*, **435**, 91

Perlman, E.S. et al. 1998, *AJ*, **115**, 1253

Pian, E. et al. 1998, *ApJ*, **492**, 17

Rachen, J. 1999, in *GeV-TeV Astronomy: Toward a major Cherenkov detector IV*, ed. B. Dingus, AIP, in press

Sambruna, R.M. 1997, *ApJ*, **474**, 639

Sambruna, R.M. 1999, astro-ph/9912060

Sambruna, R.M., Maraschi, L., & Urry, C.M. 1996, *ApJ*, **463**, 444

Sambruna, R.M. et al. 1997, *ApJ*, **474**, 639

Sambruna, R.M. et al. 1999, *ApJ*, **515**, 140

Sambruna, R.M. et al. 2000, *ApJ*, in press (astro-ph/0002215)

Sikora, M. 1994, *ApJS*, **90**, 923

Tavecchio, F., Maraschi, L., & Ghisellini, G. 1998, *ApJ*, **509**, 608

Takahashi, T. et al. 1996, *ApJ*, **470**, 89

Ulrich, M.-H., Maraschi, L., & Urry, C.M. 1997, *ARA&A*, **35**, 445

Urry, C.M. 1999, *AstroPart. Phys.*, **11**, 159

Wherle, A. et al. 1998, *ApJ*, **497** 178

Zhang, Y.H. et al. 1999, *ApJ*, **527**, 719

*Astrophysical Phenomena Revealed by Space VLBI*
*H. Hirabayashi, P.G. Edwards and D.W. Murphy (eds.)*

# VSOP Observations of TeV Gamma-Ray Sources

P.G. Edwards[1], B.G. Piner[2], S.C. Unwin[2], A.E. Wehrle[2], D.W. Murphy[1,2], H. Hirabayashi[1] & K. Fujisawa[3]

[1] *ISAS, Yoshinodai 3-1-1, Sagamihara, Kanagawa 229-8510, Japan*
[2] *JPL, 4800 Oak Grove Dr., Pasadena, CA 91109, USA*
[3] *NAO, Ohsawa 2-21-1, Mitaka, Tokyo 181-8588, Japan*

**Abstract**

VLBI Space Observatory Programme (VSOP) and ground VLBI observations of Mrk 421 and Mrk 501 are presented and the motions of milli-arcsecond scale jet components examined to compare the inferred doppler factors from the TeV-emission region with those from the parsec-scale VLBI observations.

## 1 Introduction

Mrk 421 and Mrk 501 are to date the only independently confirmed extragalactic sources at TeV energies. Short-timescale variability and correlated TeV and X-ray emission have been used to infer doppler factors of 15–40 for Mrk 421 and 1.5–20 for Mrk 501 (see e.g. the review of Catanese and Weekes 1999).

We have undertaken VSOP observations of these sources at 5 GHz to probe the milliarcsecond scale structure of these source for evidence of activity associated with this TeV activity, and have compared the VSOP images with ground-based VLBI images to study the motion of jet components in order to infer the properties of the parsec-scale jets.

## 2 Observations

The VSOP observation of Mrk 421 was made in November 1997 with the EVN and HALCA, and the Mrk 501 observation was made with HALCA and the VLBA in April 1998.

The Mrk 421 data are described in detail in Piner et al. (1999). The VSOP image, shown in Figure 1, reveals a core and jet components C6 (0.83 mas from the core) and C5 (1.63 mas). Model-fitting an elliptical gaussian component to the core yields a flux density of 370 mJy and a corresponding source frame brightness temperature of $4\times10^{11}$ K.

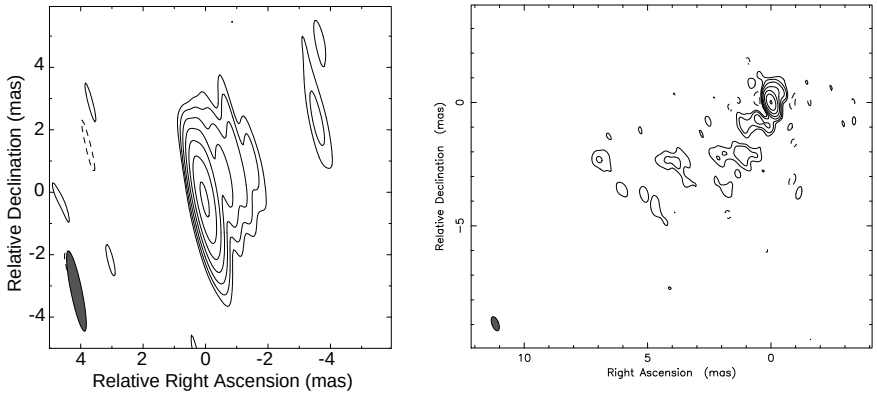


Figure 1: Left: VSOP image of Mrk 421, adapted from Piner et al. (1999). The beam (FWHM) is 2.6 x 0.4 mas at 12°. The lowest contour level is 3.6 mJy per beam, with each subsequent contour a factor of two higher. Right: VSOP image of Mrk 501. The beam (FWHM) is 0.6 x 0.3 mas at 20°. The lowest contour level is 4.7 mJy per beam, with successive contours a factor of two higher.

A preliminary VSOP image of Mrk 501 is also shown in Figure 1. Jet components ∼2.5, 4.5 and 7.5 mas from the core are evident in the VSOP image. Closer to the core the situation is more complex: the brightest feature is presumably the core, however other features near the core should be interpreted with caution as they may be artefacts of the large holes in the $(u, v)$ coverage between the ground-ground–baselines and the ground-space–baselines that are located at similar position angles to these components. Modelfitting a gaussian to the brightest feature in the core region results in a ∼470 mJy component with a brightness temperature of $4\times10^{11}$ K.

## 3 Mrk 421 Component Motions

As discussed in Piner et al. (1999), the jet components in Mrk 421 display sub-luminal speeds of $\lesssim 0.3c$ (we adopt $H_0 = 65\,\mathrm{km\,s^{-1}\,Mpc^{-1}}$ throughout this paper). A re-interpretation of the observations of Zhang and Bååth (1990), assigning their model-fit components larger uncertainties in position, is quite consistent with this result. Figure 2 plots the model-fit components for Mrk 421 within 15 mas of the core from Table 3 of Piner et al. (1999), excluding 2 GHz components within 8 mas of the

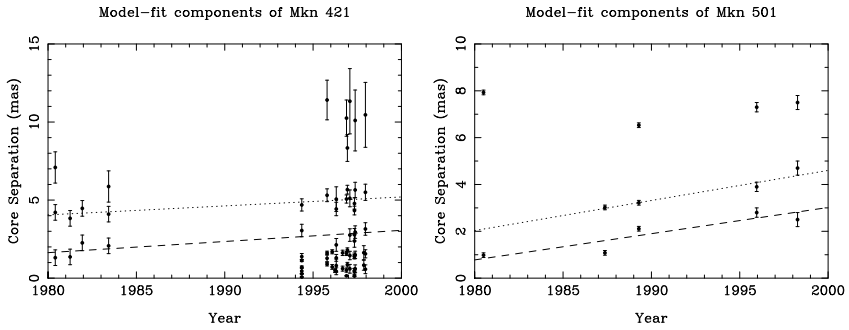


Figure 2: Component motions in Mrk 421 (left) and Mrk 501 (right). See text for details.

core and 5 GHz ground-VLBI components within 4 mas of the core as the large uncertainties on these components add unnecessary confusion.

It is tempting to try and identify the two brighter jet components of Zhang and Bååth (1990) with the more recent data. The lack of data between 1984 and 1994 renders this task open to large uncertainties, but Piner et al. found a possible match between the 2 mas and 4 mas components of Zhang and Bååth (1990) and the 5 mas (C4) and 10 mas (C3) components from the 1990s. Assuming the speeds of the components are similar, we can alternatively identify the 2 mas and 4 mas components of Zhang and Bååth (1990) with the weak 3 mas component and the 5 mas component from the 1990s, as indicated in Figure 2, which yields motions of $\sim$0.15 $c$. Regardless, the fact that the jet components display sub-luminal motions at both epochs appears beyond reproach.

## 4 Mrk 501 Component Motions

A number of different speeds have been reported for components in the Mkn 501 jet ranging from $0.27\pm0.02\,\mathrm{mas\,yr^{-1}}$ (Gabuzda et al. 1994) to $2.4\,\mathrm{mas\,yr^{-1}}$ (Giovannini et al. 1999).

The epochs and references for the data in Figure 2 are 1980.5 (Pearson and Readhead 1998), 1987.4 (Gabuzda et al. 1992), 1989.3 (Gabuzda et al. 1994), 1995.9 (the VLBA 2 cm survey, see Kellermann et al. 1998 and http://www.cv.nrao.edu/2cmsurvey) and 1998.4 (our VSOP observation). This compilation of data suggests that there are two components moving at similar apparent speeds of $\sim$0.12 $\mathrm{mas\,yr^{-1}}$, or $\sim$0.3 $c$.

## 5 Discussion

As outlined by Piner et al. (1999), there are several possible explanations for reconciling the large inferred doppler factors from TeV observations with the sub-luminal speeds determined from VLBI observations. Marscher (1999), citing the lack of emerging VLBI jet components associated the spectacular TeV flares seen from Mrk 421 in 1996 and the prolonged TeV activity of Mrk 501 in 1997, favors a change in doppler factor between the $10^{-4}$ pc–scale TeV emission region and the parsec-scale VLBI region, with most of the energy and momentum of an electron-positron dominated jet lost close to the base of the jet, and the resulting subsonic jets being decelerated and eventually dissipated on the parsec-scale. If, however, the seemingly constant sub-luminal jet speeds we have inferred for these objects are indeed correct, the components associated with the TeV activity may not yet have emerged – only further monitoring will answer this question.

**Acknowledgements.** We gratefully acknowledge the VSOP Project, which is led by ISAS in cooperation with many organizations and radio telescopes around the world.

## References

Catanese, M & Weekes, T.C. 1999, *PASP*, **111**, 1193

Gabuzda, D.C., Cawthorne, T., Roberts, D. et al. 1992, *ApJ*, **388**, 40

Gabuzda, D.C., Mullan, C., Cawthorne, T. et al. 1994, *ApJ*, **435**, 140

Giovannini, G., Feretti, L., Venturi, T. et al. 1999, in *ASP Conf. Ser.* **159***: BL Lac Phenomena*, 439 eds. L.O. Takalo & A. Sillanpää (San Francisco: Astron. Soc. Pac.), 439

Kellermann, K.I., Vermeulen, R.C., Zensus, J.A. and Cohen, M.H. 1998 *AJ*, **115**, 1295

Marscher, A.P. 1999, *Astropart. Phys.*, **11**, 19

Pearson, T.J. & Readhead, A.C.S. 1988, *ApJ*, **328**, 114

Piner, B.G., Unwin, S.C., Wehrle, A.E. et al. 1999, *ApJ*, **525**, 176

Zhang, F.J. & Bååth, L.B. 1990, A&A, **236**, 47

*Astrophysical Phenomena Revealed by Space VLBI*
*H. Hirabayashi, P.G. Edwards and D.W. Murphy (eds.)*

# Space VLBI of Parsec–Scale Jets: the Impact of VSOP

A.P. Lobanov, J.A. Zensus, T.P. Krichbaum, & A. Witzel

*Max–Planck–Institut für Radioastronomie, Auf dem Hügel 69, Bonn 53121, Germany*

**Abstract**

Resolution improvements provided by the ongoing space VLBI mission VSOP provide an excellent opportunity for studying novel aspects of the physics of compact, parsec-scale jets in active galactic nuclei. Visibilities on space baselines contain structural information that cannot be recovered by overresolving ground array data at the same frequency. We illustrate this by discussing the results from recent VSOP observations of parsec-scale jets in 0836+710 and 3C273. For both objects, the VSOP observations have allowed to directly observe plasma instabilities developing in the jets.

## 1 Introduction

The VSOP (VLBI[1] Space Observatory Programme) is a Space VLBI mission utilizing worldwide arrays of radio telescopes and an orbiting 8-meter antenna deployed on the Japanese satellite HALCA[2] (Hirabayashi et al. 1998). The satellite has an elliptical orbit with apogee at 21 000 km, perigee at 560 km, and an orbital period of 6.3 hours. In each observation, the data stream from the satellite is recorded by a network of 5 satellite tracking stations, and subsequently correlated with the data from participating ground telescopes. Regular VSOP observations started in September 1997 at 1.6 and 5 GHz. We compare here the properties of space and ground VLBI images obtained from two 5 GHz VSOP observations of compact extragalactic jets in 0836+710 and 3C 273.

## 2 VSOP and Ground VLBI Images

The VSOP observations were made in October (0836+710) and December (3C 273) of 1997. Basic description of the observations is given in

[1] Very Long Baseline Interferometry
[2] Highly Advanced Laboratory for Communication and Astronomy

Table 1: Summary of the VSOP observations

| | Ground Array | $B$ [MHz] | $N_{\rm ch}$ | $t_{\rm obs}$ [hrs] | $t_{\rm gs}$ [hrs] | $uv_{\rm gg}$ [M$\lambda$] | $uv_{\rm gs}$ [M$\lambda$] |
|---|---|---|---|---|---|---|---|
| (1) | (2) | (3) | (4) | (5) | (6) | (7) | (8) |
| 0836+710 | VLBA | 32 | 512 | 11.4 | 5.2 | 2–142 | 180–550 |
| 3C 273 | VLBA+EB | 32 | 256 | 12.5 | 6.7 | 2–137 | 100–535 |

Column designation: 2 – supporting ground VLB array; 3 – bandwidth; 4 – number of spectral channels; 5 – total observing time; 6 – observing time with ground–space baselines; 7,8 – $uv$–ranges on ground–ground and ground–space baselines.

Table 2: Parameters of the images of 0836+710

| Image | $S_{\rm tot}$ | $S_{\rm max}$ | $S_{\rm min}$ | $\sigma_{\rm RMS}$ | $D^{\rm peak}_{\rm rms}$ | Beam |
|---|---|---|---|---|---|---|
| (1) | (2) | (3) | (4) | (5) | (6) | (7) |
| VLBA | 2.167 | 0.918 | −0.001 | 0.2 | 4600:1 | 2.2, 1.5, 30.8 |
| VSOP | 2.156 | 0.432 | −0.003 | 0.5 | 900:1 | 0.9, 0.3, −36.3 |
| HALCA | 0.731 | 0.325 | −0.007 | 1.4 | 200:1 | 0.7, 0.2, −36.9 |

Column designation: 2 – total CLEAN flux [Jy]; 3 – peak flux density [Jy/beam]; 4 – lowest negative flux density [Jy/beam]; 5 – RMS noise [mJy/beam]; 6 – peak-to-RMS dynamic range; 7 – restoring beam: major axis, minor axes [mas], position angle of the major axis [deg].

Table 1. The data were correlated at the NRAO VLBA[3] correlator in Socorro NM, USA. For each source, we have produced three different images: a) ground array image (VLBI image) using only ground–ground baselines, b) space baseline image (HALCA image) with only ground–space baselines included, and c) VSOP image using the entire dataset. The respective images of 0836+710 are shown Figure 1. Table 2 compares the properties of all three images of 0836+710. The relative changes of restoring beam sizes and dynamic ranges are similar in the respective images of 3C 273 (Lobanov et al. 2000). Discussions on more specific details of imaging and properties of the images can be found elsewhere (Lobanov et al. 1998, 1999, 2000).

[3]The Very Long Baseline Array of the National Radio Astronomy Observatory. The NRAO is a facility of the National Science Foundation operated under cooperative agreement by Associated Universities, Inc.

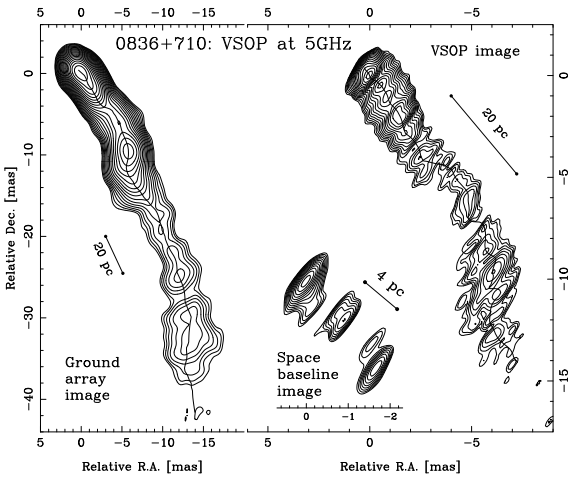


Figure 1: Ground array, VSOP, and space-baseline–only images of 0836+710 (Lobanov et al. 1998). Linear scales are given for $H_0 = 100\,\mathrm{km\,s^{-1}\,Mpc^{-1}}$ and $q_0 = 0.5$. In the ground array and VSOP images, the jet ridge line is marked. The space baseline image is obtained using only the baselines to HALCA. All structures seen in this image are consistent with those found in both the VSOP and ground array images. The contour levels are drawn as follows: $-0.9$, $0.9{\times}2^{n/2}$ mJy/beam in the ground array image; $-2$, $2{\times}2^{n/2}$ mJy/beam in the VSOP image; $-5$, $5{\times}1.5^{n}$ mJy/beam in the space baseline image. Other parameters of the images are given in Table 2

## 3 Impact of Improved Angular Resolution

### 3.1 0836+710: Plasma Instabilities in the Jet

The VSOP image of 0836+710 allows us to study the jet morphology and physical conditions on linear scales up to 1 kpc. We have shown that, on the scales of $\lesssim 700h^{-1}$ pc, the curved ridge line of the jet can be modelled by a pressure confined relativistic outflow with Lorentz factor $\gamma_\mathrm{j} \approx 11$, Mach number $M_\mathrm{j} \sim 6$, and opening half-angle $\phi_\mathrm{j} \approx 1^\circ$ (Lobanov et al. 1998). In this description, the two main factors responsible for the observed curvature of the jet ridge line are: 1) Kelvin-Helmholtz instabilities developing in the jet plasma and 2) variations of the angle, $\theta$j, between the velocity vector of the outflow and the line of sight. The derived variations of $\theta_\mathrm{j}$ are consistent with the observed variable apparent speeds along the jet.

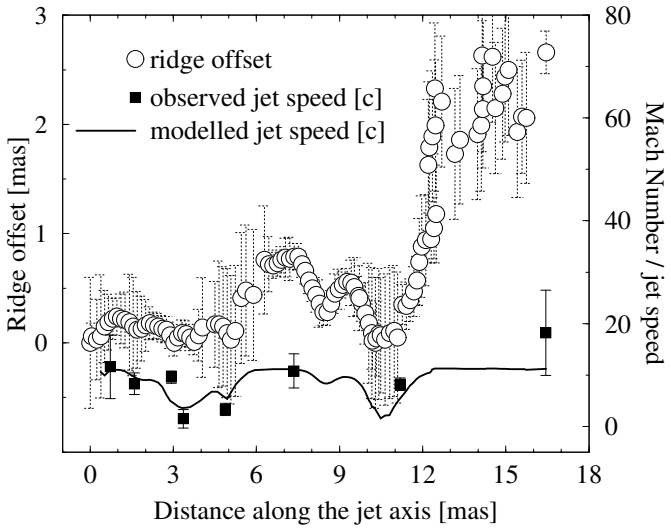


Figure 2: Relation between the ridge line and observed jet speeds in 0836+710 (Lobanov et al. 1998). Circles are measured offsets of the jet ridge line from the jet axis at P.A.$= -146°$; squares denote speeds reported by Otterbein (1996) at different locations in the jet; solid line represents apparent speed variations derived from the measured ridge line offsets, for a jet with Mach number, $M_{\rm j} = 6$, Lorentz factor, $\gamma_{\rm j} = 11$, and opening half-angle, $\phi_{\rm j} = 1°$.

The derived $\theta_{\rm j}$ changes smoothly between 3° and 65°, with largest values occurring at $\sim 3$ mas and $\sim 10$ mas distances — which are incidentally the locations where the most pronounced lateral displacements are reported (Otterbein 1996). The predicted $\beta_{\rm app}$ (plotted in Figure 2 with the solid line) is in a good agreement with the measured jet speeds. We would like to emphasize that the achieved consistency between the model and observed speeds is preserved, if the chosen direction of the jet axis are within a few degrees from the one we have used. In that case, only the derived jet Mach number would have differed from $M_{\rm j} = 6$ obtained above. Sparsity of the available speed measurements precludes better kinematic modelling and selecting the jet axis unambiguously. We expect that making such a selection would require determining the continuous velocity distribution along the jet, for which a suitable monitoring program should be designed, aimed at obtaining a sequence of high dynamic range and high fidelity VLBI images of the source.

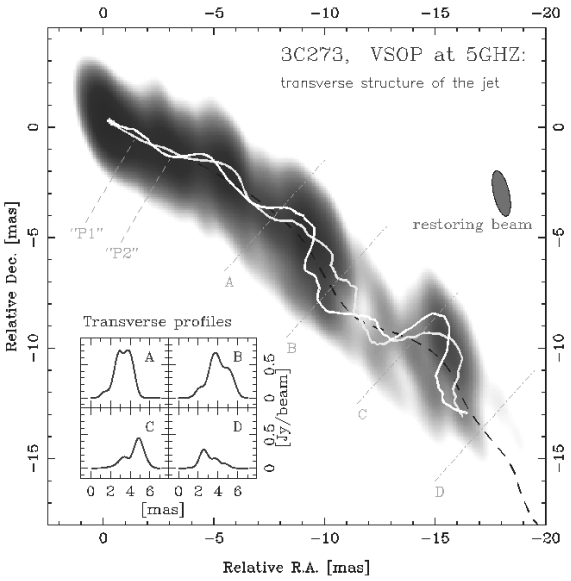


Figure 3: The 5 GHz VSOP image of the parsec-scale radio jet of 3C273 (Lobanov et al. in preparation – see also Color Figure 6). The image has a restoring beam is 2.09×0.70 mas at P.A.= 12.9° and a peak flux density of is 4.52 Jy/beam. The dashed black line is the smoothed ridge line of the jet. The dot-dashed white lines denote the locations of the 4 flux density profiles shown in the inset. It is possible to identify two internal emitting features (denoted P1 and P2) responsible for the observed transverse brightness distribution in the jet. The locations of these features are marked in the image by the grey lines. These features can be represented by Kelvin–Helmholtz instabilities developing in a relativistic plasma.

### 3.2 3C273: Transverse Structure of the Jet

The VSOP image of 3C 273 offers an even more striking example of the effect of improved angular resolution (Lobanov et al. 2000). The transverse emission distribution in the jet of 3C 273 shows remarkable deviations from a Gaussian shape, owing to the favorable orientations of the space baselines which provide a 0.7 mas resolution in the direction perpendicular to the jet axis. This is particularly visible in the emission profiles taken across the jet (Figure 3).

The ground VLBI image also resolves the jet transversely, and suggests possible edge brightening. However, only with the improved res-

olution of the VSOP image, it becomes possible to assess the true complexity of the transverse structure of the jet, with up to three emission components across the jet (i.e. in panel B in Figure 3). The stronger central component often dominates the profiles, possibly masking the presence of the third emitting feature. With the existing data, we are able to recover the locations of the two stronger emitting features (denoted P1 and P2, in Figure 3) inside the jet of 3C273. The locations of these features reveal remarkably regular, oscillating patterns which can be reconciled with the presence of Kelvin–Helmholtz instabilities developing and propagating in the relativistic plasma of the jet. We are able to obtain the wavelengths and amplitudes of at least 4 different modes of the instabilities, thereby for the first time establishing directly their presence in the jet. The measured parameters of the instabilities represent the transverse structure of the jet on scales of up to 20 milliarcseconds ($\sim$ 40 parsecs).

## 4 Conclusion

The discussed VSOP observations of 0836+710 and 3C 273 show that space VLBI arrays containing a fast–orbiting satellite element provide an excellent opportunity for high-resolution and high dynamic range imaging of parsec–scale jets in extragalactic objects, and open up new opportunities for studies of physical processes in relativistic plasmas observed in extragalactic jets.

**Acknowledgements.** We gratefully acknowledge the VSOP Project, which is led by ISAS in cooperation with many organizations and radio telescopes around the world.

## References

Hirabayashi, H., Hirosawa, H., Kobayashi, H. et al. 1998, *Science*, **281**, 1825 and erratum **282**, 1995

Lobanov, A.P., Krichbaum, T.P., Witzel, A., et al. 1998, *A&A*, **340**, 60

Lobanov, A.P., Krichbaum, T.P., et al. Witzel, A., & Zensus, J.A. 1999, *NewAR*, **43**, 741

Lobanov, A.P., Zensus, J.A., Abraham, Z., et al. 2000, *Adv. Sp. Res.*, **26**, 669

Otterbein, K. 1996, PhD thesis, Univ. of Heidelberg

*Astrophysical Phenomena Revealed by Space VLBI*
*H. Hirabayashi, P.G. Edwards and D.W. Murphy (eds.)*

# Phase-Reference Observations with VSOP

R.W. Porcas [1], M.J. Rioja [2], J. Machalski [3]
and H. Hirabayashi [4]

[1] *MPIfR, Auf dem Huegel 69, D 53121 Bonn, Germany*
[2] *OAN, Alcala de Henares, Spain*
[3] *Obs. Jagellonian Uni., Cracow, Poland*
[4] *ISAS, Kanagawa, Japan*

**Abstract**

We discuss problems associated with VLBI phase-referencing observations made with an orbiting antenna in space. Although HALCA cannot switch rapidly between sources, relative phase measurements between two close sources are possible if both are within the primary beam. We review VLBI Space Observatory Program (VSOP) observations of such pairs, and present a preliminary analysis for the source pair 1308+326 and 1308+328. For these observations the HALCA orbit was sufficiently well determined that it was possible to make a phase-reference map of 1308+326 and to perform the first ever Ground-Space VLBI relative astrometry between physically unrelated sources.

## 1 Introduction

Phase-reference mode observing has proved to be a useful technique for ground-based VLBI. The basic idea is that unwanted contributions to the visibility phase (e.g. from tropospheric and ionospheric path fluctuations) are nearly the same for two closely-spaced sources observed simultaneously or in rapid succession. For strong sources the visibility phase difference can be used directly for precision relative astrometry, whilst phase-reference mapping (Alef 1988, 1989; Beasley & Conway, 1995) can be used to image sources too weak for self-calibration. Prerequisites for success are a sufficiently strong, compact reference source, instrumental phase coherence between the sites and an accurate correlator model for the path delay difference between antennas; any uncompensated path differences arising in the propagation medium or from imperfect interferometer geometry appear in the relative phase, diluted by the source separation measured in radians.

## 2 Space VLBI and VSOP Phase-Referencing

In principle the phase-referencing technique can be extended to Space VLBI (e.g. Bartel, 1993). Problems include the possibilities that nearby reference sources are more likely to be resolved out at higher resolution, and that instrumental coherence may be limited by the space-ground link. Although there is no troposphere or ionosphere above the orbiting element, there may be large geometric delay errors due to a poor spacecraft position, and the position may be perturbed by source changes.

VSOP phase-reference observations are further restricted by the limited sensitivity of HALCA (hence fewer suitable reference sources) and the inability to change pointing sufficiently rapidly between sources. A special source-switching mode of HALCA was tested in August 1999 (VT759) on the strong source pair 0423–013/0424+006 (separation 2°) but the time between switching (30 min) was relatively long. Other investigations have been confined to observations of close pairs of sources, both of which are within the HALCA primary beam. These include 1038+528A/B (sep. 33 arcsec, V046 reported by Porcas & Rioja, 2000), 1342+662/3 (sep. 4.4 arcmin, V039 Guirado et al; Morabito, 1985), the nucleus of M81 and SN1993j (sep. 3 arcmin, W056a Bartel) and 1308+326/8 (V049), which we report on here.

## 3 VSOP Observations of 1308+326/1308+328

The two strong, flat-spectrum sources 1308+326 and 1308+328 are separated by 14.3 arcmin in PA 27°, about half of the HALCA primary beam at 5 GHz (FWHM 26 arcmin). They thus provide an ideal case for investigating the limits of phase-reference observing with VSOP. 1308+326 ($z$=0.996) is highly variable ($S$ = 2–4 Jy) and has been studied by Gabuzda et al. (1993). Geodetic VLBI observations show that its structure is also variable. 1308+328 ($z$=1.65; Machalski & Engels, 1994) is variable but weaker ($S$ = 0.3–0.6 Jy). Rioja et al. (1996) showed that it is essentially unresolved on ground baselines at 8.4 GHz, and measured the separation between the two sources to sub-mas accuracy.

VSOP observations of this pair were made from UT 1630–2230 on 29th June 1998 at 5 GHz. The ground array telescopes (VLBA and Effelsberg), which have smaller primary beams, were switched between the sources every 3 or 4 minutes. The HALCA data (2.5 h) were relayed via the Tidbinbilla tracking station. Correlation was done at the VLBA

correlator and calibration and further analysis was made using AIPS.

Fig1 shows the visibility amplitude vs. resolution for the two sources; both showed strong fringes on ground-space baselines. The weaker, but highly compact nature of 1308+328 is also evident. Maps using ground baselines only (CLEAN beam 1×1 mas) are shown in Fig. 2. At this epoch, 1308+326 consists of two, nearly equal components, separated by 1 mas. 1308+328 is almost point-like, apart from a faint (10 mJy/beam) extension of 2 mas in PA –45 (reported for the first time here). For simplicity we chose this as the reference source in our analysis.

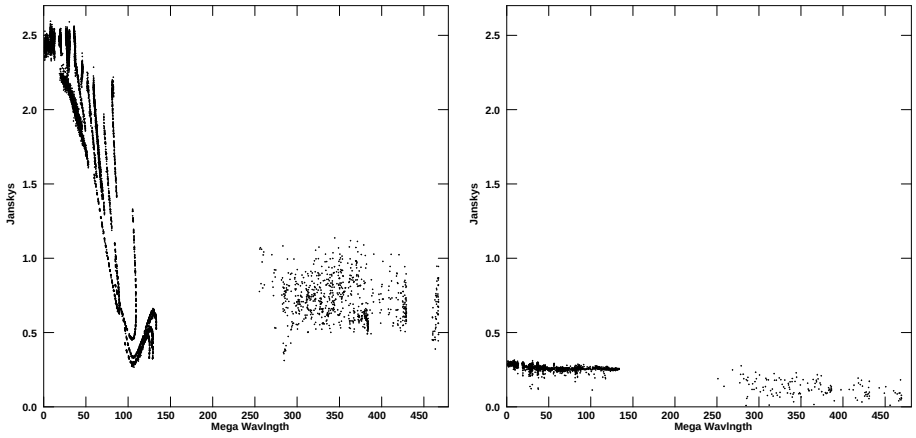


Figure 1: Amplitude of visibility function vs $(u, v)$-distance for **a** (left) 1308+326 and **b** (right) 1308+328

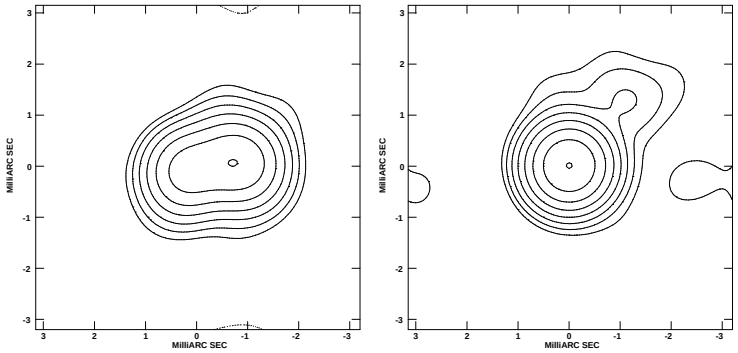


Figure 2: GRT-only maps: **a** (left) 1308+326: peak 1294, base contour 20 (mJy/beam); **b** (right) 1308+328: peak 258, base contour 2 (mJy/beam)

We started our phase-reference analysis by making VSOP hybrid maps of 1308+328 (using only the single phase self-calibration step in FRING). Maps with uniform weighting and equal data weights for all baselines are shown in Fig. 3 (CLEAN beam 0.35×0.35 mas). As expec-

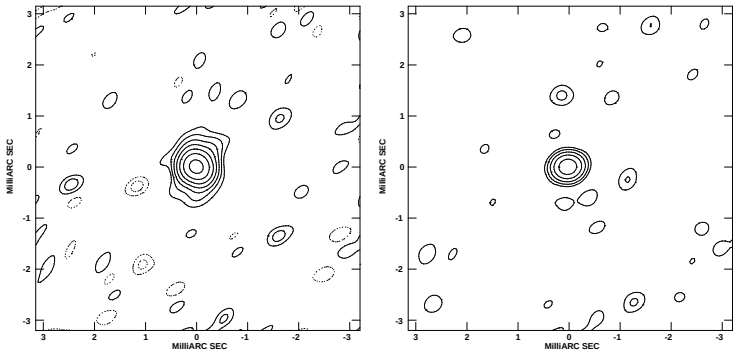


Figure 3: VSOP maps of reference source 1308+328: **a** (left) Using data from all baselines: peak 171, base contour 2 (mJy/beam); **b** (right) Using only baselines to HALCA: peak 105, base contour 4 (mJy/beam)

ted, these show a single, compact component, with 100 mJy still visible in a map made with baselines to HALCA alone (Fig. 3b).

The antenna phase calibrations determined from 1308+328 were then applied to the data of the "target" source, 1308+326, after interpolation across the observing gaps. Visibility phase plots on two baselines are shown in Fig. 4. Both are smoothly varying functions over the observing period, and represent the sum of target source structure phase, errors due to interpolation and correlator model errors (including the absence of an ionospheric path correction). It is clear that the position determination of HALCA is much better than the nominal 80 m requirement for the VSOP mission (from which one might expect phase changes up to 5 turns for the source separation of 0.004 radians).

We next made phase-reference maps of 1308+326 (Fig. 5; CLEAN beam 0.35×0.35 mas) using these calibrated visibilities, with no further phase self-calibration. The uniform-weighted map, using all baselines with equal weight (Fig. 5a) shows clearly the two compact source components, with the suggestion of an arching bridge between the two.

A map made using only baselines to HALCA (Fig. 5b) shows only one (the eastern) of these components, with a peak flux of 372 mJy/beam. A secondary component in PA –140 is clearly spurious, and can be at-

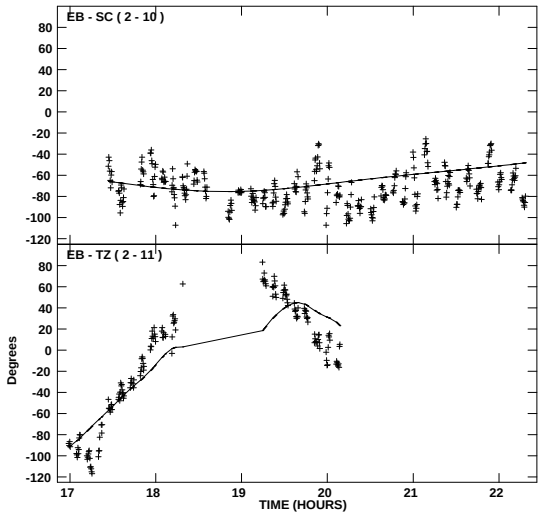


Figure 4: Phase of the 1308+326 visibility function on baselines from Effelsberg to (top) VLBA-SC and (bottom) HALCA, after applying instrumental phase corrections determined using the reference source 1308+328. Solid line is prediction from hybrid map in Fig. 6a.

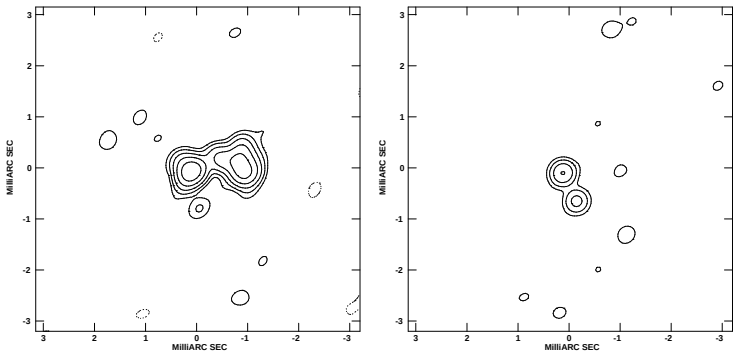


Figure 5: VSOP phase-reference maps of the target source 1308+326; **a** (left) Using data from all baselines: peak 579, base contour 20 (mJy/beam); **b** (right) Using only baselines to HALCA: peak 372, base contour 45 mJy/beam

tributed to phase errors. The difference in the positions of the peaks between Figs. 5 and 3 define astrometric corrections to the assumed source separation ($\delta$RA, $\delta$Dec). Preliminary estimates give +100, –60 $\mu$as between Figs. 5a, 3a and +90, –100 $\mu$as between Figs. 5b, 3b.

Finally, we made hybrid maps of 1308+326 by performing five iterations of phase self-calibration using CALIB, starting with the phase-reference map of Fig. 5a. These are shown in Fig. 6, with the mapping parameters as for Fig. 5. Compared to the phase-referenced maps the

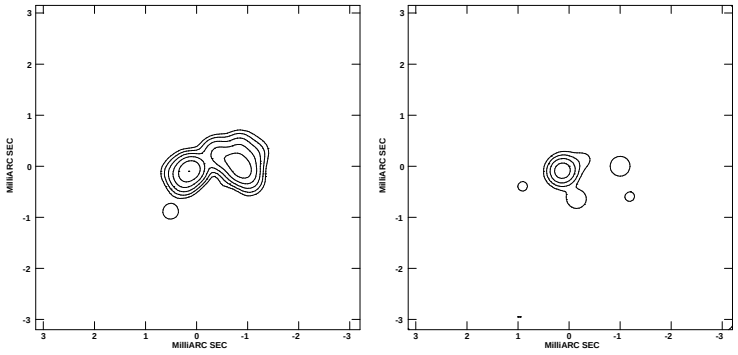


Figure 6: Hybrid maps of 1308+326: **a** (left) Using all baselines: peak 641, base contour 20 (mJy/beam); **b** (right) Using only baselines to HALCA: peak 578, base contour 45 (mJy/beam)

noise levels are much less; in particular the strong, spurious feature in Fig. 5b is considerably reduced in Fig. 6b. The peak brightness (on the eastern "core") is also increased in the hybrid maps — by 11 % in Fig. 6a and 55 % in Fig. 6b. The phase corrections derived in the CALIB phase self-calibration steps for the VLBA-SC and HALCA antennas are shown in Fig. 7. These represent the residual, differential path length errors between the two sources (with respect to the reference antenna Effelsberg), after removal of the 1308+326 source structure phase.

## 4 Conclusions

Our preliminary analysis of 5 GHz VSOP observations of the close pair of sources 1308+326/8 has shown that phase-reference observations are indeed feasible with Ground-Space VLBI.

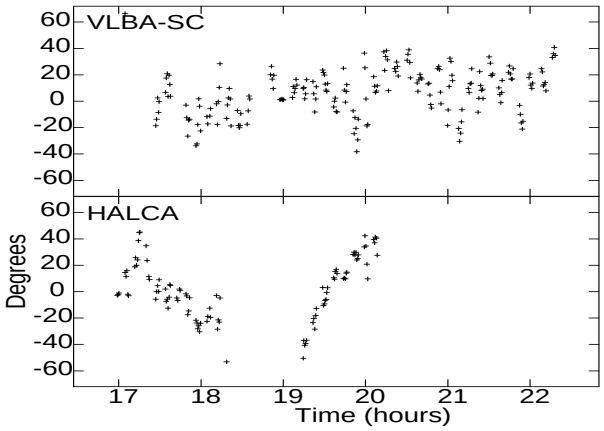


Figure 7: Antenna phase corrections for (top) VLBA-SC and (bottom) HALCA, determined using the referenced phase of 1308+326 and a hybrid map (Fig 6a)

1. The transfer of instrumental phases (determined on the reference source) to the target source was possible for ground-space baselines.

2. Phase interpolation using a 7 minute cycle worked (most of the time).

3. Phase-reference mapping, with limited dynamic range, was possible for 1308+326, using the reference source 1308+328 within the HALCA beam, 14.3 arcmin away .

4. The first ever Space VLBI relative astrometry between physically unrelated sources was achieved.

5. The orbit determination for HALCA is clearly much better than the 80 m mission requirement. The residual relative phase errors (up to 60°) imply HALCA position accuracies in the range 2–5 m. These are comparable to the uncompensated delay path differences introduced by the ionosphere at lower frequencies (e.g. 1.6 GHz) when using uncorrected residual phases from the VLBA correlator.

6. The residual relative phase errors for the source separation of 14.3 arcmin produce significant spurious features when using the ground-space baselines alone, and result in the loss of about 33 % of the expected flux.

7. One would expect the residual relative phase errors to scale proportionally with the target/reference source separation, and the observing frequency. Thus phase-referencing observations with closer source pairs should be possible with VSOP. However, a more general application of phase referencing to wider target/reference separations with future Space VLBI missions will need more precise orbit determinations. Note that Reid (1984) estimated a required baseline precision for QUASAT of 0.1 m for astrometric measurements of water-vapor masers.

**Acknowledgements.** We gratefully acknowledge the VSOP Project, which is led by ISAS in cooperation with many organizations and radio telescopes around the world. We thank P. Edwards and M. Claussen for assistance in scheduling and correlating the V049 observations and A. Roy for useful comments on the text.

## References

Alef, W. 1988, in *IAU Symp. 129: The Impact of VLBI on Astrophysics and Geophysics*, eds. M.J. Reid & J.M. Wrobel (Dordrecht: Kluwer), 523

Alef, W., 1989 in *NATO ASI Ser.: Very Long Baseline Interferometry: Techniques and Applications*, eds. M. Felli & R.E. Spencer (Dordrecht: Kluwer), 261

Bartel, N., 1993 in *Propagation Effects in Space VLBI*, ed. L. Gurvits (Arecibo: NAIC Arecibo Observatory), 90

Beasley, A.J. & Conway, J.E., 1995 in *ASP Conf. Ser.* **82***: Very Long Baseline Interferometry and the VLBA*, eds. J.A. Zensus, P.J. Diamond & P.J. Napier (San Francisco: Astron. Soc. Pac.), 327

Gabuzda, D.C., Kollgaard, R.I., Roberts, D.H. & Wardle, J.F.C., 1993, *ApJ*, **410**, 39

Machalski, J. & Engels, D., 1994, *MNRAS*, **266**, L69

Morabito, D.D., 1985, *AJ*, **90**, 1004

Porcas, R.W. & Rioja, M.J. 2000, *Adv. Sp. Res.*, **26**, 673

Reid, M.J., 1984 in *QUASAT — a VLBI observatory in space*, comp. W.R. Burke (Paris: ESA SP-213), 181

Rioja, M.J., Porcas, R.W. & Machalski, J., 1996, in *IAU Symp. 175: Extragalactic Radio Sources*, eds. R. Ekers, C. Fanti & L. Padrielli (Dordrecht: Kluwer), 122

*Astrophysical Phenomena Revealed by Space VLBI*
*H. Hirabayashi, P.G. Edwards and D.W. Murphy (eds.)*

# The Geometry of the Universe from High Resolution VLBI Data of AGN Shocks

Esko Valtaoja[1] and Kaj Wiik[1,2]

[1] *Tuorla Observatory, University of Turku*
*Väisäläntie 20, FIN-21500 Piikkiö, Finland*
[2] *Metsähovi Radio Observatory, Helsinki University of Technology*
*Metsähovintie 114, FIN-02540 Kylmälä, Finland*

**Abstract**

We propose to use the linear diameters of the shocks in AGN jets as standard rods for determining the geometry of the Universe. The unique feature of shocks is that we can directly estimate their linear diameters from total flux density monitoring data and light travel time arguments. We demonstrate the method by using a small sample of 14 22 GHz VLBI observations. The accuracy of the derived value, $q_0 \approx 0$, compares favorably with traditional methods using much larger samples.

## 1 Introduction

In principle, it is easy to determine the geometry of the Universe simply by observing how the apparent size of an object changes with distance (the redshift $z$). In an Euclidian universe the angular size of an object (the standard rod) diminishes in direct proportion to the distance, in accordance with our everyday experience. However, in a four-dimensional universe described by Einstein's theory of general relativity and the standard metric, after a minimum at around $z = 1$ the angular size of a standard rod starts to increase again and the object appears the larger the more distant it is.

The exact behaviour of the angular diameter $\theta$ on the redshift depends on the cosmological parameters. The so-called $\theta$–$z$ relation can therefore be used to determine the geometry of the universe, in particular the deceleration parameter $q_0$. Some recent supernova observations have indicated that $q_0$ may be negative, which would mean that the expansion of the universe is accelerating, and is dominated by the cosmological constant $\Lambda$ instead of visible or dark matter in any form.

Not many astronomical objects can be detected at redshifts in excess of one, and none of them is well suited to be a standard rod. All proposed rods, such as galaxy clusters or the sizes of double radio sources, have similar diameters only on the average, and they evolve significantly with the cosmological epoch. In addition, the results are confused by severe selection effects. In recent years, much effort has been directed towards using the VLBI milliarcsecond structures of radio galaxies and quasars. These have given the thus far best estimates of $q_0$, but the accuracy is hardly sufficient to differentiate between closed and open universes, and there are severe methological problems in analyzing binned data (e.g., Kellermann 1993; Gurvits 1994; Stelmach 1994; Stepanas and Saha 1995; Dabrowski et al. 1995; Gurvits et al. 1999). The problem, in short, is that we cannot measure the true linear size of an object used as a traditional standard rod.

## 2 A Normalized Standard Rod: Diameters of AGN Shocks

We propose to use the linear diameters of the shocks in AGN jets as standard rods. With modern VLBI techniques, angular sizes of these radio-emitting regions can in some cases be measured. Typical values are less than one milliarcsecond, requiring millimeter or space VLBI observations.

Assuming simply that every shock in every AGN has the same linear diameter would lead to all the well-known problems of the traditional standard rods. However, the unique feature of shocks is that we can directly estimate their linear diameters from total flux density monitoring data and light travel time arguments. The VLBI shocks correspond to radio flares seen, e.g., in the Metsähovi monitoring program (Teräsranta et al. 1998). The radio flares can be surprisingly accurately modelled with simple exponential functions, which directly give the variability timescales (Valtaoja et al. 1999). The variability timescales $\tau_{int}$, transferred to the source frame, give the linear sizes of the shocks: $L \approx kc\tau_{int}$, with $k$ an unknown factor from the source geometry. Thus, we are freed from any assumptions that the sizes of our standard rods are similar in different sources, at different times and at different cosmological epochs: using $\theta_{VLBI}/\tau_{int}$ as the standard rod, we are essentially measuring the angular size of a light-year at different redshifts.

In order to transfer the observed variability timescale, $\tau_{obs}$ into the source frame, we must know the Doppler boosting factor $D$ of the source:

$\tau_{int} = \tau_{obs} D/(1+z)$. The traditional method for estimating the Doppler boosting factors is to use synchrotron-self-Compton arguments (e.g., Guerra and Daly 1997); however, as we have recently demonstrated, such values are very unreliable and much better ones can be derived simply using total flux density variations (Lähteenmäki and Valtaoja 1999). Virtually all major total flux density outbursts in AGN have associated variability brightness temperatures far in excess of the equipartition limit (Readhead 1994; Lähteenmäki et al. 1999), indicating significant amounts of Doppler boosting: $D_{var} = (T_{b,obs}/T_{eq})^{1/3}$.

The use of variability-derived values for D has one drawback. The observed variability brightness temperature depends on the second power of the assumed angular distance $D_A$, and consequently $D_{var} \propto D_A^{2/3}$. The net result is that the 'rod length' $\theta_{VLBI}/\tau_{int}$ has a weaker dependence on the angular distance, just $D_A^{-1/3}$ instead of the usual $\theta \propto D_A^{-1}$.

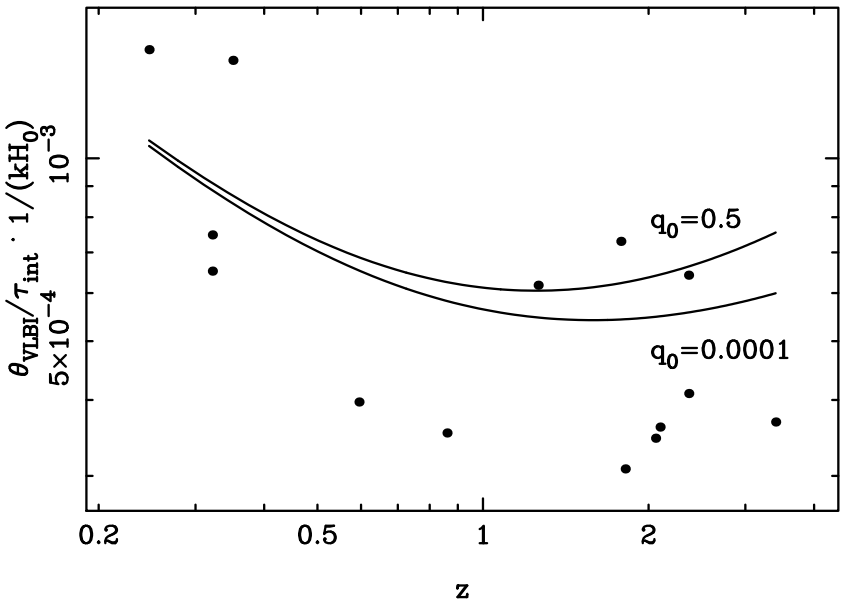


Figure 1: The scaled angular size versus redshift. The expected $z$-dependence for $q_0 = 0.5$ and 0.0001 is also shown.

## 3 First Results

Figure 1 shows our first results using two recent VLBI samples (Bloom et al. 1999 and Wiik et al., these Proceedings). Using the Levenberg-Marquardt gradient-expansion algorithm, we find that the best fit to the data is given by $q_0 = 0 \pm 0.1$ indicating an open, forever expanding universe. With more data, we will also be able to estimate the magnitude of the cosmological constant. Here we have assumed $\Lambda = 0$, since we do not yet have enough data points for a meaningful two-parameter fit. However, we note that a better fit to the data would be obtained with a negative value for $q_0$ (e.g., Krauss and Schramm 1993).

It is obvious that the shocks must be clearly resolved in transverse direction in order to obtain reliable results; high-resolution millimeter or space VLBI data are needed to test the true value of our proposed new method. Simultaneous multifrequency total flux density and VLBI observations of shocks at different stages of their development will also enable us to study variations in the geometry of the shocks - the factor $k$ (which we have assumed to be constant) relating the light travel time to the shock diameter.

## References

Bloom, S.D. et al. 1999, *ApJS*, **122**, 1

Dabrowski, Y. et al. 1995, *MNRAS*, **277**, 753

Guerra, E.J. & Daly, R.A. 1997, *ApJ*, **491**, 483

Gurvits, L.I., Kellermann, K.I. & Frey, S. 1999, *A&A*, **342**, 378

Gurvits, L.I. 1994, *ApJ*, **425**, 442

Kellermann, K.I. 1993, *Nature*, **361**, 134

Krauss, L.M. & Schramm, D.N. 1993, *ApJ*, **405**, L43

Lähteenmäki, A., Valtaoja, E. & Wiik, K. 1999, *ApJ*, **511**, 112

Lähteenmäki, A. & Valtaoja, E. 1999, *ApJ*, **521**, 493

Readhead, A.C.S. 1994, *ApJ*, **426**, 51

Stelmach, J. 1994, *ApJ*, **428**, 61

Stepanas, P.G. & Saha, P. 1995, *MNRAS*, **272**, L13

Teräsranta, H. et al. 1998, *A&AS*, **132**, 305

Valtaoja, E. et al. 1999, *ApJS*, **120**, 95

*Astrophysical Phenomena Revealed by Space VLBI*
*H. Hirabayashi, P.G. Edwards and D.W. Murphy (eds.)*

# A Next-Generation Space VLBI Observatory Assembled in Orbit

L.I. Gurvits

*JIVE, P.O.Box 2, 7990 AA, Dwingeloo, The Netherlands*

**Abstract**

A concept for an SVLBI-2 mission with a 25-30 m orbital radio telescope assembled in space is briefly outlined. The International Space Station (ISS), a permanent multi-purpose orbital manned facility, is considered as a base for the telescope assembly.

## 1 Introduction

This Symposium proves that the first letter in the acronym VLBI, so familiar to the readers of these Proceedings, means **Very** indeed: owing to VSOP, the interferometer baselines are no longer limited by the Earth's diameter. VSOP is the brightest event in the history of Space VLBI (SVLBI) which has begun with several missions proposed in Europe, the USA and the USSR in the 70's and 80's (see Ulvestad et al. 1997 and Davis 1998 for a brief review). One of the earlier proposed missions, RadioAstron (Kardashev 1997), is hoped to become operational this decade and, alongside with VSOP, forms the first generation of SVLBI missions. The technical feasibility of SVLBI was demonstrated by observations conducted with the communication satellite TDRSE in 1986 (Levy et al. 1986). VSOP moves on by testing many new features compulsory for a robust SVLBI observatory. But VSOP is only the beginning of the extraterrestrial era in VLBI. It is clear that the next steps in SVLBI (SVLBI-2 hereafter) will move toward even higher angular resolution, broader frequency coverage and better sensitivity. Of these three main SVLBI-2 characteristics, the latter seems to be of paramount importance.

There are three means of improving VLBI sensitivity:

- to decrease the system temperatures of the telescopes;
- to increase the data rate of the signal recorded;
- to increase the collecting area of each VLBI telescope.

The first option is being actively investigated, with the goal of reaching a system temperature $T_{\rm sys} \approx 10-20$ K for most operational frequencies of the ARISE mission (Ulvestad et al. 1997). This development is

matched by similar target values for the ground-based radio telescopes. However, further improvement of VLBI sensitivity due to decrease of $T_{\rm sys}$ is becoming asymptotically difficult as the values of system temperature reach single digits in Kelvin.

The second option is also being actively pursued. It is foreseen that a data rate of 1 Gbit/s will become available in a few years (Whitney 1999, Cannon 2000). However, further increase of the data rate might become problematic due to the need to overhaul the entire set of VLBI instrumentation, from the IF electronics to the data processing hard- and software. There is also a practical limit on the width of the signal: the bandwidth must not exceed a reasonable fraction of the sky frequency of the observations. In addition, a major drawback of this venue for sensitivity improvement is its irrelevance to spectral line VLBI.

The remaining option, increase of the collecting area of each element of the VLBI array, remains the only option that is practically unlimited and equally efficient for both continuum and spectral line VLBI observations. Thus, we arrive at the necessity to build a space-borne SVLBI-2 element with as large an antenna as feasible.

## 2 How and Where To Build a Large SVLBI-2 Antenna

The first generation SVLBI missions, VSOP and RadioAstron, are characterized by 10-m class parabolic reflector antennas. It is reasonable to aim at 25–30 m as the diameter of an SVLBI-2 orbital antenna. To be operational at wavelengths as short as 3 mm (e.g., the target requirement for the ARISE mission, Marscher, these Proceedings), the reflector antenna must have an rms accuracy of $\sim 0.2$ mm.

Traditionally, SVLBI is considered as a single launch mission with no in-orbit assembly operations. Three possible technologies have been investigated for forming the reflecting surface – mesh, inflatable, or solid material structure. All three options require in-orbit deployment of the antenna. A brief overview of these options and their pros and cons is given in Gurvits (2000). I reiterate here that the two contradictory requirements – overall size in excess of 25 m and sub-millimeter rms accuracy – makes any of these three options extremely challenging.

An alternative to the single launch concept is a mission using a multiple launch and in-orbit assembly of its large payload. This concept makes it possible to accommodate an antenna of considerably larger mass, and therefore larger diameter and better surface accuracy. The

multiple launch concept could be combined with all three antenna designs above. However, the most obvious advantages of the multiple launch scheme are for the solid petal antenna. Since the assembly is likely to require manned operations, it is logical to consider the International Space Station (ISS) as the base for such an SVLBI-2 mission. In general, it is imperative for the ISS to become an assembling facility for future large orbital or interplanetary missions.

The SVLBI-2 spacecraft module should have the ability to function in a free-flying regime as well as docked to the ISS. It can reach the ISS in autonomous flight or be delivered to the ISS by a Space Shuttle or other transport spacecraft. In the former case, the module must be equipped with a full set of systems for autonomous flight, rendezvous, proximity operations and docking. Most of these could be utilized for autonomous flight after assembling the radio telescope. The set of antenna elements (petals) could be delivered to the ISS by a Space Shuttle or other transport vehicle involved in the ISS logistics.

The main requirements for the module spacecraft of an SVLBI-2 mission and the overall mission operational issues are similar to those of several other applications (e.g. astrophysical and Earth science missions) that do not need to be permanently located at the station. A very high level of commonality in major mission requirements could be reached between the SVLBI-2 concept described here and the X-ray Evolving Universe Spectroscopy mission (XEUS, Bavdaz et al. 1999).

The assembly of the radio telescope would be carried out in the docked position (Figure 1). It would utilize the available robotic mechanisms on the ISS (e.g., the European Robotic Arm, ERA, and the Canadian Space Robotic Mechanisms) and would require some extravehicular activity by the station crew. A possible scenario for an SVLBI-2 radio observatory assembled in Space is described in Gurvits (2000). Here I underline two important items of this scenario: *(i)* the SVLBI-2 radio telescope occupies one of the ISS docking ports for a very limited time (approximately one month) and leaves the ISS low orbit after completion of assembly and test operations; *(ii)* the in-orbit checkout of the telescope starts while the SVLBI-2 spacecraft is docked at the ISS. The latter provides the opportunity to fix most possible problems with the SVLBI-2 spacecraft before it goes into autonomous flight.

Multiple launch and in-orbit assembly of an SVLBI-2 mission could bring technical, budgetary and logistical advantages over traditional single-launch in-orbit deployment schemes. The in-orbit assembly con-

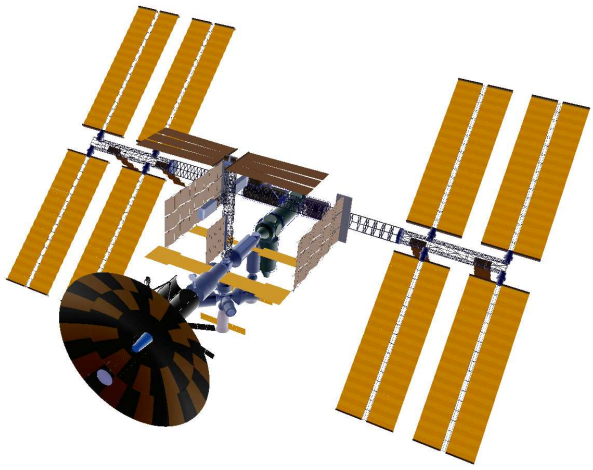

Figure 1: A 30-m radio telescope of an SVLBI-2 module assembled on the International Space Station (a concept, courtesy Aerospatiale). This configuration is temporary: after completion of the assembly and tests, the SVLBI-2 module leaves ISS for a high apogee operational orbit.

cept should therefore be explored at the earliest stages of the SVLBI-2 mission design studies. Such a scheme could also bring additional benefits (in the form of decrease in per-mission cost) by sharing substantial parts of its overall cost with other ISS applications.

**Acknowledgements.** I express my gratitude to the ESA-led team of the ISS SVLBI study. Particularly useful contributions have been made in various forms by M.-F. Busson, D. Gabuzda, C. van't Klooster, H. Olthof and J. Schiemann.

## References

Bavdaz, M., Peacock, A., Parmar, A. et al. 1999, in *Utilisation of the ISS*, ed. A. Wilson, ESA SP–433, 621

Cannon, W.H. 2000, *Adv. Sp. Res.*, **26**, No. 4, 747

Davies, J.K. 1998, *Satellite Astronomy*, (Ellis Horwood Ltd.)

Gurvits, L.I. 2000, *Adv. Sp. Res.*, **26**, No. 4, 739

Kardashev, N.S. 1997, *Experimental Astronomy*, **7**, 329

Levy, G.S. et al. 1986, *Science*, **234**, 187

Ulvestad, J.S., Gurvits, L.I. & Linfield, R.P. 1997, in *High sensitivity Radio Astronomy*, eds. N. Jackson & R.J. Davis, (CUP), 252

Whitney, A.R. 1999, *NewAR*, **43**, 527

*Astrophysical Phenomena Revealed by Space VLBI*
*H. Hirabayashi, P.G. Edwards and D.W. Murphy (eds.)*

# The Proposed ARISE Space-VLBI Mission

Alan P. Marscher

*Institute for Astrophysical Research, Boston University, 725 Commonwealth Ave., Boston, MA 02215, USA*

**Abstract**

ARISE is an antenna dedicated to space-VLBI that has been proposed to NASA as a mission for the future. The basic design is for a sensitive antenna that can observe at frequencies as high as 86 GHz. The apogee of the orbit is envisioned to be about 40,000 km in order to provide angular resolution as fine as 6 $\mu$arcsec (FWHM of longest baseline at 86 GHz). The main objective is to observe the jets of blazars as close to the central engine as possible and to measure the properties of water masers for $\sim$ 20 active galactic nuclei in order to extract information about the central massive black holes. Other possible observations include studies of intraday variability, gravitational lenses, and the regions of X-ray and $\gamma$-ray emission in blazars.

## 1 Introduction

*HALCA* has shown that VLBI with space-based antennas is possible. Indeed, the similarity of the 5 GHz *VSOP* images with 15 and 22 GHz VBLA images is a measure of the high fidelity of the former. Now that it is clear that space-VLBI can work, it is time to design new missions that extend to higher frequencies and higher orbits, leading to a quantum jump in resolution.

The *ARISE* space-VLBI mission has been proposed to NASA. The principal investigator is James Ulvestad of the National Radio Astronomy Observatory, while Arthur Chmielewski of the Jet Propulsion Laboratory is the project engineer. The author is the chair of a large international *ad hoc* scientific advisory group.

In this short contribution, the author will describe briefly the characteristics of *ARISE* and the scientific studies that it will enable, if the mission is mounted. More details of the ARISE mission are available from http://arise.jpl.nasa.gov/ .

## 2 Characteristics of *ARISE*

The original design calls for an inflatable antenna with a diameter of 25 m. Since inflatable space antennas represent new, perhaps risky technology, and since it is not clear whether such an antenna could be made smooth enough to observe with high efficiency at 86 GHz, an alternate plan is to use a smaller (12–15 m) rigid antenna. In order to maintain high sensitivity, the data rate would need to be 1 to 8 Gbits $s^{-1}$ and the system temperatures would need to be very low, 10–40 K. The receivers would be polarization-capable. The mission could be launched as early as 2008, with a nominal lifetime of 3 years.

The orbit of *ARISE* would likely be highly elliptical in order to cause precession driven by close encounters with the slightly non-spherical Earth. Such precession would allow various regions of the sky to be observed at maximum angular resolution from one several-month period to the next. The proposed apogee is about 40,000 km, which would give maximum baselines of about 50,000 km with Earth-based antennas. This would provide angular resolutions corresponding to the FWHM of the uniformly-weighted beam of 15 and 30 $\mu$arcsec at 86 and 43 GHz, respectively — about 5 times finer than with ground-based arrays. The FWHM resolution of the longest baseline would be $\sim$ 2.5 times finer still, or about 6 $\mu$arcsec at 86 GHz. The lower frequencies that would be made available on *ARISE* are the subject of debate at the present time.

There are many technical aspects that need to be worked out, such as how to get the high data rates and how to secure a sufficient number of ground stations for data transmission.

## 3 Scientific Studies with *ARISE*

The cores of blazar jets remain essentially unresolved even at 22 and 43 GHz with the VLBA (see Figure 1 and Marscher et al., these proceedings). Yet, above 30–80 GHz, the cores of most blazars become optically thin. With significantly finer resolution — as would be provided by *ARISE* — we could image the cores at 43 and 86 GHz in order to resolve the cores in both total and polarized intensity. Furthermore, the X-ray and $\gamma$-ray emitting regions of the jet are directly associated with radio flares and ejections of superluminal components (Marscher et al. and Marchenko-Jorstad et al., these proceedings). The angular resolution of arrays including *ARISE* will probably be sufficient to ex-

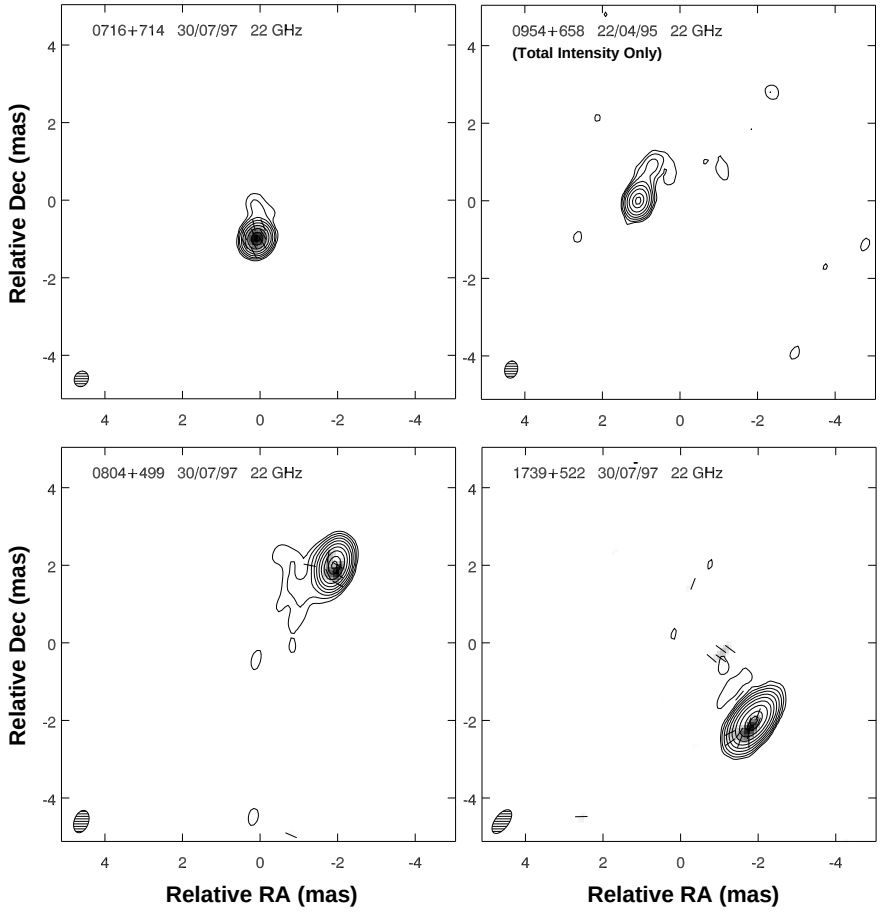


Figure 1: VLBA images of 4 $\gamma$-ray bright, intraday variable blazars at 22 GHz. Even at these high resolutions, the cores are essentially unresolved. The contours correspond to factors of 2 in total intensity, with the highest at 64%. The gray-scale shows polarized intensity, while the lines indicate the direction of the electric vectors. The maximum total intensities in Jy beam$^{-1}$ (fractional polarizations of the cores) are: 0716+714: 1.01 (6.2%); 0804+499: 1.10 (0.5%); 0954+658: 0.57 (total intensity only); 1739+522: 1.58 (1.7%).

plore these high-energy emitting regions in blazar jets. This would be particularly valuable if simultaneous monitoring observations coulds be carried out with $\gamma$-ray and X-ray satellites.

The highest brightness temperature of a source that could be resolved by arrays that include *ARISE* $\sim 5 \times 10^{13}$ K. It must be stressed that this would be an *observed* brightness temperature, not simply inferred from variability timescales. Any sources with brightness temperatures this high would require Doppler beaming factors $\gtrsim 170(1+z)$ in order to be consistent with the inverse Compton limit of incoherent synchrotron radiation, where $z$ is the redshift of the source. *ARISE* would therefore measure the range of brightness temperatures expected from intraday variables (IDVs), confirming whether they require extremely high Doppler factors or other emission models besides incoherent synchrotron radiation. Figure 1 presents high-frequency VLBA images of 4 IDVs, all of which are extremely core-dominated.

Studies of the motions of water megamasers in the outer accretion disks of relatively nearby active galactic nuclei (AGN) such as NGC 4258 can be used to determine the masses of the central black holes thought to power the nuclear activity. The higher resolution made possible by *ARISE* will allow $\sim 20$ of such systems to be studied at larger distances than is now possible.

Gravitational lenses provide effective resolution of background quasars that can be finer than 1 $\mu$arcsec, since the images are magnified by the lenses. Other studies include observations of high-redshift quasars and radio supernova remnants, which would be optimized if 5 and even 1.4 GHz receivers were to be included on *ARISE*.

## 4 Conclusion

If and when *ARISE* becomes operational, it will revolutionize our ability to image and understand the jets of blazars. Furthermore, it will open up about an order of magnitude of parameter space that will likely lead to unexpected discoveries. On the other hand, as our experience with *VSOP* has taught us, the image quality is not optimized when there is only one remote antenna. It is the author's wish that one or two other antennas — such as *VSOP-2* — could be in orbit at the same time and be included in the same arrays as *ARISE* so that truly magnificent ultrafine resolution images could be made of cosmic compact radio sources.

*Astrophysical Phenomena Revealed by Space VLBI*
*H. Hirabayashi, P.G. Edwards and D.W. Murphy (eds.)*

# Space VLBI at Low Frequencies

D.L. Jones[1], R. Allen[2], J. Basart[3], T. Bastian[4], W. Blume[1], J.-L. Bougeret[5], B. Dennison[6], M. Desch[7], K. Dwarakanath[8], W. Erickson[9], W. Farrell[7], D. Finley[4], N. Gopalswamy[7], R. Howard[10], M. Kaiser[7], N. Kassim[11], T. Kuiper[1], R. MacDowall[7], M. Mahoney[1], R. Perley[4], R. Preston[1], M. Reiner[7], P. Rodriguez[11], R. Stone[7], S. Unwin[1], K. Weiler[11], G. Woan[12] & R. Woo[1]

[1] *Jet Propulsion Laboratory, California Institute of Technology, USA*
[2] *Space Telescope Science Institute, USA*
[3] *Iowa State University, USA*
[4] *National Radio Astronomy Observatory, USA*
[5] *Observatoire de Paris, France*
[6] *Virginia Polytechnic Institute, USA*
[7] *Goddard Space Flight Center, USA*
[8] *Raman Research Institute, India*
[9] *University of Maryland, USA, & University of Tasmania, Australia*
[10] *Orbital Sciences Corp., USA*
[11] *Naval Research Laboratory, USA*
[12] *University of Glasgow, UK*

**Abstract**

At sufficiently low frequencies, no ground-based radio array will be able to produce high resolution images while looking through the ionosphere. A space-based array will be needed to explore the objects and processes which dominate the sky at the lowest radio frequencies. An imaging radio interferometer based on a large number of small, inexpensive satellites would be able to track solar radio bursts associated with coronal mass ejections out to the distance of Earth, determine the frequency and duration of early epochs of nonthermal activity in galaxies, and provide unique information about the interstellar medium. This would be a "space-space" VLBI mission, as only baselines between satellites would be used. Angular resolution would be limited only by interstellar and interplanetary scattering.

## 1 Introduction

Ground-based radio interferometers are able to produce images of the sky at frequencies down to a few tens of MHz. Some important scientific

goals, however, require imaging at even lower frequencies. Absorption and refraction by the ionosphere prevents imaging from the ground at frequencies of a few MHz and lower, so an interferometer array composed of inexpensive satellites will be needed. Suitable locations for a space-based array include very high Earth orbits, halo orbits about the Sun-Earth Lagrange points, Earth-trailing heliocentric orbits, the far side of the Moon, and (perhaps) lunar orbit. The optimal choice depends on financial considerations and the unavoidable tradeoff between a benign environment in which to maintain a multi-satellite array and the difficulty of getting enough data from the array to Earth.

## 2 Science Goals

What unique science can be done only at frequencies below $\sim 10$ MHz? There are two general areas where very low frequency observations are critical: First, sources of emission which are intrinsically limited to low frequencies (e.g., plasma oscillations and electron cyclotron masers), and second, observations of strongly frequency-dependent absorption (e.g., free-free absorption by diffuse ionized interstellar hydrogen). Type II radio bursts from interplanetary shocks driven by coronal mass ejections provide a good example of the first case. These intrinsically narrowband emissions decrease in frequency as the shock propagates farther from the Sun into regions of lower plasma density. In order to image and track type II bursts as they approach 1 AU from the Sun, observations at frequencies below 1 MHz are necessary. This would allow us to predict the arrival at Earth of coronal mass ejections, which can trigger severe geomagnetic storms. If located far enough from Earth, a low frequency array would also be able to image Earth's magnetosphere from the outside and observe how it changes in response to solar disturbances.

A sensitive map of the radio sky with arcminute angular resolution at a few MHz would be especially effective at detecting coherent emission from disks, jets, and possibly gas giant planets orbiting close to nearby stars. Most coherent processes have sharp upper-frequency limits, and can only be detected at low frequencies.

All-sky surveys at low frequencies would map the galactic distribution of low energy cosmic ray electrons and would likely discover large numbers of high redshift galaxies, "fossil" radio lobes, and large-scale interstellar shocks and shells from old galactic supernovae and $\gamma$-ray bursts. In addition, diffuse ionized hydrogen could be detected via its

absorption of radiation from extragalactic radio sources across the sky. These observations would complement H$\alpha$ emission maps, which predict large variations in free-free optical depth on angular scales of a few degrees.

## 3 Requirements for a Low Frequency Array in Space

Any space-based array for very low frequency imaging will need to meet three fundamental requirements: 1) the array must be located far enough from Earth to avoid terrestrial interference and the extended ionosphere, 2) there must be a large enough number of individual antennas in the array to produce dense, uniform $(u, v)$ coverage in all directions simultaneously, and 3) the observing bandwidth must be sufficient to provide useful sensitivity for short snapshot observations. The second and third requirements result from the nearly omnidirectional nature of reasonably sized antennas at very low frequencies. Strong variable radio sources anywhere on the sky will affect the observed total power levels, and unless such sources are imaged on short time scales their time-variable sidelobes will limit the dynamic range of observations in other directions. Simulations show that a minimum of 12 satellites will be needed, with at least 16 satellites preferred (see Figure 1 on the next page).

The maximum useful baseline length is set by interstellar and interplanetary scattering. These effects are proportional to $\nu^{-2}$ and thus are much stronger at low frequencies. For frequencies of a few MHz, maximum baselines of a few hundred km are appropriate. The degree of scattering at any given frequency is a strong function of direction on the sky. Consequently, is it important to have a wide range of baseline lengths in the array. Short projected baselines are needed in any case to allow angularly large structures in solar radio bursts and the galactic synchrotron background to be imaged.

Imaging the entire sky is a daunting task, but it can be made tractable by dividing the sky into $\sim 10^3$ fields of view and relying on parallel processing. Each field will require only a 16-bit Fourier transform in the radial direction to account for sky curvature, and $\approx 100$ deconvolving beams (see Frail et al. 1994). During deconvolution, model components from all fields must be subtracted from the full 3-D visibility data set to remove sidelobes from other fields during the next iteration of residual image production. The total computing rate required is large by current standards, but will be readily available within a few years.

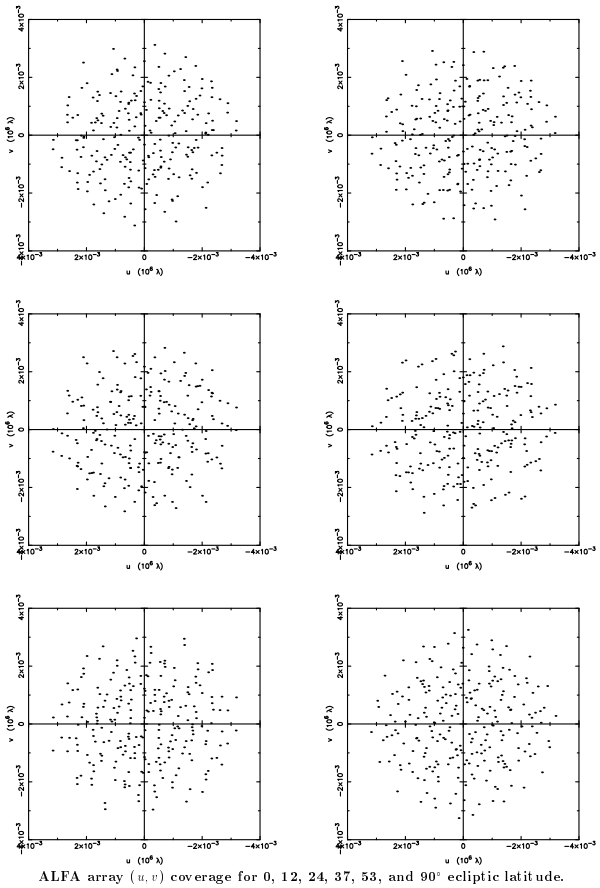


Figure 1: Snapshot (instantaneous) $u, v$ coverage at 10 MHz from a 16 satellite spherical array over a wide range of directions simultaneously.

**Acknowledgements.** Part of this work was carried out at the Jet Propulsion Laboratory, California Institute of Technology, under contract with the US National Aeronautics and Space Administration.

## References

Frail, D., Kassim, N. & Weiler, K. 1994, *AJ*, **107**, 1120

*Astrophysical Phenomena Revealed by Space VLBI*
*H. Hirabayashi, P.G. Edwards and D.W. Murphy (eds.)*

# A New Strategy for the Routine Detection & Imaging of Faint Radio Sources with VLBI

M.A. Garrett

*JIVE, Postbus 2, 7990 AA Dwingeloo, The Netherlands.*

**Abstract**

In this paper I outline a new strategy for the routine detection and imaging of faint (sub-mJy and microJy) radio sources with VLBI and SVLBI. The strategy relies on a combination of in-beam phase-referencing, wide-field VLBI imaging and simultaneous correlation of multiple field centres. A combination of these techniques, together with the steeply rising radio source counts observed at cm wavelengths, permit routine high resolution observations of radio sources previously considered too faint for conventional VLBI.

## 1 Introduction

VLBI is sensitivity limited. Most sources that can be robustly detected by conventional self-calibration techniques have peak fluxes in excess of 10 mJy. The success of phase-referencing techniques, as applied to mJy and a few sub-mJy radio sources, are often limited (particularly in terms of image fidelity) to the brighter sources for which subsequent self-calibration (over much longer solution intervals) is then possible. So far, few attempts have been made to detect sub-mJy sources, despite the fact that with a coherent integration time of 24 hours, global VLBI arrays can routinely produce images with $1\sigma$ rms noise levels better than $30\mu$Jy/beam.

Nevertheless, the focus of VLBI over the last 3 decades (and in particular Space VLBI – SVLBI) has been directed towards the study of the brightest and most compact radio sources in the sky. At these flux levels ($>$ 10mJy), the radio sky is virtually empty, with most radio sources associated with relatively distant AGN. As a result the overlap with other wave-bands is sometimes limited. In this paper, I suggest a new strategy for the *routine* detection and imaging of faint sub-mJy and $\mu$Jy radio sources. The strategy relies on a combination of in-beam phase-referencing (with obvious advantages for SVLBI but also VLBI

generally - see Fomalont et al. 1999), wide-field VLBI imaging (see Garrett et al. 1999) and simultaneous correlation of multiple field centres. These techniques, together with the steeply rising radio source counts at $\lambda$cm wavelengths, should permit high resolution, VLBI investigations of the faint sub-mJy and microJy source populations to begin.

## 2 Towards Routine Imaging of Faint Radio Sources

It is a well known and auspicious fact that the radio source counts increase steeply as one goes to fainter flux levels. At $\lambda$18cm the source counts derived from WSRT observations of the Hubble Deep Field, HDF, (Garrett et al. 2000) imply source counts of up to $\sim 40 S_{\mu Jy}^{-1}$ per square arcmin. Thus within the central regions of the primary beam of a typical 25-m VLBI antenna, one can expect to find over $\sim 100$ potential target sources with $S > 120\mu$Jy (the $3\sigma$ noise level routinely achieved in ground based VLBI images). If we extrapolate the preliminary results of Garrington, Garrett and Polatidis (1999), we can deduce that for every continuum VLBI observation conducted today, there are perhaps a dozen or so faint radio sources in the beam that might be compact enough to be detected and imaged, *in addition* to the brighter target source! This suggests a new strategy for the routine imaging of a large number of faint radio sources:
(i) *Reverse* the traditional approach of selecting the target before the calibrator (see also Garrington, Garrett & Polatidis 1999). The field chosen should satisfy the following criteria: (a) it should be an area for which high quality optical/IR, and deep, sub-arcsec resolution radio data are available (several such fields are expected to become available over the next year) and (b) the same field should also contain a reasonably bright radio source (but not too bright) that can act as a in-beam (secondary) phase-calibrator.
(ii) Split the antenna primary beam into manageable $4' \times 4'$ patches (the size of these patches is currently determined by the limiting integration time and frequency resolution provided by current generation correlators, not to mention throughput, offline storage sizes and processing speed!). Each patch can be generated via simultaneous multi-field centre processing (currently being developed for the JIVE correlator, Pogrebenko 2000) or standard multiple-pass correlation, and can share the phase corrections provided by the in-beam phase-calibrator located close to the centre of the beam.

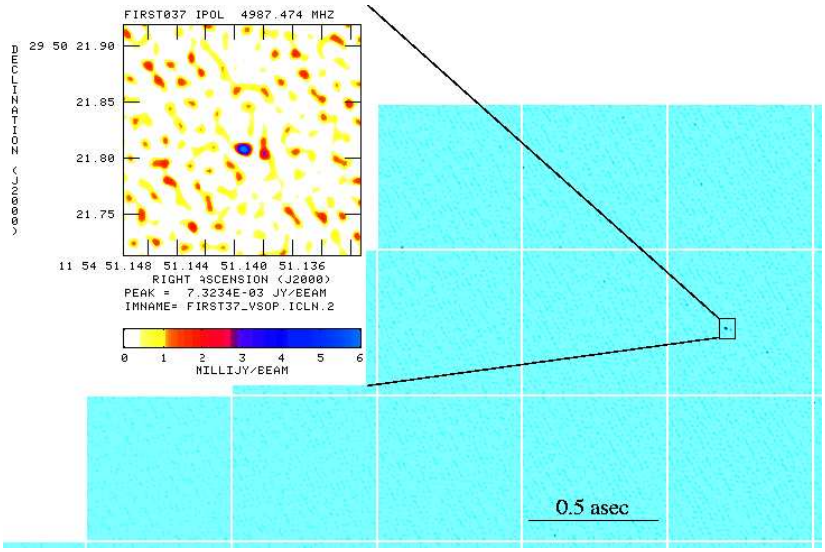


Figure 1: Wide-field VLBI dirty image of a region of sky located 1 arcminute from the phase-centre and target source. The detection of a previously known $\sim$ 10 mJy VLA FIRST source in one of the sub-fields is produced from only 10 min of (unaveraged) global 6cm VLBI data.

(iii) Divide each phase calibrated (but unaveraged) data patch into many small sub-fields of a few arcseconds across (small enough to employ 2-D FFTs and not so large that the image size becomes unmanageable - at least in terms of casual inspection by eye). FTT the data and produce a dirty map of the sub-fields of interest.

Some simple "proof-of-concept" tests have been conducted with a total of 10 minutes of Global VLBI $\lambda$6cm data (taken from the $\lambda$ 6cm Global VLBI Faint Source Survey of Garrington, Garrett & Polatidis 1999). Fig. 1 shows the clear VLBI detection of a known VLA FIRST source in a sub-field that is part of a patch of the primary beam that is located $\sim$ 1 arcminute from the phase-centre and target source. Details of the processing requirements for this (and longer runs) is beyond the scope of this paper but they are not unreasonable. A more important limitation is the minimum integration time provided by today's working correlators (these are currently inadequate to cope with SVLBI satellites at perigee — using this particular strategy — but improvements can be expected over the next few years).

## 3 The Structure of Faint Radio Sources & SVLBI-2

Exceptionally deep radio observations of the HDF (Richards et al. 1999, Muxlow et al. 1999, Garrett et al. 2000) show that the bulk of the sub-mJy and $\mu$Jy source population have steep radio spectra and are for the most part identified with distant disk or irregular, interacting galaxies (often with ISO detections). This argues strongly that these faint sources are associated with very luminous Starburst galaxies. Nevertheless, a significant fraction (perhaps as much as 30%) are probably faint AGN, especially the brighter sub-mJy sources. Using the techniques described here, the brighter AGN could be reasonable targets for the next generation of SVLBI missions now planned. Indeed, SVLBI observations are probably crucial: from simple SSA theory faint sources are also expected to be small. In addition, emission from both compact AGN and larger-scale star-forming regions (principally young SNRs, relic SNR emission and ultra-compact HII regions) might not be uncommon in the same system. Even for relatively distant ($\leq$ 350 Mpc) but ultra-luminous star-forming disk galaxies, hypernovae (such as those SNR in Arp 220 and 41.95+575 in M82) might be detected, and more importantly *resolved* by SVLBI-2 missions. The prospects of detecting these faint, steep spectrum radio sources with next generation SVLBI missions depends crucially on the availability of L or S-band receivers. The contribution future SVLBI-2 missions could make to unravelling the nature, structure and composition of the faint radio source population cannot, and should not, be underestimated.

## References

Fomalont, E.B., Goss, W.M., Beasley, A.J., Chatterjee, S. 1999, *AJ*, **117**, 3025

Garrett, M.A., Porcas, R.W., Pedlar, A. et al. 1999, *NewAR*, **43**, 519

Garrett, M.A., de Bruyn, A.G., Baan, W. & Schilizzi, R.T. 2000, IAU Symposium 199, submitted (astro-ph/0001523)

Garrington, S.T., Garrett, M.A. & Polatidis, A. 1999, *NewAR*, **43**, 629

Muxlow, T.W.B., Wilkinson, P.N., Richards, A.M.S., Kellermann, K.I., Richards, E.A., Garrett, M.A. 1999, *NewAR*, **43**, 629

Pogrebenko, S.V. 2000, EVN Document Series, in preparation

Richards, E. A., Kellermann, K. I., Fomalont, E.B., Windhorst, R.A., Partridge, R.B. 1998, *AJ*, **116**, 1039

*Astrophysical Phenomena Revealed by Space VLBI*
*H. Hirabayashi, P.G. Edwards and D.W. Murphy (eds.)*

# 1 Gbit VLBI System and Recent Observations

M. Kimura[1], J. Nakajima[2], Y. Koyama[2]

M. Sekido[2], T. Suzuyama[2], T. Kondo[2] & N. Kawaguchi[1]

[1] *NAO, Ohsawa 2-21-1, Mitaka, Tokyo 181-8588, Japan*
[2] *CRL, 893, Hirai Kashima, Ibaraki 314-0012, Japan*

**Abstract**

Since the aperture size of satellite radio-telescopes is limited, wide-band acquisition is the most effective approach to increase the sensitivity of space VLBI. The Communications Research Laboratory and National Astronomical Observatory have completed a 1-Gbit VLBI system and started astronomical and geodetic VLBI observations. This system is already working at the full 1024 Mbps (1 giga-bit/sec) rate. We introduce the Giga-bit VLBI system and describe recent observations.

## 1 Introduction

In order to improve angular resolution, we need long baselines. But, if we don't let improve sensitivity, there are only few sources which can be observed. The detection sensitivity in VLBI depends on the antenna diameter, integration time, and recording bandwidth. We think that improvement in bandwidth is the most important for next generation VLBI observing. A Giga-bit VLBI system has been jointly development by the Communication Research Laboratory and National Astronomical Observatory. We detected first fringes on 1998 July 10 and various observations are now being carried out.

## 2 Giga-Bit VLBI System

The Giga-bit VLBI system is shown in Figure 1 and the functions of the units making up the system are listed in Table 1.

The TDS-784/580 sampler was developed by Sony Tektronix. It is originally an oscilloscope, and we remodeled it as an A/D sampler for VLBI. This sampler has 4-channel 1024 M-sps A/D units with 8 bit resolution. We use only one-channel 1-bit data (1 G-sps) for our Giga-bit VLBI system.

Table 1: Function of the Giga-bit VLBI Unit.

| Unit Name | Function |
|---|---|
| TDS-784/580 | 4ch 8bit A/D Sampler |
| DRA1000 | Time control unit |
| | Data converter (VLBI data $\Longleftrightarrow$ HD-TV data) |
| GBR-1000 | Data recording and playback |
| DRA2000 | Global delay tracking |
| GICO | 1 Gbps VLBI correlator |

The DRA1000 was developed by Toshiba and Yamashita Engineering Manufacturing. This unit controls the Giga-bit VLBI system time. It converts the VLBI bit stream data into digital high-definition TV (HD-TV) image data for recording time and converts the HD-TV image data into a VLBI bit stream data for correlation.

The GBR-1000 was developed by Toshiba. It is designed for HD-TV recorders. It can record HD-TV digital image data without any compression. It is first recorder in the world to have a 1024 Mbps recording rate. This recorder uses metal-particle tape in a cassette and the recording time of each tape is one hour. This recorder unit is compatible with commercial recorders, so we can expect Toshiba technical support all around the world as well as TV broadcasting stations.

The GICO was developed by Oki Electric. This correlator's chip was developed by the National Astronomical Observatory. This chip was designed for the Nobeyama Millimeter Interferometer. It has only 4k bit memory for delay buffer and it can not remove large delay such as those encountered in global VLBI observations. To remove large delays, the DRA2000 was developed. This unit was developed by Yamashita Engineering Manufacturing. It has a 1024 Mbit buffer memory for delay tracking. Direct download from buffer memory allows data analysis on a personal computer. This was a very useful function during the development of our VLBI system.

## 3 Recent Observations

On 1999 December 25, we started high-$z$ QSO ($z > 3.5$) survey observations at 22 GHz with the Nobeyama 45 m and Kashima 34 m telescopes.


Figure 1: Giga Bit VLBI system

These observations are very sensitive and we have detected many faint sources. During these observations, we tried a real-time fringe check system. Figure 2 shows the block diagram of our real-time fringe check system. Using the DRA2000's function, a software correlator and Internet data transfer,

We could find fringes very quickly without transportation of tapes. Figure 3 shows the first fringes with software correlation of data from observation of 3C 279. Our personal computer performed this correlation in several minutes. The real-time fringe check system is very useful for our Giga-bit VLBI system. It is thought that success rate of VLBI observations will improves greatly.

Currently, the Giga-bit VLBI system has been installed in Gifu, Nobeyama, and Kashima radio observatories. We are continuing the high-$z$ QSO survey and have started geodetic VLBI observations.

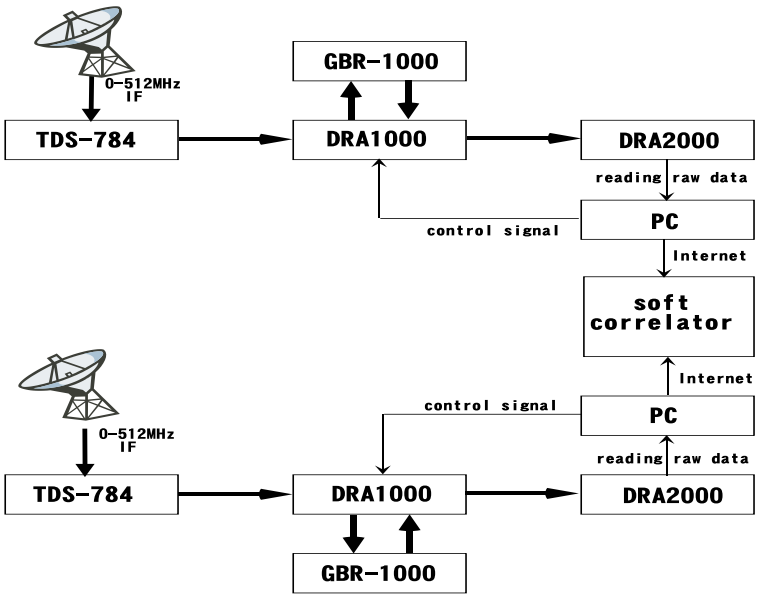


Figure 2: Real time fringe check system diagram

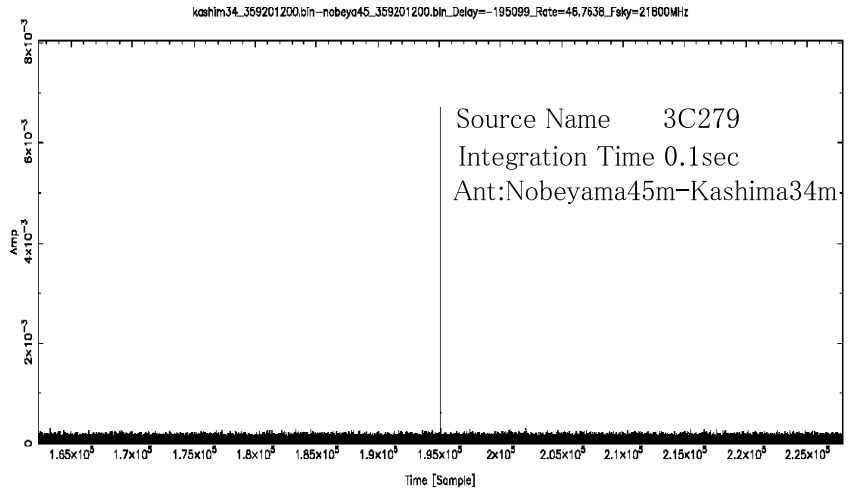


Figure 3: Result of software correlation

*Astrophysical Phenomena Revealed by Space VLBI*
*H. Hirabayashi, P.G. Edwards and D.W. Murphy (eds.)*

# The VSOP-2 Mission

H. Hirabayashi[1], D.W. Murphy[2,1], Y. Murata[1],

P.G. Edwards[1], I.M. Avruch[1], H. Kobayashi[3] & M. Inoue[3]

[1] *ISAS, Yoshinodai 3-1-1, Sagamihara, Kanagawa 229-8510, Japan*
[2] *JPL, 4800 Oak Grove Drive, Pasadena, CA 91101, USA*
[3] *NAO, Ohsawa 2-21-1, Mitaka, Tokyo 181-8588, Japan*

**Abstract**

A next generation Space VLBI mission, tentatively called VSOP-2, is already in the planning stages. In this paper, we report on the current status of this mission.

## 1 Introduction

Since May 1997 a Japanese working group for the next generation Space VLBI mission, tentatively called VSOP-2, has been studying possible mission concepts. Given a variety of constraints, it is likely that the VSOP-2 mission will use a single spacecraft in orbit co-observing with various ground telescope arrays in a similar fashion to the current VSOP mission. However, the VSOP-2 mission will provide a large increase in capability over the VSOP mission due to its higher frequency bands, larger maximum baseline length, and improved sensitivity. The VSOP-2 project would be a collaboration led by ISAS and the National Astronomical Observatory of Japan (NAOJ), with several participating university groups in Japan. Potential international partners include the space agencies NASA and ESA, as well as various foreign radio telescopes and VLBI arrays (such as the VLBA and EVN). The Japanese VERA array, now funded (Sawada-Satoh et al., these proceedings), will also be able to participate at both 22 and 43 GHz.

## 2 Strawman Mission

Based on a series of discussions, the parameters for a strawman model of the VSOP-2 have been developed and are given in Table 1. Thus, the operation of the VSOP-2 mission would be very similar to the operation of the VSOP mission. Major VLBI networks operate as facilities, and are open to the world-wide scientific community via peer-reviewed observing proposals and VSOP-2 will follow this practice, as does VSOP.

However, like the VSOP mission, a mission led survey program also seems an attractive observing strategy which nicely complements the peer-reviewed observing time.

## 3 Spacecraft Overview

A possible concept for the VSOP-2 spacecraft is shown in Figure 1. The main antenna has a diameter from 10–15 m and will be an offset parabolic reflector. The optical scheme of the telescope will include a secondary reflector (Cassegrain optics). A single $\approx$ 50 cm (37 GHz or 15 GHz) telemetry antenna will support a downlink data rate of 1 Gbps. The projected lifetime of the spacecraft is 5 years.

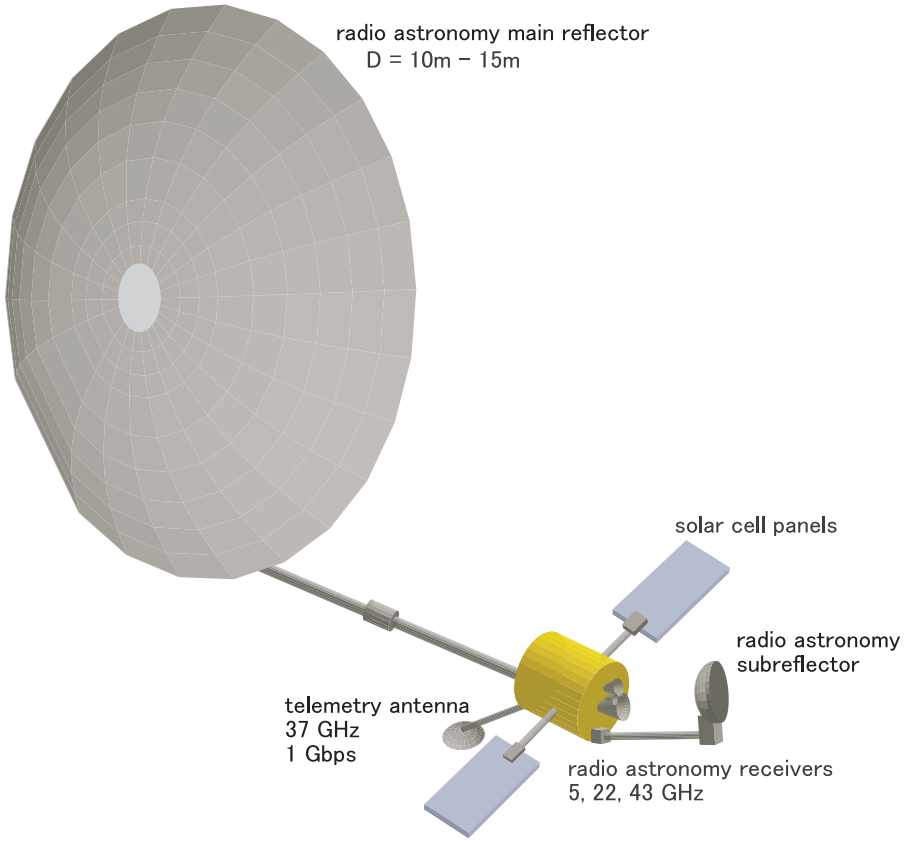


Figure 1: A concept of the VSOP-2 spacecraft

Table 1: Provisional VSOP-2 Mission Properties

| | | | |
|---|---|---|---|
| **Spacecraft: Properties** | | | |
| Lead Agency | ISAS (Japan) | | |
| Antenna Diameter (m) | 12.0 | | |
| Antenna Design | Off-set parabola | | |
| Total Spacecraft Mass (kg) | 900 | | |
| Lifetime (years) | 5 | | |
| **Spacecraft: Launch** | | | |
| Launch Vehicle | M-V | | |
| Launch Site | Kagoshima (Japan) | | |
| Launch Date | September 2007 | | |
| **Spacecraft: Orbit** | | | |
| Apogee Height (km) | 30,000 | | |
| Perigee Height (km) | 1,000 | | |
| Period (hours) | 8.9 | | |
| Inclination (°) | 31° | | |
| Perigee Precession Rate ($\dot{\omega}$) ($^\circ yr^{-1}$) | +206 | | |
| Orbit Plane Precession Rate ($\dot{\Omega}$) ($^\circ yr^{-1}$) | −132 | | |
| **Spacecraft: Science Subsystem** | | | |
| Polarization | LCP and RCP | | |
| Bandwidth/Polarization (Mbps) | 512 | | |
| Observing Bands | 5 GHz | 22 GHz | 43 GHz |
| Resolution ($\mu$as) | 130 | 50 | 25 |
| Aperture Efficiency | 0.5 | 0.4 | 0.3 |
| System Temperature (K) | 30 | 30 | 30 |
| System Equivalent Flux Density (Jy) | 1000 | 1300 | 1800 |
| 7-$\sigma$ Detection Limit (mJy)[1] | 10 | 30 | 70 |
| **Spacecraft: Tracking Network** | | | |
| Commanding | Kagoshima (Japan) | | |
| VLBI Data Acquisition | ISAS/NASA/ESA/NRAO-sites | | |
| **Ground Radio Telescopes** | | | |
| Worldwide including VLBA, EVN and VERA | | | |
| **Science Programs** | | | |
| Investigation of radio/X-ray/$\gamma$-ray emission mechanisms | | | |
| Brightness temperature Measurements | | | |
| Studies of Super-luminal Sources | | | |
| Studies of nearby AGN | | | |
| Cosmological Tests | | | |
| Extragalactic masers and circum-nuclear disks | | | |
| Galactic masers and the ISM | | | |

1. Co-observing with a single 25-m antenna on the ground with integration times of 350, 150, 60 seconds for the three observing bands, respectively.

Table 2: Comparison of VSOP and VSOP-2 Spacecraft and orbit

| | VSOP | VSOP-2 |
|---|---|---|
| Antenna diameter (m) | 8 | 10–15 |
| Frequency bands (GHz) | 1.6, 5, (22) | 5, 22, 43 |
| Typical aperture efficiency | 40% | 60% |
| Typical system temperature | 200 K | 30 K |
| Polarization | LCP-only | LCP& RCP |
| Data rate | 128 Mbps | 1024 Mbps |
| Maximum Baseline (km) | 30,000 | 40,000 |

## 4 Comparison of VSOP and VSOP-2

In Table 2, we compare some of the properties of the VSOP and VSOP-2 missions. With the spacecraft improvements the detection limit on a Earth-space baseline is reduced by more than an order of magnitude. Furthermore, the highest frequency VSOP-2 observations will have an order of magnitude increase in resolution compared with VSOP observations at 5 GHz. Also, the VSOP-2 dual polarization capability will allow all 4 Stokes parameters to be measured. Thus, crudely speaking, the VSOP-2 mission will be 400 times more capable than the VSOP mission. This increased capability will allow large areas of astrophysics to be explored than were inaccessible to the VSOP mission.

## 5 Future Developments

The VSOP-2 mission is still in the early planning stages and many things may change between what has been presented and the final mission configuration. It is expected that a proposal will be submitted to ISAS within the next year to obtain ISAS approval for this mission. If this proposal is accepted then development of the VSOP-2 mission will progress rapidly.

**Acknowledgements.** We acknowledge the efforts of many individuals and organizations around the world who have contributed to the success of the current VSOP mission and look forward to working closely with these groups in the development of the VSOP-2 mission.

*Astrophysical Phenomena Revealed by Space VLBI*
*H. Hirabayashi, P.G. Edwards and D.W. Murphy (eds.)*

# A 22 GHz Line Radiometer for the Usuda Tracking Station

Yoshiharu Asaki [1], Hideyuki Kobayashi [2], Naoki Hagiwara [3] and Masato Ishiguro [4]

[1] *ISAS, Yoshinodai 3-1-1, Sagamihara, Kanagawa 229-8510, Japan*
[2] *NAO, Ohsawa 2-21-1, Mitaka, Tokyo 181-8588, Japan*
[3] *University of Electro Communications, 1-5-1 Choufugaoka, Choufu, Tokyo, Japan*
[4] *NRO, Nobeyama, Minamimaki, Minamisaku, Nagano, Japan*

**Abstract**

Differential measurements of atmospheric water vapor line emissions measured with spaced radiometers, usually mounted on the antenna of a millimeter-wave interferometer, can be used to correct for tropospheric phase errors in the interferometric observations. In this report, we describe a novel method to compare the tropospheric phase fluctuations with 22 GHz water vapor line emissions along a single line of sight. With this method, we can investigate the direct relation between the tropospheric path delay and water vapor line emissions at various elevation angles.

## 1 Introduction

Atmospheric phase fluctuations due to the water vapor content of the lower atmosphere are one of the most serious problems for millimeter-wave VLBI and/or submillimeter-wave radio synthesis arrays. Radiometric phase correction is one of the promising methods for improving the coherence of the fringe phases. In this method, a radiometer is mounted on a radio telescope to measure the amount of water vapor along a line of sight. An example of the successful application of this method is described by Marvel and Woody (1998).

One of the interesting applications of the radiometric method is the determination of the scale factor to transfer the brightness of the water vapor to the quantity of the phase shift at the observing frequency. Since the scale factor is depends greatly on the atmospheric temperature, pressure, humidity, and elevation angle, it is quite difficult to obtain the factor from ground weather conditions at an antenna site.

The frequency standard of HALCA is transferred from a ground tracking station (Suzuki et al. 2000). Since the transferred phase is returned from the satellite to the tracking station, the atmospheric phase fluctuation along a single line of sight can be studied (Kawaguchi 1998). If a radiometer is installed on a HALCA tracking station, the direct relation between the tropospheric path delay and water vapor line emissions at various elevation angles and under various weather conditions can be investigated. In this report, we introduce our study for the development of the fringe phase correction using HALCA and the tracking station at Usuda, Japan.

## 2 Water Vapor Line Monitor

### 2.1 Instruments

The radiometer under development consists of two sections. One is an RF section to amplify a received signal at 18–26.5 GHz and then down-convert it. Since, in tracking HALCA, a link antenna transmits the up-link signal at 15.3 GHz with the level of 14 dBm, there is a possibility of causing saturation of the first LNA. Therefore, a wave guide with a high pass filter is inserted between a horn and the LNA to cut microwave power at less than 16 GHz. The received signal is down-converted to 3–11.5 GHz and transmitted to another section (IF section), which divides the signal into eight frequency channels each 900 MHz wide to obtain the line shape of the water vapor emission. The frequency table is listed in Table 1 with the equivalent receiver noise temperature.

### 2.2 Test Observations

We have conducted test observations with the radiometer. The time variation of the brightness difference, observing at the zenith, obtained by $T_{sky4} - (T_{sky1} + T_{sky8})/2$ is shown in Figure 1, where $T_{sky1}$, $T_{sky4}$, and $T_{sky8}$ are the equivalent sky noise temperatures of frequency channels 1, 4, and 8, respectively.

## 3 Schedule

We will install our radiometer on the Usuda tracking station antenna in March, 2000. The radiometer will be mounted close to the Cassegrain focus of the 10 m dish to illuminate the sub-reflector (Figure 2). The

Table 1: Frequency table of the water vapor radiometer.

| Channel | Frequency (GHz) | Receiver Noise Temperature (K°) |
|---|---|---|
| 1 | 19.15 – 20.05 | 219.2 |
| 2 | 20.05 – 20.95 | 226.3 |
| 3 | 20.95 – 21.85 | 216.5 |
| 4 | 21.85 – 22.75 | 193.1 |
| 5 | 22.75 – 23.65 | 207.5 |
| 6 | 23.65 – 24.55 | 227.3 |
| 7 | 24.55 – 25.45 | 230.6 |
| 8 | 25.45 – 26.35 | 245.3 |

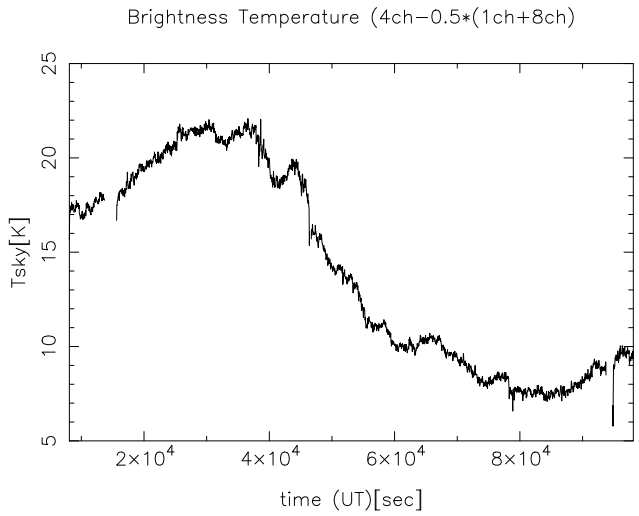


Figure 1: Time variation of the output of the radiometer.

Figure 2: Radiometer mounted on the Usuda 10 m dish for tests. It was then unmounted to conduct further tests in the laboratory.

offset angle between the lines of sight of the tracking antenna and the radiometer is 0.6°, which corresponds to a spatial distance of 11 m at 1 km. The purpose of this study is to investigate the relation between the weather conditions and elevation angles, and the brightness due to the tropospheric water vapor.

Since it will be technically more difficult to control position switching with a larger antenna and at higher frequencies than HALCA, position switching may not be fast enough to carry out phase-referencing for future space-VLBI missions. Therefore, the radiometric phase correction will be important to conduct future space-ground VLBI requiring phase correction techniques.

## References

Kawaguchi, N., Ph D thesis, Graduate University of Advanced Studies of Japan, 1998,

Suzuki, K., Kawaguchi, N., & Kasuga, T., 2000, *these Proceedings*

Marvel, K.B., & Wooday, D.P. 1998, in Proceedings of SPIE, **3357**, ed. I.G. Phillips, 442

*Astrophysical Phenomena Revealed by Space VLBI*
*H. Hirabayashi, P.G. Edwards and D.W. Murphy (eds.)*

# Experiences with the Space VLBI Geodesy Experiment

Sándor Frey, István Fejes & Zsolt Paragi

*FÖMI Satellite Geodetic Observatory, Budapest, Hungary*

**Abstract**

The primary purpose of the Space VLBI Geodesy Demonstration Experiment (GEDEX) is to test how this new potential space geodetic technique works in practice. We present our experience and outline the limitations of using VSOP data.

## 1 Introduction

Space VLBI (SVLBI) is a new observing technique extending VLBI baselines into space. Although present-day SVLBI is designed for radio astronomical purposes, the potential geodetic and geophysical applications of this space technique have been investigated since the mid-eighties (Fejes 1994, and references therein). Feasibility studies showed that SVLBI is in principle capable of *(i)* tying the terrestrial and celestial reference frames, *(ii)* determining the geocentric positions of the ground VLBI stations without collocations with other satellite-based space geodetic (e.g. satellite laser ranging or Global Positioning System) stations, and *(iii)* improving the accuracy of the SVLBI satellite orbit determination using delay and delay rate observables as new types of tracking data. Ground based VLBI is a key observing technique in geodesy and geodynamics, as it provides external reference to measure the Earth rotation and orientation, and highly accurate measurements of inter-continental baselines on the Earth (Sovers et al. 1998).

## 2 Geodesy Demonstration Experiment with VSOP Data

Studies of geodetic SVLBI were based on the assumption that the new technique is an "add on development": it can do everything what the ground based geodetic VLBI can do, but it has also valuable additional capabilities since one of the interferometer elements is orbiting around the geocenter (Fejes et al. 1996). Although this assumption is not strictly true for HALCA, it was appropriate to propose a demonstration experiment for the first-ever dedicated SVLBI satellite to test the concept

of geodetic SVLBI using real data. The primary objectives of GEDEX (Fejes et al. 1996) are to demonstrate that geodetic SVLBI can work in practice, to identify problems and to use the experience gained for formulating recommendations concerning future space VLBI missions. The GEDEX project was granted observational data from the VSOP Survey Program. Data from General Observing Time (GOT) observations can also be used. The actual status of the GEDEX data acquisition, data base and pre-processing, and the development of processing software was reported in Kulkarni et al. (1998) and Fejes (1999). An international working group was established to carry out software developments by adopting existing VLBI and/or orbit determination programs for geodetic SVLBI. We pre-processed a test VSOP experiment and made the data available for developing and testing the processing software. This work involved definition of new data formats and setting up a procedure to obtain total delay and delay rate observables.

## 3 Data Flow and Pre-Processing

The concept of GEDEX data handling is based on a central data base at the FÖMI Satellite Geodetic Observatory (SGO, Hungary), and distributed processing at the participating institutes. The FITS files routinely produced for VSOP astrophysical experiments do not contain all the necessary information to reconstruct the total delays and rates for the SVLBI baselines. In the case of the data coming from the S2 correlator at Penticton, Canada (Carlson et al. 1999), the only path fully tested so far, HALCA spacecraft a priori model delays are not included in the standard FITS file distribution, but must be obtained separately. The same applies for a priori station clock offsets and rates used at the time of correlation. Satellite reconstructed orbit data, as well as Ku band Doppler tracking data can be obtained from the Navigation Group at the Jet Propulsion Laboratory (USA). However, the format of the latter data files still requires the development of a proper program interface.

The NRAO AIPS package can be used to handle SVLBI visibility data exported on FITS archive tapes at the correlators. Special non-AIPS programs are required to import space antenna a priori delay polynomial coefficients and clock parameters into the appropriate extension tables of the FITS visibility data file. Baseline-based total delays and rates are calculated by the AIPS task CL2HF developed for ground based geodetic VLBI data reduction. Several minor modifications had to

be done before it could be used for the test data. The HF extension table is converted to a special format using a separate non-AIPS program for further processing (e.g. geodetic parameter estimation, satellite orbit improvement). This file contains the total delays, rates, their formal errors, and station clock offsets.

## 4 Preliminary Results

As a test case, we used data from the VSOP GOT experiment V003b, 1.6 GHz observation of 3C446 (Paragi et al. 2000). HALCA observed the source on 4 Dec 1997, together with the Australia Telescope Compact Array, Hartebeesthoek, Seshan and Usuda. The correlation was done at Penticton. Spacecraft *a priori* model delays and station clock offsets were received from the correlator upon request. They were incorporated in the appropriate CL extension table of the FITS visibility data file. After pre-processing, the resulting sample delay and delay rate file and the reconstructed orbit file were placed into the GEDEX data base, ready to use for developing and testing GEDEX data reduction software. Most recently, preliminary results with the modified GINS software for analysis of space geodetic technique data shows that the observed delays can be reproduced using the reconstructed orbit with an rms of 13.7 ns (U. Meyer, priv. comm.).

According to our experience, the practical implementation of the idea of geodetic VLBI using VSOP data poses several problems. They are closely related to the observing setup of the VSOP experiments. Ground based geodetic VLBI experiments are scheduled in a way which provides good temporal and spatial sampling, i.e. day-long experiments using a large network of antennas with short (few minutes) scans on many different sources separated by large angles on the sky. Current space VLBI technique is unable to provide resources for such observations. Ground based geodetic VLBI employs the technique of bandwidth synthesis (Thompson et al. 1986) to reduce the errors in group delay observable. It can be shown that the 32 MHz VSOP bands would lead to a loss of accuracy of about two orders of magnitude with respect to the usual ground based geodetic VLBI experiments. Ground based geodetic experiments use two observing frequencies (at S and X bands) to overcome the difficulties in estimating the dispersive ionospheric delay, while VSOP space VLBI observations use single frequencies. Instrumental phase-cal information, unlike in the case of most astrophysical

SVLBI observations, have crucial importance for geodetic SVLBI experiments, in order to properly separate geometric and instrumental effects. The lack of reliable phase-cal data is one of the reason why so many VSOP experiments can not qualify as a potential test case for GEDEX.

## 5 Conclusions

We established a GEDEX data base structure, defined the data pre-processing procedure, developed pre-processing programs and evaluated a test SVLBI observation according to the standards above. We determined the baseline-based total delays and delay rates for the V003b experiment. The resulted delays are in good agreement with what is expected from the reconstructed satellite orbit data. At the present stage of our work, we may conclude that space VLBI could in principle be used for geodetic experiments. However, there are many practical difficulties with VSOP space VLBI data for potential geodetic use.

**Acknowledgements.** We gratefully acknowledge the VSOP Project, which is led by the Japanese Institute of Space and Astronautical Science in cooperation with many organizations and radio telescopes around the world. This research was supported by the Hungarian Space Office. The authors wish to thank many individuals, especially D. Del Rizzo, S. Dougherty, J. Ellis, E. Fomalont, D. Gordon, Hu Xiagong, U. Meyer, N. Mottinger, Shu Fengchun for their help and comments.

## References

Carlson B.R., Dewdney P.E., Burgess T.A. et al. 1999, *PASP*, **111**, 1025

Fejes I. 1994, *Acta Geod. Geophys. Hung.*, **29**, 443

Fejes I. 1999, *Adv. Sp. Res.*, **23**, 781

Fejes I., Kawaguchi N. & Mihály Sz. 1996, *Ap&SS*, **239**, 275

Kulkarni M.N., Ádám J., Fejes I. et al. 1998, in: *Proc. IAG Symp. 119*, eds. Forsberg R., Feissel M., Dietrich R. (Berlin: Springer), 383

Paragi Z., Frey S., Fejes I. et al. 2000, *Adv. Sp. Res.*, **26**, 697

Sovers O.J., Fanselow J.L. & Jacobs C.S. 1998, *Rev. Mod. Phys.*, **70**, 1393

Thompson A.R., Moran J.M. & Swenson G.W., Jr. 1986, *Interferometry and Synthesis in Radio Astronomy* (New York: Wiley)

*Astrophysical Phenomena Revealed by Space VLBI*
*H. Hirabayashi, P.G. Edwards and D.W. Murphy (eds.)*

# Noise Reduction in the Presence of Strong Spectrally-Isolated Signals

C.R. Gwinn[1], B. Carlson[2], S. Dougherty[2,3], D. Del Rizzo[2,3], J.E. Reynolds[4], D.L. Jauncey[4], H. Hirabayashi[5], H. Kobayashi[5], Y. Murata[5], J.F.H. Quick[6] & P. M. McCulloch[7]

[1] *UCSB, Santa Barbara, California 93106, USA*
[2] *DRAO, Penticton, British Columbia, V2A 6K3, Canada*
[3] *University of Calgary, Calgary, Alberta T2N 1N4, Canada*
[4] *ATNF, Epping, New South Wales, 2121, Australia*
[5] *ISAS, Yoshinodai 3-1-1, Sagamihara, Kanagawa 229-8510, Japan*
[6] *HRAO, Krugersdorp, Transvaal, South Africa*
[7] *University of Tasmania, Hobart, 7001, Tasmania, Australia*

**Abstract**

Observational and theoretical study of data taken with VSOP and ground radio telescopes, and correlated with the DRAO correlator at Penticton, shows that the addition of a strong, spectrally-isolated signal can significantly reduce the noise level in other spectral ranges. We describe this process, and suggest applications for novel detection experiments and hardware.

## 1 Introduction

Interferometry is based upon correlation of signals from astrophysical sources at different locations. Those signals are noiselike: the signal at any instant is drawn from a Gaussian distribution. Unless the signals at the two locations are perfectly correlated, they are drawn from a covariant Gaussian distributions. The covariance of the distributions is the average correlation, the quantity that interferometry seeks to measure.

Radio-astronomical signals are nearly always digitized; in other words, they are sampled to form a discrete time series, and quantized to a finite set of possible amplitudes. Sampling limits the frequency range that can be represented. Quantization reduces the signals that can be represented within that frequency range, and therefore adds noise. For continuum signals, effects of quantization on signal, noise, and derived correlation are well understood (see, for example, Thompson et al. 1986).

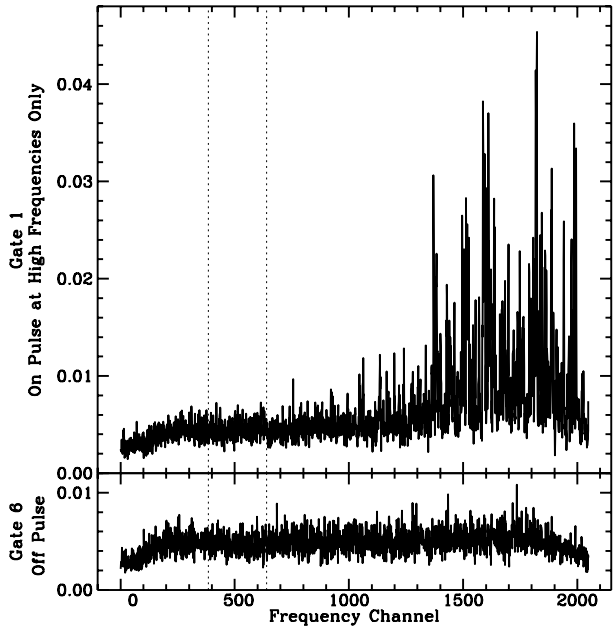


Figure 1: Spectra in gates "on" and "off" pulse. Upper panel: Gate is on pulse. Because of pulse dispersion in the interstellar plasma, the pulse has arrived only at high frequencies (high channel numbers). Scintillation produces ragged spectrum. Lower panel: Gate is off pulse. From Gwinn et al. 2000.

Radio-astronomical signals often vary spectrally. This spectral variation can be represented as covariances between the Gaussian-distributed signals observed at different times; indeed, correlation spectroscopy and spectral-line interferometry rely on measurements of these temporal correlations. A Fourier transform forms cross-power spectra from these temporal correlations. ("FX" correlators Fourier transform the signals before correlation to produce essentially identical power spectra.) In either case, noise from quantization affects the final spectrum.

Figure 1 shows cross-power spectra for the Vela pulsar, taken on the Tidbinbilla-Mopra baseline as part of VSOP observations, on 1997 December 10. The data were correlated at the Canadian VLBI correlator in Penticton, British Columbia. Correlation functions were formed in gates synchronized with the pulse, with widths of 1 msec. Because the pulsar signal varies strongly each pulse, quantizer levels are different, as expressed in terms of the standard deviation of the input signal, on

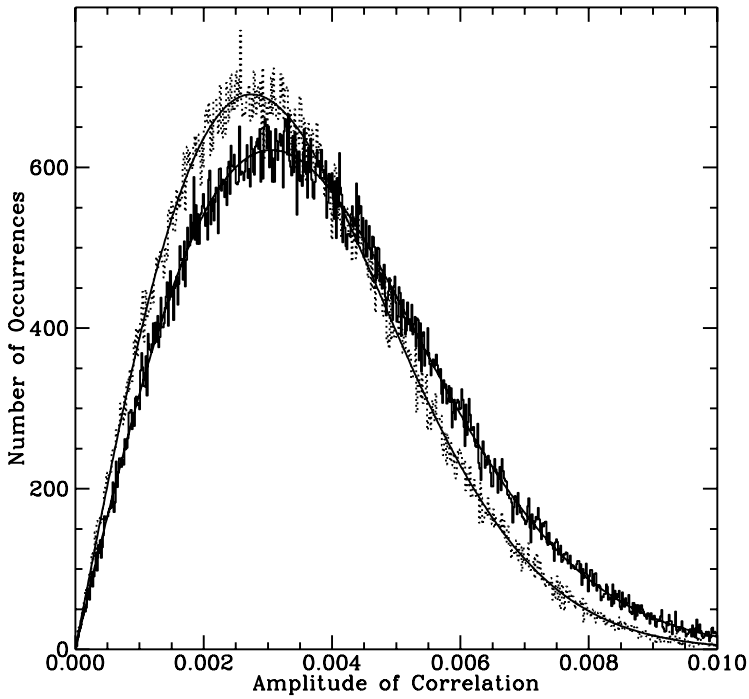


Figure 2: Noise in spectra shown in Figure 1, from channels between the vertical lines in that figure. Solid curve: Noise in "off" gate. Dotted curve: Noise in "on" gate, with pulsar. Histograms show amplitude of correlation; curves show results of fits for Gaussian noise. From Gwinn et al. 2000.

and off pulse. The effect is greatest at learge-aperture antennas, such as Tidbinbilla. Correlation in a gate near the beginning of the pulse detects strong, scintillating signal at high frequencies and no signal at low frequencies because of interstellar dispersion. Correlation in a gate off pulse shows only noise.

## 2 Quantized Spectrally-Varying Noise

Statistics for correlation of quantized, spectrally-varying, noise differ from those for continuum noise. We have computed these statistics, and compared results with computer simulations and with observations (Gwinn et al. 2000). We consider cross-correlation of two signals (or auto-correlation of one); we suppose that each signal is complex, and consists of spectrally-varying Gaussian noise. Variance and covariance

as a function of frequency thus completely characterize the signals.

When formed from many samples, the cross-power spectrum is drawn from a Gaussian distribution at each frequency, and is completely characterized by its average and variance. The average of the cross-power spectrum, over many realizations, is proportional to that of the unquantized signals (or is related linearly, for an autocorrelation). The variance of the spectrum depends on the spectra of the signals, and on the quantizer levels. Specifically, the variance of the noise of the cross-power spectrum is a product of linear functions of the normalized autocorrelation spectra of the two signals.

When a strong, spectrally-isolated signal appears in part of the band, the noise in the remainder of the band is actually reduced. This fact is predicted theoretically and observed in observations of the Vela pulsar, where dispersion causes the signal to appear first at higher frequencies (Gwinn et al. 2000). Figure 2 shows noise for the same spectral region, for the two spectra shown in Figure 1. The spectrally-isolated signal 'attracts' some of the noise added to the signal by quantization.

The fact that adding a noiselike signal in one part of the band reduces noise in another suggests the possibility of deliberately adding spectrally-clean, narrowband noise to the signal before quantization. The noise need not be identical, or even correlated, between stations; however, use of the recorded band is most efficient if noise is added to the same frequency range before correlation. Related 'dithering' techniques have been used in high-end digitization techniques, including commercially available sampling oscilloscopes (Bartz 1993). For 4-level digitization the theoretical improvement in SNR is about 20%, representing an approximately 10% increase in dish diameter.

**Acknowledgements.** We gratefully acknowledge the VSOP Project, which is led by ISAS in cooperation with many organizations and radio telescopes around the world. We thank the US National Science Foundation for financial support.

## References

Bartz, M. 1993, Microwaves & RF, **32**, 5:192

Gwinn, C.R., Carlson, B., Dougherty, S. et al. 2000, submitted to *PASP*, also astro-ph/0002064

Thompson A.R., Moran, J.M. & Swenson, G.W. 1986, *Interferometry and Synthesis in Radio Astronomy* (Wiley, New York)

*Astrophysical Phenomena Revealed by Space VLBI*
*H. Hirabayashi, P.G. Edwards and D.W. Murphy (eds.)*

# Very Long Baseline Connected Interferometry via the 2.4-Gbps ATM Network

H. Kiuchi[1], A. Kaneko[1], Y. Takahashi[1], N. Kawaguchi[2], H. Kobayashi[2,3], K. Fujisawa[2], J. Nakajima[4], T. Kondo[4], H. Uose[5], S. Iwamura[5], T. Hoshino[6], S. Iguchi[7], J. Amagai[1] & T. Yoshino[1]

[1] *CRL, Nukui-kita 4-2-1, Koganei, Tokyo 184-8795, Japan*
[2] *NAO, Ohsawa 2-21-1, Mitaka, Tokyo 181-8588, Japan*
[3] *ISAS, Yoshinodai 3-1-1, Sagamihara, Kanagawa 229-8510, Japan*
[4] *CRL, Hirai 893-1, Kashima, Ibaraki 314-0012, Japan*
[5] *NTT, Midori 3-9-11, Musashino, Tokyo 180-8585, Japan*
[6] *NTT-AT, Shinano 549-2, Totsuka, Yokohama, Kanagawa 244-0801, Japan*
[7] *UEC, Choufugaoka 1-5-1, Choufu, Tokyo 182-8585, Japan*

**Abstract**

The Communications Research Laboratory (CRL), the National Astronomical Observatory (NAO), the Institute of Space and Astronautical Science (ISAS), and the Telecommunication Network Laboratory Group of Nippon Telegraph and Telephone Corporation (NTT) have developed a very long baseline connected interferometry 6-station array with a maximum baseline length of 208 km, using a high-speed asynchronous transfer mode (ATM) network with an AAL1 that corresponds to the constant bit-rate protocol. The VLBI observed data (256 Mbps/station) is transmitted through a 2.488-Gbps [STM-16/OC-48] ATM network instead of being recorded onto magnetic tape. By combining antennas via a high-speed ATM network, a highly-sensitive connected interferometry system has been realized. The system was composed of two real-time VLBI networks: the Key-Stone Project (KSP) network of CRL (which is used for measuring crustal deformation in the Tokyo metropolitan area), and the OLIVE (Optically LInked VLBI Experiment) network of NAO and ISAS which is used for astronomy (space VLBI). These networks operated in cooperation with NTT. In order to realize connected interferometry, the acquired VLBI data (256 Mbps/station) were corrected via the ATM networks and were synthesized using the VLBI technique. The cross-correlation processing and data observation were done simultaneously.

## 1 Real-Time VLBI System

CRL developed an automated real-time VLBI system using an ATM network called the KSP network in 1996. The KSP project, which began in 1994, was developed in order to measure crustal deformation in the Tokyo metropolitan area (Kondo et al. 1998; Koyama et al. 1998). In regular geodetic KSP, VLBI experiments run every other day for 24 hours. It was found that a horizontal position uncertainty of about 2 mm and a vertical position uncertainty of about 10 mm were achieved (Koyama et al. 1998). The system was designed to operate automatically throughout the entire process; the results obtained are available to the public via the Internet (http://ksp.crl.go.jp). NAO and ISAS also developed the OLIVE real-time VLBI network in 1997 for astronomy. The network was used for monitoring the space-VLBI (VSOP: VLBI Space Observatory Programme) signals. These networks were operated in cooperation with NTT. In both systems, STM-16/OC-48 [SDH: synchronous digital hierarchy/SONET: synchronous optical network] ATM networks (Sato et al. 1990) are used. The large-size (208 km) highly-sensitive array (very long baseline connected interferometry array) was established by high-speed digital optical data links composed of both the KSP and the OLIVE networks. Four of the seven antennas; Usuda (64 m), Nobeyama (45 m), Koganei (KSP-11m), Kashima34 (34 m) / Kashima11 (KSP-11m), Miura (KSP-11m), and Tateyama (KSP-11m) were selected by the ATM cross-connect switch. The virtual telescope (the connected real-time VLBI array) was realized to observe weak radio sources.

## 2 VLBI Data Acquisition and Correlation System

Radio-signals received from astronomical radio sources at the VLBI site were converted to digital signals by the VLBI data-acquisition system — a high-end version of the K-4 system (Kiuchi et al. 1997). The data rate of the ATM transmission was selected from five possible rates (ranging from 16 to 256 Mbps). The six-baseline real-time KSP correlation system is usually operated as the very long baseline connected interferometry array. The KSP correlation processor is an XF type using field-programmable gate arrays (FPGAs) on a VME board. The correlation processor has a 512-Mbps data processing speed capability and 512 complex lags in total.

## 3 System Evaluation

The real-time VLBI system (very long baseline connected interferometry) was operated from September 1998. The very long baseline connected interferometry experiments were carried out with a 256-Mbps data rate at each station. The selection of Kashima34 (34 m) and Kashima11 (KSP-11m) was alternated. All of the radio telescopes were Az-El type antennas. The KSP system is a dual-frequency system (8 GHz-band and 2 GHz-band) for compensating ionospheric delay. The Usuda64 antenna has receivers ranging from 1.5 to 22 GHz. Nobeyama45 has receivers ranging from 22 to 110 GHz, and Kashima34 has receivers from 1.5 to 43 GHz. The VLBI observation equipment at each site includes an ATM transmitter. The Kashima34 station was the only station that transmitted its IF (intermediate frequency) analog signal – to the Kashima11 VLBI site about 600 m away. The IF analog signal is sent using commercially available fiber-optic links modulated in the radio-frequency range. The fiber-optic links were the Ortel 10341A laser diode and the Ortel 10455A photo detector. The IF signal is converted to digital signal by the KSP VLBI data-acquisition system (high-end version of the K-4). The 16-ch digital filtering was done after sampling in the VLBI data-acquisition system, the bandwidth of each channel was 8 MHz. The cross-correlation processing using the KSP six-baseline real-time correlation processor and observation were done simultaneously. Weak radio star observations were carried out, including the source HR1099. The HR1099 binary system, the radio emission of which is considered to be non-thermal in nature, is a non-eclipsing system. It is probably related to and consistent with a magnetic activity scenario. The radio behavior of HR1099 is quite characteristic: two rather different phases, quiescent and active, appear to alternate. The observation was carried out in a dual-frequency (X-band and S-band) using Usuda, Kashima34, Koganei, and Miura. The active phase of HR1099 (flare-up of X-band signal) was detected. The correlated amplitude of the quiescent phase was $3.14 \times 10^{-5}$ in X-band ($4.16 \times 10^{-5}$ in S-band) and that of active phase was $2.61 \times 10^{-4}$ in X-band ($1.77 \times 10^{-5}$ in S-band). The period of the quiescent phase is far longer than that of the active phase and the active phase detection was done between Usuda64 and KSP antennas. Unfortunately, it was not possible to operate the Kashima34 because of a gale during the flare-up detection epoch.

## 4 Conclusion

A real-time VLBI system that corresponds to the constant bit-rate protocol using the STM-16/OC-48 ATM networks with AAL1 was developed. The system was demonstrated its function successfully. This system is a significant advance in VLBI and should provide more precise information about radio astronomy.

## References

Kiuchi, H. Amagai, J. Hama, S. et al. 1997, *PASJ*, **49**, 699

Kondo, T. Kurihara, N. Koyama, Y. et al. 1998, *Geophys. Res. Letter*, **25**, 1047

Koyama, Y. Kurihara, N. Kondo, T. et al. 1998, *Earth Planets Space*, **50**, 709

Sato, K. Ohta, S. and Tokizawa, I. 1990, *IEEE Trans. Commun.*, **38**

*Astrophysical Phenomena Revealed by Space VLBI*
*H. Hirabayashi, P.G. Edwards and D.W. Murphy (eds.)*

# The Green Bank Telescope: An Overview

P.R. Jewell and Glen Langston

*NRAO, P.O. Box 2, Green Bank, WV 24944, USA*

**Abstract**

The 100 m NRAO Green Bank Telescope (GBT) will be completed in early 2000. The GBT has a large number of unique design and performance features that give it unprecedented scientific capability. We review those features, which include an offset feed (clear aperture) design, an active surface, broad frequency coverage from 100 MHz to 115 GHz, a versatile receiver selection mechanism, and a new multi-input, 256k-channel autocorrelation spectrometer.

## 1 Introduction

The Green Bank Telescope (GBT) will be among the most advanced and versatile telescopes ever constructed. The GBT, shown in Figure 1, will be completed in the summer of 2000. The GBT is a 100 m radio telescope with an unblocked aperture, fully active surface of 2004 individual panels, and laser metrology system for surface settings and pointing corrections. The GBT will operate over a wavelength range of 3 meters to 3 millimeters. Its collecting area is 7853 $m^2$, it stands 146 m high, and has a moving weight of 7700 metric tons. Although one of the largest moving structures on earth, it will ultimately have 1 arcsec

Table 1: GBT Operating Specifications

| Parameter | Constraint | Specification |
|---|---|---|
| Surface accuracy | Open loop surface | $<$ 360 $\mu m$ (rms) |
| | Closed loop/metrology | $<$ 220 $\mu m$ (rms) |
| Pointing accuracy | Conventional | 3 arcsec (rms) |
| | Closed loop/metrology | 1 arcsec (rms) |
| Slew rate | Maximum Azimuth | 40 deg/min |
| Beam size | Nominal FWHM | 720 $arcsec/\nu$ (GHz) |
| Flux sensitivity | at 20 GHz | 1.85 K/Jy |

Figure 1: Image of the GBT on 2000 January 21.

pointing accuracy and will allow observations at 3 mm wavelengths. A summary of GBT design features follows.

The NRAO in Green Bank has supported the VSOP mission with both 140 foot telescope observations and a ground tracking station for the HALCA satellite (Hirabayashi et al. 1998). The great collecting area of the GBT will valuable for future space VLBI observations requiring high sensitivity.

The GBT's characteristics (Table 1) will allow its users to address a wide range of scientific topics over a wavelength range of meters to millimeters (Tables 2, 3), including observations of young galaxies at extreme redshifts, pulsars, HI and molecular spectroscopy, ground and space VLBI, and millimeter-wave spectroscopy and continuum studies.

## 2 Construction and Commissioning

As of mid-February 2000, all antenna structural components were completed and over 80% of the surface panels were installed. Most of the

remaining work is expected to be completed in the Second Quarter of 2000, and we anticipate that the telescope will be available for the start of commissioning in the Third Quarter. Most NRAO systems, including receivers, backends, peripheral electronics, monitor and control software, and basic analysis software will be available when commissioning begins. Pointing and surface calibration and commissioning of basic systems and low frequency receivers is expected to take about 6 months. Commissioning to 50 GHz will take another 6-9 months. Operation in the 3 mm window should be available by the end of 2001.

Table 2: GBT Receivers

| Receivers | Operating Range | Status |
|---|---|---|
| Prime Focus 1 | 290 – 920 MHz | Completed |
| Prime Focus 2 | 910 – 1230 MHz | Under Construction |
| L Band | 1.15 – 1.73 GHz | Completed |
| S Band | 1.73 – 2.60 GHz | Completed |
| C Band | 3.95 – 5.85 GHz | Completed |
| X Band | 8.20 – 10.0 GHz | Completed |
| Ku Band | 12.4 – 15.4 GHz | Completed |
| K Band | 18 – 26.5 GHz | Completed |
| Ka Band | 26 – 40 GHz | Planned |
| Q Band | 40 – 50 GHz | Under construction |
| W Band | 68 – 90 GHz | Proposal stage |
| | 90 –115 GHz | Proposal stage |
| Bolometer Camera | 3 mm band | Planned |

## 3 Observing with the GBT

Much of the year 2000 will be devoted to completing and commissioning the GBT, but it is anticipated that some visitor observations will begin during the year. The first observations will be at the lower frequencies, and will allow, for example, HI and OH spectroscopy and pulsar projects. Toward the end of 2000 or in early 2001, frequencies approaching 50 GHz may be available. This will open up a range of projects that are not possible with current facilities. The first call for observing proposals is anticipated for the spring of 2000. The observing community will be notified of the dates and parameters of the first call for proposals by e-mail, newsletters, and Web announcements on the NRAO Green Bank home page (http://www.gb.nrao.edu).

Table 3: GBT Spectrometers, Continuum, and Pulsar Backends

| Backend | Specifications | Status |
|---|---|---|
| GBT Spectrometer | Maximum channels/IF: 262,144 | Integration |
| Modes: | $8 \times 800$ MHz or $32 \times 50$ MHz | |
| Pulsar: | 4096 *time bins* $\times$ 256 *channels* | |
| Spectral Processor | $2 \times 1024$ channels (40 MHz) | Completed |
| | 1, 2, 4, or 8 IF modes | |
| Digital Continuum | 16 inputs, 10 switching phases | Completed |
| | 100 nanosec phase time resolution | |
| VLBI | VLBA, VSOP and S2 Recorders | Integration |

## 4 Future Development Plans

The GBT will begin operations with excellent performance specifications and a powerful suite of instrumentation. The scientific capability of the GBT can be further exploited by the additional development of observing instrumentation and computing capability. Possible projects include enhanced pulsar backends, focal plane array receivers at several frequencies, pipeline data processing, dynamic scheduling, and remote observing capability. Particularly exciting is the potential of the GBT in the 3 mm band, where it will have unparalleled sensitivity. Receivers for point source observations (line and continuum), spectroscopic focal plane arrays, and large-format bolometer cameras for continuum observations in the 3 mm window are being investigated.

**Acknowledgements.** We gratefully acknowledge the VSOP Project, which is led by the ISAS in cooperation with many organizations and radio telescopes around the world. The National Radio Astronomy Observatory is a facility of the National Science Foundation operated under cooperative agreement by Associated Universities, Inc.

## References

Hirabayashi, H., Hirosawa, H., Kobayashi, H. et al. 1998, *Science*, **281**, 1825 and erratum **282**, 1995

*Astrophysical Phenomena Revealed by Space VLBI*
*H. Hirabayashi, P.G. Edwards and D.W. Murphy (eds.)*

# Difwrap: A Graphical User Interface for Error Analysis in Difmap

Jim Lovell

*ATNF, PO Box 76, Epping NSW 1710, Australia*

**Abstract**

Difwrap is a software package that provides a Graphical User Interface (GUI) to Difmap. The main purpose of the software is to provide a means to estimate uncertainties in source models generated by Difmap's *modelfit* task. Difwrap also allows for some limited configuration of Difmap parameters through the GUI.

## 1 Introduction

Difwrap is a program written in the Perl language to provide a Graphical User Interface (GUI) to Difmap (Shepherd et al. 1994). The main function of the software is to provide a means to estimate errors in source models generated by Difmap's *modelfit* task through a comparison of trial models with visibility data.

## 2 Model Error Analysis

The Model Error Analysis function in Difwrap is based on the process first described by Tzioumis et al. (1989). This process involves adjusting the model parameter of interest by a small amount and then fixing it. The fitting process is the run to allow the model to re-converge. This cycle of parameter adjustment and model fitting is repeated until an obvious visible difference between the model and the data is seen.

This visual inspection method to determine goodness of fit provides more realistic error estimates than a traditional chi-squared analysis because the number of degrees of freedom is typically not well known. This method also has the advantage that it allows for the inter-dependency of model components to be taken into account during model fitting. For example, if the $(u, v)$ coverage is limited, there can be a strong inter-dependency between the size and flux density of the model component.

The main problem with this method is many trial models may be needed before a good understanding of the errors can be obtained. Carrying out this task by hand is tedious and time-consuming as it requires

the generation of many model files, followed by a visual comparison of each model with the data. The model error analysis function of Difwrap removes much of this drudgery. It works in the following way:

1. The model components are presented to the user who decides which parameter (flux density, position or component size/shape) requires an error estimate.

2. The user then decides what range of parameter values require trialing and how many points to sample within that range.

3. Difwrap will then create a test model for each grid point, carry out the model fitting and store the final model and goodness of fit values.

4. When this is complete, the user can select how the goodness of fit values are to be presented. For example, if a component flux density uncertainty is being investigated, the user can choose to plot trial flux density against chi-squared of the fit. When the user selects a point on this plot the corresponding model is shown with the data for comparison. The user then indicates if the fit is acceptable or not.

5. After this inspection, the estimated error values are presented.

## 3 An Example Error Analysis

As an example of using Difwrap to obtain error estimates, an error analysis of a model for the VSOP Survey source J1316–3338 is shown.

In this example the objective is to estimate the core brightness temperature uncertainties. This requires an error analysis of the flux density and size of the core component. Firstly, the limits on the size of the component are requested. A range of Major Axis, Axial Ratio and Major Axis Position Angles are chosen with a sampling grid of 5 points in each dimension. The user then chooses to run the Difmap task *modelfit* with 10 iterations for every trial model. Difwrap is then instructed to construct the models for each of the grid points, run *modelfit* and measure the goodness of fit in each case.

On completion, Difwrap displays a "Plotting and Analysis" window which allows the user to choose how to display the results. In this case the results will be plotted as "slices" of a cube with X and Y axes of

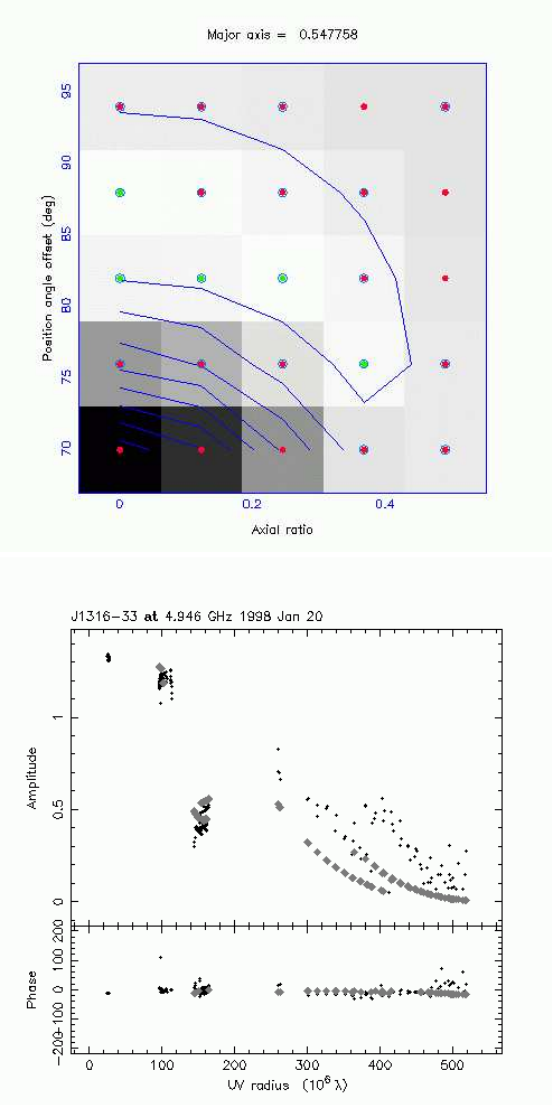


Figure 1: **Top:** RMS of the *modelfit* (logarithmic contours and greyscale) as a function of Position Angle and Axial Ratio for the best fit Major Axis. Darker pixels represent a larger rms. **Bottom:** The visibility data (black) with a model (grey) corresponding to a grid point sampled by Difwrap and plotted at top. In this case the user has plotted a model corresponding to a sampled grid point with an unacceptably high rms.

Position Angle and Axial Ratio respectively. The user steps sequentially through the gridded Major Axis values. Figure 1 shows the rms of the fit (greyscale) plotted as a function of Position Angle and Axial Ratio for the best fit Major Axis. Each pixel may be selected and the corresponding model fit is then plotted. The user may then decide if the fit is acceptable or not by changing the colour of the point plotted over each pixel. For this source, an Axial Ratio of 0 makes an acceptable fit for some position angles (implying an infinite brightness temperature) so only a lower limit on brightness temperature can be obtained. A similar error analysis to obtain limits on the core flux density results in an uncertainty in flux density of $\pm 0.12$ Jy. The lower-limit on flux density combined with the upper-limit on component area (i.e when Major Axis and Axial Ratio are at their largest) thus provides a lower limit on brightness temperature of $4.8 \times 10^{11}$ K in the source frame.

## 4 Obtaining Difwrap

Difwrap is still under development. The most recent version, together with documentation for installation and use, can be obtained from http://www.vsop.isas.ac.jp/survey/difwrap/.

**Acknowledgements.** I gratefully acknowledge the VSOP Project, which is led by the Japanese Institute of Space and Astronautical Science in cooperation with many organizations and radio telescopes around the world.

## References

Shepherd, M.C., Pearson, T.J., & Taylor, G.B. 1994, BAAS, **26**, 987

Tzioumis, A.K., Jauncey, D.L., Preston, R.A. et al. 1989, *AJ* **98**, 36

*Astrophysical Phenomena Revealed by Space VLBI*
*H. Hirabayashi, P.G. Edwards and D.W. Murphy (eds.)*

# Connection Between Superluminal Ejections and $\gamma$-Ray Flares in Blazars

S.G. Marchenko-Jorstad[1,2], A.P. Marscher[1], J.R. Mattox[1], J. Hallum[1], A.E. Wehrle[3] & S.D. Bloom[4]

[1] *Institute for Astrophysical Research, Boston University, 725 Commonwealth Ave., Boston, MA 02215, USA*
[2] *Astronomical Institute, St. Petersburg State University, Bibliotechnaya Pl. 2, Petrodvorets, St. Petersburg 198904, Russia*
[3] *Jet Propulsion Laboratory, MS 301-486, 4800 Oak Grove Dr., Pasadena, CA 91109, USA*
[4] *Box 821, Hampden-Sydney College, Hampden-Sydney, VA 23943, USA*

**Abstract**

We examine the coincidence of times of high $\gamma$-ray flux and epochs of zero separation of superluminal components from the core in EGRET blazars based on our 1993.9–1997.6 VLBA monitoring program at 22 and 43 GHz. In 19 cases of $\gamma$-ray flares for which sufficient VLBA data exist, 10 of the flares fall within $1\sigma$ uncertainty of the extrapolated epoch of zero separation from the core of a superluminal radio component. The number expected by random chance $\leq 3$ at 95% confidence. Although there are a small number of cases in which the $\gamma$-ray flux was low at the extrapolated epoch of ejection, these can be explained by accelerations or decelerations in the proper motions, as expected, for example, in bent jets.

## 1 Introduction

We have completed a program of monitoring of the milliarcsecond-scale structure of $\gamma$-ray bright blazars (42 sources) with the VLBA at 22 and 43 GHz during the period from November 1993 to July 1997. We have determined velocities of jet components in 33 sources and compare the epochs of zero separation from the (presumed stationary) core with the $\gamma$-ray light curves obtained from the 3rd EGRET catalog (Hartman et al. 1999) in order to determine whether $\gamma$-ray flares are associated with major energetic disturbances that propagate down the jet.

## 2 Detections of Gamma-Ray Flares

One of the most difficult aspects of the analysis is to detect a $\gamma$-ray flare because the light curves are very sparse. For this purpose we have determined the average $\gamma$-ray flux of every source as a weighted average value of all measurements, including the upper limits to the flux, with weight equal to $1/\sigma$, where $\sigma$ is an error of the measurement; in the case of an upper limit $\sigma$ is equal to the value of the upper limit itself. We assume that a $\gamma$-ray flare is detected if the flux measurement exceeds the average flux value by a factor of 1.9 or more and if the uncertainty in the measurement is less than the deviation of the measurement from the average value. In 29 cases the VLBA data are contemporaneous with the $\gamma$-ray observations; in 19 of these 29 cases a $\gamma$-ray flare is detected.

## 3 Discussion

### 3.1 Positive Detections

In 10 of these 19 cases the epochs of zero separation coincide, to within the 1-$\sigma$ uncertainties, with the times of the $\gamma$-ray flares. (For 0458−020, the coincidence is within the 2-$\sigma$ uncertainty. For both 1222+216 and 1226+023 there are only two epochs of VLBA observations; in these cases we assume that the 1-$\sigma$ uncertainties = 0.2 yr, similar to those of many other objects). These results are presented in Table 1, where the first column gives the name of the source, the second - redshift, the third - the ratio of the peak $\gamma$-ray flux to the average flux, the fourth - the time of the $\gamma$-ray flare, the fifth - the epoch of zero separation, and the sixth - the apparent speed ($H_0$ = 100 h km s$^{-1}$ Mpc$^{-1}$, $q_0$=0.1)

Seven sources (0234+285, 0446+112, 0917+449, 0954+658, 1606+106, 1611+343, and 1739+522) can be classified as inactive $\gamma$-ray blazars since they do not show significant variability during the $\gamma$-ray observations. No disturbances that propagate down the jet are seen in any of these sources during the period covered by our VLBA observations.

### 3.2 Marginal Detections

In the case of five additional sources (0420−014, 0716+714, 1253−055, 1406−076, and 1908−201) there is a hint of an association between $\gamma$-ray variability and ejection of superluminal jet components. For 0420−014, 1253−055, and 1406−076 the time of ejection of a component differs from the time of a $\gamma$-ray flare by less than the 3-$\sigma$ uncertainties of the

Table 1: Epochs of Zero Separation and Times of Peak $\gamma$-Ray Flux

| Name | z | Factor of $\gamma$-ray flare | Time of separation | Epoch of zero | $\beta_{app}$h |
|---|---|---|---|---|---|
| 0336−019 | 0.852 | 5.3 | 1995.266 | 1995.2±0.1 | 5.8±0.5 |
| 0440−003 | 0.844 | 3.0 | 1994.632 | 1994.7±0.2 | 8.5±0.8 |
| 0458−020 | 2.286 | 3.2 | 1994.212 | 1994.0±0.1 | 9.0±0.8 |
| 0528+134 | 2.06 | 4.0 | 1993.233 | 1993.2±1.6 | 24±14 |
| | | | | 1993.4±0.7 | 15±6 |
| 0836+710 | 2.17 | 1.9 | 1992.197 | 1992.1±0.2 | 14±1 |
| 1222+216 | 0.435 | 2.3 | 1992.984 | ∼1993.1 | ∼8.5 |
| 1226+023 | 0.158 | 2.2 | 1993.899 | ∼1994.2 | ∼3.0 |
| 1622−253 | 0.786 | 1.9 | 1995.460 | 1995.7±0.2 | 17.5±1.1 |
| | | 2.0 | 1995.729 | | |
| 1622−297 | 0.815 | 3.4 | 1995.441 | 1995.2±0.2 | 16.0±0.8 |
| | | 4.7 | 1995.460 | | |
| | | 3.9 | 1995.482 | | |
| | | 3.5 | 1995.482 | | |
| 1730−130 | 0.902 | 2.2 | 1995.510 | 1995.5±0.2 | 6.1±2.1 |

times of zero separation. For 0716+714 and 1908−201 the times of zero separation correspond to less significant increases (by factors of 1.4 and 1.3, respectively) over the mean $\gamma$-ray fluxes.

### 3.3 Negative Detections

For four sources (0219+428, 0851+202, 1510−089, 2230+114) $\gamma$-ray flares were not detected, but we can follow moving components and in three cases even multiple knots. The $\gamma$-ray measurements nearest in time to the zero separations correspond to low levels of $\gamma$-ray flux. However, because of the sparseness of the $\gamma$-ray light curves, such non-correspondence can be explained if the time scale of a high $\gamma$-ray state is of the same order as or less than the typical 1-$\sigma$ uncertainty of the epoch of zero separation (∼0.2 yr). If we assume that $\gamma$-ray flares are associated with ejections of superluminal jet components, then it is more challenging to explain the absence of moving knots connected with $\gamma$-ray flares in four sources (0827+243, 1127-145, 1219+285, and 1633+382), since if components were ejected they should have been detected by our VLBA observations. Nevertheless, there are possible explanations of such non-correspondence: the marginal significance of the $\gamma$-ray flare in 0827+243, two different possible cross-epoch identifications of components in 1219+285, and possible deceleration of a component in 1633+382).

### 3.4 Statistical Simulations

We have generated $10^6$ samples of random epochs of zero core-knot separations over a 5-year period of $\gamma$-ray observations to define the probability of random coincidences between 19 fixed epochs of $\gamma$-ray flares and ejections of superluminal jet components. A coincidence was recorded if the difference between the epoch of a $\gamma$-ray flare and an epoch of zero separation was equal to or less than 0.2 yr. The results are presented in Fig. 1, which shows that in a sample of 19 events the number of chance coincidences $\leq 3$ at the 95% confidence level. If the number of coincidences $\geq 5$ the $\gamma$-ray flares and superluminal ejections are associated with each other at the 99.9% confidence level.

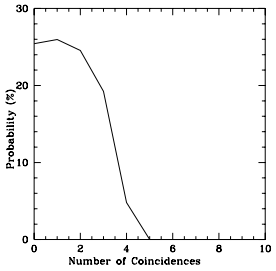


Figure 1: Probability of random coincidences between $\gamma$-ray flares and epochs of zero separation.

## 4 Conclusion

It is very striking that, despite the sparse character of the $\gamma$-ray light curves and uncertainties of epochs of zero separation of about 0.2 yr, 50% of the $\gamma$-ray flares are associated with the ejection of superluminal jet components. This implies that the $\gamma$-ray high states are not, in general, merely very short-timescale peaks of constantly fluctuating $\gamma$-ray emission, but rather correspond to major disturbances in bulk Lorentz factor and/or flow energy of the relativistic jet.

**Acknowledgements.** This work was supported in part by NASA through CGRO Guest Investigator grants NAG5-7323 and NAG5-2508, and by U.S. National Science Foundation grant AST-9802941.

## References

Hartman, R.C., Bertsch, D.L., Bloom, S.D., et al. 1999, *ApJS*, **123**, 79

*Astrophysical Phenomena Revealed by Space VLBI*
*H. Hirabayashi, P.G. Edwards and D.W. Murphy (eds.)*

# Up-Link Frequency Control Using Closed-Loop Mode

Kazumasa Suzuki[1], Noriyuki Kawaguchi[2] & Takashi Kasuga[1]

[1] *Hosei Univ., Kajinocho 3-7-2, Koganei, Tokyo 184-0002, Japan*
[2] *NAO, Ohsawa 2-21-1, Mitaka, Tokyo 181-8588, Japan*

**Abstract**

We describe the possibility of frequency stabilization on the HALCA satellite by applying a closed-loop up-link frequency control. The closed-loop mode is able to remove systematic variations of the residual delay rate and the frequency stability is greatly improved.

## 1 Introduction

The HALCA Satellite is not equipped with a hydrogen maser oscillator, and so the clock and phase are up-linked from ground tracking stations equipped with their own hydrogen maser oscillator. The received phase is Doppler shifted by the effect of the orbital motion of the satellite and fluctuated by the atmosphere. So the transferred phase must be controlled at the ground station in order to keep the received phase on the satellite constant, effectively equipping the satellite with a hydrogen maser frequency oscillator.

There are two up-link frequency control methods. One is the open-loop frequency control based on the calculation of the up-link frequency from the orbit prediction. The other is the closed-loop frequency control based on the measurement and control of the frequency offset on the satellite. At present for HALCA the open-loop control is used, although the accuracy of the orbit prediction is not so good.

In this report, we describe the possibility of high frequency stabilization on the satellite by applying a closed-loop up-link frequency control.

## 2 Merits of the Closed-Loop Mode

- An accurate orbit prediction is not necessary
- The time correction for correlation processing becomes easy.

- The possibility of real-time correlation processing becomes available.

## 3 Frequency Control Algorithm (PI Control)

1. Control is started with open-loop frequency control mode
2. Closed loop frequency control mode switched ON ($t = t_0$)
3. Estimation of true Doppler frequency

$$f_{true-dopp}(t) = \frac{\hat{f}_{up-cont}(t) - \frac{f_{down-measure}(t+T_{up+down})}{r}}{2} \quad (1)$$

4. Estimation of deviation (frequency offset on the satellite)

$$\Delta f(t) = f_{up-cont} - f_{true-dopp} \quad (2)$$

5. Calculation of manipulated variable

$$\begin{aligned} f_{up-cont}(t+5T_S) = f_{up-cont}(t+4T_S) \\ +K_P \cdot \Delta f(t) + K_I \cdot \sum_{t=t_0}^{t} \Delta f(t) \\ +f_{true-dopp}(t) - f_{true-dopp}(t-T_s) \end{aligned} \quad (3)$$

6. Decision of up-link frequency

$$f_{up}(t+5T_s) = F_{u0} - f_{up-cont}(t+5T_s) \quad (4)$$

7. Iteration of steps 3–6

$T_s$ : sampling time(1 second)
$T_{up+down}$ : propagation time
$f_{true-dopp}$ : true Doppler frequency
$f_{up-cont}$ : manipulated variable of up-link frequency
$f_{down-measure}$ : measurement variable of down-link frequency
$\Delta f$ : frequency offset
$r$ : transponding ratio (14.2[GHz]/15.3[GHz])
$K_P$ : coefficient of proportionality
$K_I$ : coefficient of integration
$f_{up}$ : up-link frequency
$F_{u0}$ : nominal up-link frequency (15.3 GHz)

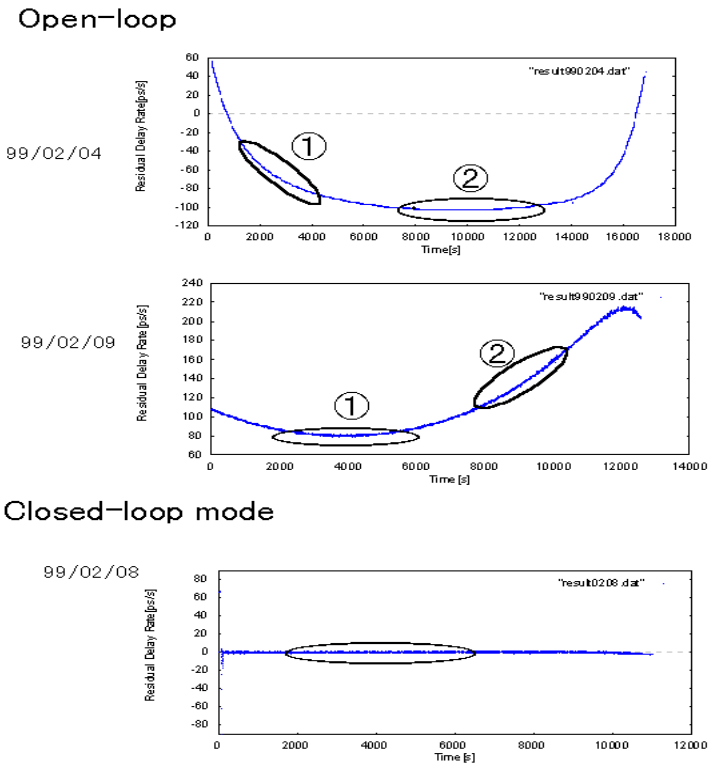


Figure 1: Result of open-loop mode and closed-loop mode.

## 4 Result

The results of the frequency control experiment are shown in Figure 1 and Figure 2. In Figure 1 the vertical axis is the residual delay rate and the horizontal axis is observation time. In Figure 2 the vertical axis is Allan standard deviation and the horizontal axis is the averaging time.

## 5 Conclusion

The closed-loop mode is able to remove the systematic variation of residual delay rate and the frequency stability is greatly improved. Therefore, it is clear that the closed-loop control is possible and offers significant improvements.

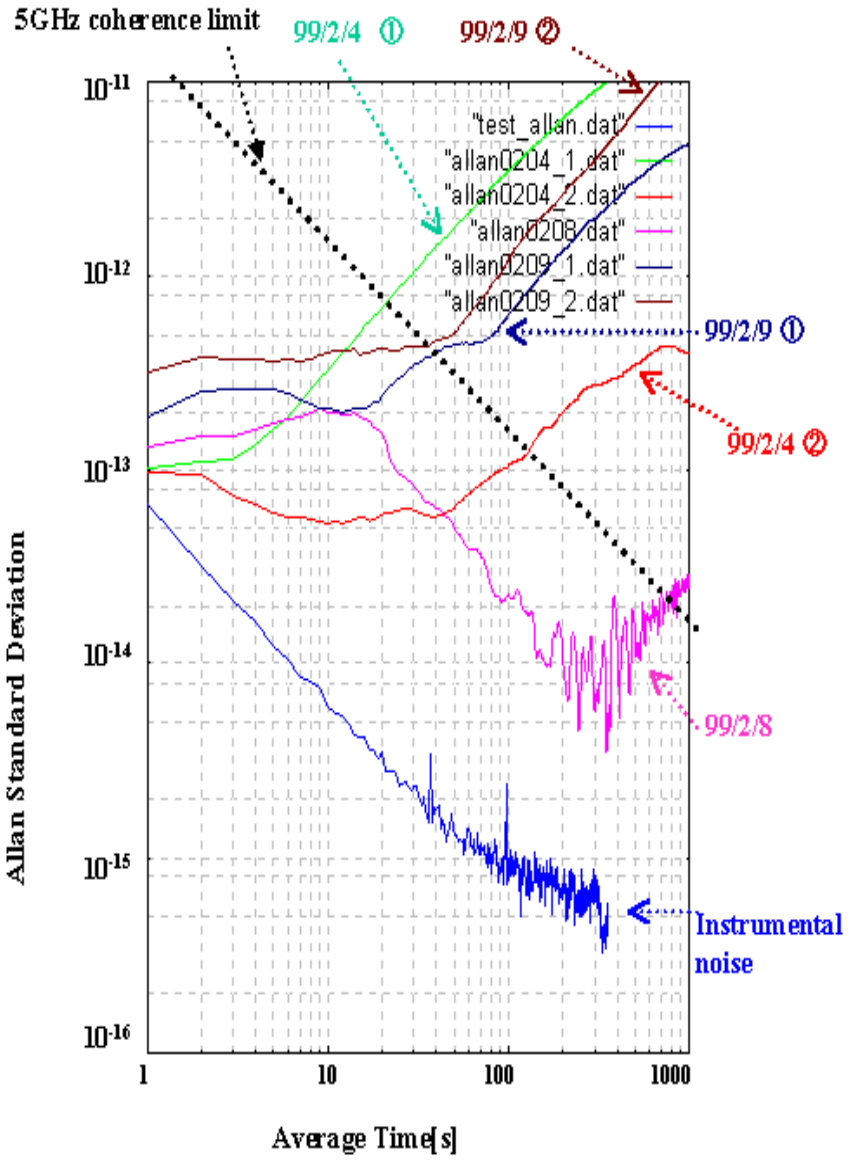


Figure 2: Frequency stability.

*Astrophysical Phenomena Revealed by Space VLBI*
*H. Hirabayashi, P.G. Edwards and D.W. Murphy (eds.)*

# VSOP Observations of Bright, Compact Southern Hemisphere AGN

S.J. Tingay [1], J.E. Reynolds [1], D.L. Jauncey [1], A.K. Tzioumis [1], R.A. Preston [2], D.W. Murphy [2], D.L. Jones [2], D.L. Meier [2], M.E. Costa [3], D. Moffet [3], P.M. McCulloch [3], G. Nicolson [4], E.A. King [1], P.G. Edwards [5], B.G. Piner [2], J.E.J. Lovell [1], H. Hirabayashi [5], M. Tornikoski [6], A. Mucke [7], H. Bignall [7], R.W. Clay [7]

[1] *ATNF, PO Box 76, Epping, NSW 2121, Australia*
[2] *JPL, 4800 Oak Grove Drive, Pasadena, CA 91109, USA*
[3] *University of Tasmania, Hobart, Tasmania 7001, Australia*
[4] *HRAO, PO Box 443, Krugersdorp 1740, Transvaal, South Africa*
[5] *ISAS, Yoshinodai 3-1-1, Sagamihara, Kanagawa 229-8510, Japan*
[6] *Metsähovi RO, Metsähovintie 114, FIN-02540, Kylmälä, Finland*
[7] *University of Adelaide, Adelaide, South Australia 5005, Australia*

**Abstract**

Observations of 11 of 23 Southern Hemisphere AGN are presented from three separate VSOP projects: comparisons of EGRET-identified and $\gamma$-ray quiet AGN, investigations of the high resolution structure in low redshift AGN, and comparisons of radio and X-ray structure in AGN jets. The observations have used HALCA in conjunction with Southern Hemisphere antennas and the VLBA, where appropriate.

## 1 Introduction

We list core model components for each source observed and calculate corresponding brightness temperatures in the co-moving frames of the sources. For a small number of sources we have derived errors on the brightness temperature estimates. Table 1 contains a list of the sources proposed/observed.

## 2 Results

Data from the Socorro, Penticton, and Mitaka correlators were reduced in standard fashion in AIPS. Images and model-fits were made in Difmap

(Shepherd et al. 1994). Error analyses, where completed, were made using the Difwrap software (Lovell, these proceedings).

Table 1: The source list from the three proposals: *Column 1*, Source name. *Column 2*, Alternate name. *Column 3*, Source type. *Column 4*, Have the data been imaged?

| Name | Alt. | Type | Image |
|---|---|---|---|
| PKS 0208−512 | | EGRET-identified AGN | YES |
| PKS 0438−436 | | $\gamma$-ray quiet AGN | YES |
| PKS 0518−458 | Pic A | low z FR-II radio galaxy | NO |
| PKS 0521−365 | | low z BL Lac | NO |
| PKS 0537−441 | | EGRET-identified AGN | YES |
| PKS 0637−752 | | $\gamma$-ray quiet AGN/X-ray jet | YES |
| PKS 1104−445 | | $\gamma$-ray quiet AGN | YES |
| PKS 1127−145 | | EGRET-identified AGN? | YES |
| PKS 1322−427 | Cen A | low z FR-I radio galaxy | NO |
| PKS 1424−418 | | EGRET-identified AGN | NO |
| PKS 1514−241 | AP Lib | low z BL Lac | NO |
| PKS 1610−771 | | $\gamma$-ray quiet AGN | YES |
| PKS 1622−253 | | EGRET-identified AGN | NO |
| PKS 1622−297 | | EGRET-identified AGN | NO |
| PKS 1718−649 | NGC 6328 | low z GPS source | YES |
| PKS 1730−130 | NRAO 530 | EGRET-identified AGN | NO |
| PKS 1908−201 | | EGRET-identified AGN | NO |
| PKS 2052−474 | | EGRET-identified AGN | NO |
| PKS 2106−413 | | $\gamma$-ray quiet AGN | NO |
| PKS 2152−699 | | low z FR-II radio galaxy | YES |
| PKS 2204−540 | | $\gamma$-ray quiet AGN | NO |
| PKS 2255−282 | | EGRET-identified AGN | YES |
| PKS 2355−534 | | $\gamma$-ray quiet AGN | YES |

The brightness temperature results tabulated below in Table 2 have been derived using Gaussian model components. In general we cannot distinguish between Gaussian, optically thin or optically thick sphere models. The Gaussian, as the most centrally concentrated surface brightness profile of the three, yields the highest estimated brightness temperatures. Brightness temperatures corresponding to optically thin spheres are a factor of 1.5 less than for Gaussians and corresponding to optically

thick spheres are a factor of 1.8 less.

| Source | S | R | $\theta^\circ$ | a | b/a | $\phi^\circ$ | $T_{b-co,G}$ |
|---|---|---|---|---|---|---|---|
| PKS 0208−512 | 0.4±0.1 | 1.0 | 90 | $0.4\pm^{0.2}_{0.3}$ | $0.5\pm^{0.1}_{0.4}$ | 50 | $0.6\pm^{50.0}_{0.4}$ |
| PKS 0438−436 | 0.94 | 0.0 | 0 | 0.3 | 0.6 | −42 | 3.5 |
| PKS 0537−441 | $0.7\pm^{0.1}_{0.2}$ | 1.0 | 180 | 0.3±0.1 | $0.8\pm^{0.2}_{0.3}$ | −67 | $0.9\pm^{3.0}_{0.6}$ |
| PKS 0637−752 | $0.9\pm^{0.5}_{0.1}$ | 0.5 | 90 | $0.6\pm^{0.3}_{0.1}$ | 0.3±0.1 | 73 | $0.7\pm^{1.6}_{0.5}$ |
| PKS 1104−445 | 0.7 | 0.0 | 0.0 | 0.4 | 0.8 | −67 | 0.8 |
| PKS 1127−145 | 0.9 | 3.7 | −99 | 0.4 | 0.5 | 73 | 1.1 |
| PKS 1610−771 | na | na | na | na | na | na | na |
| PKS 1718−649 | 0.9 | 0.0 | 0.0 | 1.0 | 0.4 | −62 | 0.1 |
| | 0.8 | 6.7 | 135 | 1.3 | 0.4 | −49 | 0.06 |
| PKS 2152−699 | 0.2 | 0.0 | 0.0 | 0.9 | 0.2 | 42 | 0.06 |
| PKS 2255−282 | 2.7 | 0.0 | 0.0 | 0.3 | 0.4 | 27 | 7.1 |
| PKS 2355−534 | 0.2 | 0.0 | 0.0 | 0.3 | 0.0 | 49 | na |

Table 2: Best fit core quantities for the VSOP data: *Column 1*, Source name. *Columns 2 to 7*, The best fit parameters derived for the component, as described in Difmap. *Column 8*, $T_{b-co,G}$, the source frame brightness temperature of the component, in units of $10^{12}$ K. Note: na denotes that the quantity could not be measured.

## 3 ATCA Lightcurves

The Australia Telescope Compact Array (ATCA) was used at 1.4, 2.3, 4.9, and 8.6 GHz to monitor 206/221 VSOP survey sources below a declination of $+10^\circ$, including most of the sources listed above that have been observed using VSOP GOT.

## 4 Conclusions

We have successfully used the Southern Hemisphere VLBI array, in conjunction with HALCA, and occasionally the VLBA, to produce the highest resolution images of these Southern Hemisphere compact radio sources to date.

Sources of several different classifications have been detected and imaged, including core dominated BL Lac objects and quasars, but also low brightness temperature sources such as radio galaxies and GHz-Peaked-Spectrum objects. The core-dominated sources have signific-

antly higher brightness temperatures than the radio galaxy and the GPS source but there is no evidence that $\gamma$-ray AGN have higher brightness temperatures than $\gamma$-ray quiet AGN, as some people expect from the suggestion that the $\gamma$-ray AGN may be more highly beamed than the $\gamma$-ray quiet AGN. However, a full error analysis of all sources needs to be undertaken before this conclusion can be quantified further.

The three most variable sources at 5 GHz are $\gamma$-ray AGN. Results for more sources are required to confirm this.

**Acknowledgements.** We gratefully acknowledge the VSOP Project, which is led by the Japanese Institute of Space and Astronautical Science in cooperation with many organizations and radio telescopes around the world.

## References

Shepherd, M.C., Pearson, T.J., & Taylor, G.B. 1994, *BAAS*, **26**, 987

*Astrophysical Phenomena Revealed by Space VLBI*
*H. Hirabayashi, P.G. Edwards and D.W. Murphy (eds.)*

# VERA Approved !

Satoko Sawada-Satoh, VERA Project Team

*NAO, Osawa 2-21-1, Mitaka, Tokyo 181-8588, Japan*

**Abstract**

A new Japanese VLBI project, VERA (VLBI Exploration of Radio Astrometry), consisting of an array of four radio telescopes, is being developed by NAO. It aims to measure distances and proper motions of astronomical maser sources distributed through our galaxy with an accuracy of a few tens of micro-arcseconds. It was funded at the end of 1999, and we have started to construct three antenna systems.

## 1 Towards the Detection of Dark Matter in Galaxy

It is known that a considerable mass of the Galaxy and the universe is in the form of dark matter. Dark matter, however, does not emit detectable electromagnetic radiation at any wavelength but can be detected only through its gravitational effect. Because of its dominance, understanding the nature and total amount of dark matter is one of the fundamental subjects in Astronomy, Astrophysics, and modern Physics.

The distribution and total amount of dark matter in the Galaxy can be studied based on the rotational motions of stars around the Galactic center. However, only nearby stars' distances and motions can be measured, and so studies of Galactic dark matter has suffered from large observational errors. VERA will investigate the three-dimensional structure and dynamics of the Galaxy and reveal the distribution and total amount of dark matter, measuring the position of astronomical maser sources with the highest accuracy ever achieved.

## 2 VERA Science Targets

The major science targets of VERA are:

- to establish the three-dimensional structure and dynamics of the Galaxy,
- to reveal the distribution and total amount of dark matter in the Galaxy,

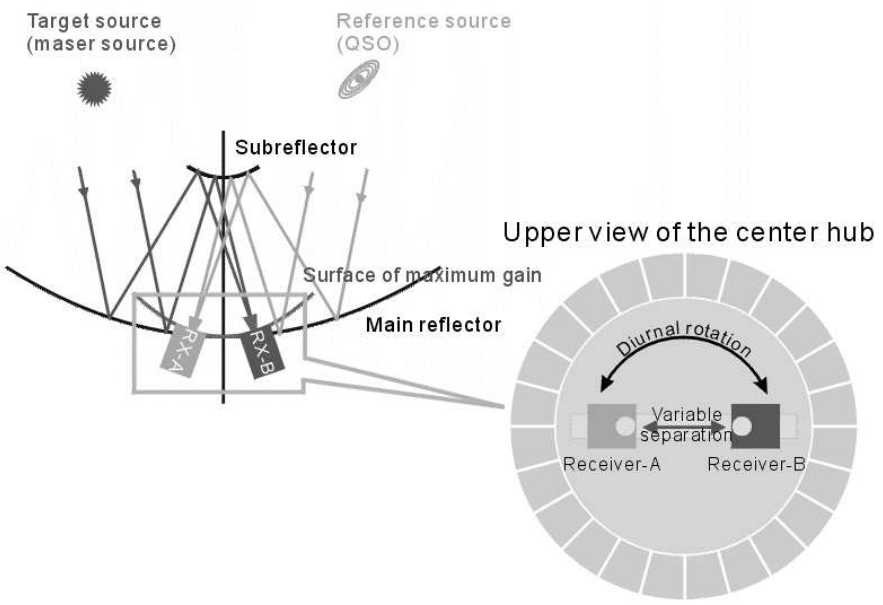


Figure 1: Dual-beam Cassegrain antenna for VERA

- to improve our understanding of the physical processes in star-forming regions and late-type stars by measuring distances and proper motions of the maser sources.
- to improve the cosmological distance scale by direct establishment of the period–luminosity relation of Mira variables and statistical parallax distances of maser sources.
- to measure proper motions of nearby active galactic nuclei and extragalactic masers,
- to support the Japanese lunar VLBI mission RISE/SELENE (Research in Selenodesy/SELenological and ENgineering Experiment) to be launched in 2004 and the next space VLBI mission (VSOP-2) as a ground array,
- to contribute to the progress of Earth science by studying the crustal deformations around Japan and the Earth's variable rotation.

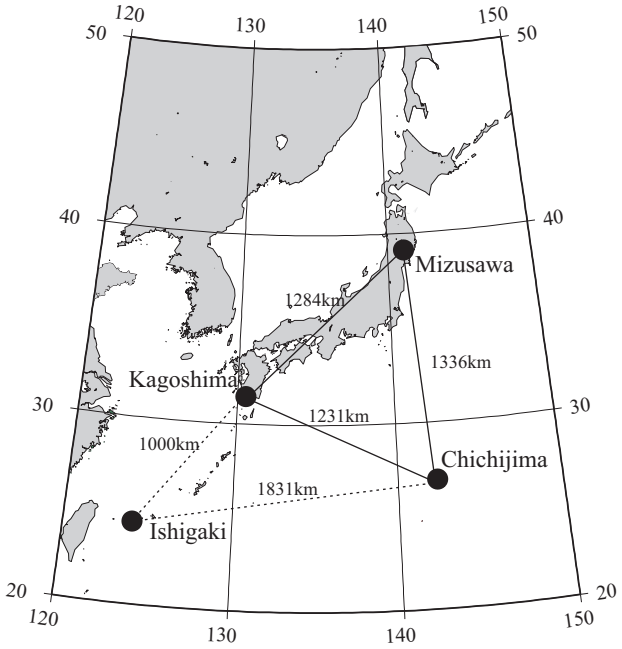


Figure 2: Location of VERA antennas

## 3 High Precision Astrometry

VERA will succeed the new approach in astronomy initiated by ESA's HIPPARCOS (High-Precision Parallax COllecting Satellite) astrometry satellite (1989–1993) with accuracy roughly 100 times higher than that achieved by the satellite. While HIPPARCOS provided accurate parallax distances for stars within 100 pc from the Sun, distance measurements with VERA will cover roughly the whole region of our Galaxy. Planned space optical interferometry missions like FAME (Full-sky Astrometric Mapping Explorer) (e.g. Horner et al. 1999) , SIM (Space Interferometry Mission) and GAIA (Global Astrometric Interferometer for Astrophysics) (Merat et al. 1999) aim at ten micro-arcsecond level astrometry, similar to VERA. VERA is unique among the challenges in using the well-established VLBI technology which achieved the highest angular resolution in astronomy. Radio observation enables us to see the objects beyond the Galactic center and gives us information on astrophysically interesting objects like star-forming regions and evolved stars.

## 4 Instrumentation

VERA will cancel the distorting effect of the atmosphere using the "phase-referencing technique" with newly designed "dual-beam antennas" (Fig. 1) which are capable of simultaneously observing a target source and a reference compact extragalactic radio source separated by up to two degrees. Model simulations and experiments using radio interferometers have shown that we could reduce the atmospheric effects below the ten micro-arcsecond level with this technique. The antennas will have a 20 m diameter Cassegrain system with S, X, K and Q band receivers. Location of antennas is shown in Fig. 2. The hardware systems in the Mizusawa–Kagoshima–Chichijima array will be constructed by the end of March, 2001, and regular observation will start in 2002. We expect in the future to build one more site at Ishigaki.

## References

Horner, M. et al., 1999, in *IAU Coll. 176: The Impact of Large-Scale Surveys on Pulsating Star Research*, eds. L. Szabados & D. Kurtz (ASP Conference Series) in press.

Merat, P. et al., 1999, *Baltic Astronomy*, **8**, 1

*Astrophysical Phenomena Revealed by Space VLBI*
*H. Hirabayashi, P.G. Edwards and D.W. Murphy (eds.)*

# Comparison of Total Flux and VLBI Properties of a Sample of Fifteen AGN at 22 GHz

Kaj Wiik[1,2], Esko Valtaoja[1] & Anne Lähteenmäki[2]

[1] *Tuorla Observatory, Väisäläntie 20, FIN-21500 Piikkiö, Finland*
[2] *Metsähovi Radio Observatory, Metsähovintie 114, FIN-02540 Kylmälä, Finland*

**Abstract**

A sample of 15 bright AGN has been observed at 22 GHz with three epoch global VLBI observations. The sample consists of all the sources in the complete 2 Jy catalogue of Valtaoja et al. (1992) that were still unobserved at 22 GHz VLBI in 1992 when the project started. We have started to compare source parameters (Doppler boost factors, shock sizes, and brightness temperatures) derived from total flux density (TFD) monitoring data and/or from VLBI.

## 1 Introduction

We have made three epoch observations of a sample of 15 bright AGN at 22 GHz global VLBI. The project started as a support survey for the 22 GHz space VLBI missions. At the time of the first epoch RadioAstron was due to be launched within some years. The observation epochs were November 1992, September 1993, and November 1996.

Lähteenmäki et al. (1999) proposed that by comparing TFD monitoring data with VLBI structure variations and apparent shock sizes, important source parameters can be estimated with higher accuracy (Valtaoja et al., 2000). Inversely, we can use this method when selecting target source candidates both for space- and mm-VLBI, where compactness and high brightness temperature are needed for successful detection.

## 2 The Sample

Our sample is based on the complete Northern hemisphere sample of compact AGN (Valtaoja et al., 1992). The selection is based on the high frequency characteristics of AGN, using the selection criterion $S_{22\ \mathrm{GHz}} >$

2 Jy combined with the experience from the Metsähovi and SEST total flux density monitoring. For this VLBI survey we selected 15 from all of the 47 complete sample sources which were not observed previously at 22 GHz VLBI: **0106+013, 0202+149, 0528+134,** 0754+100, 1219+285, **1413+135**, 1418+546, **1749+096,** 2021+614, 2134+004, 2145+067, 2201+315, 3C371, CTA102 and OK290. The sample is representative since it includes all the main classes of AGN. Five of the 15 sources observed in this project were selected to the comparison mainly because of their well definable and identifiable components (typed in boldface in the previous list).

## 3 Derivation of Doppler Boost Factors

As an example of the comparison, we will present the derivation of the Doppler boost factors and present the results for 0106+013 in Figure 1.

Doppler boost factor is defined by

$$D = [\Gamma(1 - \beta \cos\theta)]^{-1}, \tag{1}$$

where $\Gamma$ is the Lorenz-factor, $\beta$ is the component velocity relative to $c$, and $\theta$ is the viewing angle.

$D$ and redshift $z$ affect to the observables in the following way:

$$\nu_{\rm obs} = \nu_{\rm int} \left( \frac{D}{1+z} \right) \tag{2}$$

is the redshifted intrinsic radiation spectrum emitted by the moving source ($\nu_{\rm int}$).

The time dilation effects to the time scales by

$$\Delta t_{\rm obs} = \Delta t_{\rm int} \left( \frac{1+z}{D} \right) \tag{3}$$

while

$$S_{\rm obs} = S_{\rm int} \left( \frac{D}{1+z} \right)^3 \tag{4}$$

is the enhancement of the flux, where one power comes from time dilation and two powers from relativistic aberration.

If components are assumed to be spherical, aberration causes only rotation and no change in size $\Theta$:

$$\Theta_{\rm obs}^{\rm VLBI} = \Theta_{\rm int}. \tag{5}$$

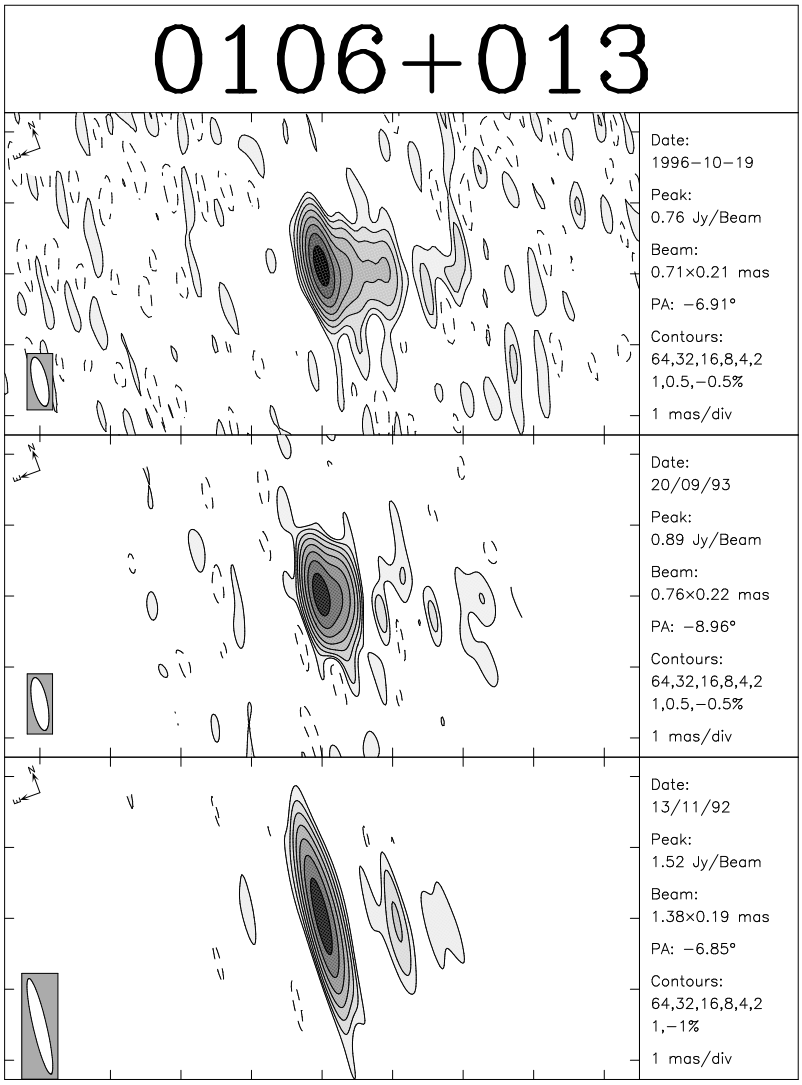


Figure 1: Three epoch VLBI observations of 0106+013. The component which is used in the Doppler boost factor estimations is just emerging from the core in the second epoch (middle panel). The component has been identified from the TFD data and it caused a peak in the total flux density around the first VLBI epoch. The new component is still merged to the core during the first epoch (bottom panel). The estimated boost factors are 2.6, 5.1, 5.3 and $<1$ for $D_1, D_2, D_3$ and $D_4$ respectively.

On the other hand, if size is estimated from the variability timescales (Valtaoja et al., 1999), time dilation must be taken into account:

$$\Theta_{\rm int} = \frac{c\,\tau_{\rm int}}{r} = \frac{H_0\,\tau_{\rm obs}}{2}\left[1 - \frac{1}{\sqrt{1+z}}\right]^{-1} D. \qquad (6)$$

The observed brightness temperatures can be calculated from the equations (2) – (**??**) for the VLBI case

$$T_{B,{\rm obs}}^{\rm VLBI} = T_{\rm B,int}\left(\frac{D}{1+z}\right), \qquad (7)$$

and for the total flux density monitoring data

$$T_{B,{\rm obs}}^{\rm TFD} = T_{\rm B,int}\left(\frac{D}{1+z}\right)^3. \qquad (8)$$

Finally the four Doppler boost factors can be expressed as

$$D_1 = \left(\frac{T_{\rm B,obs}^{\rm TFD}}{T_{\rm B,max}}\right)^{\frac{1}{3}} \quad (9) \qquad D_2 = \frac{\Theta_{\rm B,obs}^{\rm VLBI}}{\Theta_{\rm B,obs}^{\rm TFD}} \quad (11)$$

$$D_3 = \left(\frac{T_{\rm B,obs}^{\rm TFD}}{T_{\rm B,obs}^{\rm VLBI}}\right)^{\frac{1}{2}} \quad (10) \qquad D_4 = \left(\frac{T_{\rm B,obs}^{\rm VLBI}}{T_{\rm B,max}}\right). \quad (12)$$

In the comparisons we have used $T_{\rm B,max} = 5 \times 10^{10}$ K.

## 4 Conclusion

TFD variability timescales and VLBI component sizes have been successfully used to estimate Doppler boost factors for a sample of AGN. This method can also be used to estimate the component size and brightness temperature from TFD data only and thus can be used to aid selection of target source candidates both for space- and mm-VLBI.

## References

Lähteenmäki, A. et al. 1999, *ApJ*, **511**, 112

Valtaoja, E. et al. 1992, *A&AS*, **95**, 73

Valtaoja, E. et al. 1999, *ApJS*, **120**, 95

Valtaoja, E. et al. 2000, *these Proceedings*

## Index

Source List

First Author List

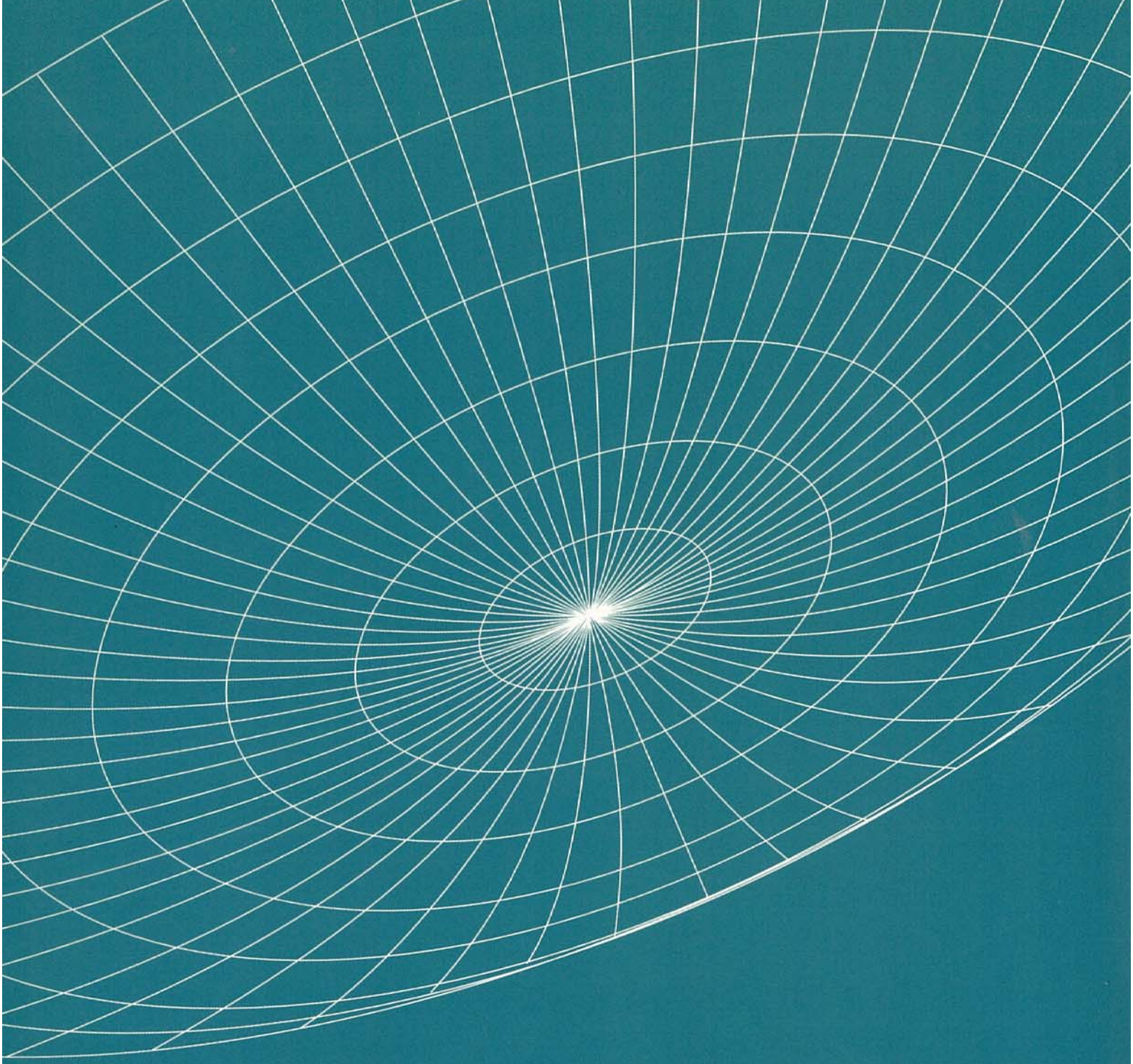

THE INSTITUTE OF SPACE AND ASTRONAUTICAL SCIENCE
3-1-1 Yoshinodai, Sagamihara, Kanagawa, 229-8510, JAPAN

vsopsymp.errata.txt

Corrections to VSOP Symposium Proceedings
---

* In the contents, the author list for the paper starting on page 79
  is incomplete and should read
  "Ignas Snellen, Wolfgang Tschager, Richard Schilizzi et al."

* In the preface, "Orian-KL" should be "Orion-KL"!!!

* The caption to Color Figure 3 refers to the source 1928+734,
  which should be 1928+738.

* In the summary section on page 49 (Murphy et al.), the sentence
  "In that time, we have observed a variety of
   structural changes in the inner jet region near the region."
  should read
  "In that time, we have observed a variety of
   structural changes in the inner jet region near the core."

* In the references on page 175 (Fomalont et al.) and page 182
  (Moellenbrock et al.) "Fomalont et al. 2000" should be updated to
  "Fomalont, E.B., Frey, S., Paragi, Z., Gurvits, L.I., Scott, W.K.,
  Edwards, P.G., Hirabayashi, H., 2000, ApJS, 131, 95"

* On page 217 (Lovell et al), the fourth line of the final paragrpah of
  section 1 should say "(see figure on page xviii)"

* In the references on page 233 (Sambruna) an extraneous "439"
  was introduced during the editing process into the reference
  for Catanese 1999.

* In the First Author List on page 327 (in the Index), the following
  line is missing
  Junor, W.       13